Synthesis, Purification, and Complexation of Polyamine Ligand Mixtures

A thesis submitted in partial fulfilment of the requirements
for the Degree of

Master of Science (Chemistry)

at the
School of Physical and Chemical Sciences

By

Sarah Ellen Lilley

University of Canterbury

June 2020

Abstract

This work focussed on synthesis of polyamine ligands by functionalisation of a linear hexamine starting material with 1,8-naphthalic anhydride to create two naphthalimide groups. This ligand was designed to be incorporated into a heterodinuclear redox-activated prodrug complex of cisplatin and cobalt. The naphthalimide groups were intended to block associative ligand exchange on the platinum centre that would otherwise result in premature release or inactivation of the prodrug.

Reaction of the impure 3,6,9,12-tetraazatetradecane-1,14-diamine starting material with 1,8-naphthalic anhydride gave a complex mixture of products, including branched and piperazine compounds and trinaphthalimides. Efforts were made to separate the desired linear dinaphthalimide product from the side products using a process of purification by complexation. This purification strategy relied on the desired compound and its complex having different properties to any side products that might lead to their separation. The copper can then be removed from the separated complex using EDTA to recover the desired dinaphthalimide ligand. Throughout this process, the copper complex of the dinaphthalimide ligand was successfully synthesised and followed by copper removal. This process led to enrichment of the desired ligand material in the reaction fractions following removal of copper with EDTA.

Attempts were made to synthesise cobalt complexes from the dinaphthalimide ligand containing mixtures. ESI-MS evidence was obtained for both the $[Co(C_{34}H_{36}N_6O_4)CO_3]^+$ and $[Co(C_{34}H_{36}N_6O_4)(NO_2)_2]^+$ complexes. Additionally, a deprotonated ligand cobalt complex was observed by ESI-MS.

Structural elucidation of a copper complex of a trinaphthalimide ligand was also performed based on crystallographic data. The trinaphthalimide ligand was synthesised from a branched isomeric impurity in a new hexamine starting material, 3,7,10,14-tetraazahexadecane-1,16-diamine. The crystal structure showed the copper centre was also coordinated to a sulfate anion in a bidentate fashion forming a five-coordinate square planar centre.

Acknowledgements

I think the acknowledgments section is both the easiest and the most difficult part of this thesis to write. I have thought many times about how to write this, and there are so many people who have contributed so massively to my journey to this point. There have been numerous moments where I have felt humbled by the help of others that recalling pages of acknowledgements is the easy part; expressing the magnitude of the contributions is the hard part. So to anyone who has been so integral to the process of my journey, which is currently culminating in this thesis, please know that these words (and the work I put into the words that follow them) cannot capture just how grateful I am.

Firstly, I want to thank the members of my supervisory team, starting with Professor Richard Hartshorn. To say that my thesis journey has been a challenge would be an understatement, but no matter how difficult I found the process you were always there to provide feedback and guidance that not only led to me being able to submit this thesis, but also made me a better scientist. My gratitude also goes to Dr Jan Wikaira, Dr Matthew Polson, and Professor Rudi Marquez. Each of you provided support and a wealth of ideas from your unique perspectives, which taught me how to adapt and expand my problem-solving skills.

To Fatemeh, Nneka, Shirley, Josh, Meghan and Rajika in the Hartshorn group, and later our labmates in the Marquez and Foley groups, as well as my friends in the wider SPCS department. Your friendship and laughter made the lab such a fun place to be, which is an environment I will sorely miss. Your relentless positivity and willingness to help when syntheses inevitably went wrong made those bad days so much brighter and I wish you all the absolute best with your careers. You are all incredible scientists and you deserve so much success. Additional thanks go to Meghan for her assistance in the work that led to Chapter 4.

I am also incredibly grateful to Gill and Laurie, Wayne, Nick, and Rob. No matter what got broken, no matter how difficult the request, and no matter how unusual the chemical, you handled everything so quickly and expertly and always with positivity. I know that the SPCS department could not run without you, and yet every request is treated like no big deal. Thank you for all your help.

Thanks also to all the technical staff involved in keeping everything running, especially Dr Matthew Polson, Dr Marie Squire and Dr Amanda Inglis. This thesis has relied heavily on ESI-MS results and no matter how many new samples I brought down that I couldn't analyse any other

way, Marie and Amanda did their best to get me results and I am so grateful for your patience and thoroughness. This thesis also relies on crystallographic information, and I am indebted to Matt for not only his role in running and analysing the structure but also for teaching me about crystallography along the way. I also want to thank the wider SPCS, and the Chemistry department. I am very grateful to have been a part of the UC chemistry family.

To the Wignall family, especially Betty and Anne. I am so incredibly grateful for your financial support, and I hope you know how much of a difference it has made to me. I apologise that my career pathway has not gone exactly the way that Betty might have hoped, but your generosity and kindness gave me the courage to make some difficult decisions. The support that your family has given me goes beyond the financial, and I cannot thank you enough.

I also want to thank the teachers who led me to where I am today. From primary school teachers who encouraged my curiosity, to my high school teachers who showed me that chemistry did not have to be just a dream and who believed in me when I could not believe in myself. To the many, many teachers along the way including lecturers and demonstrators who encouraged me along the path to where I am today. Thank you.

And finally, but by no means the least, to my incredible family. This is the hardest part for me to write because it is so difficult for me to express just how much you all mean to me, but your support has allowed me to grow into the person I am today. Whenever things were difficult you were there to help me up, and whenever things went well you were the first to celebrate my successes. I know it is a cliché, but I really could not have done this without you. So, to my Mum and Dad, my sister Bex and my partner Daniel; the only reason I could put my heart and soul into this journey is because of you all putting yours in right there with me. You have all seen me at my worst and you still looked at me like I was at my best. I hope you know that the best parts of me are a mirror of everything you have given me. To my wider family and friends, including my Uncle Jim and my Aunty Trish, you have been so understanding and given me your unconditional support which has meant so much to me. To know you is a blessing I am so grateful to have been given.

Preface

All figures and tables presented in this work were created by Sarah Lilley unless otherwise stated. The references within the figure caption indicate the source of any external data the figure was based upon.

All ESI-MS spectra are an exception to this as they were created by Dr Marie Squire or Dr Amanda Inglis within the School of Physical and Chemical Sciences, University of Canterbury. Labelling beyond standard processing was created by Sarah Lilley.

Crystallographic data collection and processing were performed by Dr Matthew Polson . An absorption corrected CIF was generated thanks to his contribution, which was used to generate the data and images used in Chapter 4.

Compounds are referred to by number throughout this work, with the first number of the code corresponding to the chapter that compound was first described in. The structures for Compounds 2.1 – 2.30 can be found in Figure 2.3 on Page 30, Compounds 3.1 – 3.3 in Figure 3.2 on Page 73 and Compounds 4.1 – 4.7 in Figure 4.1 on Page 91.

Abbreviations

Fas/FAS receptor: *Death receptor on the cell surface that is implicated in the apoptosis process*

G0, G1, S, G2: *Terms for the phases of the cell cycle. G0 is the 'resting' phase adjacent to the cycle where the cell spends the majority of its life and performs its usual functions. G1 is where the cell begins to ready for DNA replication by increasing in size and number of proteins. S phase is where the cell replicates DNA. G2 is the phase where the cell will begin to produce proteins to allow the cell to divide, ready to progress into the following mitosis phase.*

HMG Proteins: *High Mobility Group Proteins. These proteins are regulators of transcription.*

PAH: *Polyaromatic hydrocarbons.*

VEGFR Kinase: *Vascular Endothelial Growth Factor (VEGF) Receptor (VEGFR). Kinases related to the formation of blood vessels. Inhibitors of VEGFR are used in the treatment of cancers.*

Colour Coding

The following list depicts the colour scheme used to colour the atoms in three dimensional figures created within this work, both within crystal structures and within rendered models.

Carbon
(Black)

Hydrogen
(White)

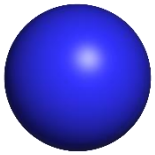

Nitrogen
(Royal Blue)

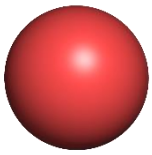

Oxygen
(Red)

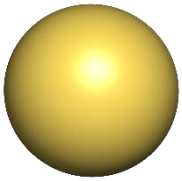

Sulfur
(Yellow)

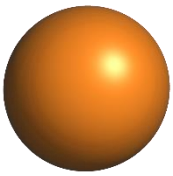

Copper
(Orange)

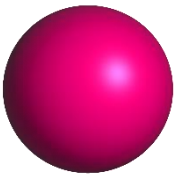

Cobalt
(Magenta)

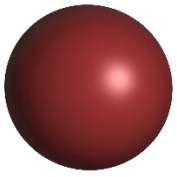

Platinum
(Burgundy)

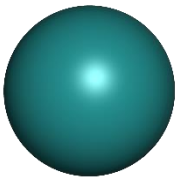

Ruthenium
(Deep Green)

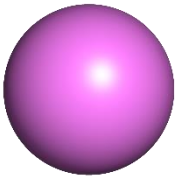

Phosphorus
(Lilac)

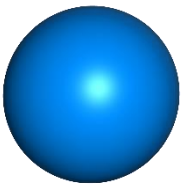

Uranium
(Bright Blue)

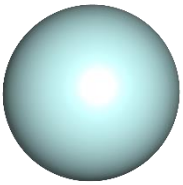

Vanadium
(Pale Blue)

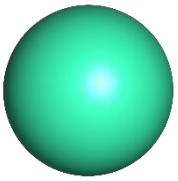

Rhenium
(Teal)

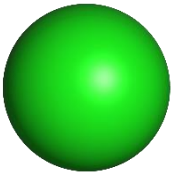

Chlorine
(Green)

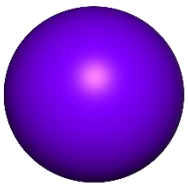

Arsenic
(Purple)

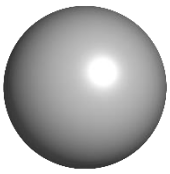

Silver
(Silver)

Table of Contents

Chapter 1: *Introduction*

1.1. Cancer

It is reported that the global cancer burden amounts to 9.6 million deaths annually, making it the second largest cause of death worldwide, with 18.1 million new diagnoses in 2018.[1] Despite being an illness that can affect any person, socioeconomic status and cancer are closely linked.[2] It is estimated that 70% of cancer deaths are among those in lower socioeconomic groups, implying that treatment success relies not only on the efficacy of the regime but also upon the cost.[3] Unfortunately, the global cost of cancer is rising every year along with the growing number of diagnoses.[1] This is attributed to both the growing population as well as the development of many nations – many of the risk factors for cancer development are associated with modernisation and industrialisation, both of which are largely shouldered by less privileged socioeconomic groups in richer nations.[2]

Cancer is a disease characterised by the uncontrolled proliferation of cells. This proliferation results in increased density of cells, termed a tumour.[3] These cells do not function in the way of a healthy cell and this, combined with the growing tumour, causes detrimental impacts to the tissue or organ in which they reside. Over time, the cancer impairs the function of the organ resulting in failure. Cancers can also metastasise, spreading from the affected organs to others through release of cancerous cells from the tumour into the bloodstream. The deadliness of cancer is due to this impact on the organs and the spread to other organs through metastasis.[3]

Cell division is essential for life and is usually a tightly controlled process involving various enzymatic pathways.[4-6] Cell division is regulated by the cell cycle which determines progression through the life cycle of a cell.[4] Most of the life of a cell is spent in a resting phase, noted as the G_0 phase (Figure 1.1).[4] During this phase, the cell is technically adjacent to the cell cycle, in a state that allows it to perform its usual activities. The cell re-enters the cell cycle by entering interphase once it begins to ready for replication.[4] Interphase consists of three stages, G_1, S and G_2.[6] The G_1 phase prepares the cell by ensuring all required resources are present and is distinguished by an increase in cell volume.[6] The S phase follows, representing the point during which DNA is replicated, creating a second complete set of DNA.[5] The cell then proceeds into the G_2 phase, where the DNA and the cell are both prepared for division before the cell enters mitosis.[6] During this short phase, the two copies of the DNA are separated and the cell begins to divide, following through the five stages of mitosis (Figure 1.1).[4-6]

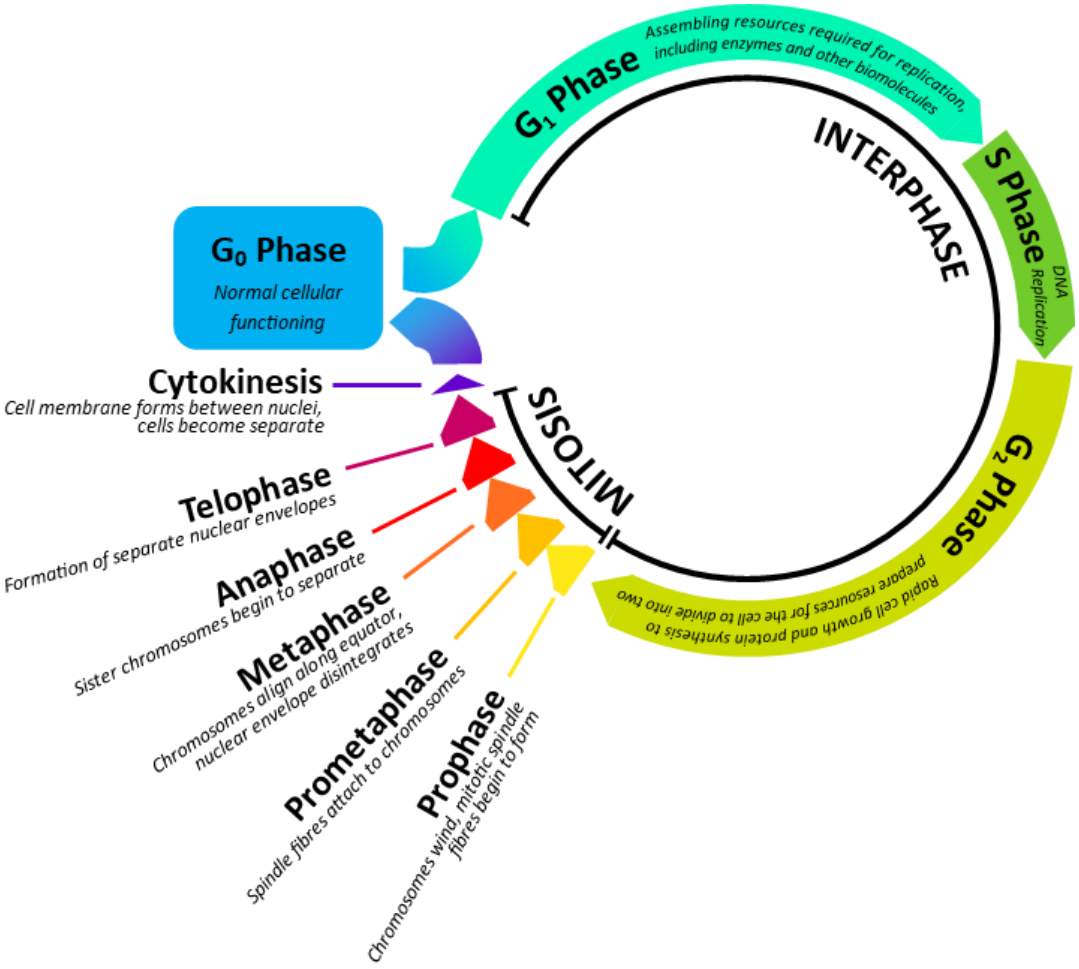

Figure 1.1: ***The cell cycle, showing relative durations and the important changes associated with each phase.***[4-6]

Before proceeding to each phase of the cycle, the cell must pass through checkpoints to ensure that the current phase is complete.[4-7] These checkpoints consists of cell signalling pathways, involving cyclins, cyclin dependant kinases and other more specialised checkpoint proteins.[7-8] These proteins are initiated by key biomolecules used as indicators of the cells readiness to progress to the next phase – presence of these molecules indicates the cell has been fully prepared by the current phase.[7] These checkpoint proteins then begin a cascade that progresses the cell into the next phase.[7]

This process attempts to limit the opportunity for something to go wrong. The more checkpoints there are along the way, the more likely it is that a potential problem with the cell will be identified leading to controlled apoptosis.[7] However, despite this, the complexity of the system also creates more points at which something could go wrong. Issues with replication that are not corrected by the cell are identified as a key mechanism for the progression of a cell line from

healthy to cancerous.[7-12] Damage to any of the biomolecules involved in replication can cause a cell to become cancerous, begin to proliferate in an uncontrolled manner, and form a tumour.

The tightly controlled cell cycle process has evolved as it minimises the opportunity for DNA damage. In fact, it is commonly agreed that the incidence of cancer due to carcinogens is dependent on two factors – the presence of the carcinogen, and the opportunity for this to affect the cell.[13-14] Most cells that become cancerous are believed to do so through damage to DNA above all other biomolecules, which is reinforced by the fact that the vast majority of identified carcinogens act on DNA.[3, 11, 15-16] DNA is at its most vulnerable during replication or during transcription of proteins, as in both cases DNA goes from double stranded, with bases protected by backbones, to single stranded.[4] During the G_0 phase, DNA is in a state termed chromatin.[4] This chromatin is wrapped around histone proteins, which act to protect the DNA both by tightly bundling the DNA around themselves and also through the association of other protection proteins to the complex.[4, 6] When undergoing transcription, a section of the DNA is unzipped and the gene copied. Damage done to the DNA during this state may be able to be rectified prior to the next use of the DNA and biomolecules – many enzymes are designed to identify the resulting lesions of DNA and associated cell machinery caused by xenobiotics.[4-6] In the case of replication, the DNA is unwound and replicated from multiple sites simultaneously and over a longer duration, and the opportunity for damage is much greater.[4, 17] It also holds true that damage sustained during this time may not have time to be repaired before the cell is preparing to divide. The presence of the second strand can mean that damage such as mismatches can be identified and replaced with the correct base through pairing to the existing correct one in the second strand. This mismatch repair mechanism may allow for damaged bases through carcinogens to be found and replaced in the process.[6] Cells that are not prepared to divide due to unrepaired DNA damage are sent down the controlled apoptosis pathway, a response that has no doubt evolved due to the need to prevent cancer. Unfortunately, this process does not always work as intended so when a carcinogen is present and there is an opportunity for it to affect DNA, rather than the cell repairing this damage or entering apoptosis, it may instead become cancerous or reproduce to form a cancerous daughter cell.

There are many physiological differences between healthy cells and cancerous cells aside from the distinctly different rates of proliferation. Often the cancerous cells have different levels of various proteins to their healthy cell counterparts, either as a direct result of the initial cause of the cancer or through indirect mechanisms due to the resulting dysfunction of the cell.[9, 18-21] A further difference relates to the cell oxygenation state. This is normally a closely monitored parameter as many biomolecules are oxidation or reduction sensitive, or rely on minor

modifications of the proximal oxidation environment in order to function.[4] Cancer cells, however, are often hypoxic due to their rapid proliferation.[9, 22] Under standard conditions, development of more tissue also requires formation or extension of blood vessels to provide nutrients and oxygen to the cell and to remove waste products. Cancer cells often replicate too quickly to allow full formation of this vasculature, instead forming a dense tumour. Some cells in the centre of this tumour are far from the blood oxygen supply and therefore have much less oxygen than is typically allowed for a cell, leading to changes in the cells redox state.[9, 22]

A further issue with cancer involves metastasis or the development of secondary cancers, which can occur through a few primary routes. Firstly, tumour cells are often loosely held together due to the rapidity of their proliferation rendering them unable to properly bind together.[6] These cells can easily become detached from the tumour and travel to other areas of the body through the bloodstream.[4] The detached cell can then implant elsewhere and begin to proliferate again, causing the development of a new tumour. Another method for secondary cancer development is through chemotherapy itself. Anticancer drugs are often carcinogenic through their mechanism of action, so while taking these medications may treat a patient's cancer, they may also result in further cancer development in future. These secondary cancers occur on average fifteen years after the initial treatment.[23]

Anticancer agents come in many forms which are often targeted to the specific form of cancer they treat. Their effects are wide ranging but primarily impact on biomolecules that are critical for cancer cell physiology, but less critical to healthy cells, or biomolecules that are more likely to be affected in cancer cells than healthy cells.[13, 24] This makes DNA a primary target for anticancer agents.[13-14] Binding to DNA and preventing replication is likely to impact cancer cells far more than healthy cells due to the proportion of time each spends in replication. Similarly, critical proteins such as topoisomerase[25] or permeability glycoprotein[26] (which is involved in efflux of drugs in multidrug resistance[27]) can be the targets, either because they are not present in most healthy cells or because they are present in much greater quantities in cancer cells. These can even be targeted to the specific cancer, such as vascular epidermal growth factor receptor (VEGFR) kinase inhibitors which are used for renal cancers[15]. Chemotherapy usually involves a combination treatment regime including both medications and methods such as surgery to remove large tumours.[13]

Unfortunately, anticancer agents have drawbacks. The fact that they target biomolecules makes them largely carcinogenic, which means they have ability to cause secondary cancers.[9, 11] Many potential new therapeutics are rejected because their toxicity level is too close to the dosage

required to get anticancer properties, however, even those that pass clinical trials have toxic impacts on the body.[11, 28] Nephrotoxicity is of particular concern as kidneys are affected during the excretion of medications and therefore can be exposed to high concentrations.[9, 29] Neurotoxicity is also of concern, as degradation of brain and nerve cells by these medications is irreversible due to the lack of regeneration of these cells.[9-10, 30]

Despite decades of ongoing research, the elusive 'cure' for cancer has not been discovered. Many have hypothesised[8, 10, 15, 31] that the nature of mitotic replication inherently links humanity to cancer; without completely changing the basis by which cells propagate we can never completely eliminate cancer development. Instead, the focus has shifted towards improving our therapeutics to allow for more effective and efficient treatment regimens resulting in fewer detrimental side effects. Many advances have been made in this direction[9-10, 15, 30, 32-35], and the focus of my research is to make further developments through the improvement of an existing anticancer drug by increasing its selectivity.

1.2. Intercalating Agents

DNA intercalators are compounds with the ability to associate with the DNA by inserting between two pairs of bases in the DNA ladder, deforming the DNA and occasionally resulting in modification to the bases, including frameshift mutageneses.[5, 36] They can also inhibit many central dogma enzymes by competing for interaction with the DNA. This results in many biological impacts, including mutation, inhibition of cell growth and cell death, making intercalators a major class of carcinogen.[36]

Intercalation is usually achievable due to the presence of extended aromatic systems that allow for π stacking with the bases.[37] π stacking involves stabilisation from the interaction of temporary and induced dipoles, also described as dispersion forces.[38] This interaction is important biochemically to stabilise both folding of proteins between aromatic amino acids and to stabilise nucleic acid strands through stacking between pairs.[39] π stacking between two benzene molecules amounts to 10 kJ mol^{-1}, which is easily overcome and therefore only imparts a small amount of stability.[38] However, heteroatoms increase the stability and in the case of DNA the interaction can amount to 40-70 kJ mol^{-1} depending on the order of the bases, the strongest interaction being between guanine-cytosine stacks.[40]

Intercalating agents are able to form relatively stable reversible interactions with DNA by inserting between bases and stacking with the aromatic bases.[37] Many therapeutics already target this interaction, and many more are under development.[8, 34, 41-47] Some of these agents

are designed to function by stabilising the DNA-intercalator-topoisomerase II ternary complex that forms when the DNA replication process is hindered by intercalation.[8]

The degree of intercalation of these agents can be determined using viscosimetry measurements, wherein the viscosity of DNA can be measured before and after the addition of intercalating agents.[34, 36] This is because the intercalation disrupts the stacking and the result is a drop in the degree of rotation the DNA would normally undergo for that step of the DNA, essentially unwinding the DNA at each intercalated step. This results in a change of viscosity, and this combined with the concentrations of both DNA and intercalator can determine the intercalative ability, and therefore efficacy, of an intercalating drug candidate.[36]

1.3. Cisplatin

Cisplatin (Figure 1.2), or *cis*-diamminedichloridoplatinum(II), was discovered to be an anticancer agent thanks to electrochemical research performed on microorganisms.[48] Microorganisms elongated throughout the experiment due to their inability to replicate, and a platinum compound was found to be the cause.[49] Platinum electrodes were chosen due to their near-inert nature, however, trace amounts of platinum compounds including one with two ammonia and two chloride ligands. could be identified in the solution. The presence of the cisplatin complex was discovered to integral to causing the disrupted replication.[50] Interestingly, the *cis* isomer of diamminedichloridoplatinum(II) is active against cancer while the *trans* isomer is not. This is due to the mechanism by which cisplatin results in the induction of cell death.

Figure 1.2: ***Cis- and trans- platin (diamminedichloridoplatinum(II)).***

Cisplatin is sparingly soluble in aqueous environments due to the overall neutral charge, and it must be administered intravenously as the low solubility precludes absorption into the blood if taken orally.[9-10] The active forms of cisplatin are the aquation products that form upon entry to the cell – chloride ligands are displaced by ligand exchange for water, coordinating through the oxygen atom (Figure 1.3). The blood concentration of chloride ions is around 100 mM whereas the cellular concentration ranges from 3 to 20 mM, and the substantial drop in concentration makes the aquation of platinum more thermodynamically favourable.[30] This process is considered essential for the subsequent efficacy of cisplatin, as the aquation products $[Pt(Cl)(NH_3)_2(OH_2)]^+$ and $[Pt(NH_3)_2(OH_2)_2]^{2+}$ are now positively charged and attracted to the

negatively charged DNA backbone. These complexes are then able to react with the nitrogenous guanine and adenine bases of the DNA ladder.[30] The positive charge on the complex also makes it more soluble in the aqueous cell environment, increasing the bioavailability.[9]

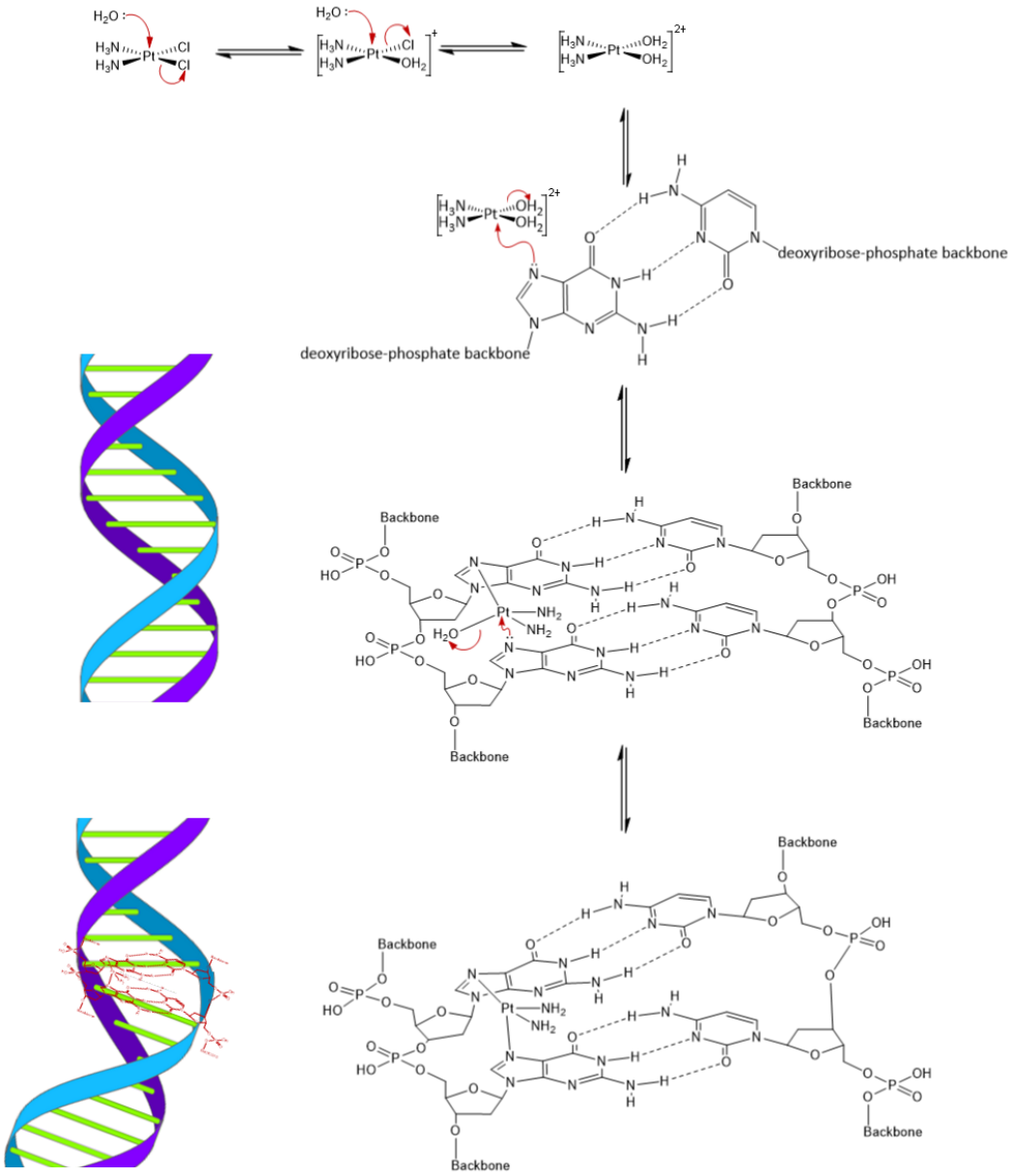

Figure 1.3: ***An example of cisplatin aquation to the diaqua product, and subsequent formation of the 1,2-intrastrand DNA adduct showing DNA deformation.***

Cisplatin is the active geometry of the complex due to its ability to form multiple kinds of intrastrand adducts to DNA, while *trans* can only make interstrand crosslinks. The adducts between adjacent guanine and/or adenine residues are the most efficient form of causing

cytotoxic DNA lesions, meaning the *trans* form is inactive as the geometry renders it incapable of forming such intrastrand crosslinks.[9, 51] Formation of the intrastrand crosslink results in cytotoxicity due to the formation of even larger DNA lesions, which consist of the DNA strand, the cisplatin adduct and various replicative machineries.[9] Enzymes such as helicase and topoisomerase that are involved in DNA replication or repair are inhibited by the lesion of the cisplatin DNA adduct, either through the direct action of cisplatin on the enzyme or due to the kinked nature of the DNA around the adduct, or a combination of the two.[9] Topoisomerase II is the enzyme responsible for relieving supercoiling in the DNA due to the process of unwinding by DNA helicase during replication. In order to perform their role, both enzymes move along the DNA double helix, helicase unwinding as it goes and topoisomerase II occasionally nicking the strand to allow the supercoiling to release before reforming the bond.[6] When encountering the cisplatin adduct, these enzymes are unable to move further along the strand, causing a DNA lesion to develop.[10] It has recently been deduced that topoisomerase II is also directly inhibited by cisplatin. Cisplatin in the adduct can bind to sulfur atoms in key residues of many proteins including topoisomerase, resulting in inhibition as it is no longer able to perform its catalytic activity.

Cisplatin within the adduct also interacts with other biomolecular targets in addition to DNA, including cell signalling caspases and High Mobility Group (HMG) proteins.[10, 51] HMG proteins compete with histones (the proteins that bind DNA to protect it while inactive after replication), preferentially binding single stranded DNA to prime and protect it in an optimised state for transcription. It has been found that HMG is able to bind to cisplatin adducts due to sulfur atoms of cysteine residues (Figure 1.4).[10] This allows the HMG protein to contribute to the formation of DNA lesions through direct interaction with cisplatin adducts. Interestingly, the HMG proteins have low binding affinity for transplatin.[9] It is also reasonable to propose that the HMG protein may be involved in delivering the cisplatin moiety to the DNA, by binding to cisplatin, associating with DNA, then allowing cisplatin to bind to the DNA. The reason why the HMG protein is able to associate with cisplatin even once cisplatin is already bound through two bonds to DNA is due to the 'softness' of the sulfur donor atom.[9] Platinum and sulfur are both soft atoms, whereas oxygen, nitrogen and even chloride are hard donor atoms. Despite the strong interaction of platinum with its nitrogen donor atoms from the DNA and ammonia ligands, sulfur atoms of the HMG cysteine residues are still able to displace a nitrogen to bind to the adduct, adding to the formation of the cytotoxic lesion. It has been shown that this interaction prevents the cell from being able to repair the adduct by removing cisplatin and is therefore important for the efficacy of the drug.[51]

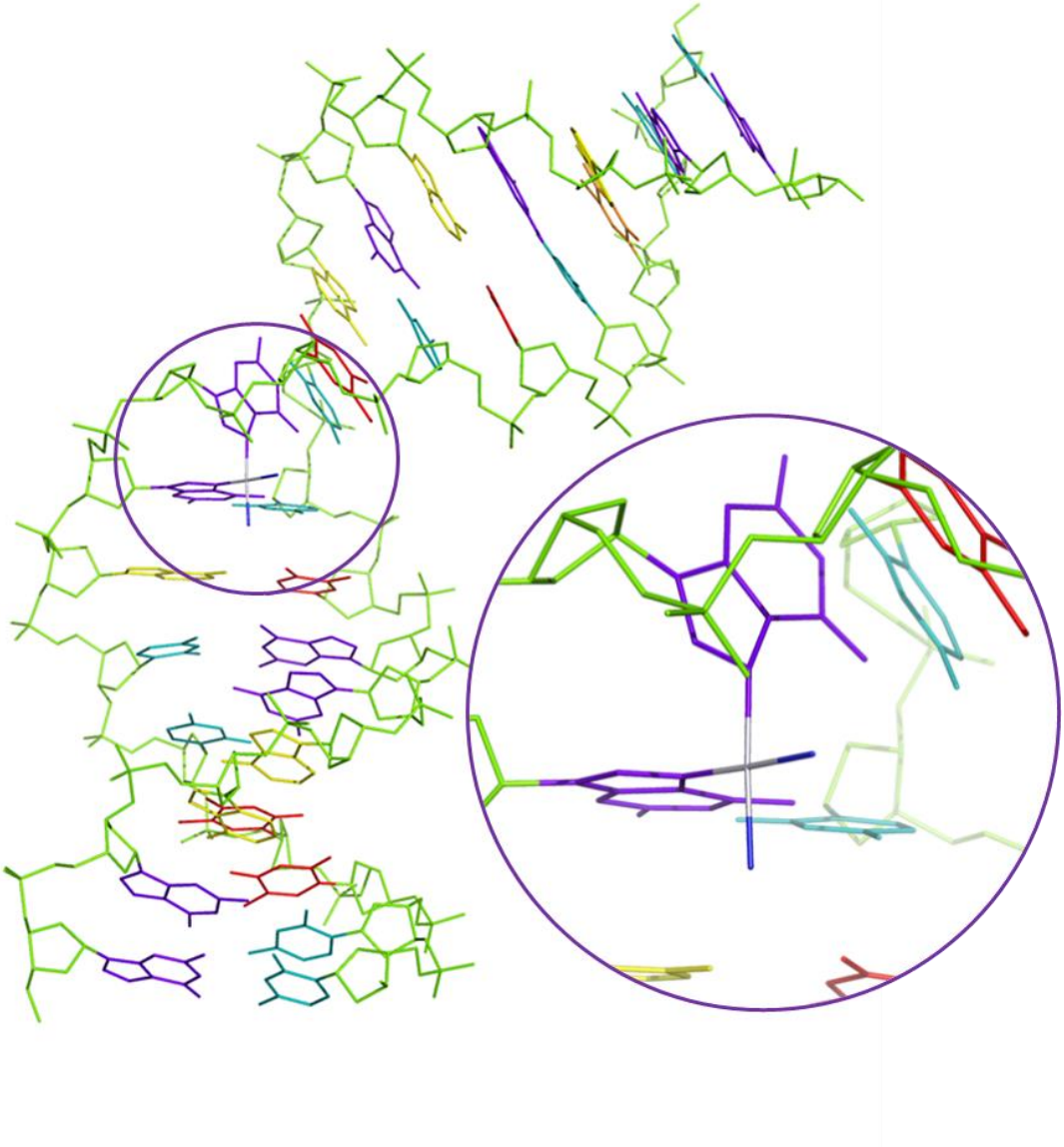

Figure 1.4: ***Crystal structure showing the DNA kink by movement of guanine residues out of alignment by cisplatin adduct formation. Note: platinum is shown silver, not burgundy, to differentiate it from the DNA strand.***

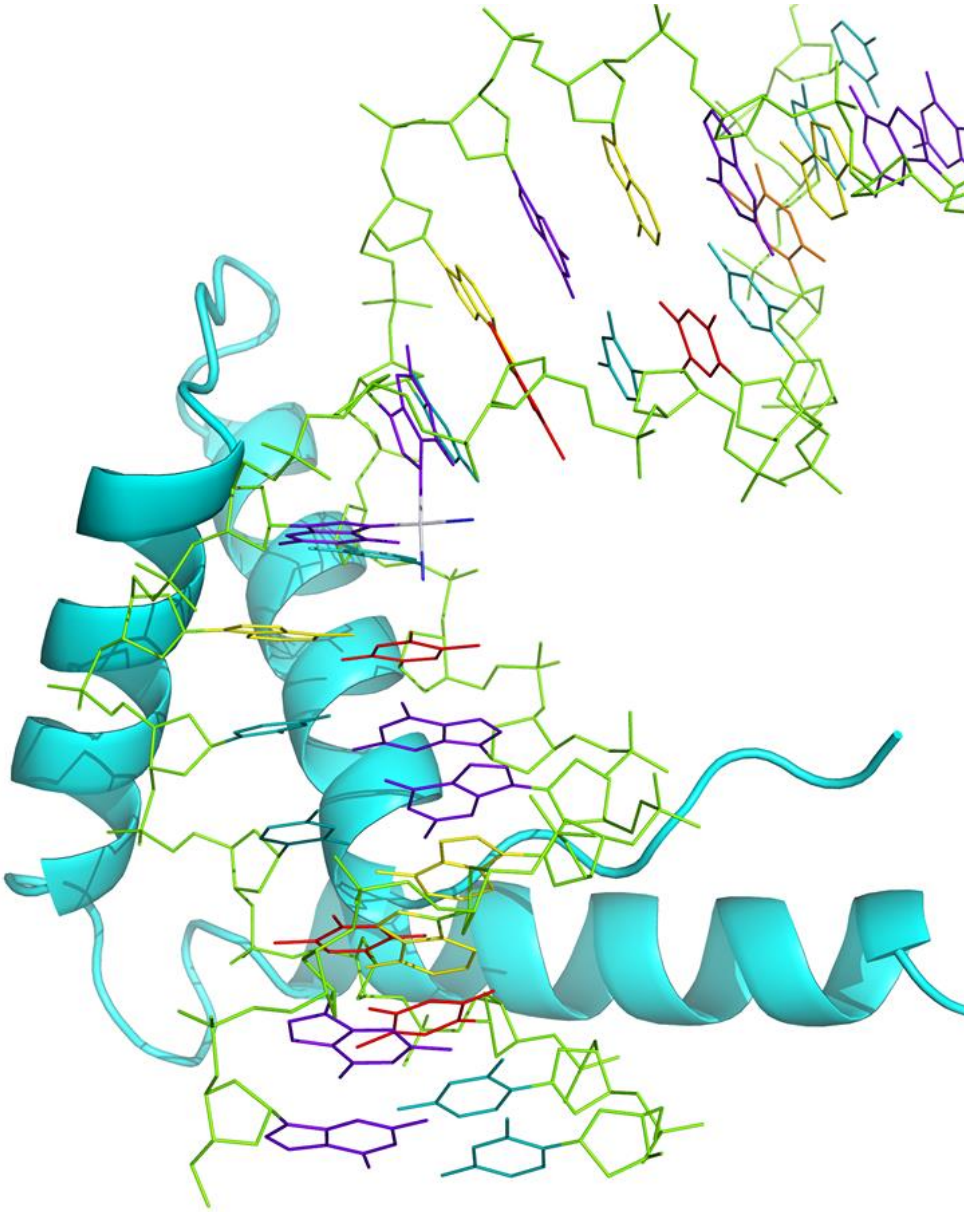

Figure 1.4 ***(continued): the same crystal structure showing the association of an HMG protein to the DNA adduct.***[51]

Cisplatin has also been implicated in cell death processes through interactions with other biomolecules. Cisplatin is known to interact with caspases and cyclins directly and indirectly through a complicated network of other proteins, resulting in the initiation of controlled cell death pathways.[9-10] Caspases are proteases generally responsible for regulating the induction and execution of apoptosis and have roles in the transduction of some phases in the cell cycle, whereas cyclins are primarily responsible for modulation of the cell cycle and signalling the transition between phases.[6] It has been shown that inhibition of caspase proteins prevents induction of apoptosis and arrests the cell cycle, preventing it from progressing.[7] Cisplatin is

involved in the activation of various initiator and executioner caspases[52]. Initiator caspases are involved in induction of apoptosis by activation of downstream caspases through the cascade of tumour necrosis factor through the FAS receptor, then procaspase-8 to cleave and therefore activate the downstream caspases.[7] These include the executioner caspases that are responsible for cleavage of various biomolecules, notably some DNA repair enzymes, an inhibitor that prevents DNA digesting caspases from acting, other nuclear proteins, and cytoskeletal proteins. Studies on various cell lines have shown that cisplatin treatment results in an increased presence of these caspases. The exact mechanism for this is not understood and is believed to be through direct binding to the caspases as addition of peptide caspase inhibitors precluded cisplatin induced activation, however, caspases have somewhat ambiguous binding sites making this difficult to confirm.[52] The combination of cisplatin activation of executioner caspases, reducing cellular levels of DNA repair machinery and initiator caspases to initiate apoptosis, contribute to the way cisplatin causes cell death.

These cisplatin mechanisms of apoptotic induction along with DNA binding are inherently selective for cancer cells, as cell death is primarily reliant on the cell entering the replicative phase of its cell cycle.[7] Cancer cells are known to replicate at a much greater rate on average than healthy cells, which spend as little as ten percent of their lifespan replicating.[5] In addition, cells have repair mechanisms to remove molecules bound to DNA to prevent cytotoxic effects.[5] As healthy cells replicate much less frequently than cancer cells, there is more opportunity for adducts to be found and removed before the cell begins replicating. Cancer cells are therefore more likely to be affected than healthy cells.

Unfortunately, despite this level of selectivity, healthy cells are still able to be affected by cisplatin treatment.[9, 11] Any cells that replicate quickly, including those involved in the production of stomach mucus and follicular cells, will be heavily impacted by treatment.[9, 11] This is responsible for the characteristic chemotherapy side effects from cisplatin; hair loss and digestive disorders including nausea.[53] Other detrimental effects have also been reported as a result of cisplatin therapies, including organ toxicity, resistance and secondary cancers.[9]

Cisplatin has been associated with specific organ toxicities that result in a lower applicable dose. Arguably, the most severe is the impact on kidneys – cisplatin accumulates in the kidneys due to excretory processes. Cisplatin is also associated with ototoxicity through apoptosis of auditory sensory cells, neuropathy and gastrointestinal toxicity.[9] The continued accumulation results in the death of cells in these systems, and the cisplatin induced apoptosis that is essential for cancer cell death also results in organ toxicity. Cisplatin must be used at a dose that is lower than

the dose at which toxicity is observed, but at a high enough dose to result in anticancer efficacy.[11] This impact is not unique to cisplatin - it affects all anticancer agents and poses a challenge that all new chemotherapeutics must overcome to enter clinical use.

Resistance to frontline drugs is also a major and developing issue in cancer treatment and has been observed in the cisplatin family of therapeutics.[9] Some forms of resistance are inherent due to an inability of the cancer cell to interact with cisplatin as expected, reducing its efficacy. An example of this is through slight mutation of caspases, which does not affect their standard activity but does prevent them from recognising cisplatin adducts and therefore prevents the cisplatin adduct from inducing apoptosis as expected.[9]

Other forms of resistance occur in an example of natural selection – cells that happen to produce a protein that reduces their susceptibility to cisplatin have a higher rate of survival than other cancer cells. These cells then reproduce, forming a tumour of resistant cells. An example of this can be seen through glutathione induced resistance.[9, 18-19, 21] Glutathione is a tripeptide (Glu-Cys-Gly) involved with maintenance of cell oxidation state through the equilibrium of glutathione with its dimerised form. The monomeric form of glutathione can act as an antioxidant and heavy metal binding agent, preventing damage from these species.[19] Thiol groups, such as the cysteine side chain, can act as reducing agents and react with oxidants in the cell. Two molecules of glutathione can be oxidised to form a dimer, donating an electron in the process to reverse oxidation processes in the cell.[18-19] This dimer can also be reduced back down to the monomeric form.[6] Glutathione is integral for maintaining cellular redox state through the ratio of free versus dimeric glutathione.[5] Cancer cells that are already higher in glutathione are able to develop resistance to cisplatin as the increased glutathione has been shown to reduce cytotoxicity of cisplatin.[18]

One of the proposed mechanisms involves increased efflux of cisplatin through xenobiotic transporters, many of which use glutathione as a substrate.[19] Glutathione-cisplatin conjugates have been observed in leukaemia cells – the thiol group of cysteine serves as an excellent ligand donor atom for soft metals, which is why glutathione is effective in removal of heavy metals.[19] A second route is through cytoprotection, as increased presence of mRNA associated with enzymes responsible for glutathione synthesis was found in cells exposed to cisplatin, however, a direct mechanism has not been elucidated to date.[19]

One way in which many of these detrimental and dose-limiting side effects can be overcome is through increased selectivity, whereby cisplatin can differentiate between healthy and cancerous cells for activity. This could allow the dosage used to be higher, potentially shortening

treatment times and thus reducing cost, both economic and emotional, of treatment. This could be achieved through coupling of cisplatin to a compound that has the ability to detect whether it is in a healthy or cancerous cell through exploitation of an innate physiological difference between the two. This project focusses on the use of cobalt to achieve this goal.

1.4. Cobalt

Cobalt is a transition metal of the first series with the electronic configuration $[Ar]4s^2 3d^7$. Cobalt exists predominantly in sulphide ores, and when mined from these ores it is often produced alongside nickel. As a transition metal, it has the ability to exist in multiple oxidation states based on the loss or gain of these 4s and 3d electrons.[54] The most common oxidation states are the 2+ state and the 3+ state, however, cobalt can exist in the 3-, 1-, 1+, 4+ and 5+ states in some rare compounds. The 2+ state occurs when the two 4s electrons are lost, and the 3+ state once a 3d electron is then also lost.[54]

An interesting feature of the 2+ and 3+ oxidation states is their vastly different labilities. Lability is defined as the speed at which the replacement of a ligand for another occurs.[54] Co^{2+} is labile, rapidly exchanging its ligands on the order of milliseconds whereas Co^{3+} is defined as inert, replacing its ligands very slowly on the timescale of minutes to hours.[54] In fact, many syntheses of Co^{3+} complexes take advantage of the higher lability of Co^{2+} by first synthesising the analogous Co^{2+} complex before oxidising it to Co^{3+}.[55] The difference in lability is related to the electronic structure of the ions in complex. As cobalt is an octahedral metal centre, ligand field theory suggests that lability is related to the occupation of the e_g orbitals - metal centres with occupied or partially occupied e_g orbitals are labile, whereas those with unoccupied e_g orbitals but full or near full t_{2g} orbitals are inert. This holds true for cobalt; Co^{2+} has seven 3d electrons, six in the t_{2g} orbitals and one in the e_g orbitals while Co^{3+} has six 3d electrons, all of which are in the t_{2g} orbitals.[54]

The ability to exist in these two oxidation states gives cobalt the ability to act as an agent to add selectivity to cisplatin. Co^{2+} complexes are labile and therefore easily exchange their ligands, whereas Co^{3+} complexes retain their ligands. The reduction from Co^{3+} to Co^{2+} could act as a targeted delivery system, utilizing this lability difference to allow for selective release of a cisplatin moiety in cancerous cells and not in healthy cells.[56] This could be done through exploitation of the inherent physiological difference in oxidation state between the two cells. A Co^{3+} complex of the cisplatin moiety would remain mostly intact in the homeostatic oxygenation state of a healthy cell, either remaining oxidised or experiencing rapid re-oxidation upon reduction. However, when it enters the hypoxic environment of some tumour cells, the cobalt

centre would be reduced to Co^{2+} and is not likely to be re-oxidised before it releases the active cisplatin agent.

1.5. Dinuclear Complexes

In order to use cobalt as a redox sensor for selective cisplatin release, the platinum and cobalt centres must be linked. These complexes are termed heterodinuclear as there are two centres that differ from each other linked through bridging ligands.[57-63] Dinuclear complexes in general were first extensively proposed by Werner and were based around the action of a metal centre in a coordination complex as a Lewis base and interacting with another metal as a Lewis acid.[63] This can occur due to coordinative unsaturation in the case of the coordinating metal, which iis observed in many examples of platinum dinuclear complexes.[63] Dinuclear complex formation can be encouraged using polydentate linear ligands. Indeed, many examples can be seen where a soft metal binds through the soft sulfur donor of ambidentate thiocyanate while a hard metal centre coordinates to the hard nitrogen donor atom.[63] Many of the first synthesised heterodinuclear complexes exploited this motif.[63] Complexation is also possible through direct metal-metal bonds, which is beyond the scope of this project.[63]

In many cases, it is favourable to form the dinuclear complex using complexes of each centre with the ligands intended to be used as bridging ligands. Stable dinuclear complexes of cobalt and platinum are already known, and hydroxide bridging ligands appear to favour formation.[62] Synthesis of the intended dinuclear complex should be attempted through synthesis of both the platinum and cobalt(III) complex with diaqua or aqua/hydroxide ligands before attempting to synthesise the dinuclear complex. This should also reduce the number of products formed as there are fewer combinations possible; whether a ligand leaves the cobalt or platinum coordination sphere to allow for complexation the result should be the same.

Aqua or hydroxide cobalt amine complexes are not usually synthesised directly, rather synthesised from a cobalt amine starting material that allows for replacement of ancillary ligands for the aqua or hydroxide ligands. There is a range of ancillary ligands that can be used to perform this function.

One of the ligands that can be displaced for aqua is nitrite, NO_2^-.[64] This ligand exchange reaction proceeds through protonation to the nitrite by acidification, resulting in NO^+ and OH^-.[65] The reaction produces the OH^- side product, and additional acid will be required to perform the ligand exchange as some will react with the nitrite ligand and some with the hydroxide produced. If the nitrite ligand is N bound (as is probable with cobalt (III) complexes), the reaction

mixture may change colours as the coordination sphere goes from having nitrogen to oxygen donor atoms. If the nitrite ligand is bound using the oxygen donor atom, the reaction progression may be difficult to track through colour alone. The solubility of the complex may also change as each nitrite ligand replaced with an aqua ligand will increase the charge on the complex by one.

Carbonate ligands are also able to be displaced through the reaction with acid.[64, 66] In this case, the carbonate is decomposed by the acid to form CO_2 and water. Again, two equivalents of acid will be required per carbonate, however, as the carbonate is bidentate this will likely require less acid for the overall process to occur than for the nitrite ligand. The carbonate binds through oxygen donor atom, as does the aqua ligand, therefore the colour change of the reaction is not likely to be useful in tracking reaction progression. The reaction produces gaseous CO_2, which is a useful indicator of the reaction progression as effervescence will be observed while the degradation of carbonate is still occurring. The charge will again change during the exchange, increasing by two for every carbonate displaced which may have an impact on the solubility of the complex. Carbonate has an additional benefit when used in this way in that it is a bidentate ligand. This means that when it is decomposed, two *cis* donor sites will be replaced with aqua ligands to produce the aqua complex.[67] This makes it more likely that the product formed will be the *cis* product, unless the other ligands allow for isomerisation. By contrast, the *trans* isomer would be possible for the nitrite complex. Carbonate complexes are often used in this manner to encourage *cis* aqua ligands as well as to reduce the number of isomers produced by the initial ligand exchange.[64]

In order to displace the intermediate ligand in favour of an aqua ligand, which is a poor ligand that is easily displaced, an acid with a sufficiently non-coordinating conjugate base must be used to prevent complexation of the conjugate base instead of the aqua ligand. Triflic acid can be also be used – the triflate anion may coordinate to the vacant donor sites yet is sufficiently labile that is can be replaced with an aqua ligand either following isolation of the triflate species or by performing the reaction under aqueous conditions.[64, 68]

Halide ligands can also be displaced in favour of aqua ligands in transition metal complexes.[62] As opposed to treatment with acid, this ligand exchange is usually performed using silver. The silver addition results in precipitation of the insoluble silver halide salt, and the halide ligand is replaced by an aqua ligand. This process is also dependent on the use of silver salts with non-coordinating anions. Generally, silver perchlorate is used as the perchlorate anion is a poor

ligand. Silver nitrate can be used for this purpose, due to the potential for perchlorates to form explosive compounds, but the nitrate anion is a ligand, albeit a poor one.

1.6. Rationale behind Ligand Design

The dinuclear motif has been synthesised by a previous student working in the Hartshorn group (Figure 1.5).[62] This was achieved using polydentate amine or polycarboxylate ligands, with a hydroxide ligand and an aqua ligand to create the cobalt(III) and platinum centres. These centres could then be reacted to synthesise the dinuclear complex.[62] Unfortunately, the resulting complexes were either unable to be isolated due to high solubility (Compounds 1.5.1, 1.5.2, 1.5.3, 1.5.4 below), or unable to be fully characterised due to their very low solubility (Compounds 1.5.5, 1.5.6, 1.5.7 below) (Figure 1.5). The latter compounds were insoluble in all solvents attempted barring dimethyl sulfoxide (DMSO), which resulted in reaction. The sulfur atom of DMSO provides a soft donor atom that can interact with the soft platinum centre.[62] As the platinum centre is square planar, it can undergo associative ligand substitution.[54] Associative substitution occurs through the new ligand binding to the metal centre before the outgoing ligand leaves. As this mechanism occurs through a higher coordinative intermediate, it is favoured by geometries with lower coordination numbers, including square planar.[54] In this manner DMSO can interact with the platinum centre through an associative mechanism and result in decomposition of the dinuclear complex.

These unintended interactions are predominantly possible due to the square planar geometry of platinum centre encouraging associative ligand exchange and the subsequent degradation of the dinuclear complex. To overcome this issue, this research focusses on surrounding the platinum centre with pendant groups to physically hinder this process. These groups should be attached to the cobalt centre to prevent loss of cisplatin functionality (so this functionality can be restored once released from the cobalt centre) and should be sufficiently large to prevent interaction of the platinum centre with the surroundings. Ideally, the pendant should contain only functional groups with poor coordinative ability to prevent them coordinating the platinum centre.

The proposed motif (Figure 1.6) involves using naphthalimide groups to perform this role, attached to a polyamine ligand coordinated to the cobalt centre. The naphthalimide candidate fulfils the requirements of the pendant group and may also have the additional benefit of their own potential anticancer efficacy as an intercalator, making this a potentially double pronged therapeutic (Figure 1.7, also see Section 1.7).

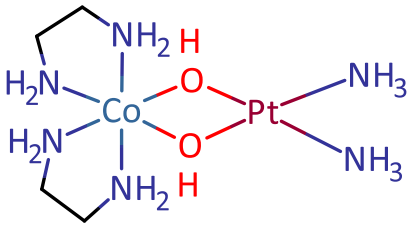

1.5.1

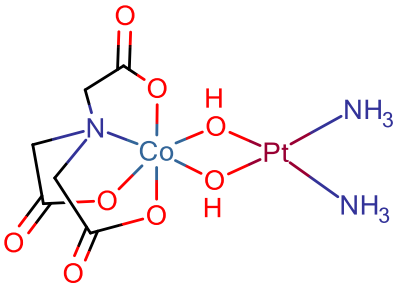

1.5.5

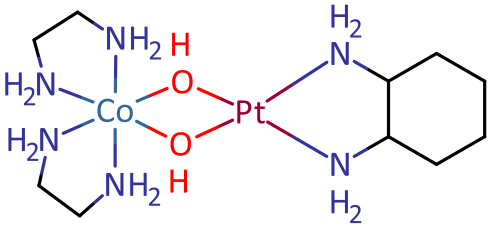

1.5.2

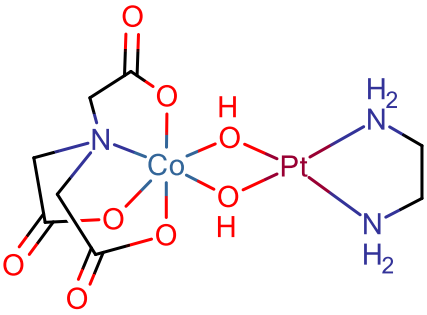

1.5.6

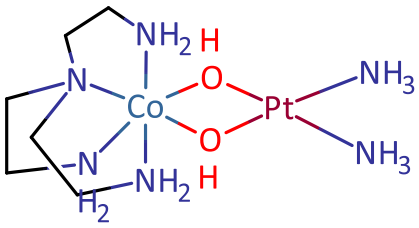

1.5.3

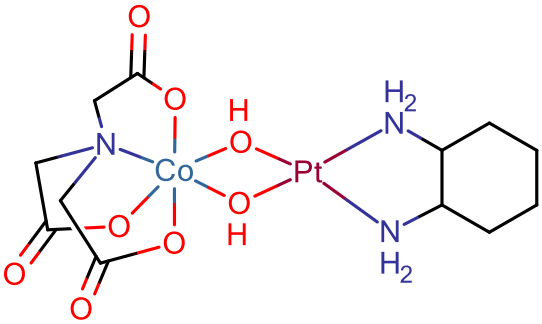

1.5.7

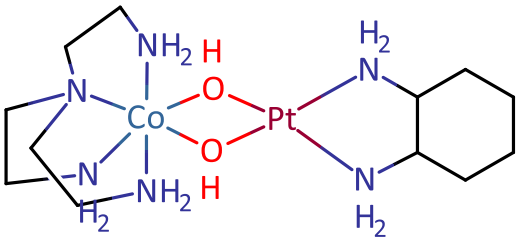

1.5.4

Figure 1.5*: 3+ Charged (1.5.1, 1.5.2, 1.5.3, 1.5.4) and neutral (1.5.5, 1.5.6, 1.5.7) complexes synthesised by a previous student working in the Hartshorn group[62]. 1.5.1, 1.5.2, 1.5.3 and 1.5.4 were too soluble for complete isolation and characterisation, whereas 1.5.5, 1.5.6 and 1.5.7 were too insoluble or reacted.*

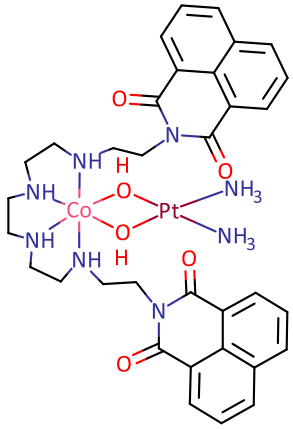

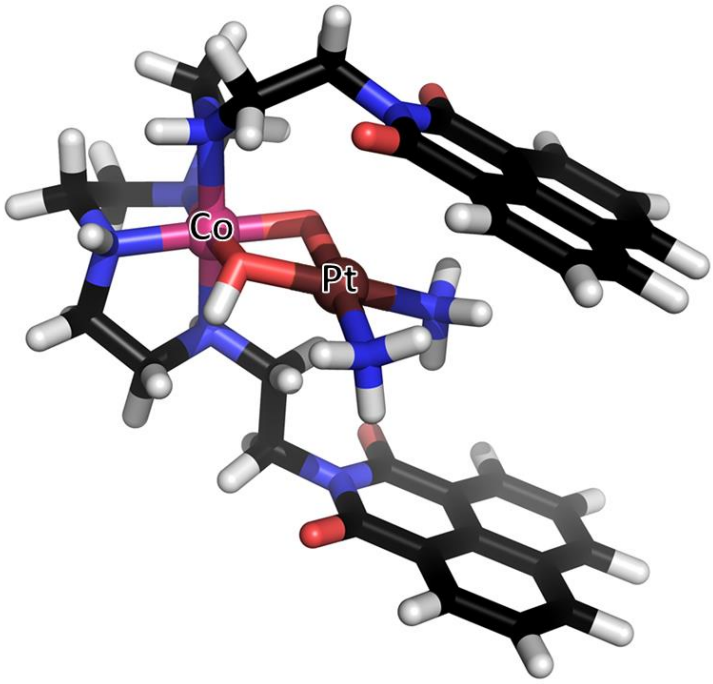

Dinuclear compound of cobalt (III) and platinum (II) – proposal

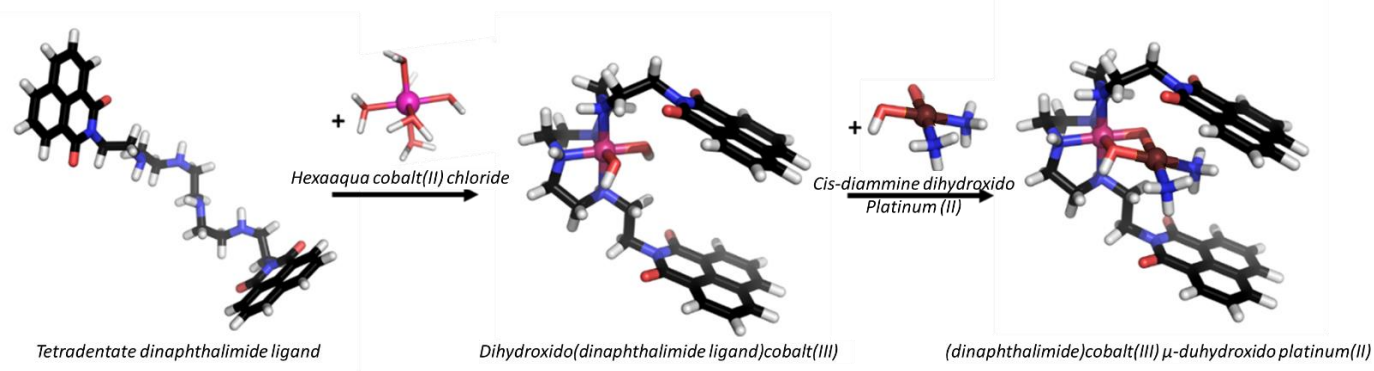

Proposed simplified synthetic pathway to the dinuclear complex

Figure 1.6: ***Proposed dinuclear motif coordinating cobalt(III) to platinum(II) through hydroxido bridging ligands, with pendants to prevent associative ligand exchange at the platinum centre.***

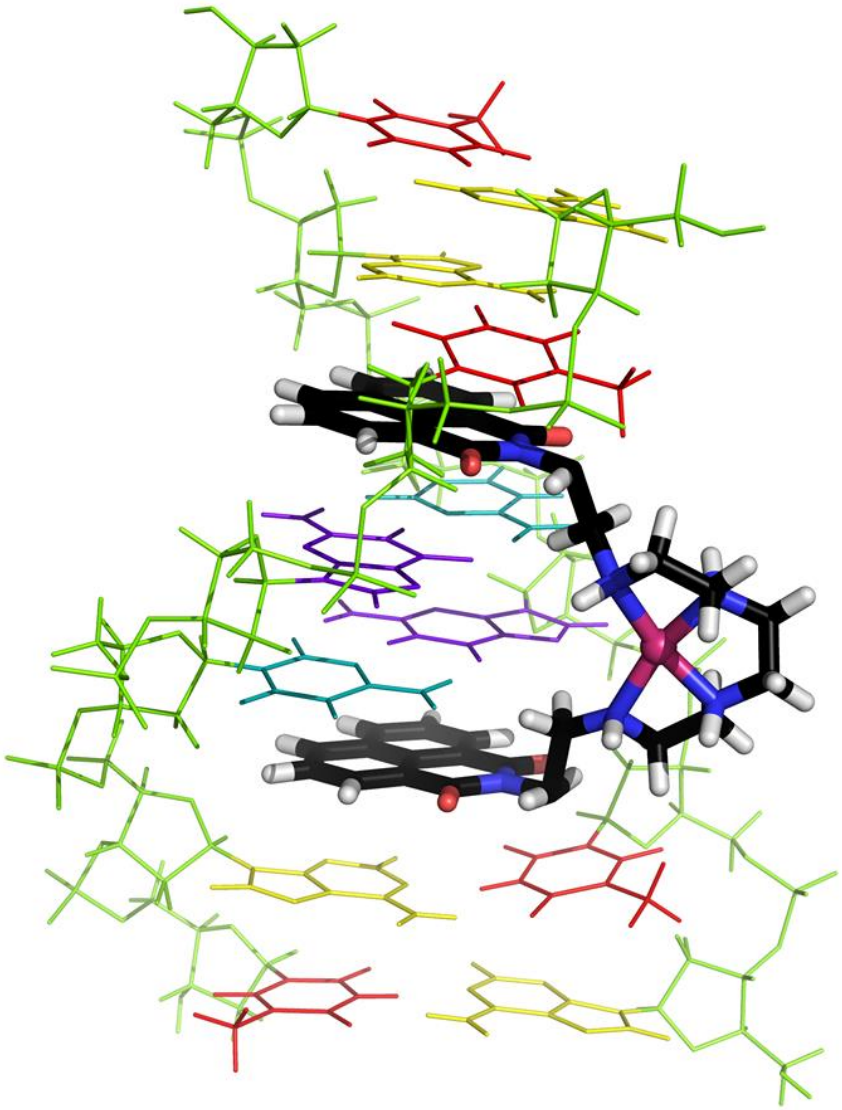

Figure 1.7: ***Rendered proposal of the cobalt centre intercalation. An existing crystal structure of a bisnaphthalimide intercalating DNA has here been modified to show the potential for the cobalt complex to coordinate.***

In order to synthesise this ligand motif, primary amines and naphthalic anhydride are reacted together to form an imide between the terminal amine and the anhydride functionality.[8, 34, 43-44] The primary amine of the starting material acts as a nucleophile on the slightly electrophilic carbon of the anhydride. This process results in the loss of water. The resulting secondary amide then reacts further to form an imide.

1.7. Naphthalimide Antitumoural Agents

The first naphthalimide therapeutic to enter clinical trials was mitonafide, a 3-nitro substituted naphthalimide synthesised by Braña *et al* (Figure 1.8).[34, 42, 69-70] The design was chosen to implement the features observed in many intercalating agents, including the naphthalene moiety and the alkyl chain.[42] It was found that the efficacy of the mitonafide motif was indeed based on its ability to act as a DNA intercalating agent through the naphthalene, which made it potent against many strains of cancer cells tested, and that the basic headgroup was essential for cytotoxicity despite lack of clear mechanism[42]. Unfortunately, the central nervous system toxicity of mitonafide in stage I precluded its use as the dose required for efficacy was too close to the dose at which toxicity occurred.[8, 70]

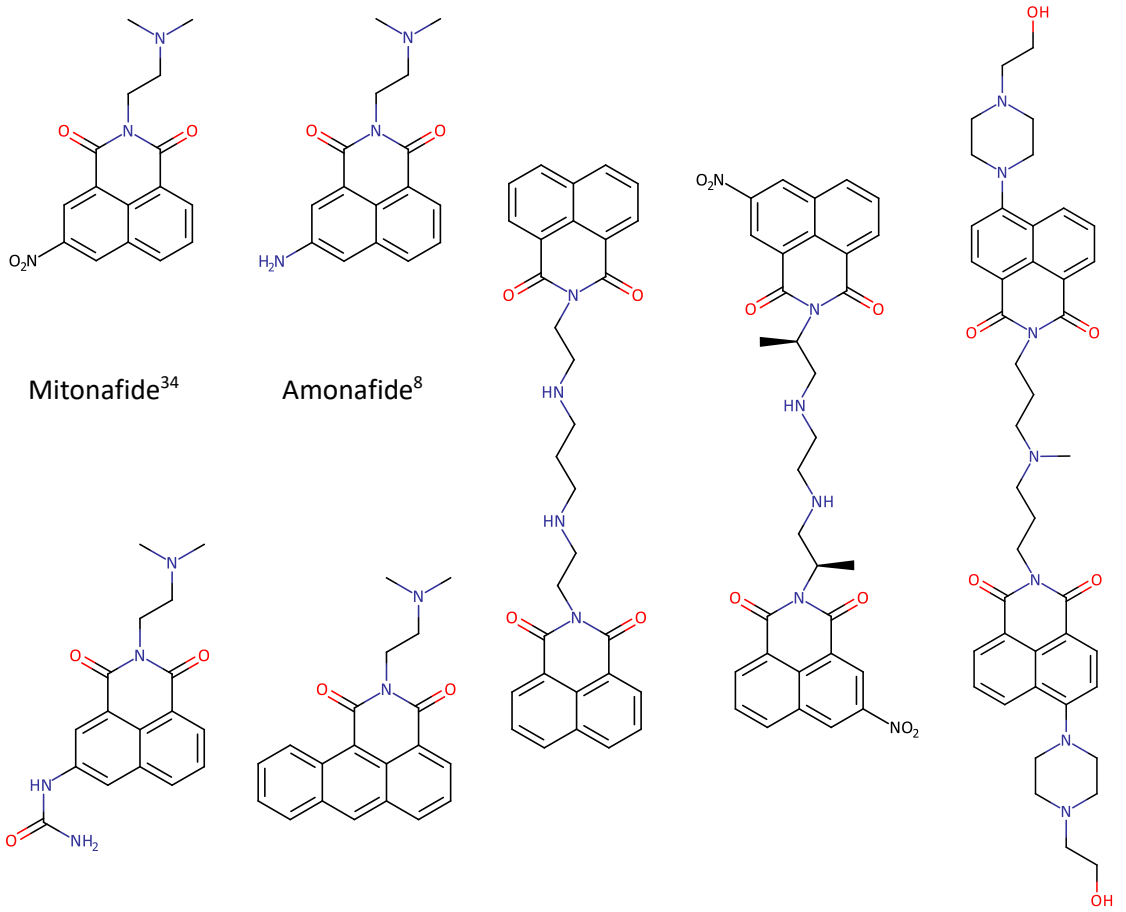

Figure 1.8: ***The structures of various naphthalimide based drug candidates.***

Amonafide quickly followed in an array of mitonafide derivatives synthesised by the Braña group, designed to reduce the toxicity.[43] The nitro group was identified as a key for DNA binding efficacy, but was also implicated in the neurotoxicity.[69] Derivatives of this functionality were key

for exploration. Amonafide differs from mitonafide by reduction of the 3-nitro group to an amine.[43] Clinical trials performed on this derivative were advanced to phase II, however, the neurotoxicity and haematoxicity precluded it from proceeding further.[73]

Following these mononapthalimides, the Braña group synthesised elinafide, a bisnaphthalimide.[44] This motif was chosen to increase the efficacy of the therapeutics thus decreasing the required dose. This can be seen in other bisintercalative molecules including ruthenium complexes with the ability to introduce strand breaks and similar aromatic anthracene derivatives.[74] The elinafide compound synthesised was discovered to intercalate along the major groove in a sequence specific manner, induce DNA strand breaks and inhibit topoisomerase.[8] Bisintercalation was confirmed through viscosity studies, showing the extent of DNA unwinding corresponded to bisintercalation rather than monointercalation.[33] Interestingly, the lack of substitution on the naphthalene moiety did not inhibit the cytotoxicity of the compound as it was the most cytotoxic of the compounds tested.[8] Elinafide has subsequently passed phase I clinical trials and entered phase II.[43]

Following the success of the naphthalimide motif, many other experimental candidates including azonafide, UNBS5162 and bisnafide have been developed as potential chemotherapeutics.[8, 72-73] In this way, the use of the dinaphthalimide ligand proposed in this study to act as a blocking group on the platinum centre may also provide a second therapeutic approach for the prodrug. Steric hindrance would likely prevent intercalation of the naphthalimide groups prior to platinum dissociation, making the dinaphthalimide group a secondary benefit of the redox sensitive prodrug candidate.

Another possible area of investigation that is relevant to explore is the solubility of the target. Previous work around the heterodinuclear system exposed issues in the purification of the compound due to solubility.[62] One way to overcome this issue would be to add substituent groups, for example nitrite or sulfite, to the aromatic moiety. Adding a polar or charged group may preclude the intercalative ability of the aromatic group, however, other charged and polar intercalators are known including ethidium bromide and berberine, as well as mitonafide above.[75]

Chapter 2: *Crude Ligand Synthesis and Attempted Purification by Complexation to Copper*

2.1. Introduction

As described in Chapter One, the tetradentate naphthalimide ligand **2.1** (Figure 2.1) was designed combining two rationale – the ability to hinder associative exchange on platinum centre of the heterodinuclear motif, and the similarity to existing anticancer agents. The pendant motif was chosen to physically block associative ligand exchange and redox chemistry on the platinum centre while still leaving the cobalt centre available to interact with the surroundings. This is important as the redox sensitive release of the cisplatin moiety relies on reduction of the cobalt centre, and synthesis of the heterodinuclear complex also relies on interaction of the platinum with the cobalt coordination sphere.

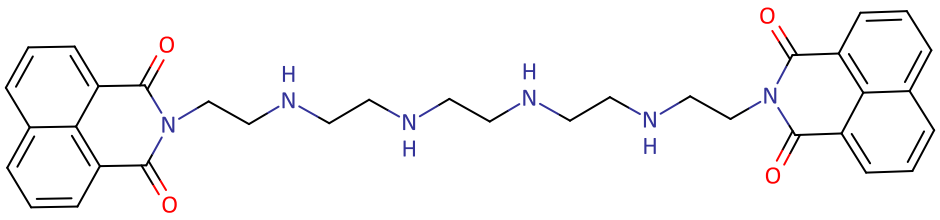

2.1

Figure 2.1: Compound 2.1 ***The desired compound, a dinaphthalimide based on the linear hexamine***

It is important to its fitness for purpose that the ligand contain these blocking pendant groups, with the pendants extending past the cobalt centre to block the platinum centre. The rest of the ligand should wrap around the cobalt and leave the cobalt as unhindered as possible. In order to coordinate to the cobalt centre, amines were chosen due to their well-known ability to form cobalt complexes.

The pendants themselves would potentially reduce the probability of ligand coordination due to their low solubility in polar solvents and the potential steric interactions of these large groups while the ligand is wrapping around the metal centre. To compensate for this the ligand was designed to contain multiple donor atoms to allow the chelate effect to encourage the coordination. To further enhance complex stability, the nitrogen donor atoms would be separated by two or three atoms to form five or six membered chelate rings once coordinated. The orientation of the ligand pendants with respect to the metal centres is itself critical to the function of the heterodinuclear compound. In order to encourage the pendants to be oriented

around the platinum centre, the ligand is designed to leave two 'vacant' coordination sites on the cobalt for later complexation to the platinum centre between the pendants. Additionally, the ligand should be able to be synthesised from common reagents in as few steps as possible.

To fulfil all these requirements, the ligand design used in this project was chosen, as shown in compound **2.1**. To give a tetradentate ligand with five membered chelate rings, 3,6,9,12-tetraazatetradecane-1,14-diamine (pentaethylenehexamine) was chosen. This amine is used industrially as well as in coordination chemistry as a hexadentate ligand directly. To form the pendants 1,8-naphthalic anhydride was chosen due to the accessibility of the material and the ease of which it can be reacted with amines to form imides. The resulting imide motif resembles existing therapeutics, opening up the prospect of a secondary therapeutic affect as described previously in Section 1.6.

This chapter describes the attempted to synthesise a tetradentate, dinaphthalimide ligand based on 3,6,9,12-tetraazatetradecane-1,14-diamine, and the subsequent attempts to enrich the samples of the target compound, **2.1**, through complexation and separation of the complex.

2.2. Experimental

2.2.1. General Procedures

All reagents were used as received, unless otherwise stated. 3,6,9,12-Tetraazatetradecane-1,14-diamine was purchased technical grade, with a specified purity of 31-32.5%. Solvents were evaporated under reduced pressure at 40-60 °C using a rotary evaporator. Silica column chromatography was performed under gravity using silica gel (Fluorochem Silica LC 60 Å) as the stationary phase and HPLC grade solvents as eluent. Reactions were monitored by thin layer chromatography where possible. TLC was performed on plastic sheets pre-coated with silica gel. The plates were visualised by the quenching of UV fluorescence and/or by staining with a ceric ammonium nitrate solution dip followed by heating with a heat gun. Melting points were obtained using samples isolated after purification without further recrystallisation.

2.2.2. Ion Exchange Chromatography

To separate crude metal complexes based on charge, ion exchange chromatography was performed under gravity using DOWEX® and Sephadex® ion exchange resins. The resins were prepared following the manufacturer's instructions and packed into glass columns. More details can be found under the relevant sections (Section 2.2.6.5, Appendix B.5).

2.2.3. Nuclear Magnetic Resonance Studies

Proton magnetic resonance spectra (^{1}H NMR) and carbon magnetic resonance spectra (^{13}C NMR) were recorded at 400 MHz or 600 MHz and 101 MHz or 151 MHz respectively and were recorded on a JEOL JNM-ECZ400S 400 MHz spectrometer with ASC64 autosampler, Agilent 400MR with Varian 7600-AS auto-sampler or JEOL JNM-ECZ600R 600 MHz spectrometer NMR equipped with an ASC30 auto-sampler. NMR samples were run primarily using 5 mm NMR tubes due to the low solubility of the compounds. D6-DMSO, $CDCl_3$, CD_3OD, 1:1 $CDCl_3$:CD_3OD and 1:1 D_2O:CD_3CN solvent systems were used, as described in the relevant experimental sections. ^{1}H and ^{13}C spectra were collected under standard conditions. Chemical shifts (δ) were reported in parts per million (ppm) and referenced to the residual solvent peak. NMR signals are described by multiplicity as singlet (s), doublet (d), triplet (t) or multiplet (m). Coupling constants (J) are quoted in Hertz to the nearest 0.1 Hz where feasible.

2.2.4. Mass Spectrometry Studies

Mass spectrometry was performed generally using a mixture of acetonitrile and water 1:1, made up into a bottle and regularly 'blank' tested for residual signals. To prepare the samples, a small amount of solid or a drop of the reaction mixture was taken into a vial and diluted through addition of 1-1.5 mL of the acetonitrile and water mixture. For dilute samples (which was defined here as samples taken directly from a reaction liquor or following elution from a column), one drop of this was used directly and added in to 1-1.5 mL of the acetonitrile and water mixture in a septum capped vial. For solids and concentrated solutions (such as those formed during *in vacuo* concentration), the diluted sample was diluted further by taking one drop and adding 1 mL of the acetonitrile water mixture. One drop of the resulting solution was added to a septum vial containing 1-1.5 mL of the acetonitrile and water solvent mixture.

Mass spectra were recorded by Dr. Marie Squire or Dr. Amanda Inglis on a BrukerMaXis4G spectrometer. The instrument was operated in a high-resolution positive ion electron spray mode, except for selected samples that were run in negative ion mode if an anionic product was probable.

2.2.5. Infrared Spectroscopy Studies

Infrared spectroscopy was performed using a Bruker FTIR spectrometer equipped with Alpha's Platinum ATR single reflection diamond and analysed using the OPUS software. Only significant absorptions outside of the fingerprint region are reported in wavenumbers with the following terms to describe intensity: w (weak), m (medium), s (strong), br (broad) or a combination of these terms.

2.2.6. Ligand Synthesis and purification by complexation

The following flowchart (Figure 2.2) is a pictorial representation of the procedure followed during the synthesis and purification by complexation experiments.

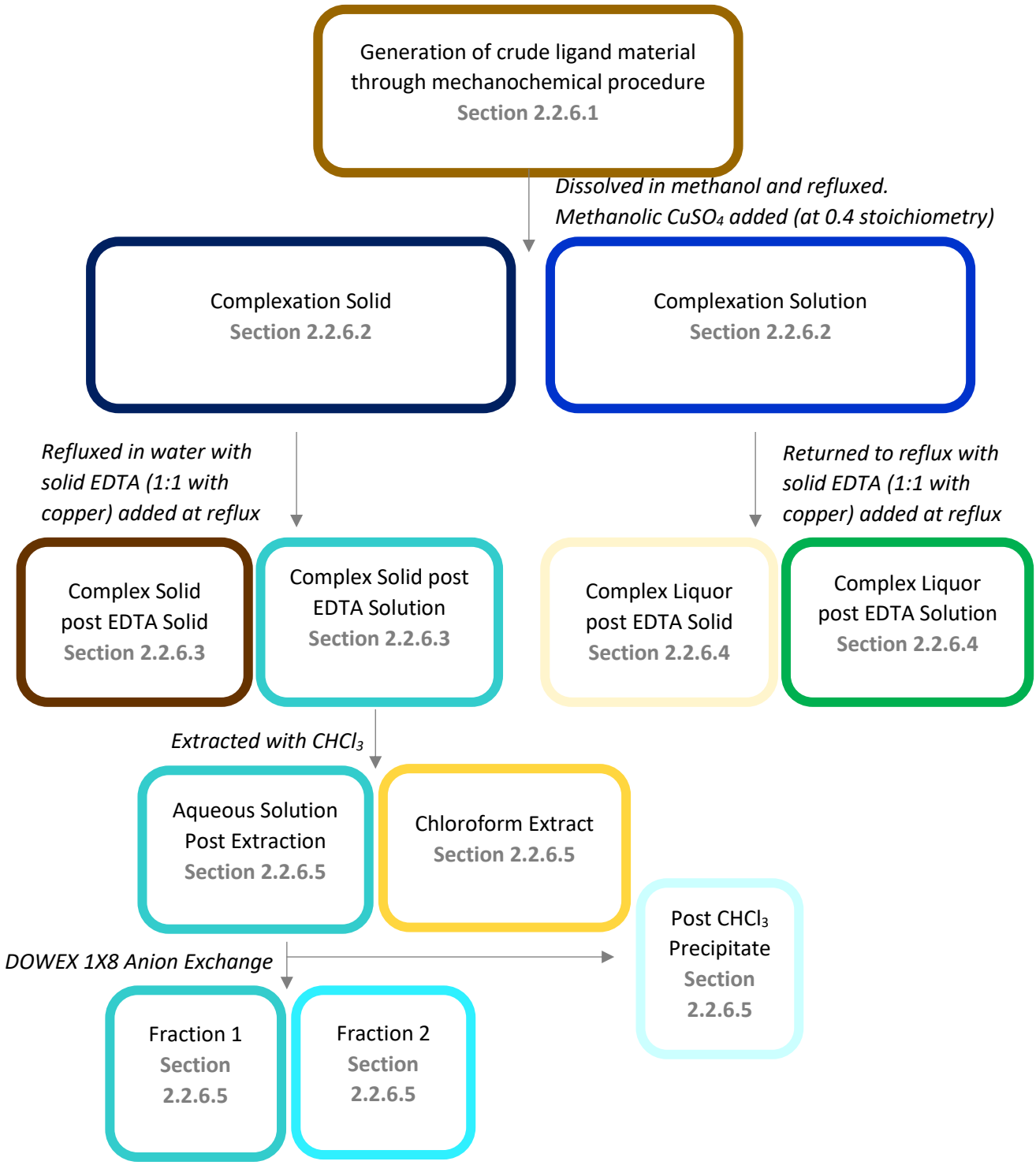

Figure 2.2: ***Flowchart depicting the purification by complexation followed, with each box representing a fraction or phase of a reaction. The methods section outlines the procedures followed to transition between the different fractions, which are labelled by the section number of the method to produce them. The colours used indicate the approximate colour of that reaction fraction.***

2.2.6.1. Ligand Synthesis

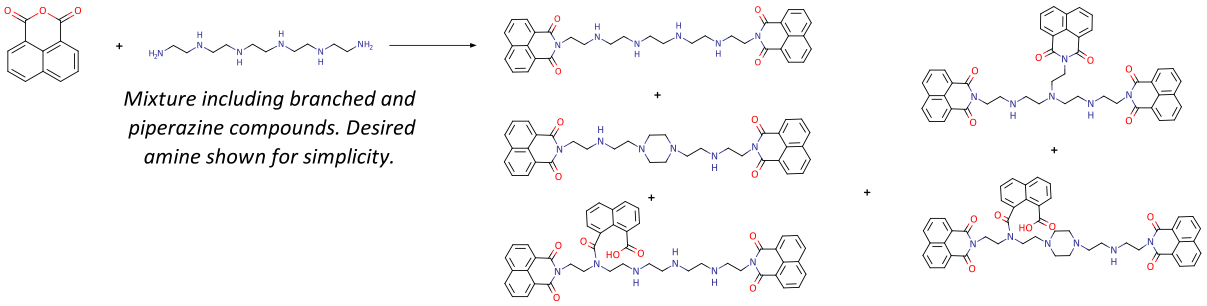

1,8-naphthalic anhydride ($C_{12}H_6O_3$ 30 g, 151 mmol) was placed in a 15 cm mortar and ground with a pestle until a fine powder was achieved. Chloroform ($CHCl_3$, 50 mL) was then added to the mortar and mixed with the anhydride to give a paste. To this, 3,6,9,12-tetraazatetradecane-1,14-diamine ($C_{10}H_{28}N_6$, 12 mL, 49 mmol) was added in a single addition and the mixture was ground for ten minutes. During this time, the mixture went from a pale beige paste to a very sticky brown then to a crumbly pale brown solid as grinding continued. Grinding ceased once the mixture became a fine pale brown powder (59.1 g).

^{1}H NMR ($CDCl_3$, 400 MHz) δ: 8.45 ppm (4H, dd, ArCH), 8.15 (4H, dd, ArCH), 7.70 (4H, ddd, ArCH), 4.25 (4H, t, CH_2 proximal to imide), 2.95 (4H, t, CH_2), 2.80 (4H, t, CH_2), 2.70 (8H, m, CH_2).

^{13}C NMR ($CDCl_3$, 151 MHz) δ: 164 ppm, 134, 131, 125, 122, 54, 51, 50, 48, 40.

Mass: 297.1478 2+ (Predicted 297.1477 for $C_{34}H_{38}N_6O_4$), 593.2884 1+ (predicted 593.2876 1+ for $C_{34}H_{37}N_6O_4$). 297.1478 2+ was one of the major peaks.

IR: 3381 cm^{-1} (m, br), 3230 (m, br), 1694 (m), 1650 (s), 1621 (m), 1587 (s), 1513 (w), 1439 (m), 1375 (m), 1346 (s, br), 1237 (s), 1202 (m), 1173 (w), 1074 (m, br).

2.2.6.2. Complexation to Copper

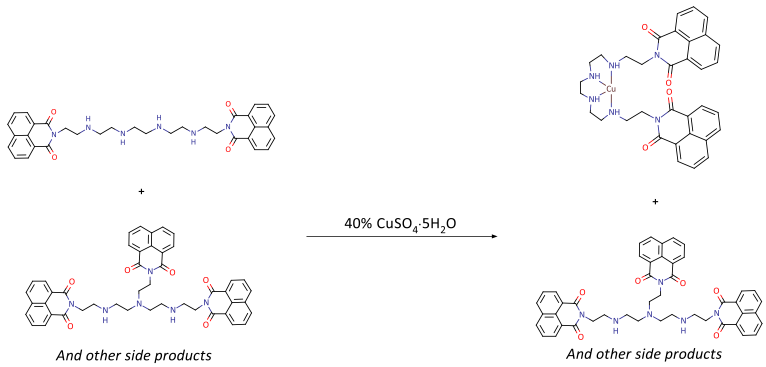

Crude ligand material (59.1 g) was placed in a 1 L round bottom flask. Methanol (500 mL) was then added with stirring. The flask was fitted with a condenser and heated at reflux on a hot plate stirrer with constant stirring. Once the reaction mixture was at reflux, copper sulfate

($CuSO_4 \cdot 5H_2O$, 9.95 g, 40 mmol) dissolved in warm methanol (200 mL) was added dropwise down the condenser. The reaction mixture gradually became blue with formation of a blue solid. The reaction mixture was heated at reflux with stirring for 3 hours. After cooling, the clear blue solution was decanted and the oily blue solid produced was washed twice with minimal methanol (less than 10 mL each) and the washings combined with the decanted solution. The methanolic liquor was refrigerated overnight and the liquid decanted off the blue oil that formed. The blue oil was combined with the solid remaining in the reaction vessel from the previous step. The solids and the reaction liquor were then characterised by ESI-MS (Table 2.3, Table 2.5, Table 2.15) and treated separately for the following steps.

2.2.6.3. Treatment of the solid material from the reaction of copper with crude ligand material

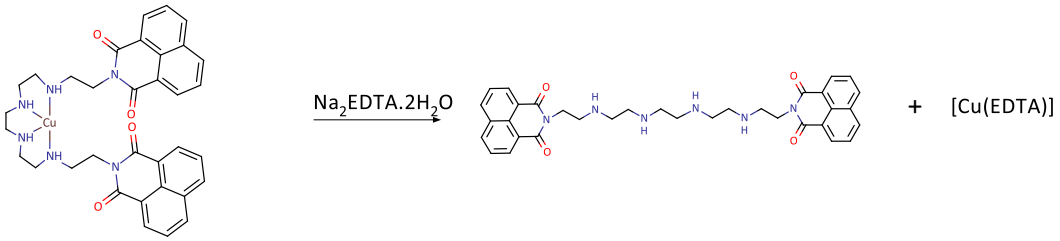

Water (700 mL) was added to the oily blue solid in the reaction vessel and this solution was brought to reflux. Disodium EDTA ($Na_2C_{10}H_{14}N_2O_8 \cdot 2H_2O$, 14.87 g 44 mmol) was added as a solid through the neck over the course of two minutes in five roughly equal portions, with the solid residue on the neck of the flask from the addition washed into the solution using five mL of water. This mixture was heated at reflux for a further three hours. The cool reaction mixture was filtered to separate the brown oil produced from the turquoise solution. The oil and the reaction solution were then characterised by ESI-MS (See Table 2.15).

2.2.6.4. Treatment of the reaction liquor from the reaction of copper with crude ligand material

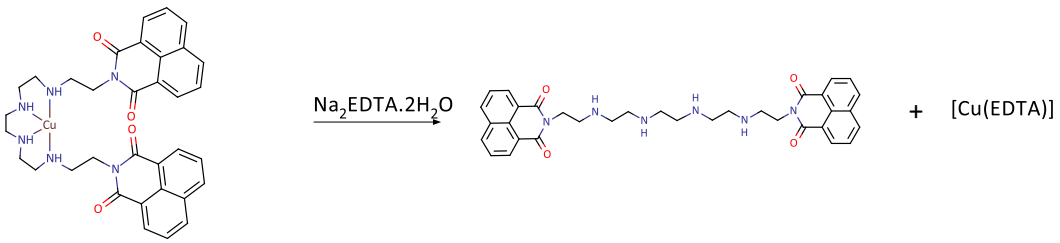

The liquor was treated with EDTA by returning the methanolic solution (~700 mL) to reflux followed by gradual addition of the solid disodium EDTA ($Na_2C_{10}H_{14}N_2O_8 \cdot 2H_2O$, 14.87 g, 44 mmol). EDTA was added over the course of two minutes in five roughly equal portions, with the solid residue on the neck of the flask from the addition washed into the solution using five mL of

methanol. This reaction was heated at reflux overnight before the reaction material was filtered to separate the resulting white powder and brownish oil from the green solution. The solids and the reaction liquor were then characterised by ESI-MS (See Table 2.15).

2.2.6.5. Treatment of the Turquoise Solution Post EDTA

The solution from the solid EDTA treatment step (Section 2.2.6.3) was taken and extracted six times with 100-150 mL of chloroform. Approximately half of the aqueous phase (~350 mL) was then run through DOWEX 1X8 resin in the chloride form to separate neutral and charged species by cation exchange. The sample was brought to pH 7-8 and loaded onto a 10 cm long 5 cm diameter column directly. The first fraction was eluted using 2 L of distilled water, giving a pale turquoise solution. The bright blue band that remained on the column was then eluted using 0.25 M NaCl solution followed by 1 M NaCl solution to ensure complete elution.

Following this, the second half of the aqueous phase was reduced to half the total volume, removing any residual chloroform, and then diluted back to twice the reaction volume in order to load it onto the column. During this process, a very pale blue precipitate formed and was collected by filtration. This precipitate was then dried under vacuum and used for subsequent reactions (0.50 g, used in Sections 3.2.2 and 3.2.5). The column fractions and the precipitate were then analysed by ESI-MS (See Table 2.15).

2.3. Results

2.3.1. Crude Material

Table 2.1: ***Crude Ligand Material ESI-MS results. Desired compound is listed first.***

Identity	m/z	Predicted m/z	Relative Intensity of reaction in Section				
			Appendix B1	Appendix B2	Appendix B3	Appendix B5	2.3.2
[**2.1**+2H$^+$] 2+	297.1472 2+	297.1477 2+ for $C_{34}H_{38}N_6O_4$	1.0	0.89	1.0	0.20	1.0
[**2.1**+1H$^+$] 1+	593.2865 1+	593.2876 1+ for $C_{34}H_{37}N_6O_4$					
[**2.4**+2H$^+$] 2+	310.1549 2+	310.1556 2+ for $C_{36}H_{40}N_6O_4$	0.68	1.0	0.93	0.19	0.90
[**2.4**+1H$^+$] 1+	619.3045	619.3033 2+ for $C_{36}H_{39}N_6O_4$					
[**2.3**+2H$^+$] 2+	387.1572 2+	387.1583 2+ for $C_{46}H_{42}N_6O_6$	0.49	0.47	0.71	0.41	0.46
[**2.3**+1H$^+$] 1+	773.3104 1+	773.3088 1+ for $C_{46}H_{41}N_6O_6$					
[**2.5**+2H$^+$] 2+	396.1623 2+	396.1636 2+ for $C_{46}H_{44}N_6O_7$	0.26	0.92	0.77	0.26	0.29
[**2.20**+2H$^+$] 2+	408.6780 2+	408.6794 2+ for $C_{48}H_{47}N_7O_6$	0.23		0.37	0.13	0.17
[**2.19**+2H$^+$] 2+	318.6673 2+	318.6688 2+ for $C_{36}H_{43}N_7O_4$	0.15			0.28	0.20
[**2.13**+2H$^+$] 2+	275.6260 2+	275.6266 2+ for $C_{32}H_{33}N_5O_4$	0.12	0.11	0.10	0.05	0.09
[**2.22**+2H$^+$] 2+	331.6754 2+	331.6767 2+ for $C_{38}H_{45}N_7O_4$	0.11		0.23		0.11
[**2.2**+2H$^+$] 2+	207.1362 2+	207.1372 2+ for $C_{22}H_{40}N_6O_2$	0.09		0.15		0.13
[**2.7**+2H$^+$] 2+	306.1526 2+	306.1558 2+ for $C_{34}H_{40}N_6O_4$	0.05	0.94	0.59		0.25
[**2.21**+2H$^+$] 2+	417.6829 2+	417.6847 2+ for $C_{48}H_{49}N_7O_7$		0.26	0.28		0.10
[**2.12**+1H$^+$] 1+	370.2235 1+	370.2243 1+ for $C_{20}H_{28}N_5O_2$	0.06	0.06	0.07		0.08
Unknown	239.0319	Unidentified	0.02		0.03		
[**2.25**+2H$^+$] 2+	254.1047 2+	254.1055 2+ for $C_{30}H_{28}N_4O_4$	0.02	0.02		0.09	0.01
[**2.18**+2H$^+$] 2+	288.6333 2+	288.6345 2+ for $C_{34}H_{35}N_5O_4$	0.05	0.10	0.08		0.05
2.26 or **2.29**	353.1961	353.1978 1+ for $C_{20}H_{25}N_4O_2$ or 2+ for $C_{40}H_{50}N_8O_4$					0.02
[**2.30**+1H$^+$] 1+	199.0393 1+	199.0395 1+ for $C_{12}H_7O_3$	0.06	0.49	0.31	0.37	0.21
Percentage of desired (**2.1** as a proportion of **2.1**, **2.3**, **2.4** and **2.5**) **Mean: 31%**			41%	27%	29%	19%	38%

The crude material produced in each reaction showed a similar overall composition which is shown in Table 2.1 as ESI-MS results, with relative intensities determined by comparison of the peak intensity to the largest peak in any given spectrum. The percentage values are given by the percentage 2.1 out of the total for 2.1, 2.3, 2.4 and 2.5. These compounds were selected as they are the most prevalent and possess the highest relative intensities of the side products. The compound numbers are in reference to the structures in Figure 2.3. These compounds are likely products of the reaction between the starting material amine mixture and 1,8-napthalic anhydride. These compounds will be listed by compound number in the results and further emphasised in the discussion. Each compound is represented by a single isomer, but in most cases many isomers are possible.

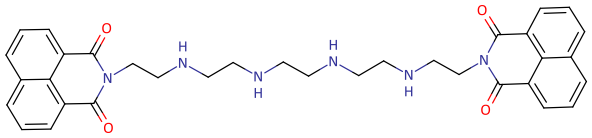

2.1

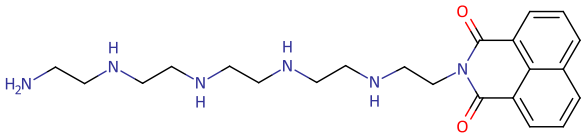

2.2: ***The linear hexamine substituted with a single naphthalimide group***

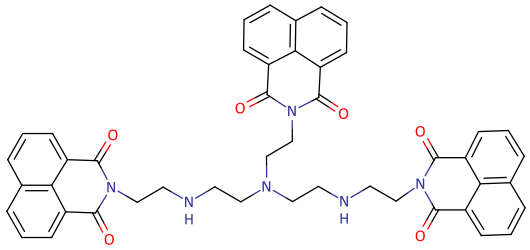

2.3: ***The branched hexamine substituted with three naphthalimide groups***

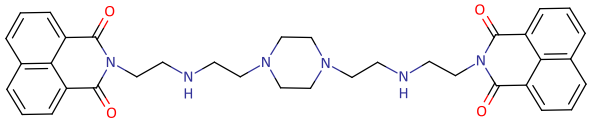

2.4: ***The piperazine derivative of the hexamine substituted with two naphthalimide groups***

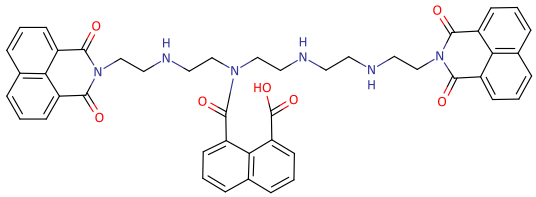

2.5: ***Hexamine substituted with two naphthalimide groups and a naphthalamide group***

Figure 2.3: ***List of the compounds identified by ESI-MS during this work. These are identified by compound number and referred to throughout the results and discussion.***

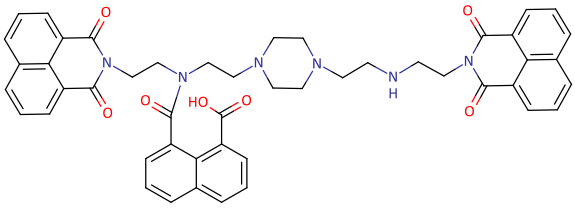

2.6: ***The piperazine derivative of the hexamine substituted with two naphthalimide groups and a naphthalamide group***

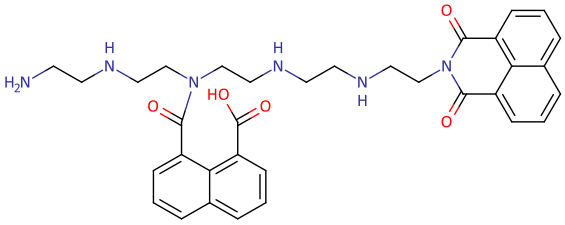

2.7: ***Hexamine substituted with a naphthalimide group and a naphthalamide group***

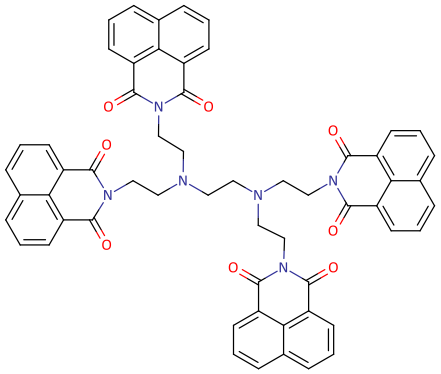

2.8: ***Dibranched hexamine substituted with four naphthalimide groups***

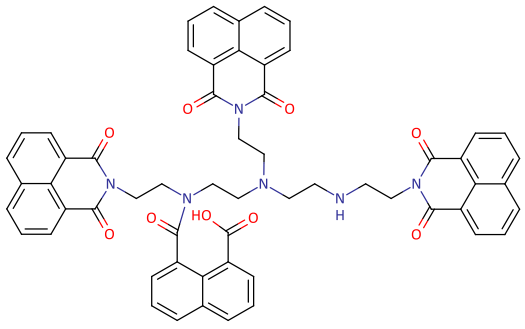

2.9: ***Branched hexamine substituted with three napthalimide groups and one naphthalamide group***

Figure 2.3 ***(continued)***

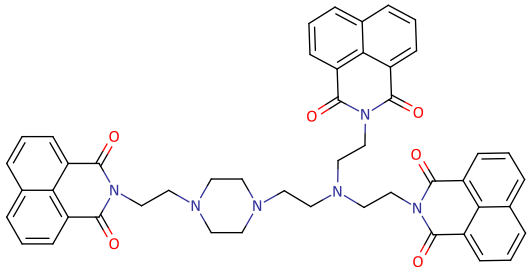

2.10: ***Piperazine derivative of the branched hexamine substituted with three naphthalimide groups***

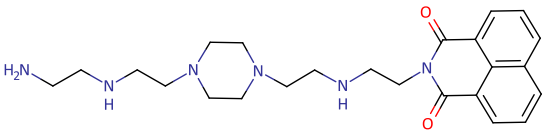

2.11: ***Piperazine derivative of the hexamine substituted with a naphthalimide group***

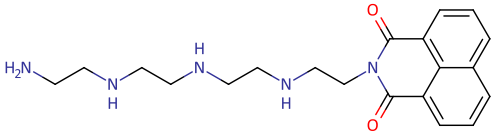

2.12: ***Pentamine substituted with one naphthalimide group***

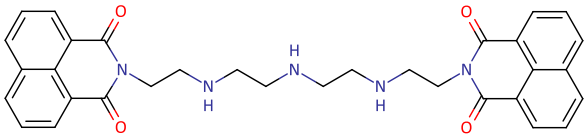

2.13: ***Pentamine substituted with two naphthalimide groups***

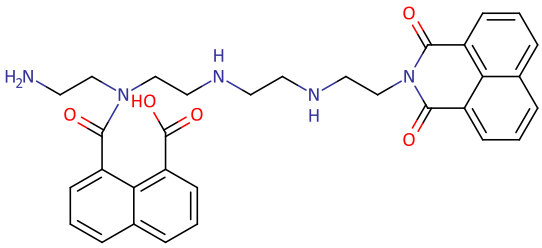

2.14: ***Pentamine substituted with one naphthalimide group and one naphthalamide group***

Figure 2.3 ***(continued)***

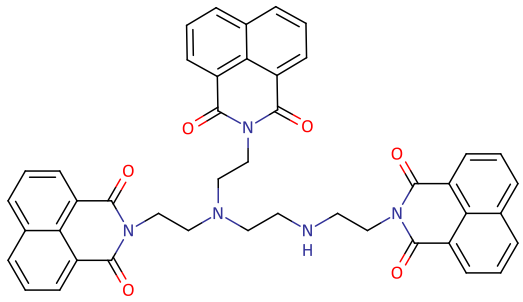

2.15: ***Branched pentamine substituted with three naphthalimide groups***

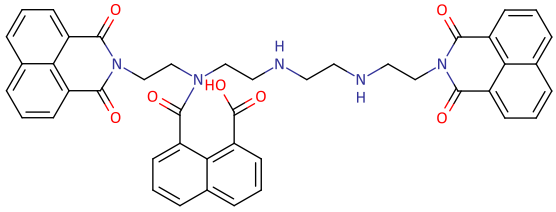

2.16: ***Pentamine substituted with two naphthalimide groups and one naphthalamide group***

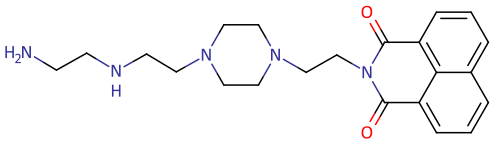

2.17: ***Piperazine derivative of the pentamine substituted with one naphthalimide group***

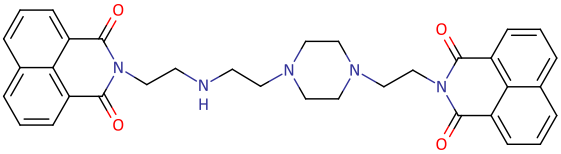

2.18: ***Piperazine derivative of the pentamine substituted with two naphthalimides***

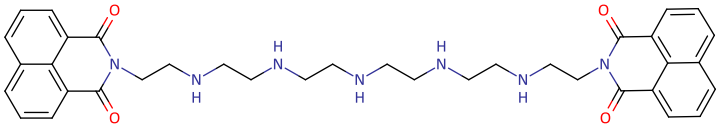

2.19: ***Heptamine substituted with two naphthalimide groups***

Figure 2.3 ***(continued)***

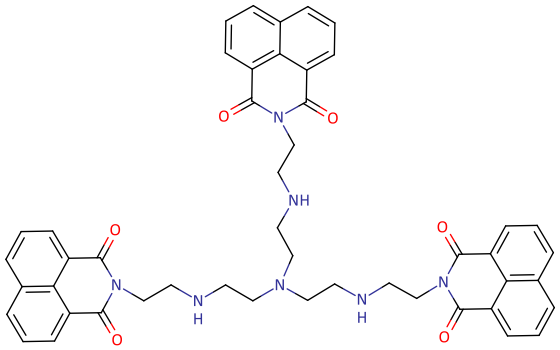

2.20: ***Branched heptamine substituted with three naphthalimide groups***

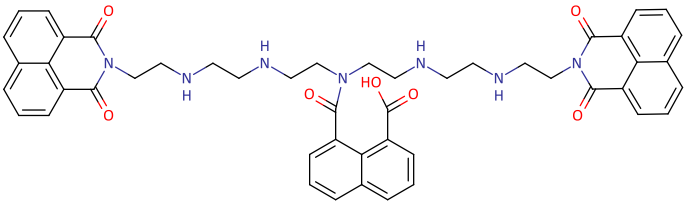

2.21: ***Heptamine substituted with two naphthalimide groups and a naphthalamide group***

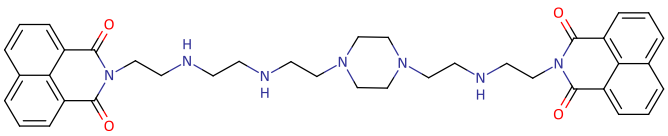

2.22: ***Piperazine derivative of the heptamine substituted with two naphthalimide groups***

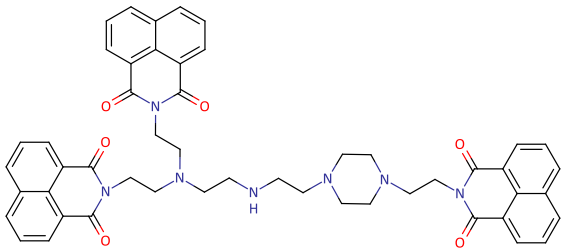

2.23: ***Piperazine derivative of the branched heptamine substituted with three naphthalimide groups***

Figure 2.3 ***(continued)***

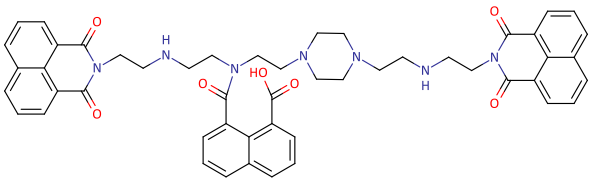

2.24: ***Piperazine derivative of the heptamine substituted with two naphthalimide groups and a naphthalamide group***

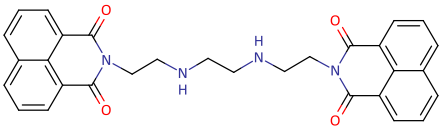

2.25: ***Tetramine substituted with two naphthalimide groups***

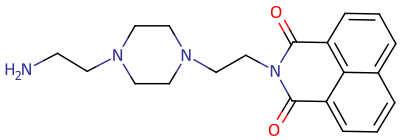

2.26: ***Piperazine derivative of the tetramine substituted with one naphthalimide group***

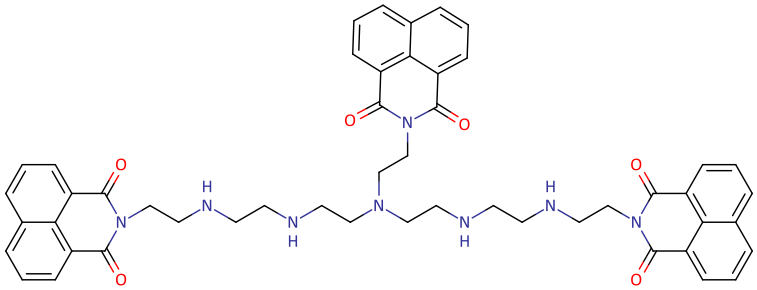

2.27: ***Branched octamine substituted with three naphthalimide groups***

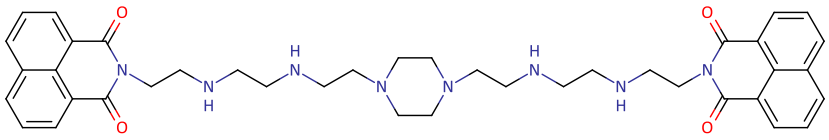

2.28: ***Piperazine derivative of the octamine substituted with two naphthalimide groups***

Figure 2.3 ***(continued)***

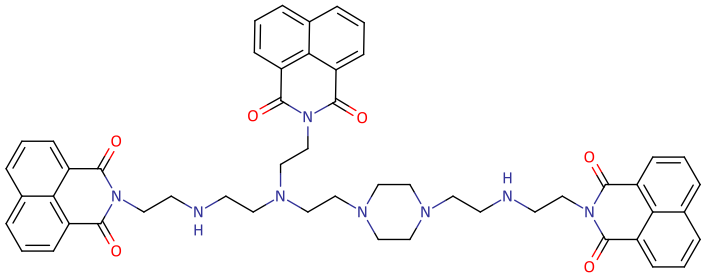

2.29: ***Piperazine derivative of the branched octamine substituted with three naphthalimide groups***

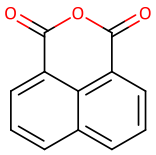

2.30: ***1,8-Naphthalic anhydride***

Figure 2.3 ***(continued)***

2.3.2. Purification by complexation

This flowchart is based upon the one shown in the experimental, and shows which species were found in each fraction of the reaction process.

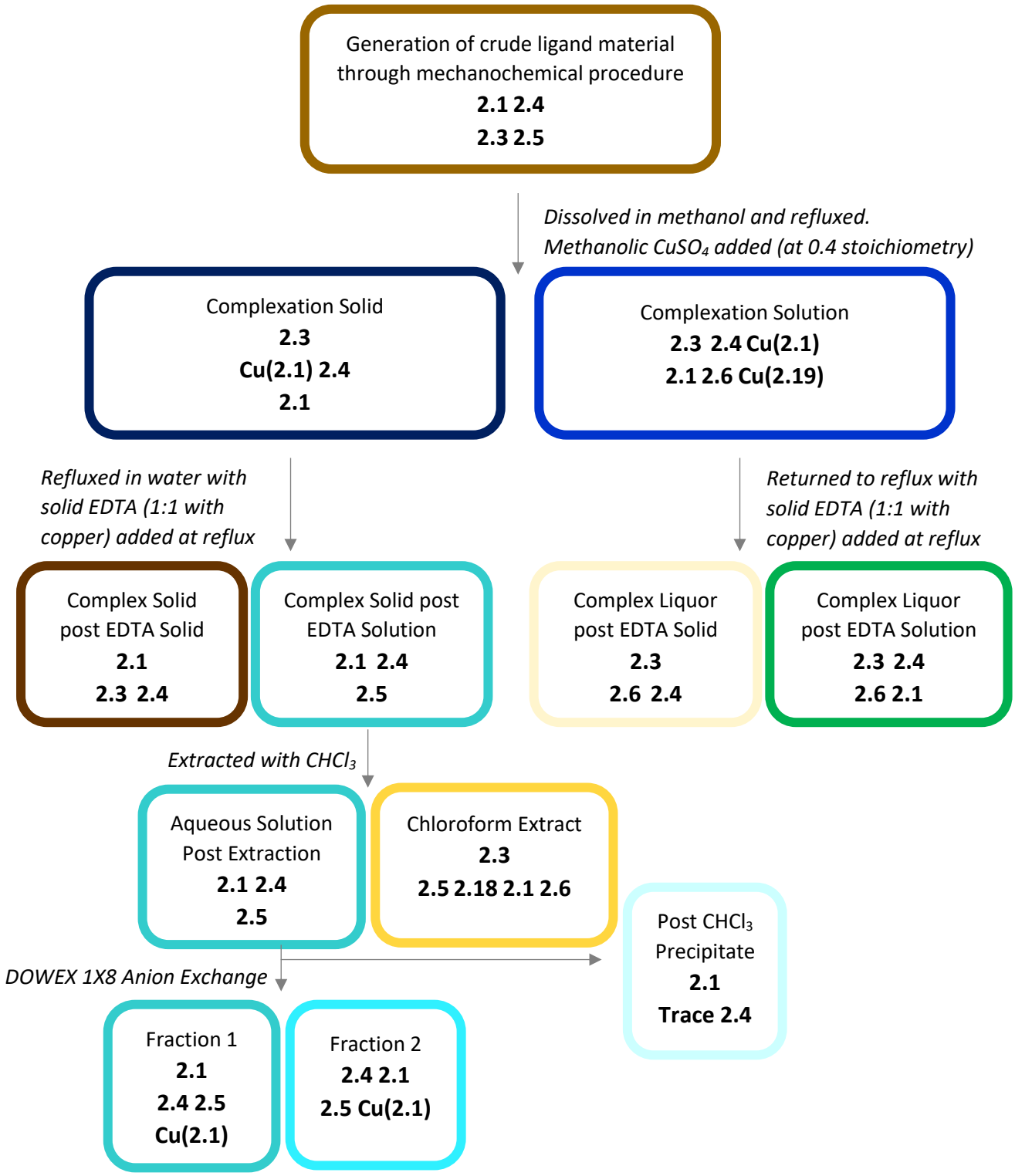

Figure 2.4: ***This flowchart shares the layout of the one in* Figure 2.2*, this time identifying the major peaks in the ESI-MS spectra for each of the different fractions to show the tracking of the desired compounds (2.1 and Cu(2.1)) through each step.***

The following tables (Table 2.3 to Table 2.14) summarise the relative intensities of major and assignable peaks in the ESI-MS spectra for each of the fractions from this reaction. Each table shows the compound assignment, the modification of the species by the ESI process, the mass to charge ratio of the found peak (and the prediction for the mass that species), and the relative intensity. For species where both the 1+ and 2+ peaks could be assigned, the species was given one relative intensity to cover both peaks. The relative intensities were found by measuring the height of each peak and dividing this by the height of the largest peak in that particular ESI-MS spectrum. This gives an indication of how much of each peak there was compared to the major peak, allowing for tracking of changes in the relative compositions of the species.

While ESI-MS is not a quantitative technique, as different species will ionise to differing extents, comparing the relative intensities of a pair of compounds between two spectra will show you whether the relative amounts of these species had changed with respect to each other. The ionisation ability of an individual species may differ from the others within the reaction mixture but should remain roughly consistent across a range of reaction compositions. This allows the species to be tracked. For example, if compound two had a relative intensity of 0.5 compared to compound one, which then drops to 0.25 in the next step of the reaction, it was clear that the amount of compound 2 had decreased, or compound one had increased. These tables were then compiled further to give Table 2.15 (see Table 2.15 for further explanation).

Table 2.2: *ESI-MS results for the crude ligand material synthesised in Section 2.2.6.1. The desired ligand compound is highlighted in green.*

Species	Identity	m/z	Predicted m/z	Relative Intensity
2.1	$[M+2H^+]$ 2+	297.1471 2+	297.1477 2+ for $C_{34}H_{38}N_6O_4$	1.0
2.4	$[M+2H^+]$ 2+	310.1550 2+	310.1556 2+ for $C_{36}H_{40}N_6O_4$	0.90
2.3	$[M+2H^+]$ 2+	387.1577 2+	387.1583 2+ for $C_{46}H_{42}N_6O_6$	0.46
2.5	$[M+2H^+]$ 2+	396.1628 2+	396.1636 2+ for $C_{46}H_{44}N_6O_7$	0.29
2.7	$[M+2H^+]$ 2+	306	306.1558 2+ for $C_{34}H_{40}N_6O_4$	0.25
2.30	$[M+1H^+]$ 1+	199.0391 1+	199.0395 1+ for $C_{12}H_7O_3$	0.21
2.19	$[M+2H^+]$ 2+	318.6673 2+	318.6688 2+ for $C_{36}H_{43}N_7O_4$	0.20
2.20	$[M+2H^+]$ 2+	408.6782 2+	408.6794 2+ for $C_{48}H_{47}N_7O_6$	0.17
2.2	$[M+2H^+]$ 2+	207.1362 2+	207.1372 2+ for $C_{22}H_{40}N_6O_2$	0.13
2.22	$[M+2H^+]$ 2+	331.6754 2+	331.6767 2+ for $C_{38}H_{45}N_7O_4$	0.11
2.21	$[M+2H^+]$ 2+	417.6834	417.6847 2+ for $C_{48}H_{49}N_7O_7$	0.10
2.13	$[M+2H^+]$ 2+	275.6256	275.6266 2+ for $C_{32}H_{33}N_5O_4$	0.09
2.12	$[M+H^+]$ 1+	370.2239	370.2243 1+ for $C_{20}H_{28}N_5O_2$	0.08
2.18	$[M+2H^+]$ 2+	288.6333	288.6345 2+ for $C_{34}H_{35}N_5O_4$	0.05
2.26	$[M+1H^+]$ 1+	353.1961	353.1978 1+ for $C_{20}H_{26}N_4O_2$	0.02

Complexation reaction of copper with crude ligand material

Table 2.3: *ESI-MS results for the solid produced by the complexation process described in Section 2.2.6.2. The desired complex is highlighted in blue.*

Species	Identity	m/z	Predicted m/z	Relative Intensity
2.3	$[M+2H^+]$ 2+	387.1563 2+	387.1583 2+ for $C_{46}H_{42}N_6O_6$	1.0
	$[M+H^+]$ 1+	773.3074 1+	773.3088 1+ for $C_{46}H_{41}N_6O_6$	
Cu(2.1)	$[M]^{2+}$	327.6031	327.6047 2+ for $[Cu(C_{34}H_{36}N_6O_4)]^{2+}$	0.43
2.4	$[M+2H^+]$ 2+	310	310.1556 2+ for $C_{36}H_{40}N_6O_4$	0.41
2.6	$[M+2H^+]$ 2+	409.1719 2+	409.1714 2+ for $C_{48}H_{46}N_6O_7$	0.13
2.13	$[M+2H^+]$ 2+	275.6256 2+	275.6266 2+ for $C_{32}H_{33}N_5O_4$	0.13
2.20	$[M+2H^+]$ 2+	408	408.6794 2+ for $C_{48}H_{47}N_7O_6$	0.10
Cu(2.19)	$[M]^{2+}$	349.1235	349.1257 2+ for $[Cu(C_{36}H_{41}N_7O_4)]^{2+}$	0.10
2.1	$[M+2H^+]$ 2+	297.1461	297.1477 2+ for $C_{34}H_{38}N_6O_4$	0.09
Cu(2.20)	$[M]^{2+}$	439.1335	439.1363 2+ for $[Cu(C_{48}H_{47}N_7O_6)]^{2+}$	0.08
2.30	$[M+H^+]$ 1+	199.0395	199.0395 1+ for $C_{12}H_7O_3$	0.08
2.5	$[M+2H^+]$ 2+	396	396.1636 2+ for $C_{46}H_{44}N_6O_7$	0.07
2.18	$[M+2H^+]$ 2+	288	288.6345 2+ for $C_{34}H_{35}N_5O_4$	0.07
2.23	$[M+2H^+]$ 2+	421	421.6872 2+ for $C_{50}H_{49}N_7O_6$	0.06
2.9	$[M+2H^+]$ 2+	486.1712	486.1741 2+ for $C_{58}H_{48}N_6O_9$	0.04

Table 2.4: *ESI-MS results for the solid produced following cooling of the complexation liquor described in Section 2.2.6.2. The desired complex is highlighted in blue.*

Species	Identity	m/z	Predicted m/z	Relative Intensity
Cu(2.1)	$[M]^{2+}$	327.6026 2+	327.6047 2+ for $[Cu(C_{34}H_{36}N_6O_4)]^{2+}$	1.0
2.3	$[M+2H^+]$ 2+	387.1553 2+	387.1583 2+ for $C_{46}H_{42}N_6O_6$	0.23
2.4	$[M+2H^+]$ 2+	310.1536 2+	310.1556 2+ for $C_{36}H_{40}N_6O_4$	0.14
2.20	$[M+2H^+]$ 2+	408.6757 2+	408.6794 2+ for $C_{48}H_{47}N_7O_6$	0.14
2.1	$[M+2H^+]$ 2+	297.1457 2+	297.1477 2+ for $C_{34}H_{38}N_6O_4$	0.12
Cu(2.20)	$[M]^{2+}$	439.1320 2+	439.1363 2+ for $[Cu(C_{48}H_{47}N_7O_6)]^{2+}$	0.05
Cu(2.19)	$[M]^{2+}$	349.1226	349.1257 2+ for $[Cu(C_{36}H_{41}N_7O_4)]^{2+}$	0.04
2.30	$[M+1H^+]$ 1+	199.0393 1+	199.0395 1+ for $C_{12}H_7O_3$	0.02
2.13	$[M+2H^+]$ 2+	275.6249 2+	275.6266 2+ for $C_{32}H_{33}N_5O_4$	0.02

Table 2.5: *ESI-MS results for the liquor produced by the complexation process described in Section 2.2.6.2. The desired complex is highlighted in blue.*

Species	Identity	m/z	Predicted m/z	Relative Intensity
2.4	$[M+2H^+]$ 2+	310.1544 2+	310.1556 2+ for $C_{36}H_{40}N_6O_4$	1.0
	$[M+H^+]$ 1+	619.3017 1+	619.3033 1+ for $C_{36}H_{39}N_6O_4$	
2.3	$[M+2H^+]$ 2+	387.1562 2+	387.1583 2+ for $C_{46}H_{42}N_6O_6$	0.95
	$[M+H^+]$ 1+	773.3075 1+	773.3088 1+ for $C_{46}H_{41}N_6O_6$	
Cu(2.1)	$[M]^{2+}$	327.6034	327.6047 2+ for $[Cu(C_{34}H_{36}N_6O_4)]^{2+}$	0.87
2.30	$[M+H^+]$ 1+	199.0399 1+	199.0395 1+ for $C_{12}H_7O_3$	0.47
2.6	$[M+2H^+]$ 2+	409.1706 2+	409.1714 2+ for $C_{48}H_{46}N_6O_7$	0.35
Cu(2.19)	$[M]^{2+}$	349.1240 2+	349.1257 2+ for $[Cu(C_{36}H_{41}N_7O_4)]^{2+}$	0.29
2.1	$[M+2H^+]$ 2+	297.1466 2+	297.1477 2+ for $C_{34}H_{38}N_6O_4$	0.28
2.13	$[M+2H^+]$ 2+	275.6258 2+	275.6266 2+ for $C_{32}H_{33}N_5O_4$	0.20
2.22	$[M+2H^+]$ 2+	331	331.6767 2+ for $C_{38}H_{45}N_7O_4$	0.16
2.18	$[M+2H^+]$ 2+	288	288.6345 2+ for $C_{34}H_{35}N_5O_4$	0.13
2.5	$[M+2H^+]$ 2+	396	396.1636 2+ for $C_{46}H_{44}N_6O_7$	0.09
2.23	$[M+2H^+]$ 2+	421	421.6872 2+ for $C_{50}H_{49}N_7O_6$	0.08
2.24	$[M+2H^+]$ 2+	430	430.6925 2+ for $C_{50}H_{51}N_7O_7$	0.04
Cu(2.20)	$[M]^{2+}$	439	439.1363 2+ for $[Cu(C_{48}H_{47}N_7O_6)]^{2+}$	0.04
2.9	$[M+2H^+]$ 2+	486.1711 2+	486.1741 2+ for $C_{58}H_{48}N_6O_9$	0.03

Treatment of Complexation Solid

Table 2.6: *ESI-MS results for the solid produced following treatment of the complexation solid with EDTA in Section 2.2.6.3. The desired ligand compound is highlighted in green.*

Species	Identity	m/z	Predicted m/z	Relative Intensity
2.1	$[M+2H^+]$ 2+	297.1467 2+	297.1477 2+ for $C_{34}H_{38}N_6O_4$	1.0
	$[M+H^+]$ 1+	593.2859 1+	593.2876 1+ for $C_{34}H_{37}N_6O_4$	
2.3	$[M+2H^+]$ 2+	387.1561 2+	387.1583 2+ for $C_{46}H_{42}N_6O_6$	0.65
2.4	$[M+2H^+]$ 2+	310	310.1556 2+ for $C_{36}H_{40}N_6O_4$	0.40
2.20	$[M+2H^+]$ 2+	408.6765 2+	408.6794 2+ for $C_{48}H_{47}N_7O_6$	0.26
2.5	$[M+2H^+]$ 2+	396	396.1636 2+ for $C_{46}H_{44}N_6O_7$	0.19
2.19	$[M+2H^+]$ 2+	318	318.6688 2+ for $C_{36}H_{43}N_7O_4$	0.07
2.12	$[M+2H^+]$ 2+	370	370.2243 1+ for $C_{20}H_{28}N_5O_2$	0.06
2.13	$[M+2H^+]$ 2+	275.6256	275.6266 2+ for $C_{32}H_{33}N_5O_4$	0.05
2.30	$[M+H^+]$ 1+	199.0396	199.0395 1+ for $C_{12}H_7O_3$	0.02
Cu(2.1)	$[M]^{2+}$	327	327.6047 2+ for $[Cu(C_{34}H_{36}N_6O_4)]^{2+}$	0.01

Table 2.7: *ESI-MS results for the solution produced following treatment of the complexation solid with EDTA in Section 2.2.6.3. The desired ligand compound is highlighted in green.*

Species	Identity	m/z	Predicted m/z	Relative Intensity
2.1	$[M+2H^+]$ 2+	297.1469 2+	297.1477 2+ for $C_{34}H_{38}N_6O_4$	1.0
	$[M+H^+]$ 1+	593.2861 1+	593.2876 1+ for $C_{34}H_{37}N_6O_4$	
2.4	$[M+2H^+]$ 2+	310	310.1556 2+ for $C_{36}H_{40}N_6O_4$	0.95
2.5	$[M+2H^+]$ 2+	396	396.1636 2+ for $C_{46}H_{44}N_6O_7$	0.32
2.22	$[M+2H^+]$ 2+	331.6749 2+	331.6767 2+ for $C_{38}H_{45}N_7O_4$	0.19
2.13	$[M+2H^+]$ 2+	275.6256 2+	275.6266 2+ for $C_{32}H_{33}N_5O_4$	0.15
2.19	$[M+2H^+]$ 2+	318	318.6688 2+ for $C_{36}H_{43}N_7O_4$	0.13
2.12	$[M+2H^+]$ 2+	370.2230	370.2243 1+ for $C_{20}H_{28}N_5O_2$	0.06
2.18	$[M+2H^+]$ 2+	288	288.6345 2+ for $C_{34}H_{35}N_5O_4$	0.04
2.17	$[M+2H^+]$ 2+	198.6233	198.6239 2+ for $C_{22}H_{31}N_5O_2$	0.02

Treatment of Complexation Liquor

Table 2.8: *ESI-MS results for the solution produced following treatment of the complexation liquor with EDTA as described in Section 2.2.6.4. The desired ligand compound is highlighted in green.*

Species	Identity	m/z	Predicted m/z	Relative Intensity
2.4	$[M+2H^+]$ 2+	310.1552 2+	310.1556 2+ for $C_{36}H_{40}N_6O_4$	1.0
2.3	$[M+2H^+]$ 2+	387.1570 2+	387.1583 2+ for $C_{46}H_{42}N_6O_6$	1.0
2.6	$[M+2H^+]$ 2+	409.1717 2+	409.1714 2+ for $C_{48}H_{46}N_6O_7$	0.53
2.5	$[M+2H^+]$ 2+	396	396.1636 2+ for $C_{46}H_{44}N_6O_7$	0.33
2.1	$[M+2H^+]$ 2+	297.1474 2+	297.1477 2+ for $C_{34}H_{38}N_6O_4$	0.30
2.30	$[M+1H^+]$ 1+	199.0400 1+	199.0395 1+ for $C_{12}H_7O_3$	0.27
2.22	$[M+2H^+]$ 2+	331.6753 2+	331.6767 2+ for $C_{38}H_{45}N_7O_4$	0.16
2.13	$[M+2H^+]$ 2+	275.6262 2+	275.6266 2+ for $C_{32}H_{33}N_5O_4$	0.11
Unknown	1+	354.0115	Unknown	0.07
2.16	$[M+2H^+]$ 2+	374.6408	374.6425 2+ for $C_{44}H_{39}N_5O_7$	0.07

ESI-MS of Complexation Liquor Post EDTA Solid:

Table 2.9: *ESI-MS results for the solid produced following treatment of the complexation liquor with EDTA as described in Section 2.2.6.4. The desired ligand compound is highlighted in green.*

Species	Identity	m/z	Predicted m/z	Relative Intensity
Unknown	1+	293.0985 1+	Unknown	1.0
2.3	$[M+2H^+]$ 2+	387.1562 2+	387.1583 2+ for $C_{46}H_{42}N_6O_6$	0.73
	$[M+H^+]$ 1+	773.3091 1+	773.3088 1+ for $C_{46}H_{41}N_6O_6$	
2.4	$[M+2H^+]$ 2+	310	310.1556 2+ for $C_{36}H_{40}N_6O_4$	0.27
2.6	$[M+2H^+]$ 2+	409.1707 2+	409.1714 2+ for $C_{48}H_{46}N_6O_7$	0.19
2.5	$[M+2H^+]$ 2+	396	396.1636 2+ for $C_{46}H_{44}N_6O_7$	0.14
2.1	$[M+2H^+]$ 2+	297	297.1477 2+ for $C_{34}H_{38}N_6O_4$	0.10
2.9	$[M+2H^+]$ 2+	486.1702	486.1741 2+ for $C_{58}H_{48}N_6O_9$	0.08
2.30	$[M+H^+]$ 1+	199.0394	199.0395 1+ for $C_{12}H_7O_3$	0.05
2.13	$[M+2H^+]$ 2+	275.6256	275.6266 2+ for $C_{32}H_{33}N_5O_4$	0.05
2.18	$[M+2H^+]$ 2+	288	288.6345 2+ for $C_{34}H_{35}N_5O_4$	0.03

Chloroform Extraction of Complexation Solid Post EDTA Solution

Table 2.10: *ESI-MS results for the chloroform extract from the solution produced following treatment of the complexation solid with EDTA as described in Section 2.2.6.4 and 2.2.6.5. The desired ligand compound is highlighted in green.*

Species	Identity	m/z	Predicted m/z	Relative Intensity
2.3	$[M+2H^+]$ 2+	387.1564 2+	387.1583 2+ for $C_{46}H_{42}N_6O_6$	1.0
2.5	$[M+2H^+]$ 2+	396	396.1636 2+ for $C_{46}H_{44}N_6O_7$	0.18
2.30	$[M+H^+]$ 1+	199.0395	199.0395 1+ for $C_{12}H_7O_3$	0.15
2.9	$[M+2H^+]$ 2+	486.1714 2+	486.1741 2+ for $C_{58}H_{48}N_6O_9$	0.14
2.18	$[M+2H^+]$ 2+	288.6332 2+	288.6345 2+ for $C_{34}H_{35}N_5O_4$	0.11
2.1	$[M+2H^+]$ 2+	297	297.1477 2+ for $C_{34}H_{38}N_6O_4$	0.08
2.6	$[M+2H^+]$ 2+	409	409.1714 2+ for $C_{48}H_{46}N_6O_7$	0.07
2.4	$[M+2H^+]$ 2+	310	310.1556 2+ for $C_{36}H_{40}N_6O_4$	0.05
2.20	$[M+2H^+]$ 2+	408	408.6794 2+ for $C_{48}H_{47}N_7O_6$	0.05
2.13	$[M+2H^+]$ 2+	275	275.6266 2+ for $C_{32}H_{33}N_5O_4$	0.04

Table 2.11: *ESI-MS results for the solution following chloroform extraction of the solution produced following treatment of the complexation solid with EDTA as described in Section 2.2.6.4 and 2.2.6.5. The desired ligand is highlighted in green.*

Species	Identity	m/z	Predicted m/z	Relative Intensity
2.1	$[M+2H^+]$ 2+	297.1460 2+	297.1477 2+ for $C_{34}H_{38}N_6O_4$	1.0
	$[M+1H^+]$ 1+	593.2841 1+	593.2876 1+ for $C_{34}H_{37}N_6O_4$	
2.4	$[M+2H^+]$ 2+	310.1536 2+	310.1556 2+ for $C_{36}H_{40}N_6O_4$	0.86
2.5	$[M+2H^+]$ 2+	396.1601 2+	396.1636 2+ for $C_{46}H_{44}N_6O_7$	0.41
2.22	$[M+2H^+]$ 2+	331.6738 2+	331.6767 2+ for $C_{38}H_{45}N_7O_4$	0.20
Unknown	1+	354.0107 1+	Unknown	0.15
2.13	$[M+2H^+]$ 2+	275.6248	275.6266 2+ for $C_{32}H_{33}N_5O_4$	0.10
2.12	$[M+2H^+]$ 2+	370.2220	370.2243 1+ for $C_{20}H_{28}N_5O_2$	0.08
2.17	$[M+2H^+]$ 2+	198.6228	198.6239 2+ for $C_{22}H_{31}N_5O_2$	0.04

Table 2.12: *ESI-MS results for the precipitate produced from the solution following chloroform extraction as described in Section 2.2.6.4 and 2.2.6.5. The desired ligand is highlighted in green.*

Species	Identity	m/z	Predicted m/z	Relative Intensity
2.1	$[M+2H^+]$ 2+	297.1465 2+	297.1477 2+ for $C_{34}H_{38}N_6O_4$	1.0
	$[M+1H^+]$ 1+	593.2863 1+	593.2876 1+ for $C_{34}H_{37}N_6O_4$	
2.4	$[M+2H^+]$ 2+	310.1538 2+	310.1556 2+ for $C_{36}H_{40}N_6O_4$	0.12
2.12	$[M+H^+]$ 1+	370.2232	370.2243 1+ for $C_{20}H_{28}N_5O_2$	0.09

Column of Complexation Solid Post EDTA Solution Post Chloroform Extraction

Table 2.13: *ESI-MS results for Fraction 1 of the anion exchange column of the solution remaining following chloroform extraction as described in Section 2.2.6.4 and 2.2.6.5. The desired ligand is highlighted in green.*

Species	Identity	m/z	Predicted m/z	Relative Intensity
2.1	$[M+2H^+]$ 2+	297.1468 2+	297.1477 2+ for $C_{34}H_{38}N_6O_4$	1.0
	$[M+1H^+]$ 1+	593.2859 1+	593.2876 1+ for $C_{34}H_{37}N_6O_4$	
2.4	$[M+2H^+]$ 2+	310.1543 2+	310.1556 2+ for $C_{36}H_{40}N_6O_4$	0.79
	$[M+1H^+]$ 1+	619.3019 1+	619.3033 1+ for $C_{36}H_{39}N_6O_4$	
2.5	$[M+2H^+]$ 2+	396.1611 2+	396.1636 2+ for $C_{46}H_{44}N_6O_7$	0.28
2.22	$[M+2H^+]$ 2+	331.6747 2+	331.6767 2+ for $C_{38}H_{45}N_7O_4$	0.27
Cu(2.12.1)	$[M]^{2+}$	327	327.6047 2+ for $[Cu(C_{34}H_{36}N_6O_4)]^{2+}$	0.26
2.13	$[M+2H^+]$ 2+	275.6255 2+	275.6266 2+ for $C_{32}H_{33}N_5O_4$	0.16
	$[M+1H^+]$ 1+	550.2430 1+	550.2455 1+ for $C_{32}H_{32}N_5O_4$	
2.12	$[M+H^+]$ 1+	370.2231	370.2243 1+ for $C_{20}H_{28}N_5O_2$	0.08
Cu(2.19)	$[M]^{2+}$	349.1239	349.1257 2+ for $[Cu(C_{36}H_{41}N_7O_4)]^{2+}$	0.06
Cu(2.20)	$[M]^{2+}$	439.2802 2+	439.1363 2+ for $[Cu(C_{48}H_{47}N_7O_6)]^{2+}$	0.07
2.17	$[M+2H^+]$ 2+	198.6234 2+	198.6239 2+ for $C_{22}H_{31}N_5O_2$	0.05

Table 2.14: *ESI-MS results for Fraction 2 of the anion exchange column of the solution remaining following chloroform extraction of the solution produced following treatment of the complexation solid with EDTA as described in Section 2.2.6.4 and 2.2.6.5. The desired ligand compound is highlighted in green.*

Species	Identity	m/z	Predicted m/z	Relative Intensity
2.4	$[M+2H^+]$ 2+	310.1538 2+	310.1556 2+ for $C_{36}H_{40}N_6O_4$	1.0
	$[M+1H^+]$ 1+	619.3009 1+	619.3033 1+ for $C_{36}H_{39}N_6O_4$	
2.1	$[M+2H^+]$ 2+	297.1462 2+	297.1477 2+ for $C_{34}H_{38}N_6O_4$	0.95
	$[M+1H^+]$ 1+	593.2849 1+	593.2876 1+ for $C_{34}H_{37}N_6O_4$	
2.5	$[M+2H^+]$ 2+	396.1604 2+	396.1636 2+ for $C_{46}H_{44}N_6O_7$	0.39
Cu(2.1)	$[M]^{2+}$	327.6027	327.6047 2+ for $[Cu(C_{34}H_{36}N_6O_4)]^{2+}$	0.29
2.22	$[M+2H^+]$ 2+	331.6748 2+	331.6767 2+ for $C_{38}H_{45}N_7O_4$	0.28
2.13	$[M+2H^+]$ 2+	275.6255 2+	275.6266 2+ for $C_{32}H_{33}N_5O_4$	0.15
	$[M+1H^+]$ 1+	550.2437 1+	550.2455 1+ for $C_{32}H_{32}N_5O_4$	
Cu(2.19)	$[M]^{2+}$	349.1233	349.1257 2+ for $[Cu(C_{36}H_{41}N_7O_4)]^{2+}$	0.07
2.12	$[M+H^+]$ 1+	370.2232	370.2243 1+ for $C_{20}H_{28}N_5O_2$	0.07
Cu(2.20)	$[M]^{2+}$	439.2792	439.1363 2+ for $[Cu(C_{48}H_{47}N_7O_6)]^{2+}$	0.06
2.17	$[M+2H^+]$ 2+	198.6230 2+	198.6239 2+ for $C_{22}H_{31}N_5O_2$	0.05

Table 2.15*: Summarised ESI-MS results from the reaction fractions of the purification by complexation shown in Section 2.2.6. The values are expressed as relative intensities for the species of interest compared to the largest peak in that spectrum. The final row percentages for the desired compound was calculated by the desired product divided by the sum of the most common side products.* **2.1, 2.4, Cu(2.1), 2.3** *and* **2.5***. The desired compound was* **2.1** *except where* **Cu(2.1)** *was the desired compound, as highlighted, with free ligand highlighted green and complex highlighted blue. The columns in this table correspond to the boxes of the flowcharts in* **Figure 2.2** *and* **Figure 2.4***.*

Identity	m/z	Predicted m/z	Relative Intensity												
			Crude Ligand	Complex Solid	Complex Liquor	Cooling Solid	Solid EDTA Solid	Solid EDTA Solution	$CHCl_3$ Extract	Solution Post $CHCl_3$	Solid from post extract	Column Band 1	Column Band 2	Liquor ETDA Solid	Liquor EDTA Solution
[**2.17**+2H$^+$] 2+	198.6234 2+	198.6239 2+ for $C_{22}H_{31}N_5O_2$						0.02		0.04		0.05	0.05		
[**2.30** +1H$^+$] 1+	199.0391 1+	199.0395 1+ for $C_{12}H_7O_3$	0.21	0.08	0.47	0.02	0.02		0.15					0.05	0.27
[**2.2**+2H$^+$] 2+	207.1362 2+	207.1372 2+ for $C_{22}H_{40}N_6O_2$	0.13												
[**2.13**+2H$^+$] 2+	275.6256 2+	275.6266 2+ for $C_{32}H_{33}N_5O_4$	0.09	0.13	0.20	0.02	0.05	0.15	0.04	0.10		0.16	0.15	0.05	0.11
[**2.18**+2H$^+$] 2+	288.6332 2+	288.6345 2+ for $C_{34}H_{35}N_5O_4$	0.05	0.07	0.13			0.04	0.11					0.03	
[**2.1**+2H$^+$] 2+	297.1471 2+	297.1477 2+ for $C_{34}H_{38}N_6O_4$	1.0	0.09	0.28	0.12	1.0	1.0	0.08	1.0	1.0	1.0	0.95	0.10	0.30
[**2.7**+2H$^+$] 2+	306.1520 2+	306.1558 2+ for $C_{34}H_{40}N_6O_4$	0.25												
[**2.4**+2H$^+$] 2+	310.1550 2+	310.1556 2+ for $C_{36}H_{40}N_6O_4$	0.90	0.41	1.0	0.14	0.40	0.95	0.05	0.86	0.12	0.79	1.0	0.27	1.0
[**2.19** +2H$^+$] 2+	318.6673 2+	318.6688 2+ for $C_{36}H_{43}N_7O_4$	0.20				0.07	0.13							
[Cu(**2.1**)]$^{2+}$	327.6026 2+	327.6047 2+ for [Cu($C_{34}H_{36}N_6O_4$)]$^{2+}$		0.43	0.87	1.0	0.01					0.26	0.29		
[**2.22**+2H$^+$] 2+	331.6754 2+	331.6767 2+ for $C_{38}H_{45}N_7O_4$	0.11		0.16			0.19		0.20		0.27	0.28		0.16
[Cu(**2.19**)]$^{2+}$	349.1226 2+	349.1257 2+ for [Cu($C_{36}H_{41}N_7O_4$)]$^{2+}$		0.10	0.29	0.04						0.06	0.07		
[**2.12**+1H$^+$] 1+	370.2239 2+	370.2243 1+ for $C_{20}H_{28}N_5O_2$	0.08				0.06	0.06		0.08	0.09	0.08	0.07		
[**2.16**+2H$^+$] 2+	374.6400	374.6425 2+ for $C_{44}H_{39}N_5O_7$												0.04	0.07
[**2.3** +2H$^+$] 2+	387.1577 2+	387.1583 2+ for $C_{46}H_{42}N_6O_6$	0.46	1.0	0.95	0.23	0.65		1.0					0.73	1.0
[**2.5**+2H$^+$] 2+	396.1628 2+	396.1636 2+ for $C_{46}H_{44}N_6O_7$	0.29	0.07	0.09		0.19	0.32	0.18	0.41		0.28	0.39	0.14	0.33
[**2.20**+2H$^+$] 2+	408.6782 2+	408.6794 2+ for $C_{48}H_{47}N_7O_6$	0.17	0.10		0.14	0.26		0.05						
[**2.6**+2H$^+$] 2+	409.1717 2+	409.1714 2+ for $C_{48}H_{46}N_6O_7$		0.13	0.35				0.07					0.19	0.53
[**2.21**+2H$^+$] 2+	417.6834 2+	417.6847 2+ for $C_{48}H_{49}N_7O_7$	0.10												
[**2.23**+2H$^+$] 2+	421.6849 2+	421.6872 2+ for $C_{50}H_{49}N_7O_6$		0.06	0.08										
[**2.24**+2H$^+$] 2+	430.6902	430.6925 2+ for $C_{50}H_{51}N_7O_7$			0.04										
[Cu(**2.20**)]$^{2+}$	439.1320 2+	439.1363 2+ for [Cu($C_{48}H_{47}N_7O_6$)]$^{2+}$		0.08	0.04	0.05						0.07	0.06		
[**2.9**+ 2H$^+$] 2+	486.1714 2+	486.1741 2+ for $C_{58}H_{48}N_6O_9$		0.04	0.03				0.14					0.08	
Percentage of desired compound (compared to major side products)			38%	22%	27%	67%	44%	44%	6%	44%	89%	43%	36%	8%	11%

2.3.3. Summary of Results

The intention of this work was to purify the desired ligand, 2.1, through complexation to copper followed by recovery of the ligand. Iterations of the reaction was performed in an attempt to refine the reaction conditions towards purifying the desired ligand following the steps of the reaction. The criterion for judging enrichment was made on the basis ESI-MS results, where relative intensities for various compounds were compared to trace the increased or decreased presence of a compound before and after a reaction step. From the flowcharts and tables of ESI-MS results, (See Appendix A and B for more) it can be seen that the complexation reaction generally produced a blue oily solid and a blue liquor, of which the desired compound exists predominantly in the solid. The reaction of the solid with aqueous EDTA produced a brown oily solid and bright blue liquor, of which the greatest relative intensity of the desired compound 2.1 was observed in the liquor. Both the solid and the liquor show an enrichment of 2.1 compared to crude material.

The modifications to the reaction, increasing the ratio of copper, changing the addition of copper from aqueous to methanolic and use of anhydrous copper sulfate led to the method using 40% stoichiometric pentahydrate copper added as a methanolic solution. This method can be observed to give the greatest enrichment of 2.1 with the least waste of this compound to the fractions where lower detection was observed.

2.4. Discussion

2.4.1. Amine Starting Material

It became evident early in the project that the amine starting material used contained substantial impurities. These impurities were detected by ESI-MS where species with additional or fewer -CH_2CH_2NH- groups were detected, and by ^{13}C NMR. The ^{13}C NMR spectrum allowed for identification of carbon atoms in different environments with respect to the amine group they are connected to. Carbon atoms bonded to primary amines tend to have signals between 35 and 45 ppm, carbon atoms next to secondary amines between 45 and 55 ppm and carbon atoms next to tertiary amines between 50 and 60 ppm.[38, 76]

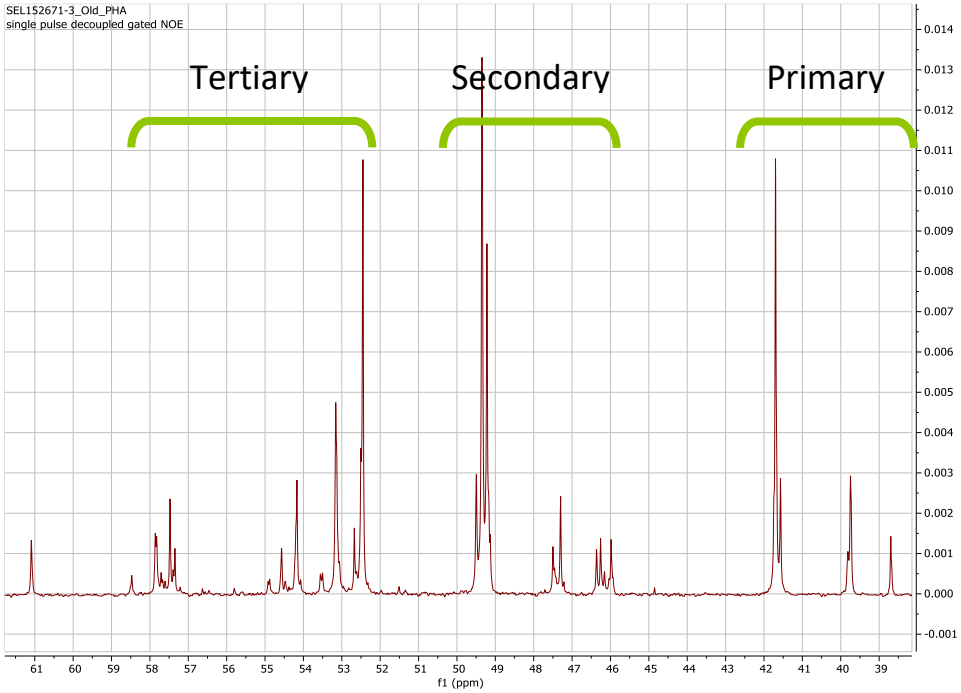

Figure 2.5: ***^{13}C NMR spectrum of the amine, highlighting the peaks in the regions of the NMR spectrum where carbon atoms adjacent to primary, secondary, and tertiary amines are typically observed.***

In the ^{13}C NMR spectrum (Figure 2.5) there was evidence of carbon atoms next to tertiary amines. The desired compound should have had no tertiary amines, so this information indicated that branched isomers or piperazines must be present in the mixture (Figure 2.6).

Peak picking the ^{13}C NMR spectrum gave 30 individual peaks, including some possible multiplets/overlaps (so the number would increase if these peaks are not multiplets or are separated from each other). The maximum realistic number of peaks expected for the four isomers was 22, showing that there were other unknown compounds present in the mixture. This coupled with the overall complexity of the peaks and integral uncertainty (due to the fact

that the relaxation times were not known) has meant that assignment was not achievable. However, integration of the relevant sections of the ^{13}C NMR allowed for an estimate as to the degree of branching (Table 2.16)

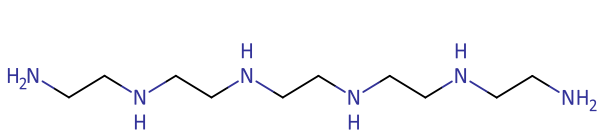

Linear polyamine (desired compound)

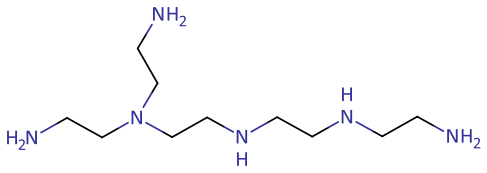

Asymmetric monobranched

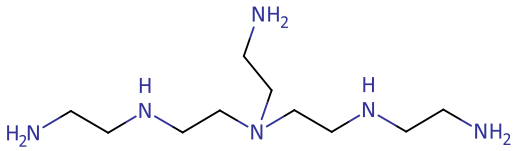

Symmetric monobranched

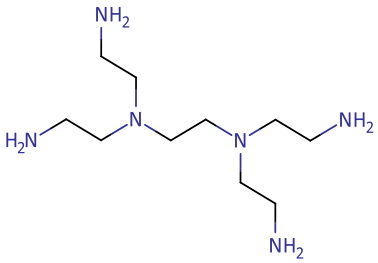

Dibranched

Figure 2.6: ***Polyamine isomers of 3,6,9,12-tetraazatetradecane-1,14-diamine ($C_{10}H_{28}N_6$)***

Table 2.16: *Ratio of carbon atoms adjacent to primary, secondary and tertiary amines for each of the probable 3,6,9,12-tetraazatetradecane-1,14-diamine isomers present in the starting material*

Isomer	C next to 1° N	C next to 2° N	C next to 3° N	Ratio
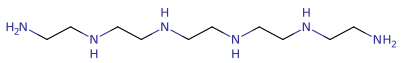	2	8	0	2:8:0 (1:4:0)
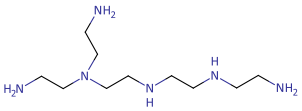	3	4	3	3:4:3
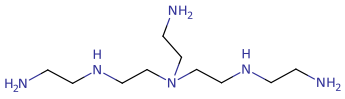	3	4	3	3:4:3
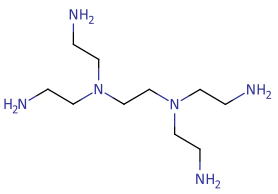	4	0	6	4:0:6 (2:0:3)

Arbitrarily, if the mixture was assumed to be composed of a 1:1:1:1 mixture of each isomer, the ratio of carbon atoms next to primary, secondary and tertiary amines would be 12:16:12 (primary:secondary:tertiary), or 0.75:1.00:0.75. Integration of the ^{13}C spectrum gave a ratio of 0.50:1.00:0.78, suggesting more secondary and tertiary amines were present than for a 1:1:1:1 mixture. Multiple attempts were made to assign this spectrum and to determine the true ratio based on the integrals, including using excel to create and then solve equations to fit the data, to no success.

ESI-MS evidence was especially indicative of the impurities observed in the amine starting material. The major peak observed in the ESI-MS spectrum corresponds to the desired mass for the named amine, which could correspond to both the desired linear amine as well as any branched isomers. Peaks were also evident for the amines with additional or fewer -CH_2-CH_2-NH- units (Figure 2.7, Figure 2.8) which again were likely composed of linear and branched isomers. In addition to this, signals consistent with piperazine compounds were also able to be detected. These originated from the reaction to form the polyamine and formed as a by-product, more detail of which can be seen in Figure 2.9, Figure 2.10 and Figure 2.11 below. The piperazine compounds formed during the synthesis of the polyamine would have had a different molecular mass to the equivalent polyamine compound by 28 $gmol^{-1}$, and many such signals were located in the mass spectrum for the amine starting material (Figure 2.7).

Terminal piperazines would reduce the number of primary amines while increasing the number of tertiary amines, while central piperazines decrease the number of secondary amines in favour of tertiary amines. Presence of these compounds would also explain the complexity of the NMR spectrum as there are multiple isomers depending on the position of the piperazine moiety.

A final class of side products may be present in the reaction mixture, adding further complexity to the starting material. Cyclic versions of the polyamines may have also been present in the reaction however, their presence was difficult to determine as the cyclic compounds of the linear amines are isomers of the piperazine compounds. The linear piperazine compounds were assumed to be present as piperazine compounds with multiple piperazine groups or the isomeric cyclic piperazine compounds were detected, showing that piperazines can be formed. Additionally, in later sections, the compounds of piperazine masses were seen to react with naphthalic anhydride which was not likely to be possible if the mass was entirely composed of cyclic compounds unless they contained multiple branches.

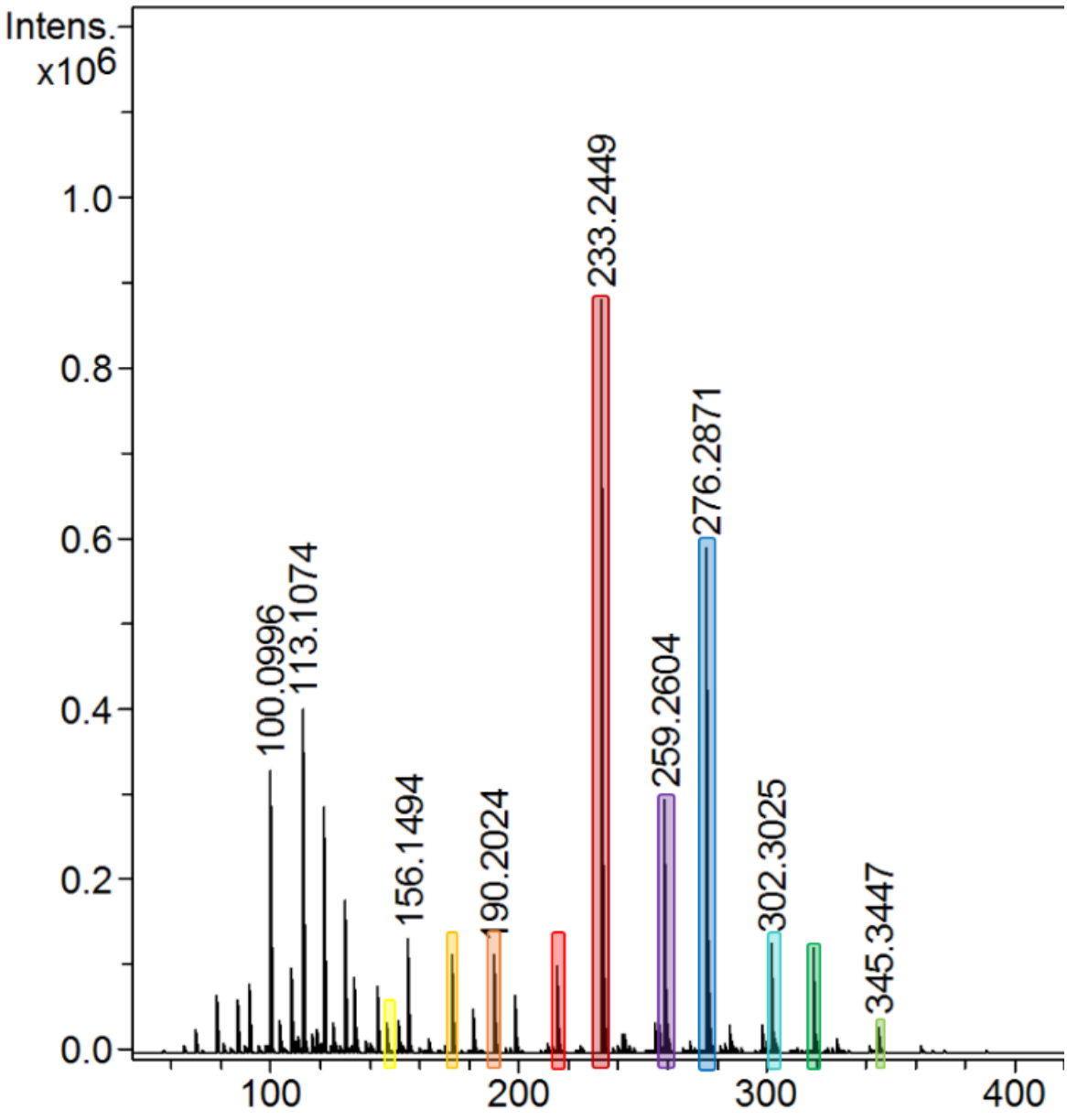

Figure 2.7: ***ESI-MS spectrum of the starting material amine, with peaks colour coded to correspond to the species identified in*** **Figure 2.8.** ***The peaks that are not labelled on this spectrum for clarity have been identified and their assignment given in*** **Figure 2.8.**

.

$C_6H_{18}N_4$	$C_8H_{20}N_4$	$C_8H_{23}N_5$	$C_{10}H_{25}N_5$	$C_{10}H_{28}N_6$
147.1604	**173.1759**	**190.2024**	**216.2181**	**233.2449**
(147.1610, 0.04)	(173.1761, 0.13)	(190.2032, 0.13)	(216.2183, 0.22)	(233.2454, 1.0)
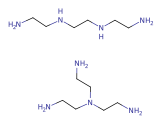	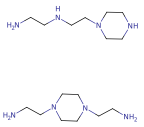	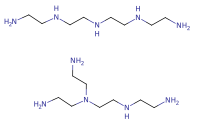	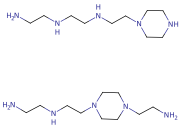	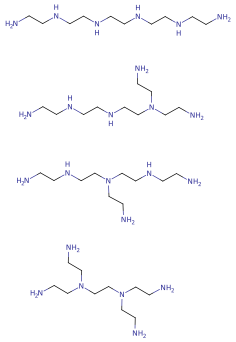

$C_{12}H_{30}N_6$	$C_{12}H_{33}N_7$	$C_{14}H_{35}N_7$	$C_{14}H_{38}N_8$	$C_{16}H_{40}N_8$
259.2604	**276.2871**	**302.3025**	**319.3292**	**345.3447**
(259.2610, 0.52)	(276.2875, 0.66)	(302.3032, 0.18)	(319.3292, 0.14)	(345.3454, 0.04)
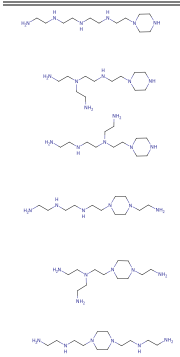	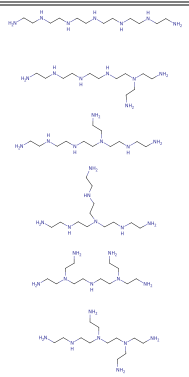	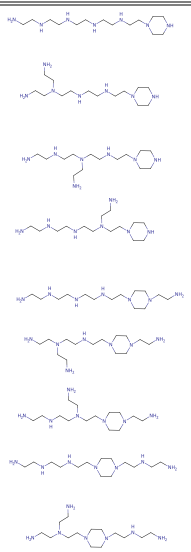	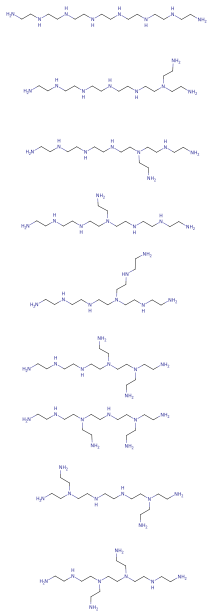	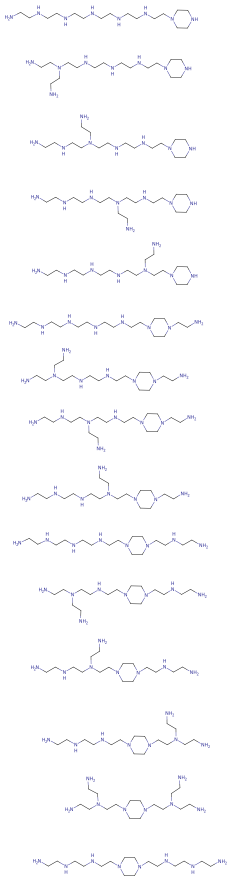

Figure 2.8: ***The top rows show the masses and formulae of identified compounds present in the reaction mixture, with the observed mass in bold and colour coded and the predicted mass and relative intensity (compared to the desired mass) in brackets. The isomers matching that mass and formula is then shown in the columns beneath the mass. Note: the isomers shown may not be exhaustive of all the isomeric possibilities. Cyclic species including improbable larger macrocycles are not shown.***

The peaks corresponding to the masses of free amines were not normally detected following reaction, indicating the presence of cyclic compounds may be unlikely. Additional expansion of the ESI-MS results for the crude ligand synthesis, focussing on the 0-250 m/z region, would potentially identify any trace amine corresponding to the cyclic species following reaction. Branched cyclic species on the other hand would have had the potential to react with naphthalic anhydride so presence or lack of masses corresponding to the free amine in the spectrum would not be able to confirm whether these cyclic compounds exist.

The relative intensities assigned to the piperazine compounds above therefore cannot be identified as corresponding entirely to the piperazines nor to the cyclic compounds, however, due to the inability for cyclic compounds to react as observed and the presence of cyclic piperazines these peaks were assigned as piperazines for simplicity. This was not an assumption that the entire peak was composed of the piperazines, but rather a way to highlight the compounds that were able to react in the reactions performed in this work and were therefore of interest to this study. ESI-MS peaks corresponding to compounds potentially containing either a piperazine moiety and cyclic character or multiple piperazine moieties indicated that the piperazine compounds existed in the mixture (Table 2.17).

Table 2.17: *Cyclic piperazine derivatives detected in the ESI-MS spectrum of the amine starting material. These may also correspond to linear molecules containing two or three piperazine groups, respectively.*

Compound	Identity	m/z	Predicted m/z	Relative Intensity
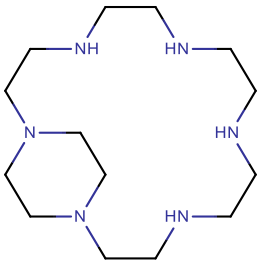	Cyclic hexamine with one piperazine moiety, or linear hexamine with two piperazines	143.1415 2+	143.1422 2+ for $C_{14}H_{33}N_6$	0.09
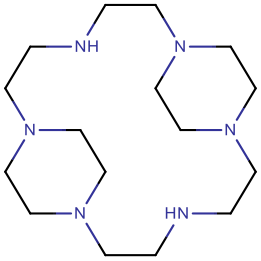	Cyclic hexamine with two piperazine moieties, or linear hexamine with three piperazines	156.1494	156.1501 2+ for $C_{16}H_{35}N_6$	0.15

The amine chosen, 3,6,9,12-tetraazatetradecane-1,14-diamine, was identified by both NMR and ESI-MS as having many impurities present. To understand where these impurities may have originated from, the method of producing this amine was researched in the literature. The amine was likely produced through one of the following methods, as the majority of commercial ethyleneamines were produced in this way (in 2005 it was reported that 65% of commercial amines were produced using the EDC method)[77-78]:

1. EDC (ethylene dichloride) method (Figure 2.9). This method involves reacting 1,2-dichloroethane with ammonia, producing 1,2-disubstitutedalkanes of varying lengths *via* a nucleophilic substitution. The more 1,2-dichloroethane that is added, the greater the number of -CH_2CH_2NH- units in the final molecules. The mixture that is produced will contain a large mix of amines of different molecular weights based on the number of repeated units. The reaction also produces HCl as a side product which is neutralised with NaOH. The nucleophilic substitution unfortunately favours formation of both linear and branched products as the nucleophilicity of primary and secondary and amines are similar, with the trend generally being that secondary amines are more nucleophilic than primary unless they are substantially sterically hindered. Therefore, branched products are likely to form. As these have the same molecular mass, they will be difficult to separate from each other, as well as from the similar mass compounds with extra units.[79]

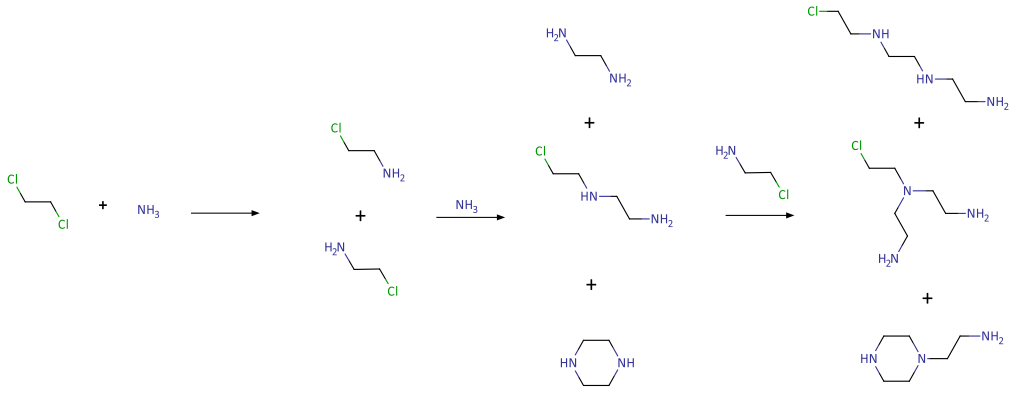

Figure 2.9: ***Summary of the EDC method for production of ethylene amines, showing common products and their subsequent reaction products, including piperazine and branched side products.***

2. MEA/RA (monoethanolamine reductive amination) method (Figure 2.10). 2-Aminoethan-1-ol is oxidised using a nickel hydrogenation/dehydrogenation catalyst to give 2-aminoethanal. This then reacts with either ammonia or existing amines to produce an amine which then undergoes hydrogenation to give the product amine.

Again, this method is capable of producing various longer amines including branched compounds.[80]

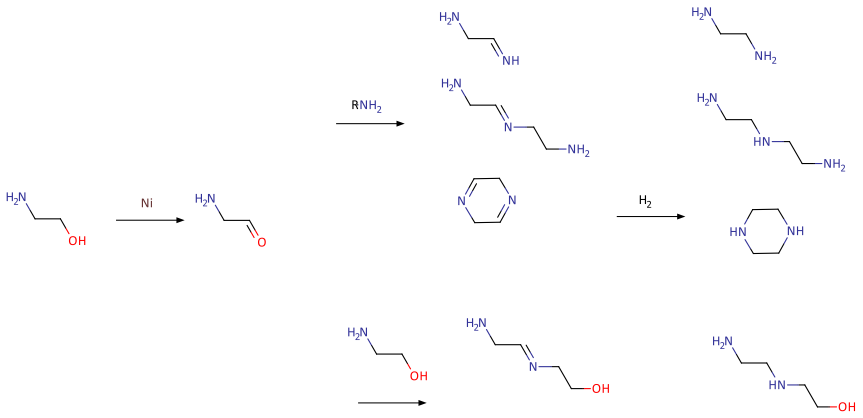

Figure 2.10: ***Summary of the MEA/RA method for production of ethylene amines, showing common products and their subsequent reaction products, including piperazine and branched side products.***

3. Ethylene oxide method (Figure 2.11). This method is less commonly used, however, reacts following a similar process to the MEA/RA method. Ethylene oxide is reacted with ammonia to produce 2-aminoethan-1-ol, which then reacts further to give ethyleneamines[77]. This also produces 2,2'-azanediylbis(ethan-1-ol) and 2,2',2''-nitrilotris(ethan-1-ol), along with the branched side products.

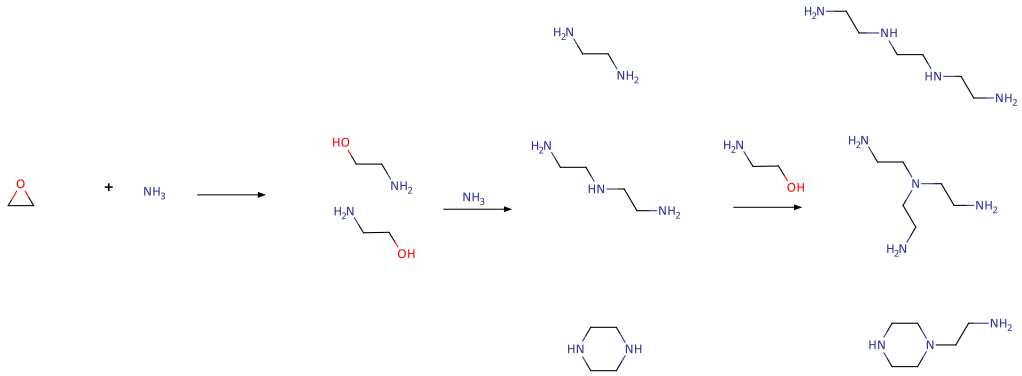

Figure 2.11: ***Summary of the ethylene oxide method for production of ethylene amines, showing common products and their subsequent reaction products, including piperazine and branched side products.***

In these syntheses and in the syntheses using other less common methods, the resulting mixture is then fractionally distilled in attempt to isolate the amines of different molecular weights from each other.[78, 81]

All three methods involve reacting ethyleneamine compounds with additional units, essentially building the amines from $-CH_2CH_2NH-$ units. For an amine composed of five of these units, as for the desired compound, there are four possible isomers: a linear polyamine, an asymmetric

monobranched polyamine, a symmetric monobranched polyamine, and a dibranched polyamine. The method used to produce the ethyleneamines is also used to produce piperazine which is a common side product in the reaction to produce linear polyamines.[78] Piperazine forms when two molecules of 1,2-dichloroethane react with one molecule of ammonia each as well as reacting together to form a ring. The piperazine product can then react further to become longer chain piperazine derivatives.

The fractional distillation process to separate the resulting mixture into different components was not completely effective, leaving many of the compounds of different masses in the fraction containing the desired compound along with isomers of the same mass. Synthesis of the ligand based on this polyamine mixture was likely to produce a similarly broad range of compounds.

Attempts have been made to purify this amine outside of the direct scope of this work, including silica column chromatography using triethylamine to prevent smearing by deactivating the silica. The column was then run using DCM:Methanol 9:1 through to 4:1. Some separation into a number of bands was observed on TLC yet the NMR spectra of fractions showed separation was incomplete. Direct complexation to copper followed by Sephadex column chromatography was also attempted by mixing the amine starting material with copper sulfate and loading this onto a Sephadex column. Elution gave some appearance of banding with a large amount of smearing. This again resulted in a mixture of compounds in the fractions collected.

Given the complexity of the mixture, any attempt to purify the amine will be difficult and it was unsurprising that these attempts were unsuccessful. Future work surrounding purification of this amine could include further distillation of the amine or synthesis of the naphthalimide directly. Direct synthesis of the desired linear amine has not been attempted to date due to the prospect of generating a similarly complicated mixture of compounds to the purchased chemical. If the synthesis were attempted it could be performed using aminoethane-1-ol, reacting with naphthalic anhydride, activating the alcohol and reacting this with pure 3,6-diazaoctane-1,8-diamine (Figure 2.12). This may still result in branched molecules forming which may be able to be separated based on their large difference in mass from the naphthalimide groups.

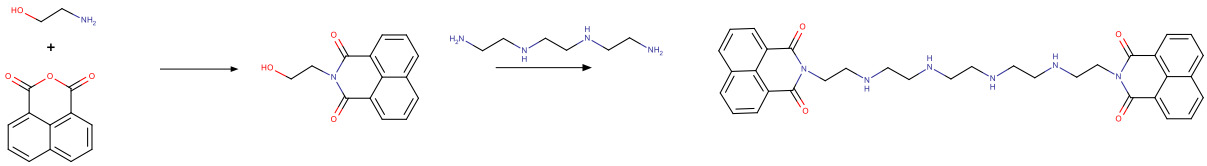

Figure 2.12: ***Future work proposal. Isomeric possibilities and side products not shown.***

2.4.2. Crude Ligand Material

After attempts to purify the amine were unsuccessful, effort was focussed instead on separating the desired naphthalimide compound 2.1 from the crude ligand mixture following the reaction of the amine with naphthalic anhydride. This was a logical approach not only because of the inability to separate free amine, but also due to the observation that mononaphthalimide, dinaphthalimide and trinaphthalimide products can all form simultaneously from the synthesis and purification would therefore be required anyway.

The mechanochemical procedure was an adaption of one described by Arya *et al* and involves directly grinding aromatic anhydrides with primary amines in a mortar and pestle for ten minutes, achieving a yield of approximately 90%.[82] The method by Arya *et al* was performed to synthesise mono- and diimides from primary amines and 9,10-dihydroanthracene-9,10-a,b-succinic anhydride, a reaction similar to that described in this work in that the primary amine was reacted with a bulky anhydride to form imides. This method was preferred over the solvent-reflux method described by Braña *et* al in their synthesis of compound 2.1 as the mechanochemical procedure can be performed in greater quantities, in shorter time scales and was a greener chemistry approach with less work up than the solution-based method. This was because the lack of solvent allows for easy handling of greater amounts of starting materials without the added hazard of the bulk solvent. The reaction duration was shorter, going from hours at reflux to minutes of mechanochemistry. Additionally, the work up involved was quick drying of the powdery sample rather than concentration *in vacuo*, recovery from the vessel and subsequent drying of the oily product that resulted when the reaction was performed in this fashion. Reactions at reflux were attempted and the range of impurities was not observed to decrease by ESI-MS (with emphasis placed on the presence of the mononaphthalimide species) and therefore the solvated procedure was abandoned.

A series of experiments were conducted in which the stoichiometry of the starting materials was varied in attempts to obtain product richer in the desired compound. It was found that side products were always a substantial contaminant of the desired product, however, the nature of these side products varied with the stoichiometric ratio. The method was adjusted to use a slight excess of naphthalic anhydride, approximately a 1:3 molar ratio as opposed to the stoichiometric 1:2. The method was also adjusted to include the use of a small volume of chloroform to aid mixing.

The stoichiometry of the reaction was tailored to prevent the formation of the mononaphthalimide product 2.2 even though this increased production of the product where a

third naphthalic anhydride group had reacted (Figure 2.16). This was because the impurity produced with an additional naphthalene moiety was likely to be more easily separated from the others through their poorer complexation with copper (See Section 2.4.3). As the mononaphthalimide was likely to be a good ligand it would not be separated from the desired compound during the copper complexation technique used to purify, while the molecules with additional naphthalimides potentially could be.

The mass of crude material gained from this reaction was generally slightly greater than the mass of the starting materials used. The material was allowed to dry before weighing and use to allow evaporation of the chloroform used and the water generated in the synthesis, however, the increased mass suggests that the water was retained by the material and that the material may be hygroscopic despite its low solubility in water. Further possibilities include reactions with carbon dioxide in the air. Products from such reactions were not observed.

Multiple different compounds were detected by ESI-MS (Figure 2.13), and of these compounds, all had multiple possible isomers. As a result, the complexity of the mixture cannot be fully determined by ESI-MS. The discussion will focus instead on the group of isomers described by the mass detected, with some discussion surrounding the isomers that may be present. The compounds detected include mono-, di- and trinaphthalimide and naphthalamide products of the piperazine tetramine, pentaamine, piperazine pentaamine, hexamine, piperazine hexamine, heptamine and piperazine heptamine compounds. The distribution observed was also similar to that of the starting material, with the largest peaks corresponding to the hexamines and the piperazine derived hexamine products.

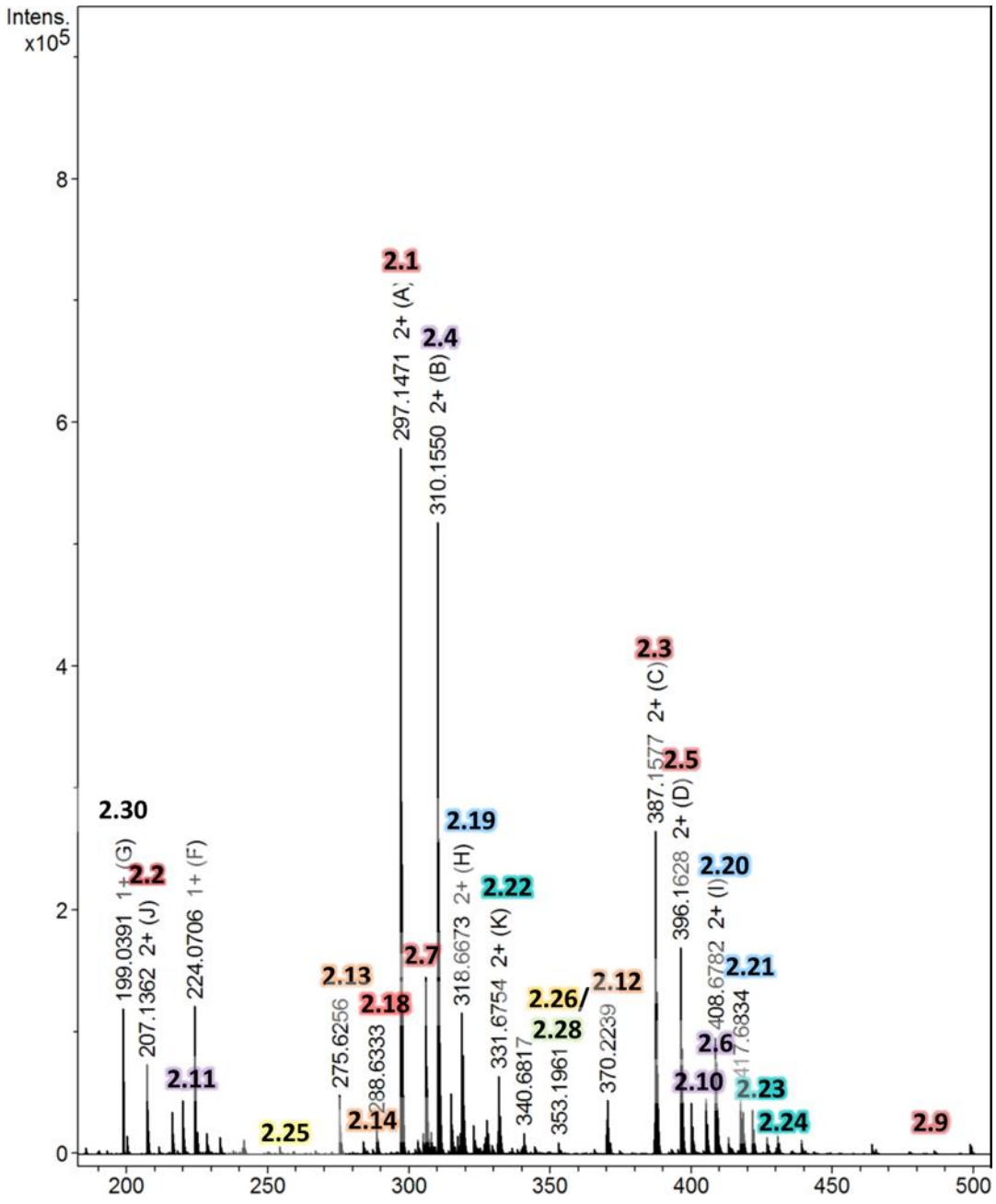

Figure 2.13: ***ESI-MS spectrum showing different compounds detected following reaction of the amine with naphthalic anhydride. These compounds have been assigned and labelled with both the compound number and the colour of the amine that would yield this compound as per Figure 2.7.***

The NMR information collected on the crude synthetic product also indicates a complex mixture, even in the poor-quality spectra which were able to be obtained. There were peaks in the ^{13}C NMR spectrum (Figure 2.14) characteristic of carbon atoms adjacent to primary (36-38 ppm), secondary (44-47 ppm) and tertiary (51-54 ppm) nitrogen atoms. The peaks were in different locations to the free amine, which may be due to the solvent difference or the peaks of the

aromatic carbons but was likely due to the different environments of the nitrogen atoms (including both the addition of naphthalimides and their electronic effects as well as changes to overall symmetry). The aromatic carbon atoms would likely show as peaks past 100 ppm. Of note was the presence of peaks that may correspond to carbon atoms next to primary nitrogen atoms, as this would imply that there were branched isomers that did not have naphthalimide attached to every terminal nitrogen atom.

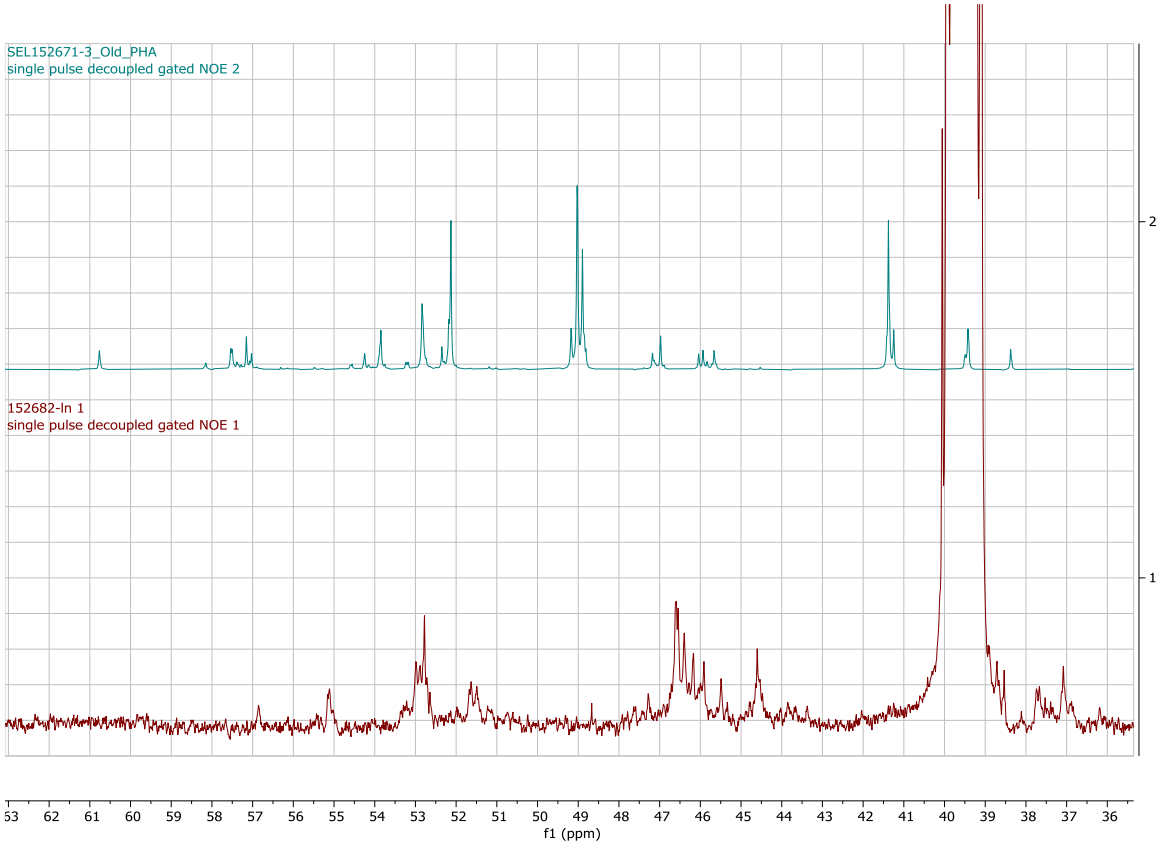

Figure 2.14: ***^{13}C NMR spectrum of the alkyl region of the crude material alongside the free amine (top) and crude ligand mixture (lower).***

The ^{1}H NMR spectrum (Figure 2.15) showed a ratio of 6:18 aromatic:alkyl protons when integrated, with 9 protons of these appearing as an amine region and 1 removed for the solvent. The expected ratio, based on reaction stoichiometry, would be 6:9.33 for unreacted material, 6:8 for dinaphthalimide material with unreacted additional anhydride and 6:7.33 for trinaphthalimide material. This decrease was due to the loss of protons on the nitrogen atoms as imide formation occurred. The ratio from the NMR appeared to be more complex as it did not correspond to any ratio above, likely due to overlap of the amine peak with alkyl protons or presence of water.

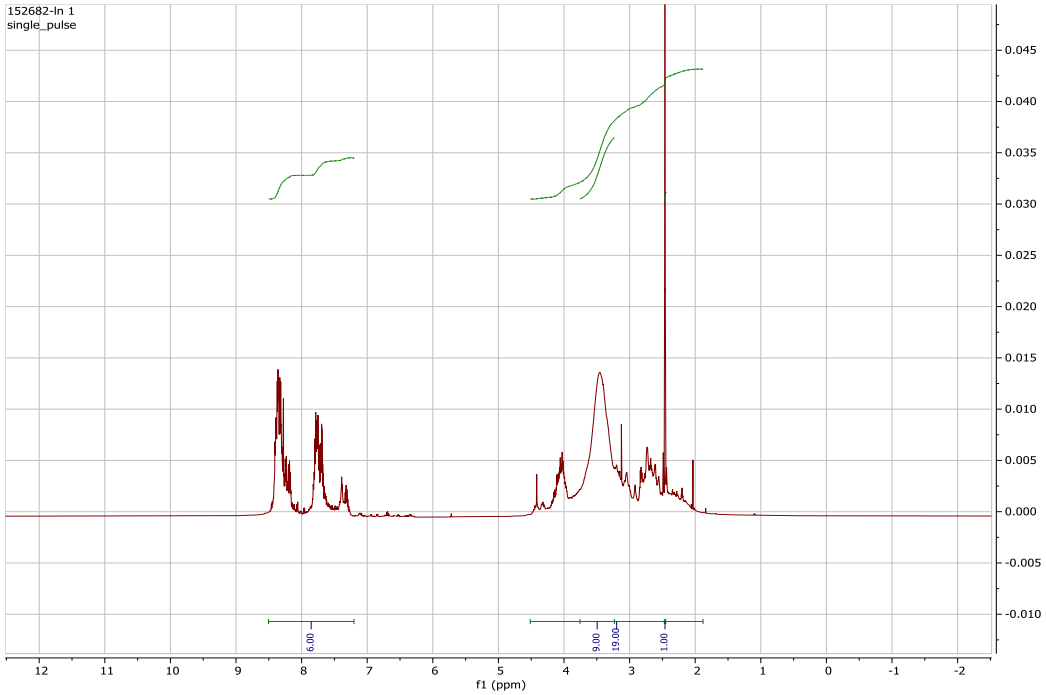

Figure 2.15: ***^{1}H NMR spectrum of the crude ligand material, showing the overlap and complexity of the peaks, which were not able to be fully assigned. Integrations of the aromatic and alkyl regions of the spectrum are also shown. Spectra of drier material was not able to be obtained.***

Despite the issues surrounding the complexity of this mixture, the ESI-MS analyses highlighted the presence of the desired compound mass in high amounts. This indicated that the intended dinaphthalimide of the hexamine and the related isomers are substantial components of the crude reaction material. As observed in Table 2.1, the composition as detected by ESI-MS varies between syntheses, suggesting that there is some level of inconsistency in the product even when produced identically.

2.4.3. Purification by Complexation

The synthesis of the ligand produced a range of compounds due to the low purity of the amine starting material. The products of these impurities may have had fewer available donor atoms than the desired compound (Figure 2.16). As a result, they would have had a lower coordinative ability than the desired compound and would be outcompeted for coordination in the presence of limited metal availability. As the chelate theory predicts, the more nitrogen atoms with free lone pairs in the molecule, the better the ligand will be. Considering only the molecules derived from the linear and mono-branched hexamine, the mononaphthalimide ligand 2.2 will form the most thermodynamically favourable complex, followed by the dinaphthalimide **2.1**, followed by the dinaphthalimide ligand with additional amide substitution 2.5. This means it was possible that the mixture where excess anhydride was used will be able to be purified by complexation.

This is because the additionally substituted ligands would have been unlikely to coordinate in favour of the desired product, and therefore the complex and the residual starting material mixture can be separated to yield the copper complex of the desired product. The only better ligand depicted (2.2) was unlikely to be present in the crude material due to the excess naphthalic anhydride used encouraging its conversion to the dinaphthalimide species.

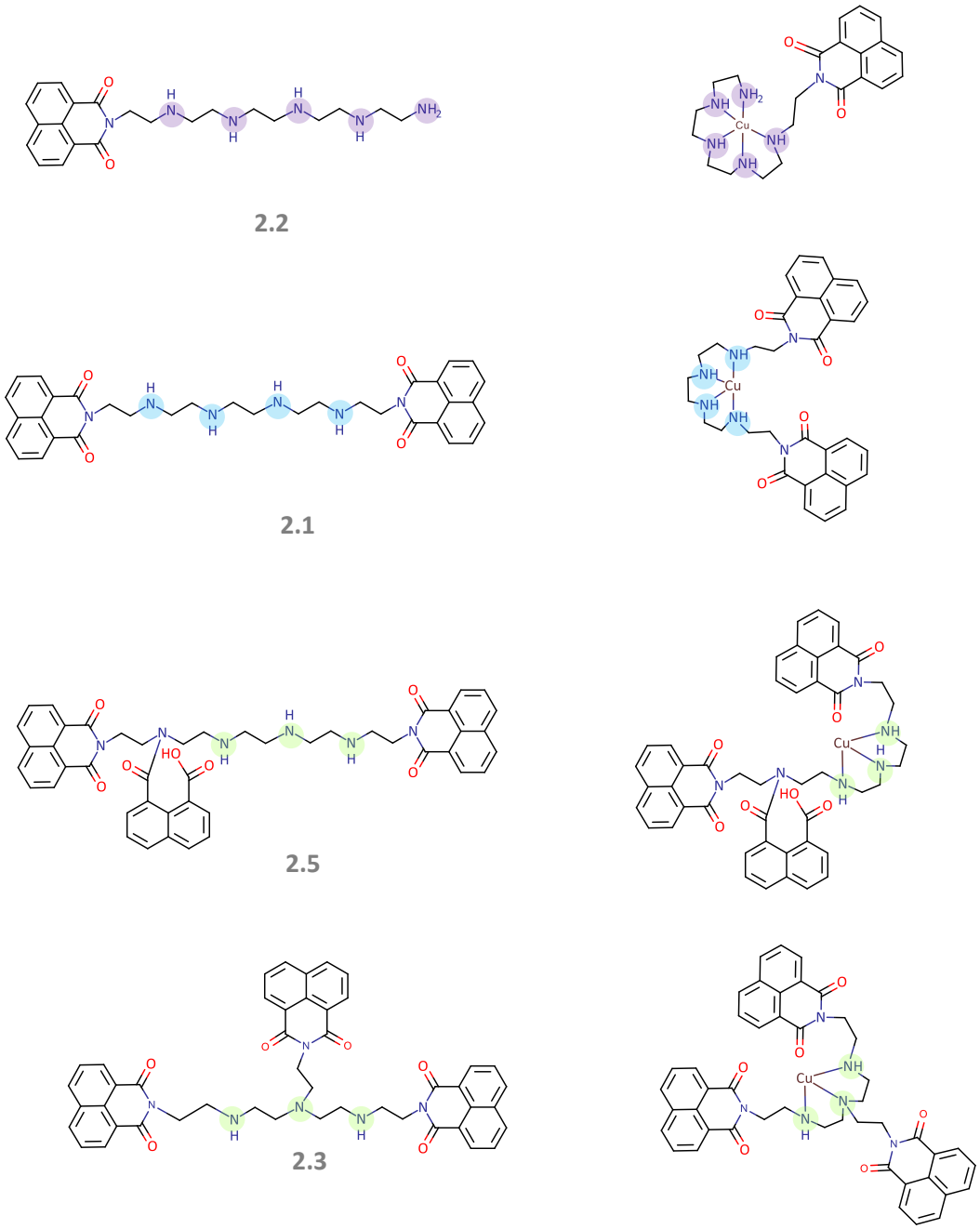

Figure 2.16: ***Compounds 2.1, 2.2, 2.3 and 2.5 are shown (left) with their copper complexes (right). The figure also shows the number of coordination sites for coordination to metal centres and the predicted complexes of these compounds with copper (right). Note that the coordination geometry and ligand isomer is shown as a simplification and there are many possible options.***

For the piperazine compounds, the piperazine moiety reduces the strength of some donor atoms. This is due to the geometry required for the piperazine compound to coordinate. The piperazine moiety is a six membered ring and will therefore be most stable in a chair orientation (Figure 2.17). In this orientation, the lone pair of electrons on the nitrogen atoms are oriented in different directions to each other, meaning that it is not possible for both nitrogen atoms to coordinate to the same metal while in the chair geometry. The piperazine group must adopt a boat-like conformation to coordinate both nitrogen donors to the metal centre. This of course comes with a reduction in stability due to the ring strain of the boat conformation, so the piperazine derivative was likely to be a poorer ligand than the equivalent linear compound.

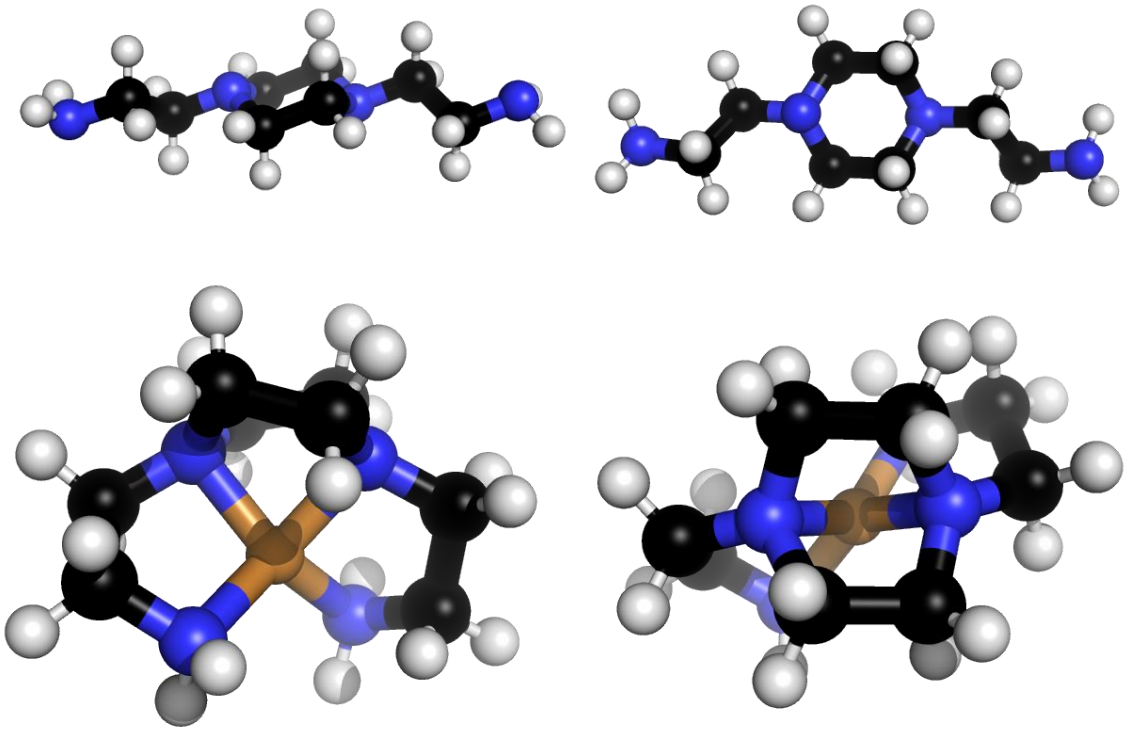

Figure 2.17: ***The most favourable orientation for the piperazine moiety both free (above) and coordinated (below). This highlights the difference in the orientation, with the left side showing the distortion from chair form to boat upon coordination, and the right showing the distortion to the hexagonal shape of the ring when viewed from above the plane of the ring.***

Unfortunately, the purification by complexation strategy will not allow for elimination of the longer side products as these will be better ligands than the desired compound due to their available donor atoms for coordination. None of the purification attempts to date have been able to overcome this issue.

2.4.3.1. Purification by Complexation Reaction Stages

The process of purification by complexation, as seen in the flowcharts in Sections 2.2.6 and Appendix A, involved taking the crude ligand material and reacting it with copper at a less than stoichiometric ratio under reflux. The crude ligand mixture of the desired compound and side products was dissolved in methanol and the copper salt added as a solution. This was intended to produce a complexation product of the copper centre with the best ligands available, ideally the desired ligand, and the remaining side products would hopefully stay in solution unchanged. Following separation of the complexation product from the unreacted side products, the complexation products were reacted with EDTA to remove the copper and leave the free ligand behind. It was expected that the complexation product from the previous step would produce an aqueous solution of the copper EDTA complex and the desired ligand would precipitate for collection. In this way, the desired compound could be separated from the side products.

The complexation reaction produced a solid and a liquor, with the solid containing the greater proportion of the desired complex Cu(2.1), which was detected as up to 68% and an average of 41% of the complexation solid (Table 2.18; see the table for the explanation on how percentages were calculated). This result represents an enrichment compared to the crude product, which had a maximum composition of 41% and average of 31% desired ligand, 2.1. This reaction then led to further enrichment as this solid was treated with EDTA, leading to a solution that had a maximum composition of 69% and mean of 51% desired ligand, 2.1. This aqueous fraction was still contaminated with undesired side products, and the attempted extraction with chloroform to collect the desired compound led to removal of much of the undesired side products and a subsequent enrichment of the desired compound 2.1. This enrichment in the remaining solution following extraction was observed as a maximum composition of 85% and a mean of 63%. It was evident that the desired compound can be enriched during this process by comparison to the crude material.

Unfortunately, the phase in which the greatest enrichment was observed by ESI-MS (aqueous phase in Section 2.2.6.3) contained substantial Cu(EDTA) presence, meaning the true enrichment is not known. Attempts to separate these species through anion exchange chromatography led to some separation, yet the fractions collected retained some blue colour indicating that complex was still present. The purity of the recovered fractions also appeared to decrease, with a lower percentage composition for the desired compound once the solution had been run through the column (Table 2.11 and Table 2.13). The reason for this is unknown.

The solid produced during the same reaction (Section 2.2.6.3) as the aqueous phase just described also demonstrated an increased enrichment compared to crude material. While this

increase was overall not as substantial, increasing by only a few percent, in the reaction described in Section 2.2.6.3 the increase in enrichment was the same for both the solid and the aqueous phases. This suggests that the solid could also be used as although the enrichment was not as great, the bulk of the material ended up in this phase. Additionally, even though the enrichment was not as great in some cases, the phase considered more enriched was determined to be so based on numbers which excluded the substantial Cu(EDTA) side product present within that phase. As such, the enrichment is likely much lower than calculated.

A discussion around each fraction of the reaction following the purification by complexation protocol as discussed in the experimental section, followed by a discussion on the individual variations made to the method and their consequences, can be found in Appendices C and D.

Table 2.18: *Summary of results tables, showing the percentage composition values of the desired compound, based on relative intensities by ESI-MS as per the results tables. The columns show the percentage composition for the desired compound in each fraction, and the rows show the iteration of the reaction. The penultimate row shows the mean value of the percentage compositions and the final row shows the range. Where the desired compound was the free ligand, the mean is highlighted in green, and where the desired compound was the copper complex the mean is highlighted in blue.*

	Crude Ligand	Complex Solid	Complex Liquor	Cooling Solid	Solid EDTA Solid	Solid EDTA Solution	Liquor EDTA Solid	Liquor EDTA Solution	Solid EDTA Solution $CHCl_3$ Extract	Solid EDTA Solution Post $CHCl_3$
33% Aqueous Copper (Appendix B.1)	41	12	9	16	4	23	39	2		
33% Methanolic Copper (Appendix B.2)	27	61	12	10	7	54	6	4		
33% Methanolic Copper Repetition (Appendix B.3)	29	38	14	14	14	38	15	9	21	50
40% Methanolic Copper (Appendix B.4)	29	44	14	20	25	69	7	14	10	52
40% Methanolic Anhydrous Copper (Appendix B.5)	19	68	14		17	61	3	4	21	84
40% Methanolic Copper 3.5x Scale (Appendix B.6)	19	39	16		23	67	15	10	11	85
40% Methanolic Copper 7.5x Scale (Table 2.15)	38	22	27	67	44	44	8	11	6	44
Mean	**31***	**41**	**15**	**25**	**19**	**51**	**13**	**8**	**14**	**63**
Maximum and Minimum values (range)	19 to 41 (22)	12 to 68 (56)	9 to 27 (18)	10 to 67 (57)	4 to 44 (40)	23 to 69 (46)	3 to 39 (36)	2 to 14 (12)	6 to 21 (15)	44 to 85 (41)

*As this column includes duplicates from experiments that used the same starting material, the mean value excludes these duplicates, taking each value once.

2.4.3.2. Variations to the Purification by Complexation method

Many variations to the method were made in attempts to refine the process towards fractions with the greatest enrichment of the desired ligand. The method described in this chapter was

the final method used during this work and appeared to give the greatest enrichment of the desired compound.

From the results obtained from these experiments, it appeared that using aqueous copper sulfate resulted in little to no enrichment when compared to crude material by ESI-MS, while switching to methanolic addition of copper sulfate increased the enrichment. Additionally, switching from 33% stoichiometric to 40% stoichiometric copper also resulted in an increased enrichment to the desired compound in various reaction fractions. The use of anhydrous copper as opposed to the pentahydrate appeared to have increased the enrichment, but the poor solubility of the anhydrous copper in methanol made this method substantially more difficult to accurately perform and reproduce. Future work surrounding the use of the pentahydrate in a larger reaction volume to recreate the concentration of the anhydrous reaction may produce interesting results as the increased reaction volume may have been the true reason for this increased enrichment (See the Appendix D subsection on the pentahydrate versus anhydrous copper for more).

The results from this process show that, while enrichment of the desired compound was achieved, this was at the substantial detriment of the yield. As such, it was difficult to determine which of the variations described was most successful and further work around repetition of the methods would need to be performed. The greatest overall enrichment of the desired compound was observed in the post chloroform extraction solution of the EDTA treated complexation solid from the 40% methanolic copper reaction performed on 3.5x scale (Appendix B.6), however, as identified above this aqueous fraction contained predominantly the Cu(EDTA) complex and so the true enrichment is unknown. Additionally, lack of repetitions makes it difficult to comment fully on which method was best.

The methods and results for these variations can be found in Appendix A, and a further discussion surrounding the impact of the variations can be found in Appendix D.

2.4.4. Conclusions

During this study, a polyamine mixture containing a multitude of related ethyleneamines was reacted with naphthalic anhydride in the attempt to synthesise a dinaphthalimide tetradentate ligand for use in dinuclear complex syntheses. While this compound was synthesised, a range of other compounds were also detected due to the other amines present in the starting material. Purification by complexation was applied to attempt to separate out the desired compound from the by-products. This strategy was approached as the various naphthalimide side products were likely to have different properties which might allow them to be separated. This included

the theory that the majority of the side products were likely to be poorer ligands than the desired compound.

During this study enrichment and isolation of the desired complex was achieved to a much greater enrichment than in the crude material. This occurred through the collection of the solid precipitate following complexation and subsequent treatment with EDTA (Figure 2.18). The enriched compound was detected in the solution following the EDTA treatment. While this then gave reasonably enriched material (as judged by ESI-MS) through both anion exchange chromatography and through precipitation from water, the reaction was very low yielding and much of the desired compound was lost to other fractions during the work up. As such, future work should be attempted to optimise the quantity of the material recovered, not just the quality.

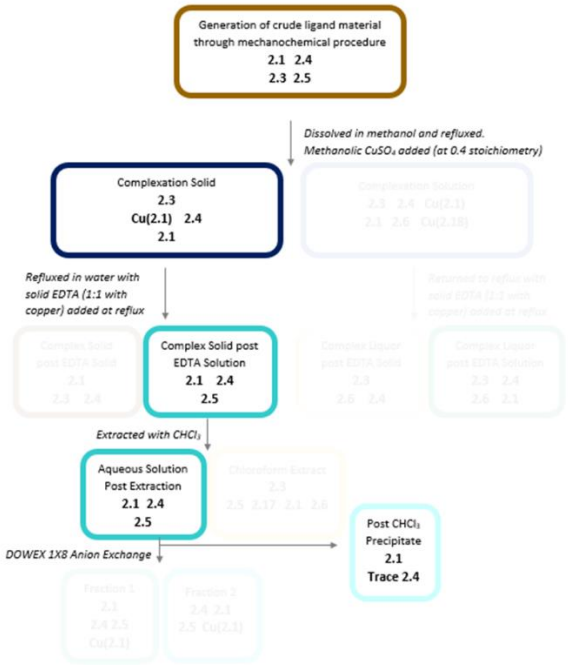

Figure 2.18: ***The flowchart from* Figure 2.4 *modified to highlight the path to the material that showed the greatest enrichment of the desired compound 2.1.***

Through the experiments where variables surrounding the copper were altered, the reaction conditions were able to be somewhat refined. It became evident that methanolic addition of a 40% stoichiometric solution of copper sulfate pentahydrate was the best set of conditions trialled for this reaction and resulted in the greatest enrichment of the compound compared to the side products. Repeated experimentation showed that the process was fairly reproducible and that the process was able to be scaled up.

Chapter 3: *Cobalt Complexes*

3.1. Introduction

The intention of this project was to synthesise a heterodinuclear anticancer drug by coupling cobalt(III) and platinum(II) centres. As described in Section 1.3, the dinuclear complex was designed to act as a prodrug of cisplatin, retaining its anticancer efficacy once activated. The cobalt centre, as in Sections 1.4 and 1.5, is to be coupled to the platinum centre to give the platinum anticancer centre increased selectivity. The desired ligand 2.1 was designed to physically block the interactions on the platinum centre that. Led to complex degradation.

The tetradentate ligand synthesised in Chapter 2 would form a complex with cobalt(III) that leaves two vacant coordination sites. To allow for the water ligands ultimately required for dinuclear complex synthesis, carbonate and nitrite ligands were chosen as candidates for this work (as seen in Section 1.5). Literature examples of tetradentate amine complexes of cobalt(III) with both nitrite and carbonate ligands are known, as are studies where these ligands are subsequently replaced by other ligands. [83, 84, 85, 86, 87, 88]

To form these complexes the cobalt centre must first be complexed to nitrite or carbonate ligands, forming $[Co(NO_2)_6]^{3-}$ or $[Co(CO_3)_3]^{3-}$ complexes, which are then reacted with the tetradentate ligand. Many tetradentate amine ligand complexes have been synthesised in this manner, such as in the syntheses of complexes $[Co(cyclam)(NO_2)_2]^+$, $[Co(dimethylcyclam)OCO_2]^+$, $[Co(trpyn)OCO_2]^+$, $[Co(pmea)OCO_2]^+$, $[Co(abap)OCO_2]^+$ and $[Co(trien)(NO_2)_2]^+$ (Figure 3.1). In these syntheses, the cobalt(III) complex is first formed followed by ligand exchange of either NO_2^- or CO_3^{2-} ligands for the tetradentate amines. The yields of these complexes range from 18% to 81%, with the lowest percentage corresponding to formation of crystals of a compound that turned out to be a dinuclear complex. In general, these syntheses appear to be relatively high yielding, producing sufficient material to allow for further reaction steps as desired. As a result, similar strategies were employed within this work.

(dimethylcyclam = meso-5,12-dimethyl-1,4,8,11-tetraazacyclotetradecane; trpyn = tris(2-(1-pyrazolyl)ethyl)amine); pmea = bis(2-pyridylmethyl)-2-(2-pyridylethyl)amine; abap = N-(2-Aminoethyl)-N-(3-aminopropyl)-1,3-propanediamine; trien = triethylenetetramine).

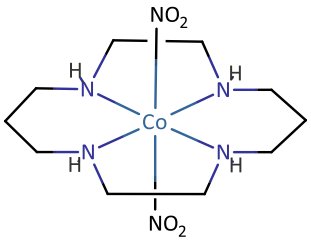

$[Co(cyclam)(NO_2)_2]^{+}$ [83]

Yield: Not given

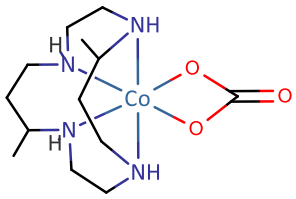

$[Co(dimethylcyclam)OCO_2]^{+}$ [84, 85]

Yield: 65%

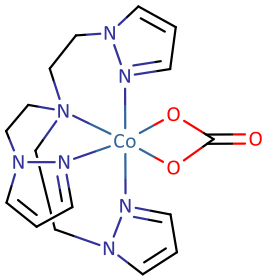

$[Co(trpyn)OCO_2]^{+}$ [86]

Yield: 24%

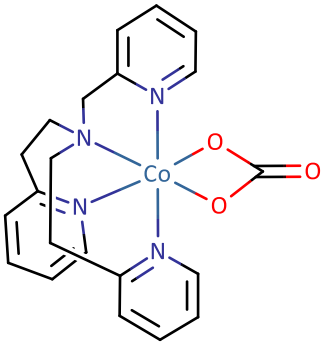

$[Co(pmea)OCO_2]^{+}$ [86]

Yield: 18% as $ZnCl_3$ dinuclear complex

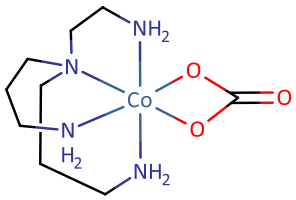

$[Co(abap)OCO_2]^{+}$ [87]

Yield: 50%

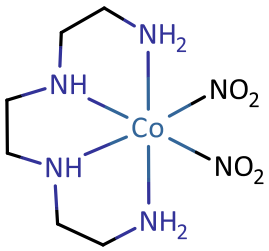

$[Co(trien)(NO_2)_2]^{+}$ [88]

Yield: 81%

Figure 3.1: ***Tetramine complexes of cobalt(III), synthesised by displacement of NO_2^- or CO_3^{2-} ligands with the tetradentate ligand.***

3.2. Experimental

Cobalt starting materials were purchased and used directly. The ligands used were synthesised as previously described. General methods and procedures can be found in Sections 2.2.1-2.2.5.

3.2.1. $[Co(C_{34}H_{36}N_6O_4)(CO_3)]^+$ from crude ligand material as produced in Section 2.2.6.1

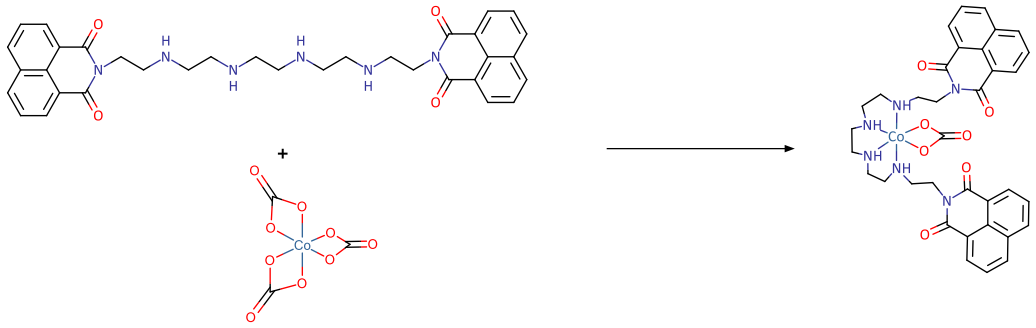

Carbonato(3-(14-{2,4-dioxo-3-azatricyclo[7.3.1.0^{5,13}]trideca-1(13),5,7,9,11-pentaen-3-yl}-3,6,9,12-tetraazatetradecan-1-yl)-3-azatricyclo[7.3.1.0^{5,13}]trideca-1(13),5,7,9,11-pentaene-2,4-dione)cobalt(III)

Following the method by Mori and Douglas[89], cobalt chloride ($[Co(OH_2)_6]Cl_2$, 3.2 g 13.4 mmol) was dissolved in distilled water (3.2 mL) and hydrogen peroxide (2 mL, 30 %) added. A separate solution of potassium bicarbonate ($KHCO_3$, 6.4 g 63.9 mmol) in distilled water (6.4 mL) was placed on a magnetic stirrer in a beaker and the cobalt chloride solution added dropwise with stirring over the course of thirty minutes. The colour change observed was from pink to a deep green solution immediately with formation of a deep green precipitate over time.

While the cobalt solution was being added to the potassium bicarbonate solution, crude tetradentate ligand **2.1** ($C_{34}H_{36}N_6O_4$, 8.0 g 13.5 mmol) was added to methanol (125 mL) in a 250 mL round bottom flask and brought to reflux by placing on a hot plate stirrer. Once at reflux, and the addition of cobalt solution to potassium bicarbonate solution was completed, the resulting green mixture was added to the methanolic ligand solution. The beaker was rinsed with distilled water (2 mL) which was also added to the mixture at reflux. The resulting mixture was then heated with stirring for 20 hours to give a burgundy solution with some deep green solid. The solid was then removed by filtration while the mixture was still warm. Upon cooling, the liquor produced an oily burgundy solid (m.p. 89-96 °C) with the liquor remaining burgundy. The liquor was then decanted from the oil and placed in the refrigerator overnight.

Analysis of Solid:

Mass: [M +H^+] 1+: *m/z* 711.1986 1+ (Predicted 711.1977). Not the major peak, major peaks assigned to side products from the ligand material (including 387.1570 2+, assigned as 2.3 predicted 387.1583 2+ for $C_{46}H_{42}N_6O_6$).

IR: 1696 (m), 1655 (s), 1621 (m), 1586 (s), 1512 (w), 1437 (w) 1377 (m), 1343 (s), 1290 (w), 1234 (s), 1170 (m).

See results for analysis of other phases (Section 3.3.1, Appendix E).

3.2.2. $[Co(C_{34}H_{36}N_6O_4)(CO_3)]^+$ using enriched ligand material from Section 2.2.6.5

This reaction was performed as per Section 3.2.1 with the following amendments:

- $[Co(OH_2)_6]Cl_2$ (0.1 g, 0.42 mmol) was dissolved in distilled water (0.5 mL) and 30% hydrogen peroxide (0.25 mL) added.
- Potassium bicarbonate ($KHCO_3$ 0.2 g) was dissolved in distilled water (0.5 mL)
- The cobalt chloride solution added dropwise with stirring over the course of five minutes
- enriched tetradentate ligand **2.1** ($C_{34}H_{36}N_6O_4$, 0.25 g 0.42 mmol) was added to methanol (25 mL) in a 50 mL round bottom flask
- The beaker from the cobalt carbonato synthesis was rinsed with distilled water (0.5 mL) which was also added to the refluxing solution.

Difference in the results obtained between the methods include the substantially reduced detection of ligand side products and lack of formation of an oil following cooling of the reaction liquor.

Analysis of Solid:

Mass: [M +H^+] 1+: *m/z* 711.1986 1+ (Predicted 711.1977 for $[Co(C_{34}H_{36}N_6O_4)(CO_3)]^+$). Not the major peak, major peak 325.1013 2+ (assigned as 3.3, predicted 325.1026 2+ for $[Co(C_{34}H_{35}N_6O_4)]^{2+}$)

See results for analysis of other phases (Section 3.3.1, Appendix E).

3.2.3. $[Co(C_{34}H_{36}N_6O_4)(NO_2)_2]^+$ from crude ligand material produced as in Section 2.2.6.1 (excess cobalt)

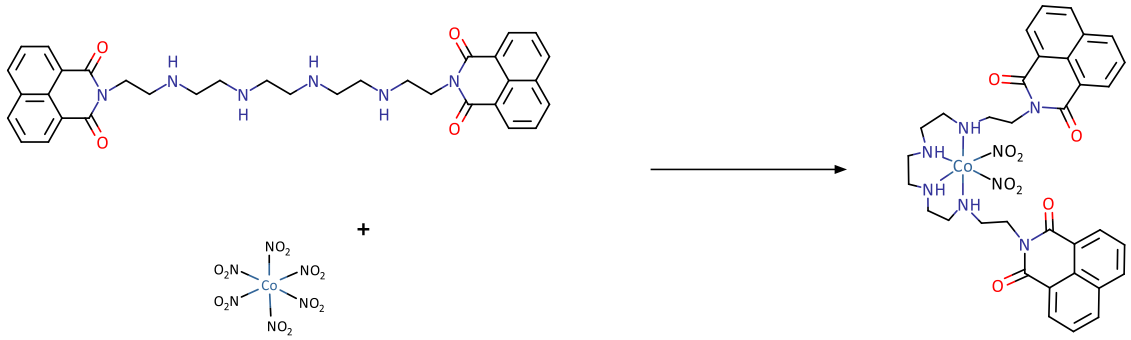

Dinitrito(3-(14-{2,4-dioxo-3-azatricyclo[7.3.1.0^{5,13}]trideca-1(13),5,7,9,11-pentaen-3-yl}-3,6,9,12-tetraazatetradecan-1-yl)-3-azatricyclo[7.3.1.0^{5,13}]trideca-1(13),5,7,9,11-pentaene-2,4-dione)cobalt(III)

Cobalt nitrate ($Co(NO_3)_2{\cdot}6H_2O$, 1.00 g 3.5 mmol) was dissolved in water (10 mL) and stirred into a solution of potassium nitrite (KNO_2, 2.00 g, 24.4 mmol) dissolved in water (15 mL). The resulting solution was stirred for 30 minutes at 70°C. Acetic acid (50 % v/v, 3.25 mL 27 mmol) was added and the slurry allowed to settle overnight. This slurry was then filtered and the solid collected.

A solution of crude tetradentate ligand 2.1 ($C_{34}H_{36}N_6O_4$, 1.00 g 1.7 mmol) dissolved in methanol (20 mL) was brought to reflux using a hotplate stirrer. This recovered solid (mass unknown as solid was used directly) was added to the solution in a single addition. The resulting mixture was heated at reflux and stirred overnight. Alternatively, sodium cobaltinitrite ($Na_3[Co(NO_2)_6]$ 1.9 g, 4.7 mmol) was dissolved in methanol used in place of the filtered product and reaction continued analogously. The reaction resulted in production of a yellowish precipitate and orange solution which was warm filtered to give bright yellow orange solid material that was visually indistinguishable from the $[Co(NO_2)_6]^{3-}$ starting material and was similarly soluble in water. ESI-MS analysis of this solid gave no assignable peaks, which was the same as was observed for the starting material. The filtrate yielded an orange-brown precipitate (0.1 g) once cooled in the fridge, which was then further characterised by IR, ESI-MS, and melting point. (m.p. 101-104 °C).

Analysis of solid from cooling overnight:

Mass: $[M+H^+]$ 1+: *m/z* 743.1990 1+ (Predicted 743.1983 1+ for $[Co(C_{34}H_{36}N_6O_4)(NO_2)_2]^+$ major peak)

IR: 1694 (m), 1651 (s), 1624 (m), 1587 (s), 1512 (w), 1460 (w), 1438 (w), 1412 (m, br), 1360 (m), 1342 (m), 1305 (m), 1235 (s)

See results for analysis of other phases (Section 3.3.1, Appendix E).

3.2.4. $[Co(C_{34}H_{36}N_6O_4)(NO_2)_2]^+$ from crude ligand material produced as in Section 2.2.6.1 (stoichiometric)

Sodium cobaltinitrite ($Na_3[Co(NO_2)_6]$ 5.45 g, 13.5 mmol) was added to a refluxing solution of tetradentate ligand 2.1 ($C_{34}H_{36}N_6O_4$, 8 g 13.5 mmol) dissolved in methanol (125 mL). This mixture was then heated at reflux and stirred for 19 hours. The reaction resulted in production of a brown, beige and orange precipitate and an orange solution which was warm filtered and refrigerated overnight to produce an orange oily solid.

Analysis of Oily Solid:

Mass: [M +H^+] 1+: *m/z* 743.1993 1+ (Predicted 743.1983 1+ for $[Co(C_{34}H_{36}N_6O_4)(NO_2)_2]^+$ minor peak, major peak was 387.1579 2+, assigned as 2.3 predicted 387.1583 2+ for $C_{46}H_{42}N_6O_6$)

See results for analysis of other phases (Section 3.3.1, Appendix E).

3.2.5. $[Co(C_{34}H_{36}N_6O_4)(NO_2)_2]^+$ using enriched ligand material from Section 2.2.6.5 (stoichiometric)

Purified tetradentate ligand 2.1 ($C_{34}H_{36}N_6O_4$, 0.25 g 0.42 mmol) was dissolved in methanol (25 mL) in a 50 mL round bottom flask and brought to reflux. Sodium cobaltinitrite ($Na_3[Co(NO_2)_6]$ 0.17 g, 0.42 mmol) was added as a solid and washed into the solution using methanol. The orange mixture was heated for 19 hours and resulted in production of a pale blue precipitate, a yellow orange precipitate and orange solution which was warm filtered.

Analysis of Orange Solid:

Mass: [M +H^+] 1+: *m/z* 743.1991 1+ (Predicted 743.1983 1+ for $[Co(C_{34}H_{36}N_6O_4)(NO_2)_2]^+$ minor peak, major peak was 325.1031 2+, assigned as 3.3 predicted 325.1026 2+ for $[Co(C_{34}H_{35}N_6O_4)]^{2+}$)

See results for analysis of other phases (Section 3.3.1, Appendix E).

3.3. Results

Figure 3.2 shows the cobalt complexes discussed further in this chapter.

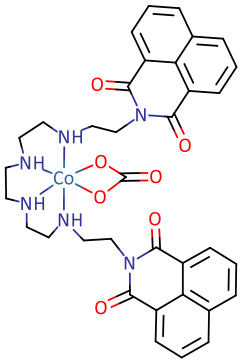

3.1: $[Co(2.1)CO_3]^+$ complex, 711.1984 1+ (predicted 711.1977 1+ for $[Co(C_{34}H_{36}N_6O_4)CO_3]^+$)

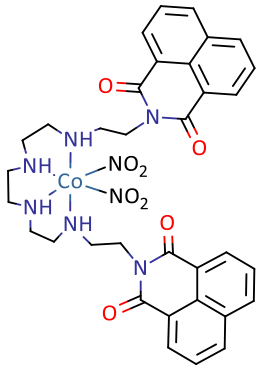

3.2: $[Co(2.1)NO_2]^+$ complex, 743.1991 1+ (predicted 743.1989 1+ for $[Co(C_{34}H_{36}N_6O_4)(NO_2)_2]^+$)

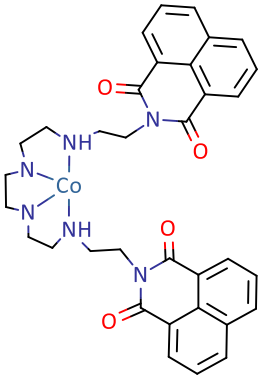

3.3: $[Co(2.1\ -2H^+)]^{2+}$ complex, 325.1009 2+ (predicted 325.1026 2+ for $[Co(C_{34}H_{35}N_6O_4)]^{2+}$)

Figure 3.2: ***These structures correspond to the structures discussed in this chapter. The structures are deliberately shown without geometry and as only one isomeric possibility, both for simplicity and because elucidation of these details was not achieved during this work.***

3.3.1. $[Co(C_{34}H_{36}N_6O_4)(CO_3)]^+$ Syntheses

3.3.1.1. ESI-MS of Synthesis using Crude Ligand

The following table summarises the ESI-MS results from the synthesis of $[Co(2.1)CO_3]^+$ using crude ligand material, as described in Section 3.2.1. The ESI-MS results are quoted as relative intensities which were calculated as per Chapter 2; by measuring the peaks and dividing each peak height by that of the major peak in the mixture. The percentage compositions of each fraction are given in the final row. The percentage composition was calculated as the percentage of the desired compound (2.1 in the first column, $[Co(2.1)CO_3]^+$ in the following three columns) compared to the major products of the reaction, 2.1, 2.3, 2.4, 2.5 and $[Co(2.1)CO_3]^+$. The free ligand 2.1 is highlighted in green, and the $[Co(2.1)CO_3]^+$ complex is highlighted in lavender.

Table 3.1: *ESI-MS results for the synthesis of $[Co(C_{34}H_{36}N_6O_4)(CO_3)]^+$ using crude ligand material.*

Identity	m/z	Predicted m/z	Relative Intensity			
			Crude Ligand	Solid	Liquor	Cooling Solid
[**2.30**+1H⁺] 1+	199.0394 1+	199.0395 1+ for $C_{12}H_7O_3$	0.31		0.12	
[**2.2**+2H⁺] 2+	207. 2+	207.1372 2+ for $C_{22}H_{40}N_6O_2$	0.15			
[**2.25**+2H⁺] 2+	254.1036 2+	254.1055 2+ for $C_{30}H_{28}N_4O_4$		0.01		
[**2.13**+2H⁺] 2+	275.6259 2+	275.6266 2+ for $C_{32}H_{33}N_5O_4$	0.10	0.02		0.03
[**2.18**+2H⁺] 2+	288.6330 2+	288.6345 2+ for $C_{34}H_{35}N_5O_4$				0.03
[**2.1**+2H⁺] 2+	297.1470 2+	297.1477 2+ for $C_{34}H_{38}N_6O_4$	1.0		0.05	
[**2.4**+2H⁺] 2+	310.1549 2+	310.1556 2+ for $C_{36}H_{40}N_6O_4$	0.93	0.20	1.0	0.23
[**2.7**+2H⁺] 2+	306.1520 2+	306.1558 2+ for $C_{34}H_{40}N_6O_4$	0.59			
[Co(**2.1**)]⁺-H⁺	325.1011 2+	325.1026 2+ for $[Co(C_{34}H_{35}N_6O_4)]^{2+}$		0.05		0.06
[**2.15**+2H⁺] 2+	365.6359 1+	365.6372 2+ for $C_{44}H_{35}N_5O_6$				0.02
[**2.12**+1H⁺] 1+	370.2235 2+	370.2243 1+ for $C_{20}H_{28}N_5O_2$	0.07			
[**2.3** +2H⁺] 2+	387.1568 2+	387.1583 2+ for $C_{46}H_{42}N_6O_6$	0.71	1.0	0.37	1.0
[**2.5**+2H⁺] 2+	396.1623 2+	396.1636 2+ for $C_{46}H_{44}N_6O_7$	0.77	0.12	0.07	
[**2.20**+2H⁺] 2+	408.6776 2+	408.6794 2+ for $C_{48}H_{47}N_7O_6$	?0.37?		0.12	0.14
[**2.21**+2H⁺] 2+	417.6829 2+	417.6847 2+ for $C_{48}H_{49}N_7O_7$	0.28			
[**2.23**+2H⁺] 2+	421.6852 2+	421.6872 2+ for $C_{50}H_{49}N_7O_6$		0.09		
[Co(**2.1**)CO_3]⁺	711.1974 1+	711.1977 1+ for $[Co(C_{34}H_{36}N_6O_4)CO_3]^+$		0.01	0.05	0.03
Percentage of desired compound in the fraction composition			29%	1%	3%	2%

3.3.1.2. ESI-MS of Synthesis using Enriched Ligand

The following table summarises the ESI-MS results from the synthesis of $[Co(2.1)CO_3]^+$ using crude ligand material, as described in Section 3.2.2. The ESI-MS results are quoted as relative intensities which were calculated as per Chapter 2; by measuring the peaks and dividing each peak height by that of the major peak in the mixture. The percentage compositions of each fraction are given in the final row. The percentage composition was calculated as the percentage of the desired compound (2.1 in the first column, $[Co(2.1)CO_3]^+$ in the following two columns) compared to the major products of the reaction, 2.1, 2.3, 2.4, 2.5 and $[Co(2.1)CO_3]^+$. The free ligand 2.1 is highlighted in green, and the $[Co(2.1)CO_3]^+$ complex is highlighted in lavender.

Table 3.2 *ESI-MS results for the synthesis of $[Co(C_{34}H_{36}N_6O_4)(CO_3)]^+$ using enriched ligand material.*

Identity	m/z	Predicted m/z	Relative Intensity		
			Crude Ligand	Solid	Liquor
[**2.1**+2H$^+$] 2+	297.1465 2+	297.1477 2+ for $C_{34}H_{38}N_6O_4$	1.0	0.04	1.0
[**2.4**+2H$^+$] 2+	310.1538 2+	310.1556 2+ for $C_{36}H_{40}N_6O_4$	0.12	0.05	0.88
[Co(**2.1**)]$^+$-H$^+$	325.1013 2+	325.1026 2+ for $[Co(C_{34}H_{35}N_6O_4)]^{2+}$		1.0	0.07
[Co(**2.1**)(OH)]$^{2+}$	334.1068 2+	334.1079 2+ for $[Co(C_{34}H_{36}N_6O_4)(OH)]^{2+}$		0.37	
[**2.12**+1H$^+$] 1+	370.2232 2+	370.2243 1+ for $C_{20}H_{28}N_5O_2$	0.09		
[**2.5**+2H$^+$] 2+	396.2388 2+	396.1636 2+ for $C_{46}H_{44}N_6O_7$			0.05
[Co(**2.1**)CO_3]$^+$	711.1981 1+	711.1977 1+ for $[Co(C_{34}H_{36}N_6O_4)CO_3]^+$		0.21	0.02
[Co(**2.1**)CO_3OH_2]$^+$	729.2101 1+	729.2083 1+ for $[Co(C_{34}H_{36}N_6O_4)(CO_3)(OH_2)]^+$		0.05	
Percentage of desired compound in the fraction composition			83%	16%	1%

3.3.2. $[Co(C_{34}H_{36}N_6O_4)(NO_2)_2]^+$ Syntheses

3.3.2.1. ESI-MS Results of the Synthesis using Crude Ligand Material (Excess Cobalt)

The following table summarises the ESI-MS results from the synthesis of $[Co(2.1)(NO_2)_2]^+$ using crude ligand material, as described in Section 3.2.3. The ESI-MS results are quoted as relative intensities which were calculated as per Chapter 2; by measuring the peaks and dividing each peak height by that of the major peak in the mixture. The percentage compositions of each fraction are given in the final row. The percentage composition was calculated as the percentage of the desired compound (2.1 in the first column, $[Co(2.1)(NO_2)_2]^+$ in the following three columns) compared to the major products of the reaction, 2.1, 2.3, 2.4, 2.5 and $[Co(2.1)(NO_2)_2]^+$. The free ligand 2.1 is highlighted in green, and the $[Co(2.1)(NO_2)_2]^+$ complex is highlighted in orange. See Figure 3.3 for a detailed analysis of the peak corresponding to $[Co(2.1)(NO_2)_2]^+$ in the ESI-MS spectrum.

Table 3.3: *ESI-MS results for the synthesis of $[Co(C_{34}H_{36}N_6O_4)(NO_2)_2]^+$ using crude ligand material and excess cobalt.*

Identity	m/z	Predicted m/z	Relative Intensity			
			Crude Ligand	Solid	Liquor	Cooling Solid
[**2.17**+2H⁺] 2+	198.6229 2+	198.6239 2+ for $C_{22}H_{31}N_5O_2$	0.40			
[**2.25**+2H⁺] 2+	254.1030 2+	254.1055 2+ for $C_{30}H_{28}N_4O_4$	0.29			
[**2.13**+2H⁺] 2+	275.6254 2+	275.6266 2+ for $C_{32}H_{33}N_5O_4$	0.55			
[**2.18**+2H⁺] 2+	288.6335 2+	288.6345 2+ for $C_{34}H_{35}N_5O_4$	0.14			
[**2.1**+2H⁺] 2+	297.1464 2+	297.1477 2+ for $C_{34}H_{38}N_6O_4$	0.92			
[**2.4**+2H⁺] 2+	310.1539 2+	310.1556 2+ for $C_{36}H_{40}N_6O_4$	1.0			
[**2.19**+2H⁺] 2+	318.6673 2+	318.6688 2+ for $C_{36}H_{43}N_7O_4$	0.57			
[Co(**2.1**)]⁺-H⁺	325.1020 2+	325.1026 2+ for $[Co(C_{34}H_{35}N_6O_4)]^{2+}$		1.0		
[**2.3** +2H⁺] 2+	387.1565 2+	387.1583 2+ for $C_{46}H_{42}N_6O_6$	0.07			
[**2.5**+2H⁺] 2+	396.2387 2+	396.1636 2+ for $C_{46}H_{44}N_6O_7$	0.15			
[**2.11**+2H⁺] 2+	439.2807 1+	439.2822 1+ for $C_{24}H_{35}N_6O_2$	0.11			
$[Co(\mathbf{2.12})(NO_2)_2]^+$	520.1346 1+	520.1355 1+ for $[Co(C_{20}H_{28}N_5O_2)(NO_2)_2]^+$			0.13	
Unknown	605.2519 1+	Unknown		0.32	0.19	0.14
Unknown	677.2844 1+	Unknown		0.82	0.23	0.25
$[Co(\mathbf{2.1})CO_3]^+$	711.1984 1+	711.1977 1+ for $[Co(C_{34}H_{36}N_6O_4)CO_3]^+$		0.56		
$[Co(\mathbf{2.1})(NO_2)_2]^+$	743.1987 1+	743.1989 1+ for $[Co(C_{34}H_{36}N_6O_4)(NO_2)_2]^+$		Not Detected	1.0	1.0
Percentage of desired compound in the fraction composition			43%	0%	100%	100%

Oily Solid IR: 1694 (m), 1651 (s), 1624 (m), 1587 (s), 1512 (w), **1460 (w)**, 1438 (w), **1412 (m, br)**, **1360 (m)**, **1342 (m)**, **1305 (m)**, 1235 (s)

Crude Ligand IR: 1694 (m), 1650 (s), 1621 (m), 1587 (s), 1513 (w), 1439 (m), **1375 (m)**, **1346 (s, br)**, 1237 (s)

The two IR spectra peaks indicate that while the complexation material contains peaks corresponding to the naphthalimide moiety of the free ligand, there were differences between the two spectra. Common peaks have been left as plain text while the peaks that exist in only one of the two spectra are bolded. This indicated that some new peaks were present, and some existing peaks had disappeared, in the non-fingerprint region of the complex IR spectra.

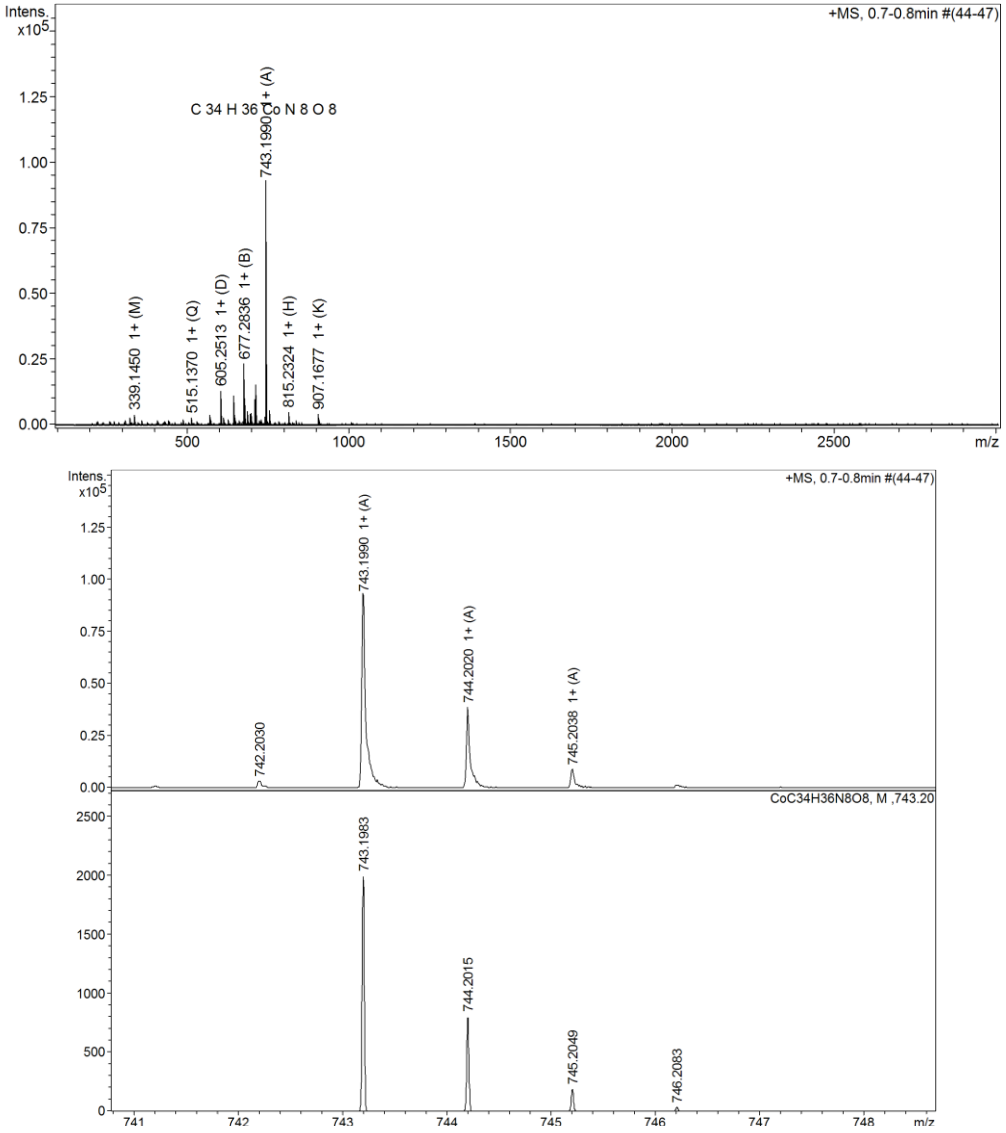

Figure 3.3: ***ESI-MS spectra showing the result of the synthesis of [Co($C_{34}H_{36}N_6O_4$)(NO_2)$_2$] (743.1990 1+, predicted 743.1993, top spectrum). The sample isotope pattern and mass values (middle) compare well to the prediction (bottom) for this sample.***

3.3.2.2. ESI-MS Results of the Synthesis using Crude Ligand Material (Stoichiometric)

The following table summarises the ESI-MS results from the synthesis of $[Co(2.1)(NO_2)_2]^+$ using crude ligand material, as described in Section 3.2.4. The ESI-MS results are quoted as relative intensities which were calculated as per Chapter 2; by measuring the peaks and dividing each peak height by that of the major peak in the mixture. The percentage compositions of each fraction are given in the final row. The free ligand 2.1 is highlighted in green, and the $[Co(2.1)(NO_2)_2]^+$ complex is highlighted in orange.

Table 3.4: *ESI-MS results for the synthesis of $[Co(C_{34}H_{36}N_6O_4)(NO_2)_2]^+$ using crude ligand material and stoichiometric cobalt.*

Identity	m/z	Predicted m/z	Relative Intensity						
			Crude Ligand	Brown Solid	Beige Solid	Orange Solid	Filter Oil	Liquor	Cooling Solid
[**2.30** +1H$^+$] 1+	199.0394 1+	199.0395 1+ for $C_{12}H_7O_3$	0.31	0.11	0.53	0.02	0.04		
[**2.2**+2H$^+$] 2+	207 2+	207.1372 2+ for $C_{22}H_{40}N_6O_2$	0.15						
[**2.13**+2H$^+$] 2+	275.6259 2+	275.6266 2+ for $C_{32}H_{33}N_5O_4$	0.10			0.02	0.13		
[**2.18**+2H$^+$] 2+	288.6329 2+	288.6345 2+ for $C_{34}H_{35}N_5O_4$				0.05		0.09	
[**2.1**+2H$^+$] 2+	297.1470 2+	297.1477 2+ for $C_{34}H_{38}N_6O_4$	1.0				0.18		
[**2.7**+2H$^+$] 2+	306.1520 2+	306.1558 2+ for $C_{34}H_{40}N_6O_4$	0.59						
[**2.4**+2H$^+$] 2+	310.1549 2+	310.1556 2+ for $C_{36}H_{40}N_6O_4$	0.93	0.25	0.27	0.45		1.0	0.13
[Co(**2.1**)]$^+$-H$^+$	325.1013 2+	325.1026 2+ for $[Co(C_{34}H_{35}N_6O_4)]^{2+}$		0.43	0.09		0.21		
[**2.12**+1H$^+$] 1+	370.2235 2+	370.2243 1+ for $C_{20}H_{28}N_5O_2$	0.07						
[**2.3** +2H$^+$] 2+	387.1565 2+	387.1583 2+ for $C_{46}H_{42}N_6O_6$	0.71	1.0	0.34	1.0	1.0	0.86	1.0
[**2.5**+2H$^+$] 2+	396.1623 2+	396.1636 2+ for $C_{46}H_{44}N_6O_7$	0.77		0.39	0.19	0.32	0.24	
[**2.20**+2H$^+$] 2+	408.6775 2+	408.6794 2+ for $C_{48}H_{47}N_7O_6$	?0.37?				0.45	0.15	
[**2.21**+2H$^+$] 2+	417.6829 2+	417.6847 2+ for $C_{48}H_{49}N_7O_7$	0.28						
[**2.9**+2H$^+$] 2+	486.1727 2+	486.1741 2+ for $C_{58}H_{48}N_6O_9$		0.10	0.09				
[Co(**2.1**)CO_3]$^+$	711.1984 1+	711.1977 1+ for $[Co(C_{34}H_{36}N_6O_4)CO_3]^+$		0.11		0.09		0.08	0.36
[Co(**2.1**)$(NO_2)_2$]$^+$	743.1993 1+	743.1989 1+ for $[Co(C_{34}H_{36}N_6O_4)(NO_2)_2]^+$		Not Detected	Not Detected	0.02	Not Detected	Not Detected	0.05
Percentage of desired compound in the fraction composition			29%	0%	0%	1%	0%	0%	4%

3.3.2.3. ESI-MS Results of the Synthesis using Enriched Ligand Material (Stoichiometric)

The following table summarises the ESI-MS results from the synthesis of $[Co(2.1)(NO_2)_2]^+$ using crude ligand material, as described in Section 3.2.5. The ESI-MS results are quoted as relative intensities which were calculated as per Chapter 2; by measuring the peaks and dividing each peak height by that of the major peak in the mixture. The percentage compositions of each fraction are given in the final row. The percentage composition was calculated as the percentage of the desired compound (2.1 in the first column, $[Co(2.1)(NO_2)_2]^+$ in the following columns) compared to the major products of the reaction, 2.1, 2.3, 2.4, 2.5 and $[Co(2.1)(NO_2)_2]^+$. The free ligand 2.1 is highlighted in green, and the $[Co(2.1)(NO_2)_2]^+$ complex is highlighted in orange.

Table 3.5: *ESI-MS results for the synthesis of $[Co(C_{34}H_{36}N_6O_4)(NO_2)_2]^+$ using enriched ligand material and stoichiometric cobalt.*

Identity	m/z	Predicted m/z	Relative Intensity			
			Crude Ligand	Blue Solid	Orange Solid	Liquor
[**2.18**+2H⁺] 2+	288.2903 2+	288.6345 2+ for $C_{34}H_{35}N_5O_4$		0.15		
[**2.1**+2H⁺] 2+	297.1465 2+	297.1477 2+ for $C_{34}H_{38}N_6O_4$	1.0			0.32
[**2.4**+2H⁺] 2+	310.1538 2+	310.1556 2+ for $C_{36}H_{40}N_6O_4$	0.12	0.43	0.39	0.24
$[Co(\mathbf{2.1})]^+ - H^+$	325.1009 2+	325.1026 2+ for $[Co(C_{34}H_{35}N_6O_4)]^{2+}$		1.0	1.0	1.0
[**2.12**+1H⁺] 1+	370.2232 2+	370.2243 1+ for $C_{20}H_{28}N_5O_2$	0.09			
$[Co(\mathbf{2.1})CO_3]^+$	711.1984 1+	711.1977 1+ for $[Co(C_{34}H_{36}N_6O_4)CO_3]^+$		0.13	0.23	0.27
$[Co(\mathbf{2.1})(NO_2)_2]^+$	743.1991. 1+	743.1989 1+ for $[Co(C_{34}H_{36}N_6O_4)(NO_2)_2]^+$		Not Detected	0.03	0.08
Percentage of desired compound in the fraction composition			83%	0%	2%	4%

3.3.3 Summary of Results

This chapter explores the synthesis and analysis of cobalt complexes of the tetradentate ligand 2.1, synthesised from both crude and enriched starting materials. The results have shown through the detection of the desired mass by ESI-MS that the desired complexes were synthesised. The $[Co(2.1)CO_3]^+$ complex, 3.1, was detected in all corresponding syntheses by ESI-MS as 711.1984 1+ (predicted 711.1977 1+ for $[Co(C_{34}H_{36}N_6O_4)CO_3]^+$), and the $[Co(2.1)(NO_2)_2]^+$ complex, 3.2, was detected in all corresponding syntheses as 743.1991 1+ (predicted 743.1989 1+ for $[Co(C_{34}H_{36}N_6O_4)(NO_2)_2]^+$).

While these compounds were detected, they were present in low amounts. Complexes were synthesised using both enriched and crude material to afford the desired product. Interestingly, the use of enriched material yielded purer complexes (as the crude ligand syntheses predictably resulted in the detection of ligand side products in the complexation mixture) yet the relative intensity of the desired complexes were still low. This was partially due to a substantial contaminant appearing in many spectra that would correspond to cobalt complexed to the

ligand after it had undergone a deprotonation; $[Co(2.1)]^{+}$ $-H^{+}$, 325.1026 2+ for $[Co(C_{34}H_{35}N_6O_4)]^{2+}$. This side product was discussed in more depth throughout the discussion and in Appendix F. The large peak of the 325 2+ mass in many spectra results in the desired complex peak appearing as a small peak relative to it, which indicated that the presence of the 325 2+ peak may be giving the desired compound peak a diminished appearance.

The appearance of free ligand in the complex syntheses, both using crude and enriched material, reinforces that the ligand may have had issues complexing whether it be due to the differing solubilities of the metal centre and the ligand or due to the steric effects of the pendant naphthalimide groups. This was not a surprising finding given that many syntheses were attempted before these complexes were successfully detected by ESI-MS. Further work into the optimisation of the complexation conditions should be pursued to encourage full ligand complexation. The excess free ligand indicated that further complexation may be possible, and increasing the cobalt content is one area in which optimisation could focus. Given that the best sample of any complex came from a synthesis with “excess” cobalt (Section 3.2.2), and only trace amounts of free ligand were detected in any of the phases by ESI-MS, this avenue should be the first to be explored further. Additional future work into complexes that have either smaller pendant groups or greater aqueous solubility is also desirable to pursue greater yields.

The following discussion around formation of these complexes will include relative intensity and percentage composition values as for the discussion of Chapter 2. As in Chapter 2, these values should be treated as a guide only as ESI-MS is a non-quantitative technique. Changes of relative intensity of two compounds relative to each other can be used to determine the conversion of starting material to product or purification of the desired compound. The differing abilities of compounds to ionise by ESI means that the percentage compositions cannot be taken as exact but rather must only be used to compare the difference fractions to determine which had the greatest presence of the desired compound versus side products. The percentage compositions were found from relative intensities, and therefore were calculated in the same way for each reaction fraction. In this way, a fraction with 10% of the composition identified as the desired complex can be compared to one with 5% composition to determine that the former contains a higher proportion of the desired compound, while the actual exact percentages remain unknown.

3.4. Discussion

3.4.1. Cobalt Carbonate Syntheses

Mass spectrometry showed presence of a peak corresponding to complex formation, 711.1984 1+ (predicted 711.1977 for $[Co(C_{34}H_{36}N_6O_4)CO_3]^+$); however, this was not a major peak. The predicted isotope pattern for this structure matched that seen in the native spectrum well (Figure 3.3). The highest relative intensity found during the reported work here was 0.21, corresponding to 16% of the composition being the complex (Table 3.1).

This solid was separated from the reaction liquor by hot filtration. The liquor itself was a clear burgundy solution that gradually became slightly opaque and forms an oil upon cooling. The liquor and the oil it produced were largely very similar, containing the desired compound along with side products from the crude ligand reaction. The oil had a slightly higher relative intensity of cobalt complexes when compared to the liquor. In both cases, side products from the ligand material represented the major peaks in the ESI-MS spectra.

The syntheses performed using crude ligand material produced the corresponding contaminated products, wherein the ligand side products were found in all phases of the reaction mixture. The synthesis using the enriched ligand material produced a less complicated ESI-MS spectra for each phase, however, free ligand remained in the solution indicating completion was incomplete.

There was also evidence of another complex in the fractions with the mass 325.1020 2+ and its pair at 649.1982 1+. This mass corresponds to $[Co(C_{34}H_{35}N_6O_4)]^{2+}$ and $[Co(C_{34}H_{34}N_6O_4)]^+$, which would be a complex of the desired compound to cobalt without additional ligands and deprotonated once and twice respectively (3.3). This complex was unexpected given the ESI-MS was run in positive ion mode which should favour protonation, yet the ESI-MS peak matched well to the assigned formula with the isotope pattern of the simulated and native spectra correlating well (Figure 3.4). Prediction software for this mass was also unable to find any other logical formula that matched this mass as well as the one given here.

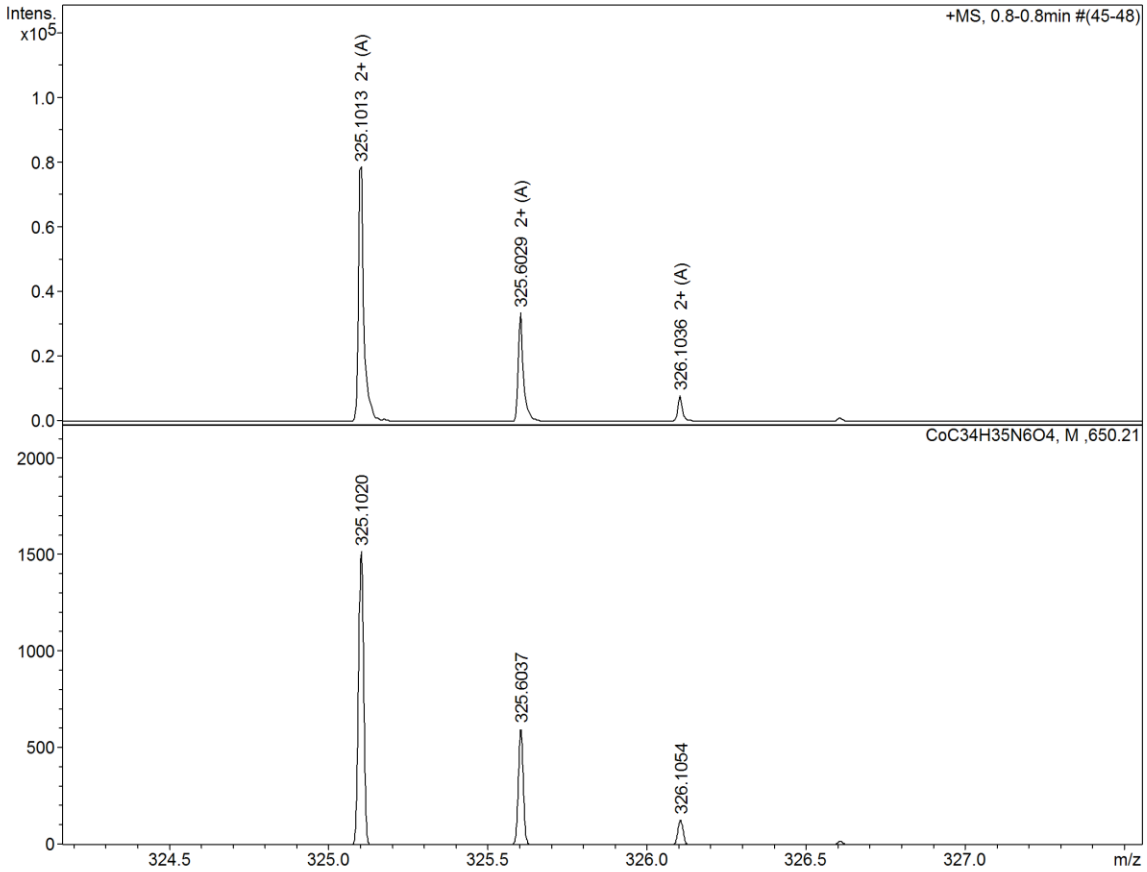

Figure 3.4: ***Native (above) and simulated (below) spectra for the 325.1013 2+ peak, showing the isotopic pattern match.***

To form a complex with this structure, it was possible that the amines within the molecule had become deprotonated. This could either be due to the other amines present in solution acting as bases, or due to the ESI process required to analyse the samples. It was unclear as to whether this species existed in solution or whether it formed in the process of analysing the sample. The structure of this species is difficult to determine as there are a few potential binding modes. The first involves the nitrogen atom of the imide acting as a donor atom, which is unlikely due to both the resonance of the naphthalimide and the steric bulk preventing the metal to be proximal to the nitrogen for coordination.

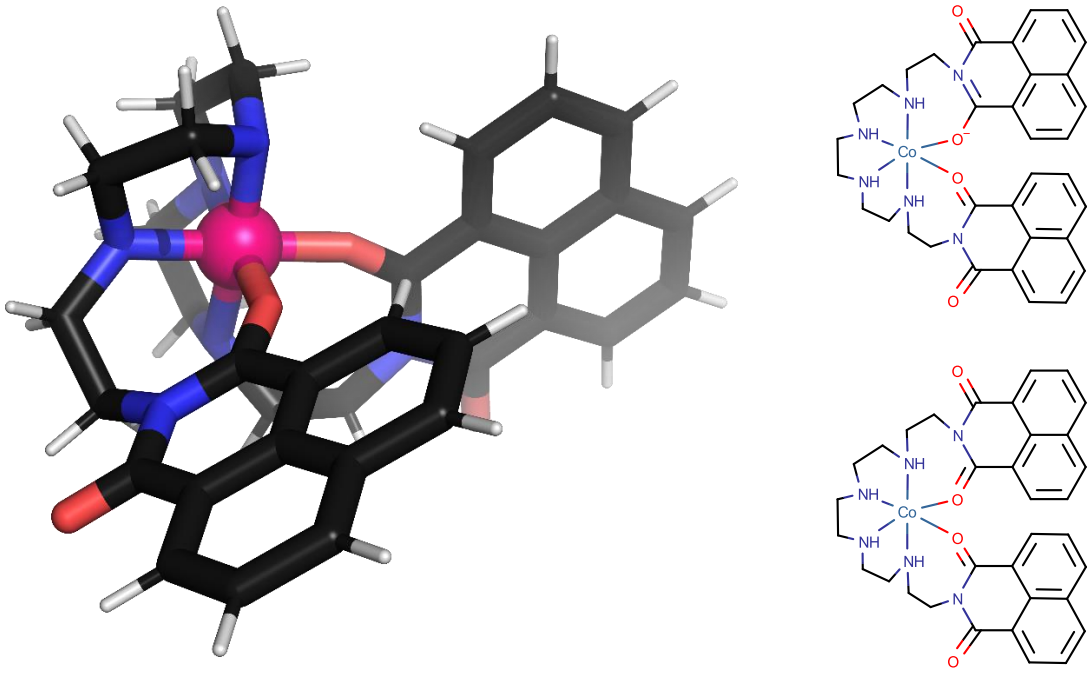

Figure 3.5: ***One proposed binding modes for the deprotonated ligand cobalt complex, showing coordination through the oxygen donor atoms in 3D (left) as an iminolate (upper 2D) or through lone pairs (lower 2D). Note that the deprotonation is not displayed in the lower 2D structure here as it is unclear where this would occur but is assumed to be an amine proton.***

A second option is through coordination to the lone pairs on the imide carbonyl groups, possibly as an iminolate (Figure 3.5). This would form a seven membered ring, and as such may be a poorer coordination mode. A naphthalimide structure bound through the oxygen donor atom is known, and the literature example forms an eight membered chelate ring indicating that the structure proposed here is feasible (Figure 3.6).

Another option would be a combination of these two binding modes with five total nitrogen donor atoms and one oxygen. Finally, it is possible but unlikely that the cobalt(III) centre was four coordinate. Such structures are known[90] and were formed through reactions in non-coordinating solvents with tetradentate ligands. The reaction solvent in this reaction contained both coordinating ions and was weakly coordinating so this is not as likely to have occurred in solution, but may have occurred in the largely solvent free environment of ESI-MS. It would be difficult to distinguish this compound from the desired complex visually as it would likely be pink or red if it contains a cobalt coordination sphere of four or five nitrogen donor atoms and one or two oxygen donor atom/s.

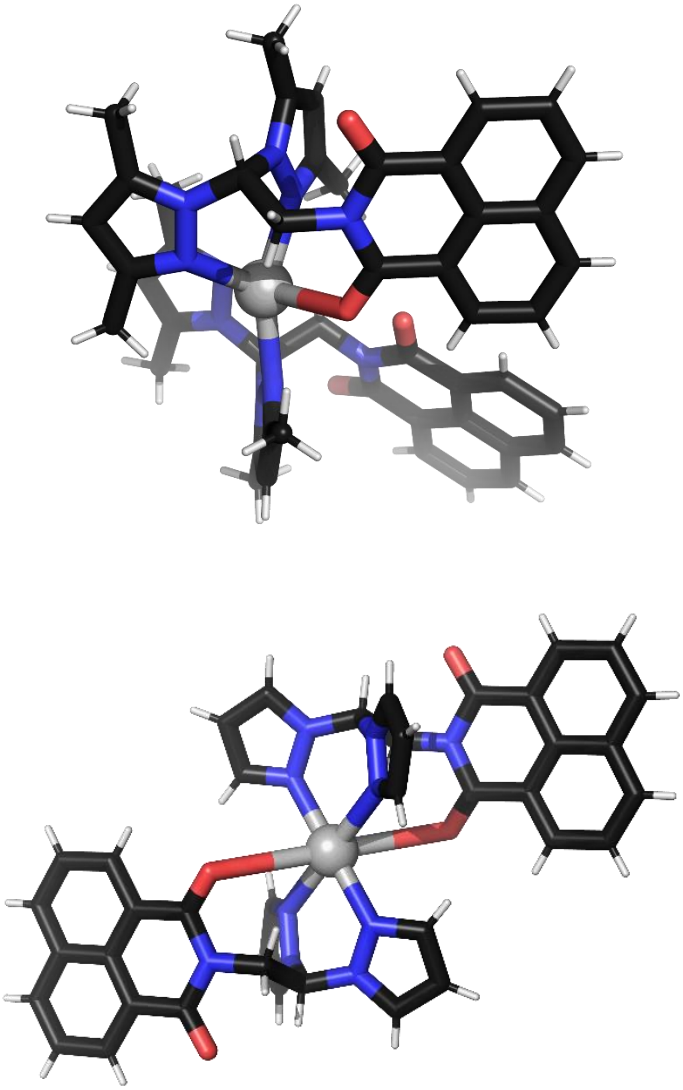

Figure 3.6: ***Literature structures 636006 and 636004 demonstrating an oxygen bound naphthalimide moiety, forming an eight membered chelate ring.[91] Bond determined by Olex2. This bond was shown in Olex2 and had a length of 2.8 Å in the first structure and 3.2 Å in the second structure, which is a long but plausible bond length.***

3.4.2. Cobaltinitrite Syntheses

As for Section 3.4.1, both crude and enriched ligand syntheses resulted in the production of complex 3.2. This was detected in low amounts in many phases of the reaction, and as the major component in one fraction. This was the reaction involving crude ligand and excess cobalt, which produced an oil upon cooling of the reaction liquor that contained close to 100% complex 3.2 (Table 3.3).

The synthetic procedure for production of the dinitrite complex was adapted from Werner's original method for tetraamminedinitritocobalt(III).[92] A stoichiometric amount of potassium

cobalt nitrite and tetradentate ligand, which was dissolved in methanol, were heated until the reaction was observed by production of solid. In the original method this only required three minutes; in the current adaptation the reaction was allowed to proceed overnight due to the increased complexity and lower solubility of the ligand. The solution was then filtered to remove unreacted potassium cobaltinitrite and the filtrate cooled to allow for precipitation of brown-yellow powder. The potassium cobaltinitrite species required for this synthesis was produced using the second method described by Vendilo *et al.*[93]

The reaction of the ligand material with the cobaltinitrite starting material produced solid material and an orange liquor, which upon cooling produced an orange-brown oil. The solid that was produced immediately during the reaction can be separated into two primary categories: cobaltinitrite starting material and other products. The cobaltinitrite starting material has low solubility in methanol and was either added to the methanolic ligand solution as a methanol slurry or as a solid. The addition of the material to the refluxing methanolic ligand solution resulted in solid remaining in the mixture. At the end of the reaction, the orange solid could be separated from the other solids and showed the same solubility and intense yellow colouring in water as the starting material. ESI-MS in positive and negative ion mode (as the complex would be expected to be 3-) of this solid did not detect the compound, which was in keeping with the lack of detection of the cobaltinitrite starting material when analysed directly. This did not confirm with certainty that the solid was starting material, but the lack of other complex detection showed that it was not the desired compound.

The remainder of the reaction solid from each reaction contains predominantly side products, the exact nature of which was discussed in Appendix F.2 as it pertains to each iteration of the reaction. The desired compound was detected in the solids in trace amounts.

The hot filtering followed by cooling and collection of the precipitate formed allowed for separation of impurities from the desired compound. The desired compound was detected in the purest form in the oil produced after the reaction liquor had been cooled, as determined by ESI-MS. In this fraction, the desired complex was the major peak, with side products present at less than a quarter of the height (0.25 or less relative intensity) of the desired complex peak. The ESI-MS of this precipitate showed a good match of the major peak isotope pattern to a simulated pattern for the expected product (Figure 3.3). The starting materials were a mustard yellow colour, however, the solid analysed was more orange-brown. The IR data (Section 3.3.2.1) showed some ligand starting material peaks in the complexation product, indicating that the ligand was present, along with some new peaks outside of the fingerprint region (which was

very different) not seen in the free ligand spectrum. This indicated that complexation may have occurred, and the new cobalt-nitrogen bonds were present in the spectrum.

Finding the complex in its purest form in this oil was logical based around the structure of this complex. With a 1+ charge, the complex was likely to be more polar than the free ligand and as a result may show a lower solubility in methanol than the free ligand did, causing it to precipitate following cooling. The complex was less charged than the cobalt starting material, which had a 3- charge, and the separation of these two complexes by hot filtering then allowing the reaction to cool thereby reducing the desired complex solubility, was rationale behind the method design. The yield of this oil was relatively low with less than 0.1 g of the product formed from 1 g of crude ligand, however, the ESI-MS spectrum of this oil appeared to have very few other species, indicating that this sample was enriched especially by comparison to the other phases (Table 3.3). Unfortunately, during the following repetitions of this method it was difficult to reproduce the enrichment demonstrated in the first method described, even when using the enriched ligand material. More detail on this can be seen in the discussion for each iteration in Appendix F.

The reaction liquor for this reaction also contained predominantly side products. This was to be expected as mentioned above the intended complex and the cobalt starting material were both charged and therefore likely less soluble in the methanol of the reaction solvent than the crude ligand material was. The exact composition of the liquor again varied by reaction and was predominantly composed of the side products with only traces of the desired complex detected by ESI-MS (less than 0.05 relative intensity, Table 3.3, Table 3.4).

Aside from the desired compound, other cobalt complexes were detected in the reaction components. Interestingly, this included a 711.1984 1+ peak that matched the predicted mass for the carbonate complex. This peak in the carbonate synthesis matched the expected isotope pattern for this compound, and the peak masses were very similar (711.1984 1+ here versus 711.1986 1+ in the previous section). Additionally, the relative intensities of these peaks compared to ligand side products was very similar, 0.11 versus 0.05 (Table 3.1 and Table 3.4). This was not likely to be caused by cross contamination of the mixture as this peak was frequently seen across numerous reaction mixtures in multiple fractions. There was a possibility that traces of complex 3.1 could have formed *in situ*. Dissolution of carbon dioxide into the solution would be favoured by the presence of basic amines reacting with the carbonic acid formed, producing carbonate and protonated amines. The resulting carbonate anion can bind to the metal centre as a bidentate ligand, which gives it the ability to displace monodentate ligands

such as nitrite in a complex. It was possible that following dissolution in methanol[94], the reaction of carbon dioxide with water proceeds as above, forming carbonate that then complexes cobalt. A synthesis of the $[Co(CO_3)]^{3-}$ complex involving the bubbling of a stream of carbon dioxide through the reaction mixture[95] as the source of carbonate is reported in the literature, indicating that this is a reliable way to synthesise the carbonate ligand. In the experiments by Fumiyo *et al*, a platinum triethylphosphine complex was reacted with Tl(acac) in methanol under atmospheric conditions which produced a platinum triethylphosphine carbonato complex in 3%.[96] When carbon dioxide was bubbled through the solution, the yield increased to 18%. This indicated that the formation of carbonate complexes in methanolic solutions can be performed under standard atmospheric conditions. To identify whether this was occurring in this reaction, further reaction under a completely inert atmosphere would need to be performed. Additionally, deliberate bubbling of CO_2 may encourage the carbonate complex to form, indicating that this could be an avenue for future synthesis of the carbonate complex.

An air oxidation synthesis in this work involving a cobalt sulfate starting material and ligand 2.1 also appeared to have produced the carbonate complex as determined by presence of the 711.1982 1+ peak in the ESI-MS spectrum of the reaction mixture. During this synthesis air was bubbled continuously through the reaction solution, which appeared to have provided the oxygen to oxidise the cobalt as expected as well as the carbon dioxide to form carbonate anions.

The 325.1013 2+ and 649.1963 1+ peak pair assigned to compound 3.3 were also detected in these syntheses, numerous times as the major peak. It remains unclear as to whether this species existed in solution or was a remnant of the ESI process. As the desired dinitrito species had been observed in spectra as the major peak with no evidence of the 325 peak (Table 3.3) it seems as though the 325 species was not solely produced by decomposition of the intended complexes during the ESI-MS process. This would favour the hypothesis that the 325 peak results from complexation of the ligand to cobalt directly, rather than from the degradation of the existing complexes. It remains unclear as to whether the deprotonated ligand complex forms in solution or during the ESI process.

The colours of the samples from which the 325 2+ peak was detected were orange in these syntheses, which was not the colour expected for a cobalt complex with four nitrogen and two oxygen donor atoms, a probable binding mode for this complex. It was possible that this complex only forms in the ESI process, or that the binding mode was not as speculated. It was also possible that the complex was in low amounts leading to masking of the colour by other compounds. This seems unlikely given that it was often a major peak, but there was the

potential for formation of negatively or neutrally charged complexes which could be the major product, masking the 3.3 compound appear to be the major product when detected by ESI-MS (discussed further in Appendix F). This product also may show a dramatically better ionisation ability than the other complexes, appearing as a larger peak which seems unlikely given that it had also been detected in small relative intensities.

The 325 2+ peak has also been observed in previous cobalt syntheses during this study with ligand 2.1, including an attempted complexation with $[Co(en)_2Cl_2]^+$ and an air oxidation reaction using cobalt sulfate as the starting material. In both of these cases, the 325 peak was a major peak in the ESI-MS spectrum, reinforcing the observations made in this chapter. Further evidence of deprotonated ligands complexing was observed during one of the copper syntheses in the previous chapter, where a peak in the ESI-MS spectrum corresponding to the deprotonated Cu(2.1) complex was detected (Figure 3.7). The isotope pattern matched between the simulated and native peaks, standing as further evidence of the deprotonation of the ligand.

The reactions performed using stoichiometric cobalt did not show the same level of enrichment in any phase as was observed in the synthesis using excess cobalt. Not only did the complex appear in these reactions as a trace component of many phases, free ligand material was also detected in many fractions indicating that optimisation of the reaction conditions is required to obtain a higher yield of the highly enriched material detected in this work. Similarly to the previous section, the use of enriched ligand material compared to crude material led to a less complicated product mixture, however, the major products from this reaction were the 325 2+ and 711 1+ peaks of the side product complexes, and the desired 743 1+ peaks remained at a low intensity.

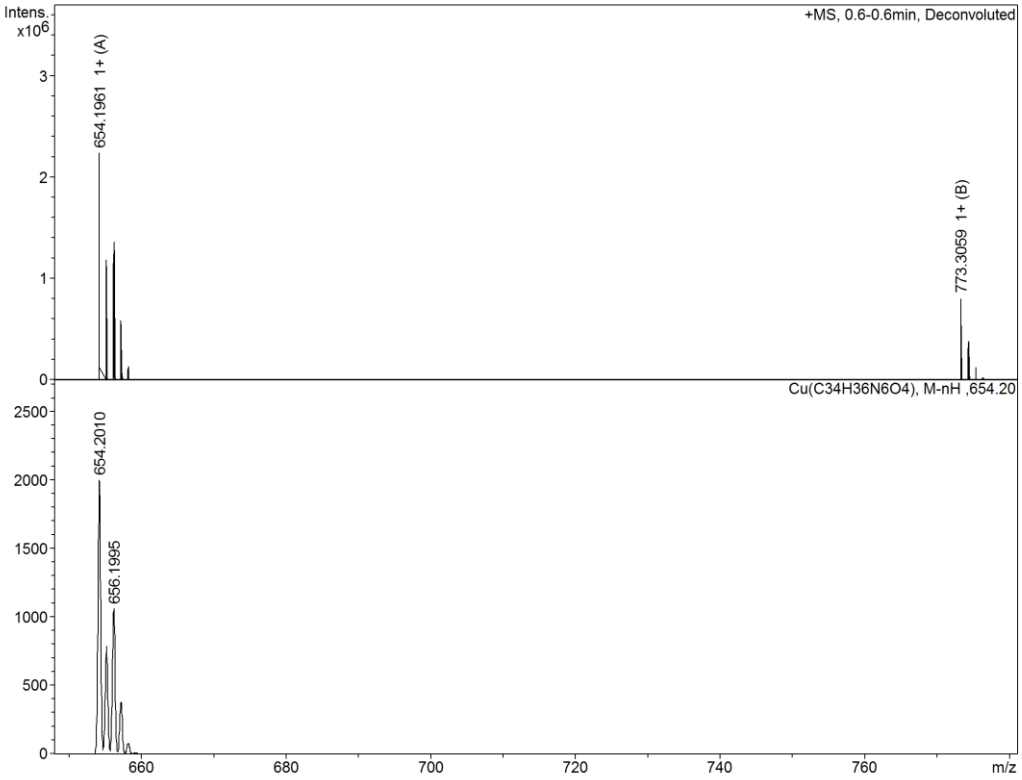

Figure 3.7: ***Peak in the Copper(2.1) synthesis showing the isotope pattern in the native (above) and simulated (below) spectra. The peak corresponds to the mass for a complex formed between copper and a deprotonated 2.1 ligand.***

3.4.3. Conclusions

This chapter explored the successful syntheses of cobalt complexes using both crude and enriched ligand material. The complexes produced were detected in low amounts in many of the fractions, with the highest detection in the oil produced upon cooling of the reaction liquors. The crude material produced the correspondingly contaminated products in most cases, and while the enriched ligand material did produce material with fewer side products the yield was low and utilised a material that was difficult to obtain (from Section 2.2.6.5). As such, there were benefits and detriments around employing either strategy to synthesise these complexes.

The highest observation by ESI-MS in the reaction composition of the $[Co(2.1)CO_3]^+$ complex, 3.1, was achieved in the solid produced by the reaction with enriched ligand material. Unfortunately, this solid was dark green indicating that residual cobalt starting material, which was not detected by ESI-MS, was also present so the true composition was unknown. The other detections all occurred in trace amounts so determination of an alternative best method would require further experimentation. Prior work showed that crude material could produce higher relative intensities of the desired complex, but the detection was variable. Interestingly, detection of this compound mass by ESI-MS appeared to be better in some of the

$[Co(2.1)(NO_2)_2]^+$ syntheses, which is also cause for further experimentation to determine if this complex can be formed in other ways.

The greatest percentage of the reaction composition for $[Co(2.1)(NO_2)_2]^+$, 3.2, was observed in the reaction utilising crude ligand material and excess cobaltinitrite starting material. This reaction produced an oil upon cooling of the reaction solution, both fractions of which contained a very high fraction of the complex 3.2 with the complex peak being the major peak of the reaction fractions. The stoichiometric crude and enriched syntheses also showed production of complex, but in much lower yields.

Across the syntheses the identification of another potential complex was possible. A peak for 325.1020 2+ (predicted 325.1026 2+ for $[Co(C_{34}H_{35}N_6O_4)]^{2+}$) was identified throughout. This peak was assigned as a complex of cobalt with a deprotonated ligand 2.1 coordinated without additional ligands. The 'vacant' cobalt binding sites may be occupied by the ligand naphthalimide carbonyls or through formation and complexation of an iminolate. It is unclear whether the complex forms due to the degradation of the desired complexes in the ESI process, complexes that exist synthetically or as a remnant of the ESI process in general. This species was identified in both crude and enriched ligand syntheses, with a much greater prevalence in the enriched ligand syntheses. This may be due to the lack of other species around to mask their presence in the enriched syntheses, as it was also detected as the major peak in some crude ligand fractions. The presence of this complex could indicate that product formation was higher than previously judged if it had degraded to become this compound. Further work surrounding the characterisation and attempts to isolate this compound may help to determine how it forms.

Chapter 4: *Copper Naphthalimide Ligand Complex Crystallography*

4.1. Introduction

This chapter largely focusses on the structure obtained through crystallographic data collection and structural elucidation. The crystals formed during the process of complexation of a new ligand material to copper and were subsequently analysed by X-ray diffractometry. The production of the ligand was performed in the same way as in Chapter 2, using 1,8-naphthalic anhydride to produce pendants through mechanochemical reaction conditions. The amine starting material, N,N'-bis(3-(2-aminoethylamino)propyl)ethane-1,2-diamine 4.1, was used in place of the previously described hexamine, 3,6,9,12-tetraazatetradecane-1,14-diamine. Their structures differ in the length of two of the links between nitrogen atoms; the amine focused on in this chapter had two propyl chains where the previous amine had five ethylene chains. This amine was chosen to both provide a hopefully purer starting material for synthesis, and to modify the cobalt coordination environment with two six-membered chelate rings as opposed to the previous five membered rings. As five and six membered chelate rings are the most stable for a cation in the first transition series, this modification may also encourage complexation.

The original complex in this chapter was synthesised by myself and my colleague Meghan Ricciardi, an undergraduate exchange student whom I supervised and worked alongside through a short research project. The crystallographic work was performed by and alongside Dr Matthew Polson.

Figure 4.1 depicts the theoretical and observed compounds discussed in this chapter.

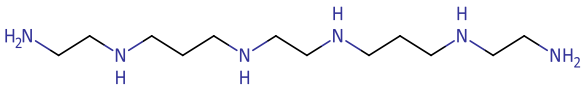

4.1 ***Intended polyamine starting material***

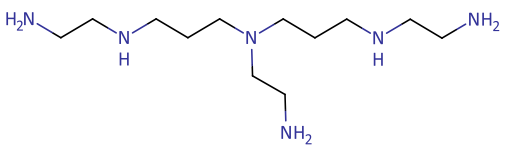

4.2 ***Branched isomer of polyamine starting material***

Figure 4.1: ***Structures of the proposed and observed compounds discussed in this chapter.***

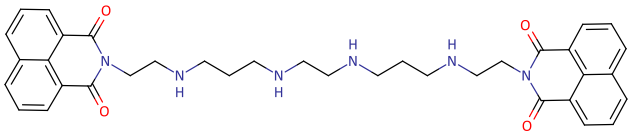

4.3 *Dinaphthalimide ligand formed from 4.1*

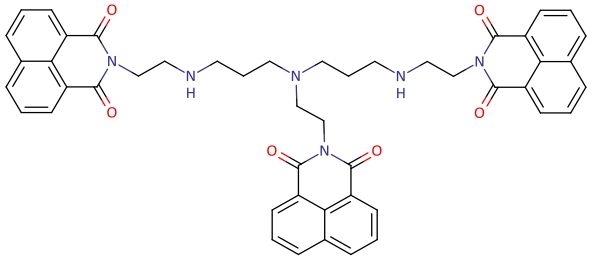

4.4 *Trinaphthalimide ligand formed from 4.2*

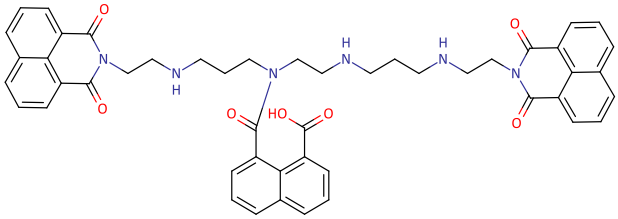

4.5 *Ligand formed from 4.1 with two naphthalimide groups and a naphthalamide group*

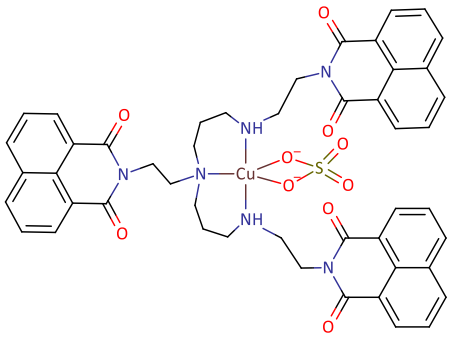

4.6 *Crystal structure formed by complexation of 4.4*

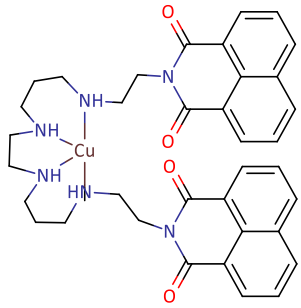

4.7 *Proposed complex formed with 4.3, not observed during this work*

Figure 4.1 (continued)

4.2. Experimental

General methods can be found in Sections 2.2.1 - 2.2.5.

4.2.1. Single Crystal X-Ray Crystallography

X-ray data was collected on a Supernova instrument with a focused microsource Cu Kα [λ = 1.54184 Å] radiation and an ATLAS CCD area detector. CrysAlisPro 171.36.28 was used for the data collection and data processing. The crystals were mounted on nylon loop using polyethylene glycol. All structures were solved using direct methods with SHELXT and refined on *wF*2 using all data by full matrix least square procedures with SHELXL using OLEX-2 for visualisation. Graphical presentation of crystallographic data was prepared using OLEX-2 and Mercury.

4.2.2. Amine Starting Material

^{1}H NMR ($CDCl_3$ 400 MHz) δ 2.36 (t, *J* = 6.0 Hz, 4H, -NH-C$\underline{H_2}$-CH_2-NH_2), 2.28 (s, 4H, -NH-C$\underline{H_2}$-C$\underline{H_2}$-NH-) 2.25 – 2.19 (m (dt?), 8H, -NH-C$\underline{H_2}$-CH_2-C$\underline{H_2}$-NH-), 2.06 (dq, *J* = 14.2, 7.1 Hz, 4H, -C$\underline{H_2}$-NH_2), 1.23 (dp, *J* = 14.1, 6.8 Hz, 4H, -NH-CH_2-C$\underline{H_2}$-CH_2-NH-), 0.99 (s, 8H, N$\underline{H}$).

^{13}C NMR ($CDCl_3$ 101 MHz) δ 51.81 (2C, -$\underline{C}H_2$-NH_2), 48.67 (2C, -NH-$\underline{C}H_2$-$\underline{C}H_2$-NH-), 47.50 (2C, -$\underline{N}$-$\underline{C}H_2$-CH_2-CH_2-NH-), 47.39 (2C, -$\underline{N}$-CH_2-CH_2-$\underline{C}H_2$-NH-), 40.89 (2C, -NH-CH_2-$\underline{C}H_2$-NH_2), 29.59 (2C, -$\underline{N}$-$\underline{C}H_2$-$\underline{C}H_2$-CH_2-NH-)

Mass: [M +1H$^+$] 1+: *m/z* 261.2695 1+ (Predicted 261.2767), major peak

4.2.3. Synthesis of Naphthalimide Derivatised Amine

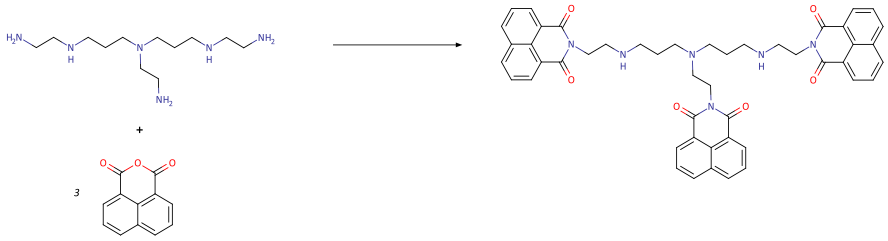

1,8-naphthalic anhydride ($C_{12}H_6O_3$ 5.00 g, 25 mmol) was placed in a 10 cm mortar and ground with a pestle until a fine powder was achieved. Chloroform (20 mL) was then added to the mortar and mixed with the anhydride to give a paste. To this, 3,7,10,14-tetraazahexadecane-1,16-diamine ($C_{12}H_{32}N_6$, 2 mL approx. 8 mmol) was added in a single addition and the mixture was ground for ten minutes. During this time, the mixture went from a pale beige paste to a very sticky brown and then to a crumbly pale brown solid as grinding continued. Grinding ceased once the mixture became a sticky pale brown powder.

^{1}H NMR (D_2O, 400 MHz) δ: 8.79 – 8.71 (m, 4H, ArCH), 8.66 – 8.58 (m, 4H, ArCH), 8.08 (m, 4H ArCH), 4.38 (t, *J* = 7.0 Hz, 4H, CH_2 next to imide), 4.25 – 4.17 (m, 4H, CH_2 outer ethyl next to 2° N), 3.12 – 3.02 (m, 4H, outer propyl CH_2), 3.02 – 2.86 (m, 4H, inner propyl CH_2), 2.11 (s, 4H, inner ethyl CH_2), 2.09 – 1.92 (m, 4H, central propyl CH_2).

4.2.4. Formation of Copper Complexes

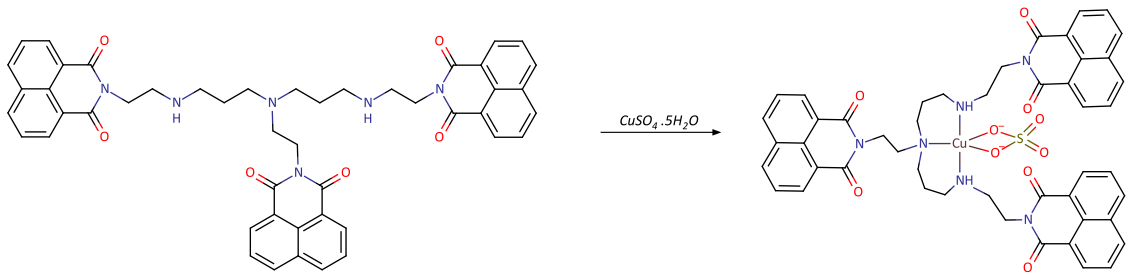

Crude ligand material ($C_{36}H_{42}N_6O_4$, 1.6 g, 2.57 mmol) was dissolved in methanol (100 mL) and filtered. The filtrate was added to a 500 mL conical flask and warmed on a steam bath. Copper sulfate ($CuSO_4 \cdot 5H_2O$, 0.4 g, 1.6 mmol) dissolved in warm methanol (25 mL) and added to the conical flask. The reaction mixture gradually became blue with formation of a blue solid. The reaction mixture was heated on the steambath with occasional swirling for 3 hours. The reaction resulted in formation of an oily blue solid and a blue liquor. Allowing this to stand resulted in formation of bright blue plate-like crystals over the course of two weeks. The mass was not obtained to avoid deterioration of the crystals upon drying, however, there were crystals scattered across the entire surface of the flask, forming upwards of 100 mg of crystalline material.

Suitable crystals were selected and mounted on nylon loops using perfluoronated PEG on a SuperNova, Dual, Cu at zero, Atlas diffractometer. The crystals were kept at 120.01(10) K during data collection. Using Olex2[97], the structures were solved with the ShelXT[98] structure solution program using Intrinsic Phasing and refined with the ShelXL[99] refinement package using Least Squares minimisation.

Numerical face indexed absorption corrections were done on all structures unless otherwise noted.

Unless otherwise stated, hydrogens attached to carbons were inserted in the appropriate positions and refined as riding atoms with thermal parameters 1.2 (aromatic carbons) or 1.5 (all other carbons) times that of the parent atom. Hydrogens attached to nitrogen or oxygen were located in the residual electron density map, the distance to the parent atom was fixed at 0.86 Å and the thermal parameter fixed to 1.5 times that of the parent atom.

Crystal Data for $C_{48}H_{44}N_6O_{10}SCu$ (M =960.51 g/mol): Monoclinic, space group $P2_1/c$ (no. 14), a = 15.2747(13) Å, b = 22.5822(11) Å, c = 15.3342(13) Å, α = 90°, β = 109.197(9)°, γ = 90°, V = 4995.2(7) $Å^3$, Z = 4, T = 120.01(10) K, μ(CuKα) = 1.510 mm^{-1}, ρ_{calc} = 1.277 g/cm^3, 9908 reflections measured (3.626° ≤ 2Θ ≤ 75.831°), 5943 unique (R_{int} = 0.0682, R_{sigma} = 0.102) which were used in all calculations. The final R_1 was 0.0568 (I > 2σ(I)) and wR_2 was 0.1557 (all data).

Mass: Complex not detected by ESI-MS. Detection corresponds to the free ligand.

[M +2H$^+$] 2+: *m/z* 401.1740 2+ (predicted 401.1739 2+ for $C_{48}H_{46}N_6O_6$)

[M +1H$^+$] 1+: *m/z* 801.3411 1+ (predicted 801.3400 1+ for $C_{48}H_{45}N_6O_6$)

[M +3H$^+$] 3+: *m/z* 267.7849 3+ (predicted 267.7852 3+ for $C_{48}H_{47}N_6O_6$)
Relative Intensity: 1.0

[M +2H$^+$] 2+: *m/z* 311.1634 2+ (predicted 311.1633 2+ for $C_{36}H_{42}N_6O_4$)
Relative Intensity: 0.11

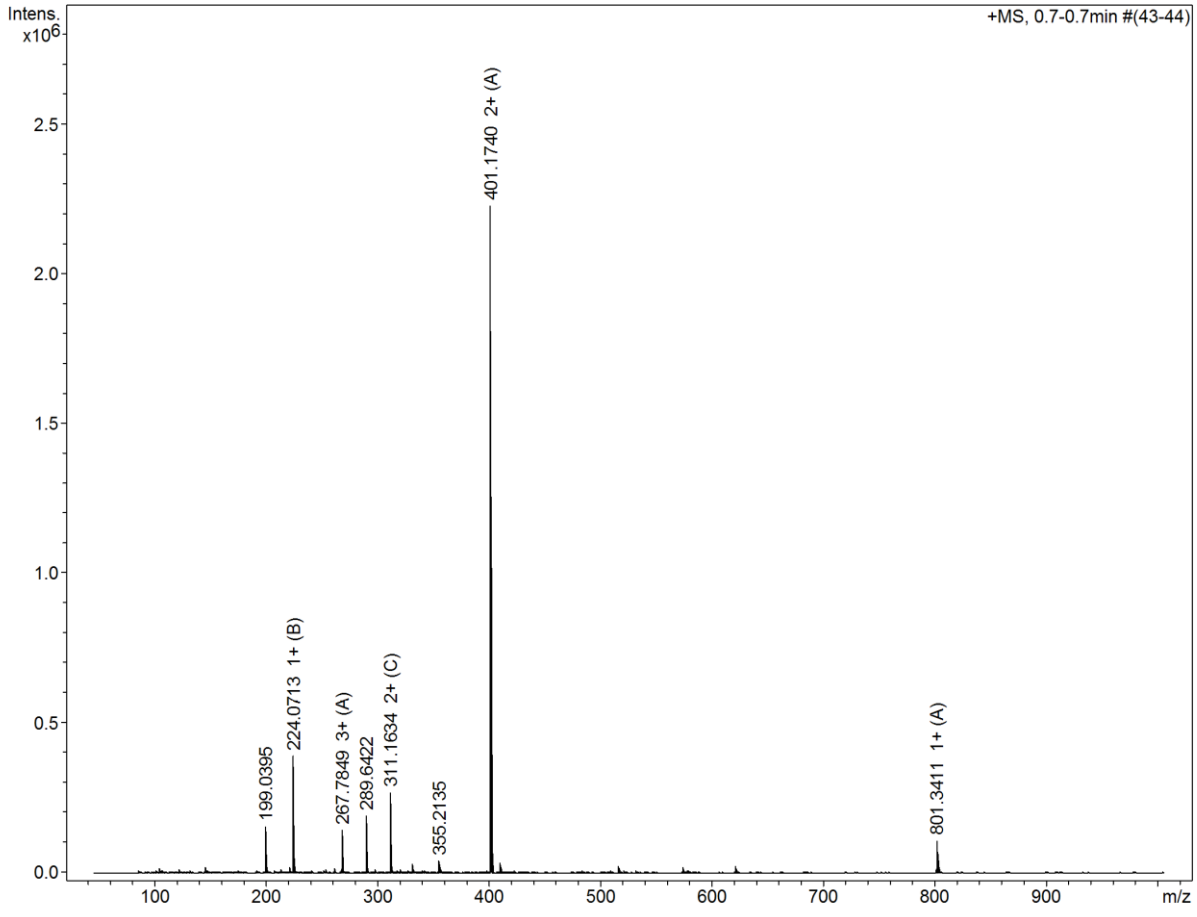

Figure 4.2: ***ESI-MS spectrum of a sample of the crystals that led to the collected structure***

IR of the crystal material: 1692 (s), 1651 (s), 1640 (m), 1589 (m), 1457 (w, br), 1438 (m), 1407 (w), 1387 (m), 1339 (s), 1236 (s), 1172 (w), 1106 (w, br), 1059 (w)

4.3. Results

4.3.1. $[Cu(C_{48}H_{44}N_6O_6)SO_4]$ Complex Crystal Structure

Figure 4.3 depicts the structure elucidated from the crystallographic data. The structure shows a copper centre bound to a tridentate branched trinaphthalimide ligand and a bidentate sulfate anion, forming a neural complex. The crystal parameters for this structure are given in Table 4.1.

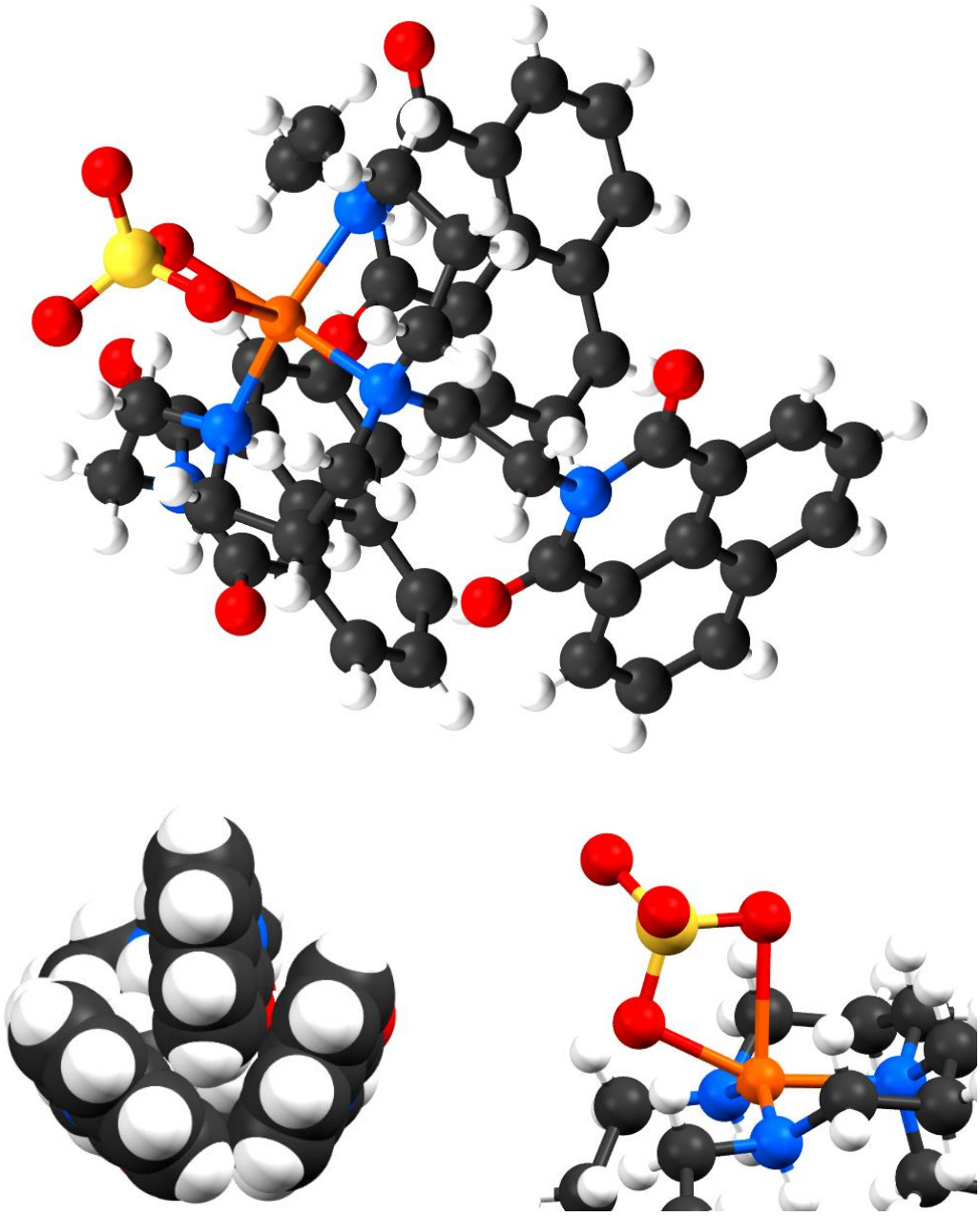

Figure 4.3: ***Crystal structure of the copper naphthalimide complex, including a space fill view of the naphthalimide pendants and a closer alternative view of the coordination sphere.***

Table 4.1: *Collection and solution parameters for the crystal structure reported in this work.*

Crystallographic Parameters	
Identification code	SEL01a
Empirical formula	$C_{48}H_{44}CuN_6O_{10}S$
Formula weight	960.51 g mol^{-1}
Temperature/K	120.01(10) K
Crystal system	Monoclinic
Space group	$P2_1/c$
a/Å	15.2747(13)
b/Å	22.5822(11)
c/Å	15.3342(13)
α/°	90
β/°	109.197(9)
γ/°	90
Volume/$Å^3$	4995.2(7)
Z	4
$\rho_{calc}g/cm^3$	1.277
μ/mm^{-1}	1.510
F(000)	1996
Crystal size/mm^3	0.122 x 0.078 x 0.014
Radiation	CuK_α (λ = 1.54184)
2Θ range for data collection/°	3.626 to 75.831
Index ranges	-18≤ h ≤13, -27≤ k ≤21, -17≤ l ≤19
Reflections collected	9908
Independent reflections	5943 [R_{int} = 0.0682, I/σ = 0.102]
Data/restraints/parameters	5943/2/601
Goodness-of-fit on F^2	0.965
Final R indexes [I>=2σ (I)]	R_1=0.0568, wR_2=0.1317
Final R indexes [all data]	R_1=0.0984, wR_2=0.1557
Largest diff. peak/hole / e $Å^{-3}$	0.317, -0.554
CCDC	TBC

The unit cell contained four molecules, with one molecule in the asymmetric unit (Figure 4.4 and 4.5). The formula of the compound was identified as $C_{48}H_{44}CuN_6O_{10}S$ which corresponds to the expected formula for a compound containing a copper centre bound to a sulfate and the polyamine ligand formed with three naphthalimide pendants. The structure contained three molecules of ethanol within the asymmetric structure (to give a total of 12 in the unit cell), which failed to refine due to disorder. The electron density associated with these ethanol molecules was removed using Olex2's solvent mask. The amine hydrogens were located in the electron difference map with N-H distance restrained to 0.86 Å and the position was allowed to refine. The U_{iso} for the hydrogen atoms were fixed to the atom they were attached to at 1.5x.

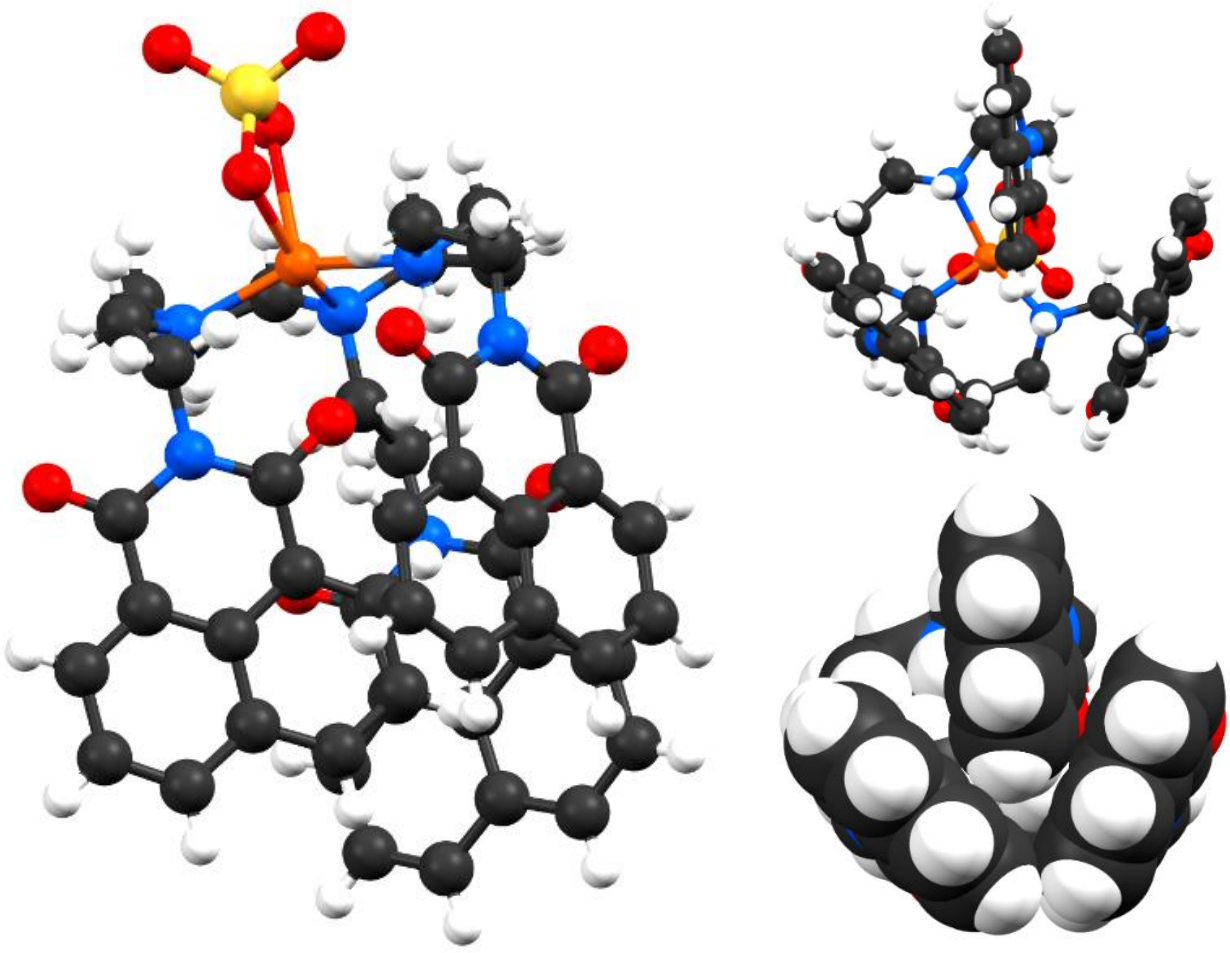

Figure 4.4: ***Structure of the Copper Naphthalimide product synthesised in this work, rotated to show the orientation of the pendants to each other. The third image is a space fill of the naphthalimide pendants to show their relative orientation.***

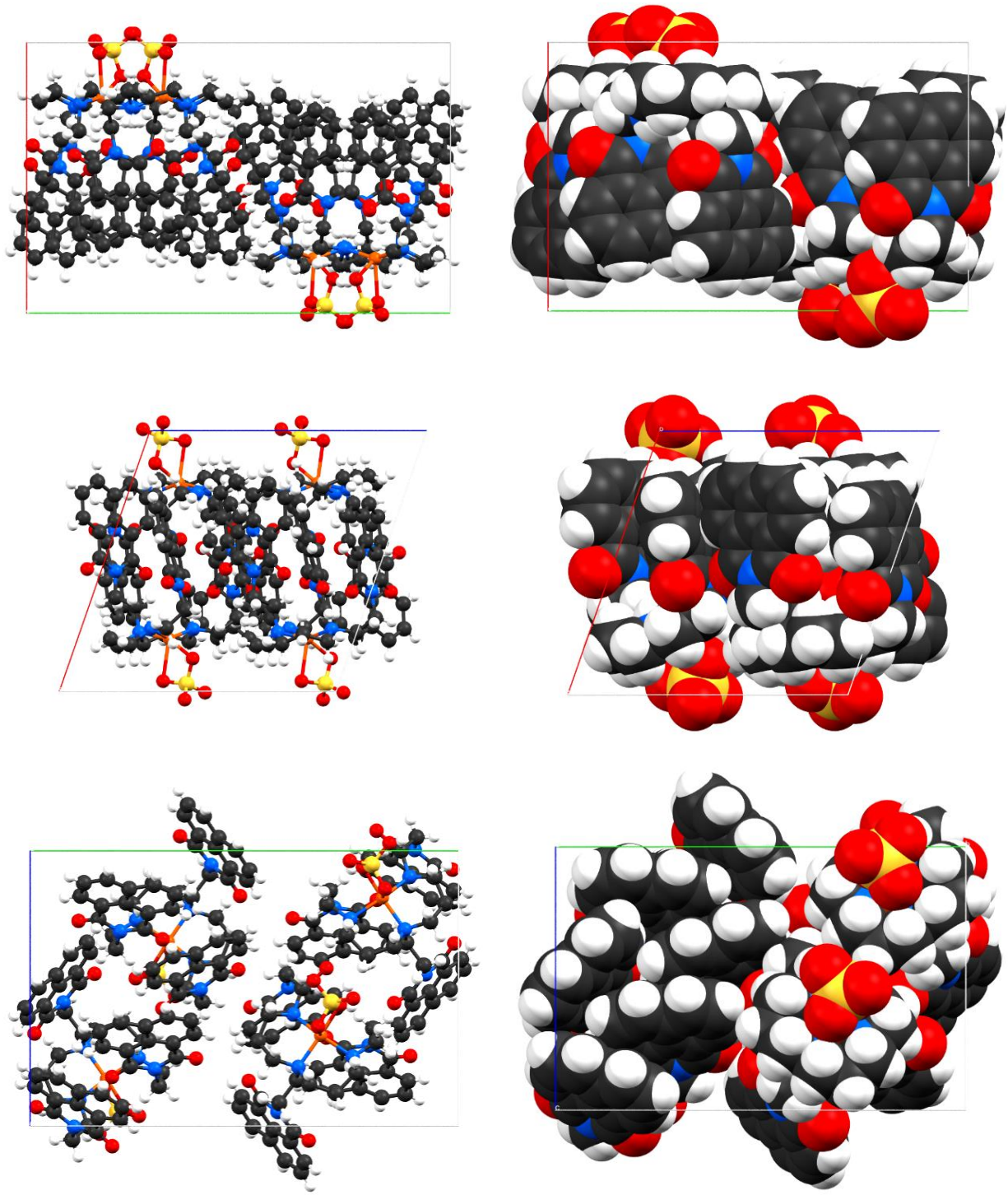

Figure 4.4 continued: ***Side by side ball and stick (left) and spacefill (right) views of the unit cell packing of the crystal structure***

The collected structure showed the copper centre was bound to three nitrogen and two oxygen donor atoms. The bond angles of the coordination sphere can be seen in Figure 4.5 and Table 4.2, while the bond lengths are given in Figure 4.6 and Table 4.3.

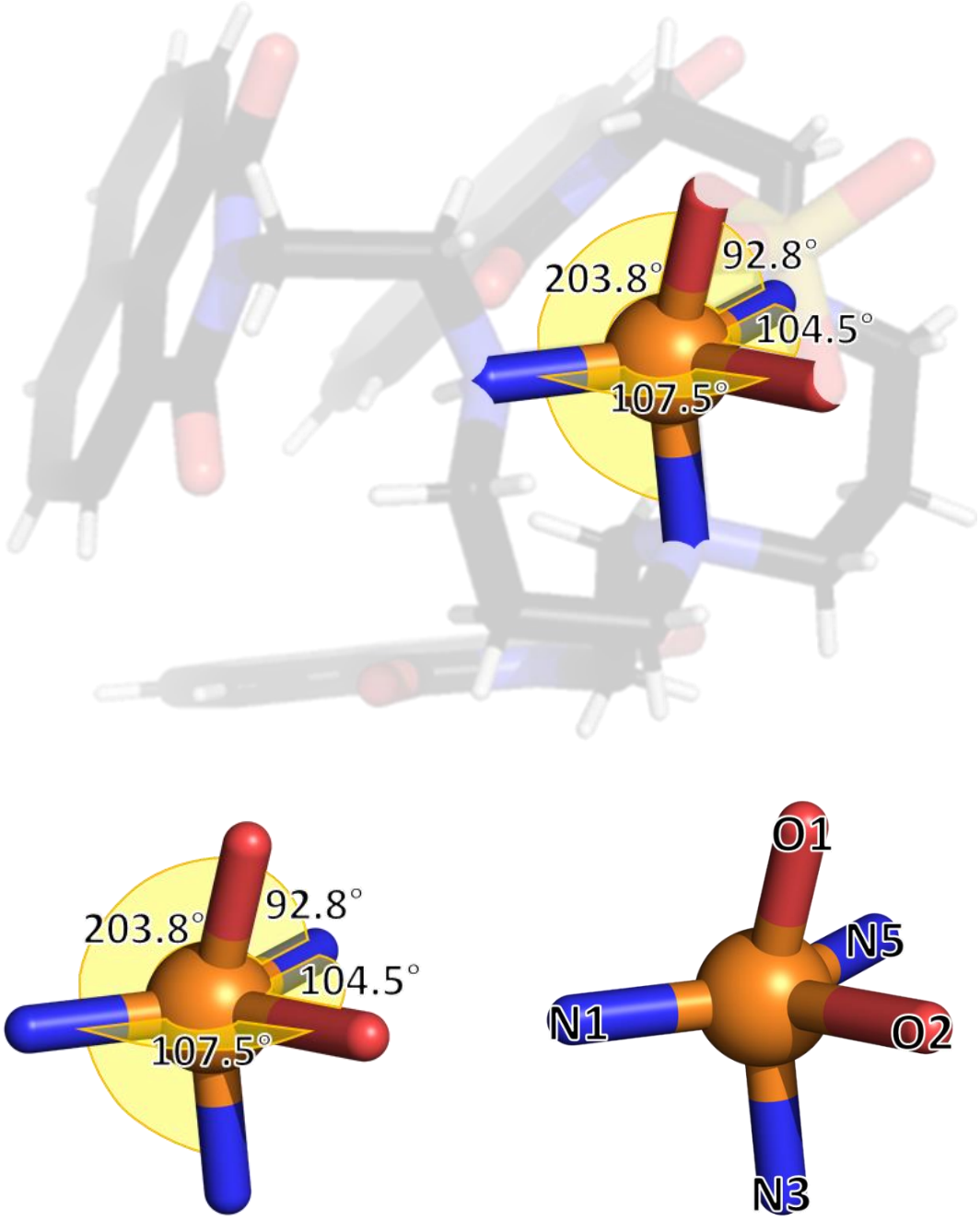

Figure 4.5: ***Selected bond angles for the coordination sphere, showing the sphere in context of the full structure (top), in isolation (left) and the atom numbering (right).***

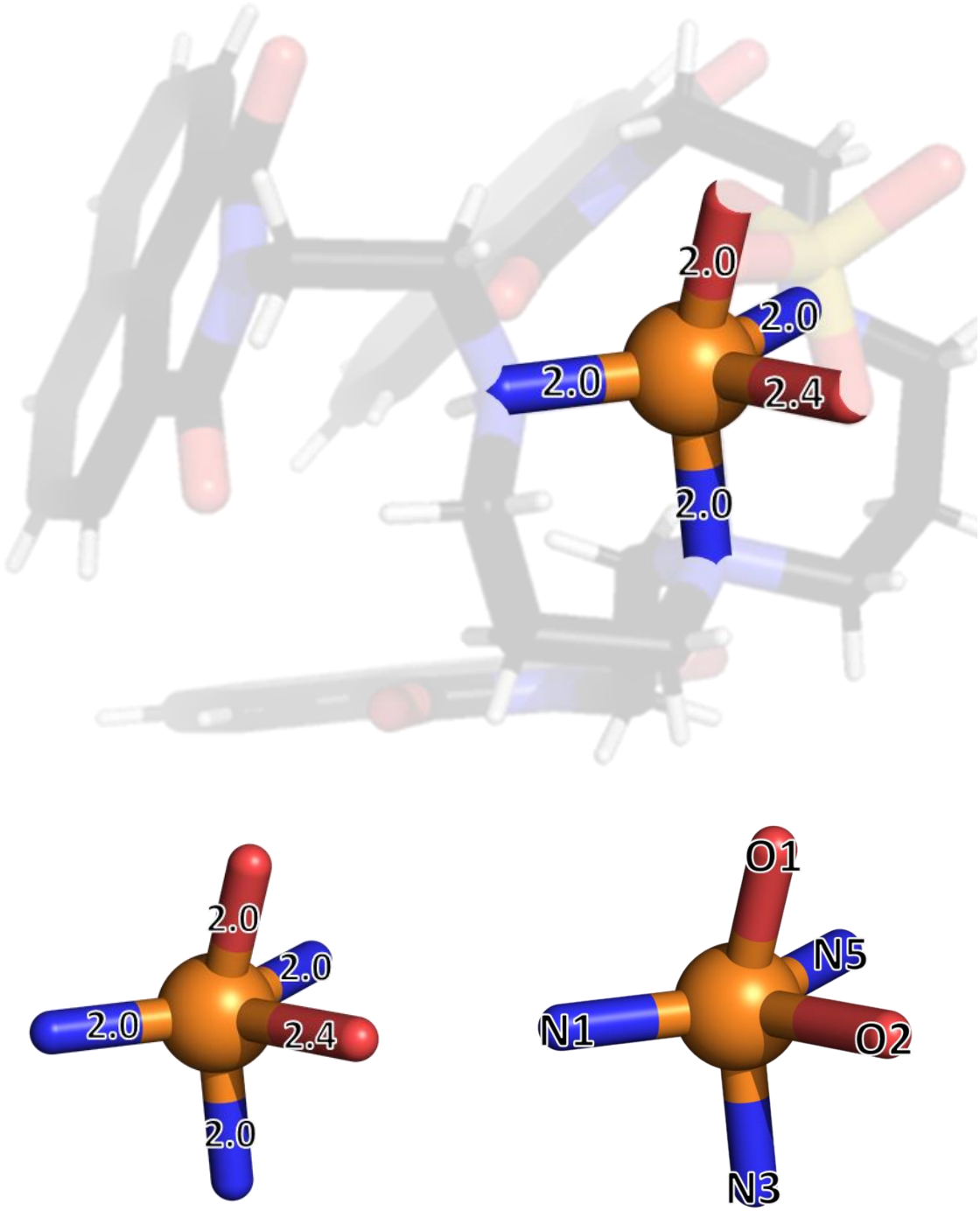

Figure 4.6: ***Bond lengths for the collected structure coordination sphere, showing the sphere in context of the full structure (top), in isolation (left) and the atom numbering (right).***

Table 4.2: *Coordination Sphere Bond Angles. The first column shows which atoms are being considered in the angle. The second column shows the bond angles and error values from the crystal structure elucidation.*

Atoms forming the bond angle	Bond Angle including errors
N1 – Cu – N3	94.60(12)°
N1 – Cu – N5	147.10(13)°
N1 – Cu – O1	93.63(12)°
N1 – Cu – O2	107.46(12)°
N3 – Cu – N5	92.29(12)°
N3 – Cu – O1	156.19(13)°
N3 – Cu – O2	91.41(12)°
N5 – Cu – O1	92.84(11)°
N5 – Cu – O2	104.48(12)°
O1 – Cu – O2	64.80(11)°

Table 4.3: *Collected Structure Bond Lengths The first column lists the atoms in the bond. The second column shows the bond lengths and error values from the crystal structure elucidation.*

Bonded Atoms	Bond Length including errors
Cu – N1	2.037(3) Å
Cu – N3	2.052(3) Å
Cu – N5	2.031(3) Å
Cu – O1	1.998(3) Å
Cu – O2	2.378(3) Å

4.3.2. Repetition of Crystallisation Conditions

Both the trinaphthalimide ligand synthesised from the amine corresponding to the branched species, 4.4, and the dinaphthalimide ligand synthesised from the linear species, 4.3, were again detected in the repetition. Attempts to produce crystalline material were unsuccessful.

4.3.3. Summary of Results

This chapter focusses on the synthesis and structural elucidation of a copper tridentate naphthalimide complex. This complex was formed from a branched impurity in the amine starting material that was used to form a tetradentate dinaphthalimide ligand from a linear hexamine. The branched impurity lead to the formation of a trinaphthalimide and subsequently

tridentate species that formed a complex to copper, with a sulfate anion coordinating to the two vacant coordination sites around the copper centre. No complex of the desired dinaphthalimide ligand product was observed. The crystal structure complex was not detected by ESI-MS, which was possibly due to the neutral charge on the complex. The crystal structure had approximately four molecules of disordered solvent per unit cell which were removed by solvent masking to obtain the final structure.

4.4. Discussion

4.4.1. Crystal Structure Analysis

The crystal structure confirmed that at least one branched amine was present in the starting material, which was speculated upon based on the ESI-MS results. It also showed that the naphthalimide pendant motif was indeed forming during the reactions, which to date had only been confirmed by ESI-MS evidence. ESI-MS of the crystal showed the major peak corresponding to the free ligand 4.4. The amount of this varies in the ESI-MS spectra between syntheses and was detected as a major peak in some reactions.

4.4.1.1. Coordination Sphere Bond Angles and Geometry

The geometry of the copper centre was a distorted square based pyramid, with multiple bond angles experiencing distortion (Table 4.2, Figure 4.5). The decision to call the geometry more square pyramidal was based on the τ_5 method outlined by Addison and Rao[100]. This method uses the two largest bond angles in the coordination sphere, termed α and β, according to the formula $\tau = \frac{\beta-\alpha}{60°}$, where τ becomes a number between 0 and 1. 1 corresponds to pure trigonal bipyramid (as the difference between the two largest angles was 60°, or the difference between the 180° axial and 120° equatorial angles) while 0 corresponds to pure square based pyramidal (as the difference between the two largest angles was 0°, as both the longest angles are in the base of the pyramid and therefore are both 180°). In this system, the two largest angles were 147.1° and 156.2°. When the calculation was performed using the values of 156.2° as β and 147.1° as α, τ=0.15, making the geometry predominantly square pyramidal. τ values as extreme as 0.1 and 1.0 are reported in the original paper. It appears likely in this situation that the small bidentate sulfate bonding angle distorted the geometry, particularly in angles involving the Cu – O1 bond. The six membered chelate rings of the naphthalimide ligand also appear to have slightly distorted the geometry. Both of these impacts are discussed further below.

The geometry consisted of the oxygen atom O2 in an approximately axial position, and one oxygen and three nitrogen atoms in equatorial positions (Table 4.3, Figure 4.6). A square based pyramid would have 90° and 180° equatorial-equatorial angles and 90° axial-equatorial angles. In the collected structure, four bond angles assigned as equatorial-equatorial are 92.3°, 92.8°, 93.6° and 94.6°, which were all close to the expected 90° angle for a square based pyramid. The values are slightly larger than expected due to the N1 – Cu – N5 (147.1°) and N3 – Cu – O1 (156.2°) angles deviating from the expected 180°. This has led to the equatorial positions sitting slightly out of plane, with N1 and N5 sitting slightly below the expected plane and N3 and O1 sitting slightly above it. The four bond angles designated as axial-equatorial were 64.8°, 91.4°,

104.5° and 107.5°, which deviated from the expected 90°, especially the outlier of 64.8°. Interestingly, these axial-equatorial angles were all different and span a wide range of 42.7° (16.1° with the outlier excluded). As mentioned above and discussed in more detail below, the deviations observed were likely caused by the balance of the strained four membered sulfate chelate ring and wider six membered naphthalimide ligand chelate rings.

4.4.1.2. Sulfate Coordination

The small bond angle between the two oxygen atoms (64.9°) was likely caused by the constraint of the sulfate moiety which forms a four atom chelate ring when coordinated. This small chelate ring restricts the system, resulting in a smaller bond angles than is typically observed in copper complexes. The O – S – O bond angle between the coordinated oxygens, 103.8°, is smaller than the non-coordinated O – S – O angles, 109.5°, 109.9°, 109.9°, 111.0° and 112.4° (Table 4.2), which indicates that the strain was experienced across the four membered chelate ring. The larger bond angles are caused by the sulfur-oxygen double bonds which give larger bond angles than the single bonded O – S – O. The theory that the four membered chelate ring had this impact was reinforced by the fact that the bond angles around the sulfate moiety are comparable to those previously observed in crystal structures; see Table 4.2 for more.[101]

Most notable of the literature structures compared here are the structures (CCDC deposition numbers 168978, 1308854, 1264272 and 753668) which also show sulfate bound as a bidentate ligand to the same metal centre, especially the structure that had a five-coordinate copper centre. The angles of the bidentate O – M – O bonds are 52.3°, 57.4°, 65.5° and 67.4° (with an average of 61.6° including this work) and the metal to oxygen bond lengths are 2.98 Å and 1.99 Å; 2.13 Å and 2.13 Å; 2.12 Å and 2.17 Å; and 2.44 Å and 2.45 Å. This compares well to the structure listed in this work, which had a bidentate sulfate bond angle of 64.8° and bond lengths of 2.0 Å and 2.4 Å. One of these bond lengths was slightly shorter than those observed in the above structures while the other was on the longer side, both of which appear to be within the expected lengths for the copper sulfate oxygen bond. The structure (168978) with a copper centre bound to a bidentate sulfate had a bidentate angle of 53.2°, which was even smaller than the angle seen in this work, and also features different copper to sulfate oxygen bond lengths, the longer of which was longer than that observed in this work and likely accounts for the shorter angle observed in the literature structure.

Table 4.4: *Bond angles and their designations for various coordinated sulfate groups in crystal structures. The angles are defined as being bidentate (the angle between two oxygen atoms connected to the same metal centre), bridging (the angle between two oxygen atoms connected to different metal centres) or are undesignated (one or both of the oxygen atoms are not bound to a metal centre). These angles are shown predominantly as measured from the sulfur atom, with the last column showing the angles as measured from the metal centre as appropriate.*

CCDC Reference and Structure	Angle 1 (O1 – S – O2)	Angle 2 (O1 – S – O3)	Angle 3 (O1 – S – O4)	Angle 4 (O2 – S – O3)	Angle 5 (O2 – S – O4)	Angle 6 (O3 – S – O4)	Binding Mode/s	Angle of O – M – O
This work 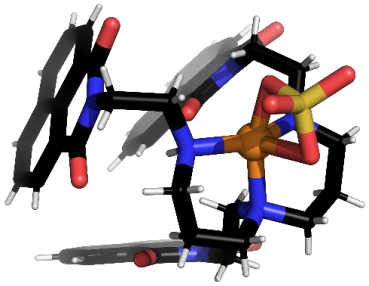	103.9*	109.9	109.5	112.4	109.9	111.0	Bidentate	64.8*
168978[102] 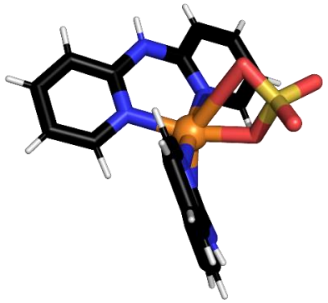	108.0*	106.7	108.5	110.0	112.9	110.4	Bidentate	53.2*

Table 4.4 (continued)

CCDC Reference and Structure	Angle 1 (O1 – S – O2)	Angle 2 (O1 – S – O3)	Angle 3 (O1 – S – O4)	Angle 4 (O2 – S – O3)	Angle 5 (O2 – S – O4)	Angle 6 (O3 – S – O4)	Binding Mode/s	Angle of O – M – O
1264272[103] 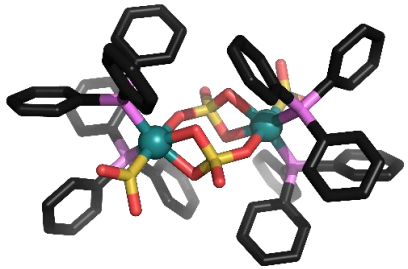	101.9*	109.6 μ	112.5	110.8 μ	112.1	109.6	Bidentate, Bridging	65.5*, 85.6 μ, 84.1 μ.
753964[104] 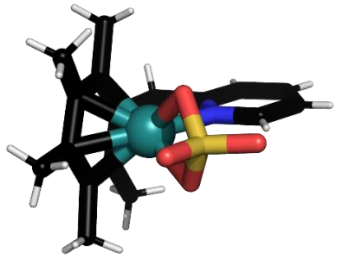	100.2*	110.7	110.2	110.7	107.7	114.0	Bidentate	67.4*

Table 4.4 (continued)

CCDC Reference and Structure	Angle 1 (O1 – S – O2)	Angle 2 (O1 – S – O3)	Angle 3 (O1 – S – O4)	Angle 4 (O2 – S – O3)	Angle 5 (O2 – S – O4)	Angle 6 (O3 – S – O4)	Binding Mode/s	Angle of O – M – O
1308854[105] 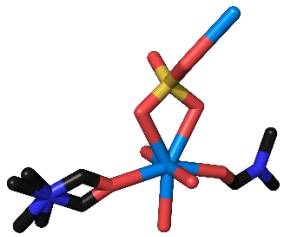	103.5*	109.8 μ	110.7	106.8 μ	114.2	111.5	Bidentate, Bridging	57.4*, 149.7 μ, 152.9 μ
178531[106] 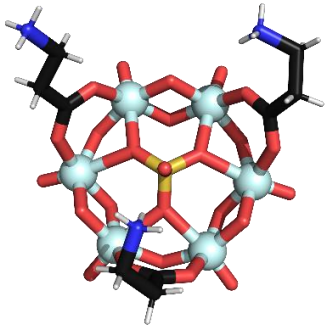	109.3	111.5	111.9	107.4 μ	108.4 μ	108.3 μ	Bridging	NA

Table 4.4 (continued)

CCDC Reference and Structure	Angle 1 (O1 – S – O2)	Angle 2 (O1 – S – O3)	Angle 3 (O1 – S – O4)	Angle 4 (O2 – S – O3)	Angle 5 (O2 – S – O4)	Angle 6 (O3 – S – O4)	Binding Mode/s	Angle of O – M – O
129805[107] 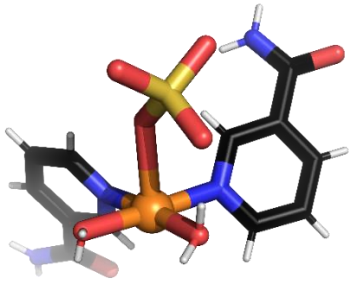	111.5	109.5	109.3	109.0	109.4	108.2	Monodentate	NA
131233[108] 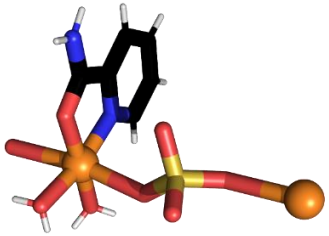	110.8 μ	109.5	110.0	110.1	107.6	108.9	Bridging	175.6 μ

Table 4.4 (continued)

CCDC Reference and Structure	Angle 1 (O1 – S – O2)	Angle 2 (O1 – S – O3)	Angle 3 (O1 – S – O4)	Angle 4 (O2 – S – O3)	Angle 5 (O2 – S – O4)	Angle 6 (O3 – S – O4)	Binding Mode/s	Angle of O – M – O
1605787[101] 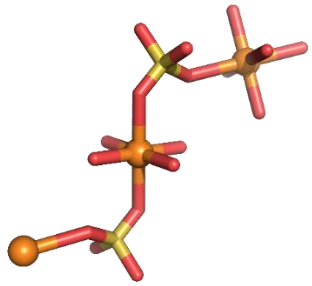	109.1 μ	114.3	110.6	109.4	111.6	101.8	Bridging	180.0 μ

Key: * = bidentate angle, μ = bridging angle. No symbol indicates at least one oxygen is not coordinated.

Average O – S – O angle for all oxygens: 109.4°

Average O – S – O angle for unbound oxygens: 110.2°

Average O – S – O angle for bridging structures: 108.9°

Average O – S – O angle for bidentate structures: 103.5°

Average O – M – O angle for bidentate structures: 61.7° (See Table 4.5)

The bidentate coordination in general seems unfavourable, both due to the strained coordinate bond angles and due to the limited number of similar structures in the literature when compared to a bridging or monodentate binding mode. The lengthening of the second bond to the sulfate anion appeared to be a balance between the unfavourable angle and copper becoming four coordinate. A review[109] comparing structures found that the average bond angle for oxygen-containing four-membered chelate rings was 57°, which was comparable to this structure and the other bidentate sulfate ligand structures listed above. The bidentate binding may have been observed in the structure reported in this wordue to the interactions of the aromatic systems encouraging the crystal formation and resulting in a more favourable structure than one that could form using bridging sulfate. It was also possible that the crowding of the naphthalimides in this structure encouraged the bidentate binding mode by precluding coordination of another species due to the lack of space remaining around the cooper centres.

Table 4.5 summarises the O – M – O bond angle and bond lengths for the bidentate sulfate structures. Again the copper structure 168978[102], which showed a lengthening of one copper to oxygen bond compared to the other bonds, is of particular interest. As mentioned previously, this highlights the lengthening of the metal to oxygen bond because of the unfavourable coordination angle.

Table 4.5: *Comparison of O – M – O bond angles for metal centres coordinated to a bidentate sulfate anion.*

Structure	O – M – O Bond Angle	O – M Bond Lengths	Image	Geometry
This Work 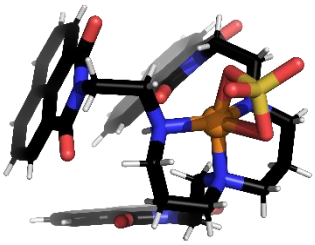	O – Cu – O 64.8°	1.99 Å 2.38 Å	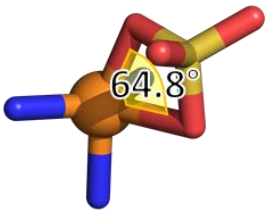	τ_5 = 0.15, Square Pyramidal
1308854[105] 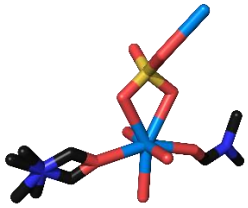	O – U – O 57.4°	2.44 Å 2.45 Å	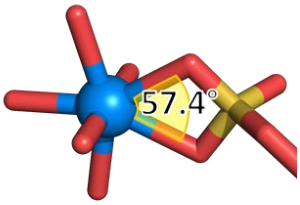	Distorted Capped Octahedral
1264272[103] 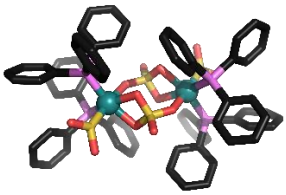	O – Ru – O 65.5°	2.17 Å 2.12 Å	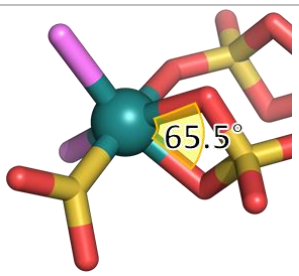	Distorted Octahedral
753964[104] 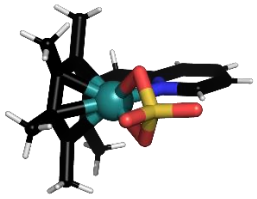	O – Ru – O 66.7°	2.1 Å 2.1 Å		Distorted Octahedral
168978[102] 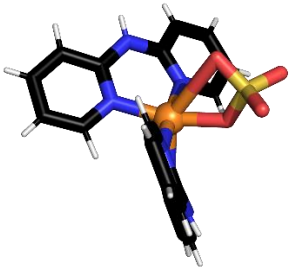	O – Cu – O 53.2°	3.0 Å 2.0 Å	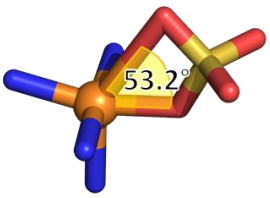	Distorted Octahedral

4.4.1.3. Naphthalimide Ligand Coordination

It is not uncommon for copper complexes to adopt distorted geometries, with five coordinate complexes generally adopting square pyramidal structures along with the less common trigonal bipyramidal, and many structures existing as a distorted version of either geometry.[109] Four coordinate complexes also demonstrate multiple geometric possibilities and were seen as both square planar and tetrahedral geometries, as well as with structures with properties of each geometry.[109] Other structures displaying a distortion similar to the crystal structure reported in this work have been observed and it appeared to be due to the strain imparted on the complex by the ligand geometry. In particular, rigid ligands can force the metal centre into a different geometry in order to coordinate but will still form stable complexes.[110-113]

As mentioned earlier in this discussion, the six membered chelate rings may have encouraged the distortion towards a square pyramid due to their larger bond angles than for five membered chelate rings. This was difficult to fully determine as copper structures often experience distortion. Two five membered ring structures are shown in Table 4.6, where each contains a bidentate and a tridentate ligand on a copper(II) centre. These both demonstrate a distorted square pyramidal geometry similar to that seen in the work reported in this chapter; the Aguilo[110] *et al* structure has a $\tau_5 = 0.25$, while the Kumar[111] *et al* structure has $\tau_5 = 0.19$. In these structures, the distortion likely arose due to the constraints from the ligands enforcing a set bond angle between coordinating atoms. The coordination sphere of the Kumar *et* al structure was composed of five nitrogen atoms. The structure reported by Aguilo *et al* also showed a distorted geometry. The coordination sphere, as for the collected structure, was composed of three nitrogen donor atoms from a tridentate ligand and two oxygen donor atoms from a bidentate ligand. The distortion was again likely due to the constraint from the bidentate ligand, which forms a five membered chelate ring with the copper centre and gives a bond angle of 81.9°. The N – Cu – N bond angles for nitrogen atoms in the same five membered chelate ring in these structures are summarised in Table 4.6.

Table 4.6: *Bond angles for the literature five membered chelate ring compounds that display similar τ_5 values to the structure collected in this work.*

Bonds	Angle	Structure	Coordination Sphere
Kumar *et al*		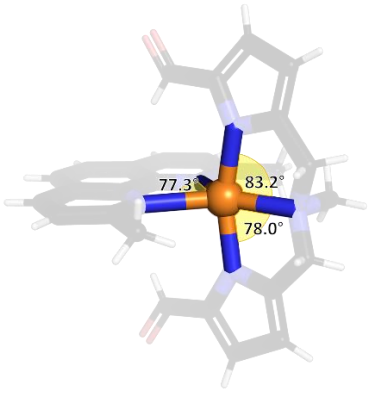	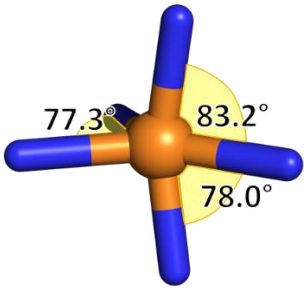
N1 – Cu – N2	78.0°		
N2 – Cu – N3	83.2°		
N4 – Cu – N5	77.3°		
Aguilo *et al*		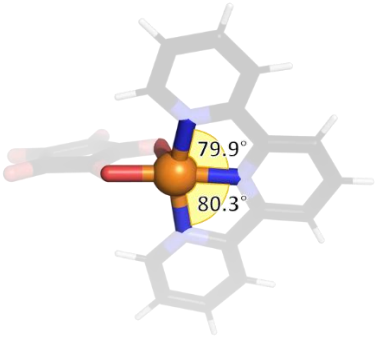	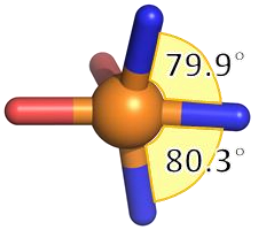
N1 – Cu – N2	79.9°		
N2 – Cu – N3	80.3°		
Average	79.7°		

Structures with six membered chelate rings also demonstrate distortion, favouring larger bond angles[109]. The structures below include copper centres with six membered chelate rings , formed by nitrogen donor atoms in a tridentate ligand separated by propyl chains. The backbone of this ligand was equivalent to the backbone of the donor atom connectivity of the ligand used in this work. The structures listed below have τ_5 = 0.03-0.69, with an average of 0.34. Most of the structures are therefore square pyramidal and comparable to the collected structure. All of the N – Cu – N angles listed were close to the expected 90° for a square pyramid.

The impact of the six membered chelate ring on the bond angle appeared to increase the N – Cu – N bond angle. The N – Cu – N bond angles from the five membered chelate rings were compared the values give an average of 79.7°. By comparison, the six membered chelate rings give an average angle of 92.5°. From this, it was evident that the six membered chelate rings encourage a larger coordination angle.

Table 4.7: *Literature N – Cu – N bond angles, τ_5 values and coordination geometry.*

Bonds	Structure	Angle	τ_5 and Geometry
This work			
N1 – Cu – N3 N3 – Cu – N5	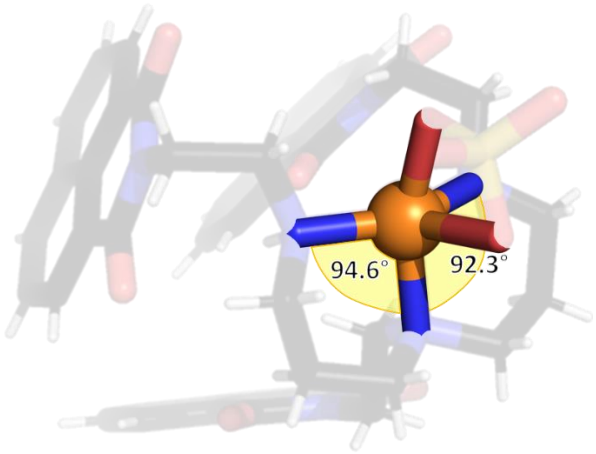	94.6° 92.3°	0.15, Square Pyramidal
242150[114]			
N13 – Cu – N14 N14 – Cu – N15	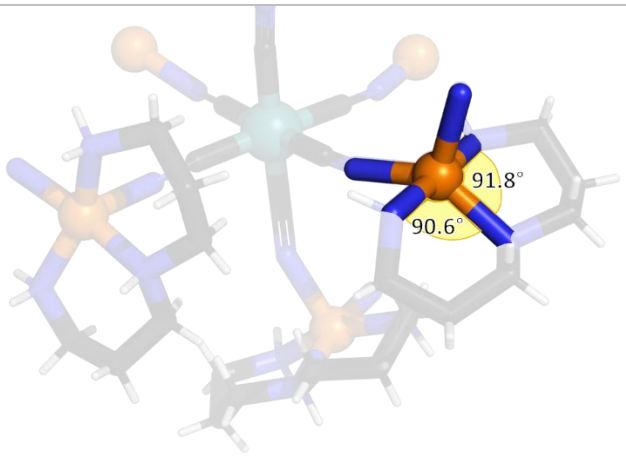	91.8° 90.6°	0.61, Trigonal Bipyramidal
278095[115]			
N2 – Cu – N3 N3 – Cu – N4	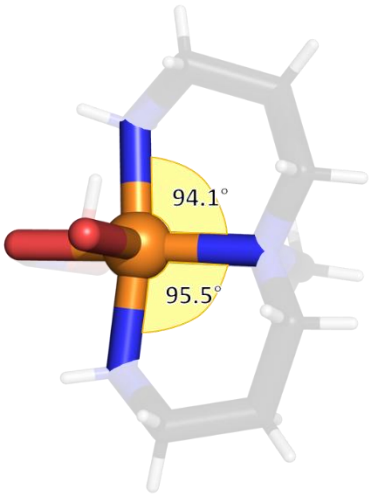	94.1° 95.5°	0.03, Square Pyramidal

Table 4.7 (continued)

Bonds	Structure	Angle	τ_5 and Geometry
	600401		
N1 – Cu – N2	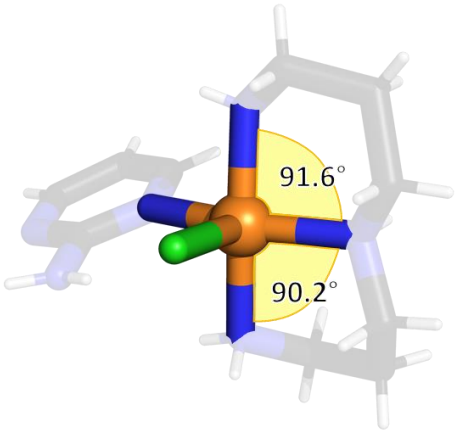	91.6°	0.19, Square Pyramidal
N2 – Cu – N3		90.2°	
	725160[116]		
N1 – Cu – N5	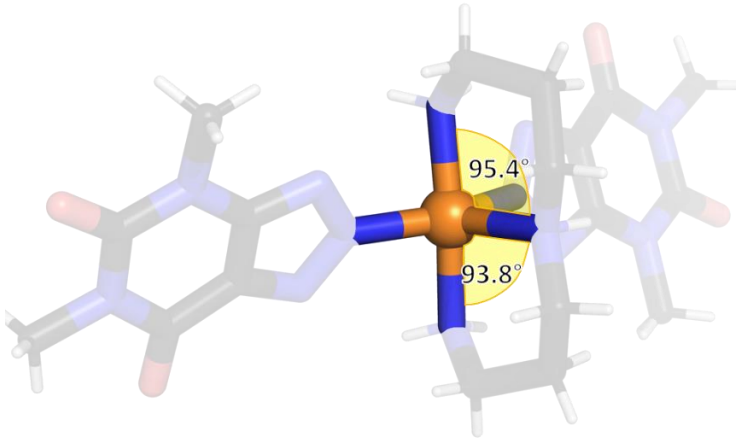	95.4°	0.34, Square Pyramidal
N5 – Cu – N9		93.8°	
	979301[117]		
N1 – Cu – N2	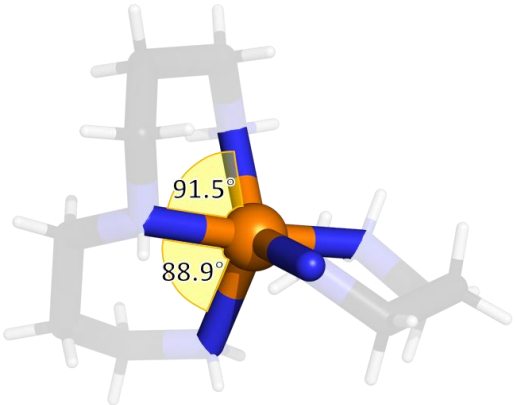	91.5°	0.69, Trigonal Bipyramidal
N2 – Cu – N3		88.9°	
	Average:	92.5°	0.34

The orientation of the tridentate ligands forming six membered chelate rings was relatively consistent across the structures, with the three nitrogen donor atoms located largely in the same plane as each other. A few exceptions to this occur, and these structures have tended towards more trigonal bipyramidal geometries as determined by the τ angles. This appeared to have occurred due to the bidentate ligand present encouraging the alternative form of wrapping, and as a result, the more trigonal bipyramidal geometry. This was also observed in the structure presented in this chapter; the bidentate sulfate ligand had encouraged a slightly more trigonal bipyramidal geometry.

4.4.1.4. Coordination Sphere Bond Lengths

The bond lengths of the coordination sphere consist of four approximately 2.0 Å bond lengths and one 2.4 Å bond length (Figure 4.6, Table 4.3). This longer bond appeared to be due to the balance between an unfavourable bond angle and an unfavourable bond length for the second sulfate oxygen, or the balance of the unfavourable bond angle with instead forming the lower four coordinate complex.

Jahn-Teller distortion is observed frequently in six coordinate octahedral copper(II) complexes as lengthening or shortening of the axial bonds[118] and was considered as a possibility for this distortion. It is also observed in lower coordinate complexes of copper(II)[119] as well as in trigonal bipyramidal complexes of other first row transition metals[120-121]. Generally, it is observed as a lengthening of the equatorial coordinate bonds[122], which was observed in one of three equatorial bonds in this structure. It was more likely that the extension observed in the Cu – O bond was due to the sulfate anion acting as a bidentate ligand and forming a four membered chelate ring, as this was also observed in the bidentate sulfate structures listed above.

The bond distances seen in the collected sample were consistent with those seen in copper(II) complexes rather than copper(I); a Cu-N coordinate bond for a copper(II) complex is generally between 1.8-2.2 angstroms in length, versus the shorter 1.6-1.8 for copper(I) complexes[123]. This was expected for this complex as copper(II) was used in the starting material. This also indicated that the complex will indeed be neutral due to the 2+ charge on the metal centre, the neutral ligand and the SO_4^{2-} ancillary ligand.

4.4.1.5. Naphthalimide Pendants

Another notable feature of the crystal structure was the distortion of the pendant naphthalimide moiety away from expected planarity (Figure 4.7). Distortion of aromatic systems is known in the context of polycyclic aromatic hydrocarbons (PAHs) and was most observed in extended systems or in systems where substituents on the molecules causes steric strain that

was mitigated through ring distortion.[124] In this case, the system consisted of only three rings without substantial steric strain, excepting possible intermolecular interactions. It seems unlikely that this distortion arose purely for similar reasons to those seen in PAH systems. This distortion was very minorly observed in the naphthalic anhydride starting material[125], and was very evident in the crystal structure for naphthalimide.[126] This is a difficult parameter to measure as it is not a traditionally observed torsion and was occurring in multiple directions to give the final result. Therefore, measuring the twisting was difficult to perform and this comparison was purely visual. The increase in distortion from the anhydride starting material to the imide product may correlate to the replacement of the anhydride oxygen for the imide nitrogen atom. In the collected structure, the three pendants were distorted in different ways, with the two terminal pendants twisting in a similar fashion and the middle differing by curving along the molecule instead. This could be due to the electronic or steric effects of either the tertiary nitrogen atom the linker connects to or the way the ring was located between the other two enforcing a certain conformation.

It was unclear as to whether the observed twisting had implications for the stability of the pendants or their use in further complexation, and as such literature structures were analysed to see if they experienced similar distortion (Figure 4.8). The twisting may impact of the ability of the ligand to act as an intercalator, which was proposed as an additional functionality of these targets in Chapter 1. Naphthalimide structures have been used as intercalators in other studies to much success, which would suggest that the twisting may not have had an effect. Other literature compounds have also been observed demonstrating this twisting, some to a greater extent than observed in this work. It appears to trend towards greater distortion if groups were added to the naphthalene moiety, with it possibly encouraging twisting due to electronic effects. Addition of aromatic substituents to the naphthalimide may alleviate the twisting, which other variants to the imide group including coordination of an oxygen atom did not. Substitution to the naphthalimide with amines appear to intensify the distortion. A larger study would need to be done to determine these trends further, and a measurement system to account for the distortion across the whole naphthalimide group away from the expected planarity would be required for more in-depth analysis.

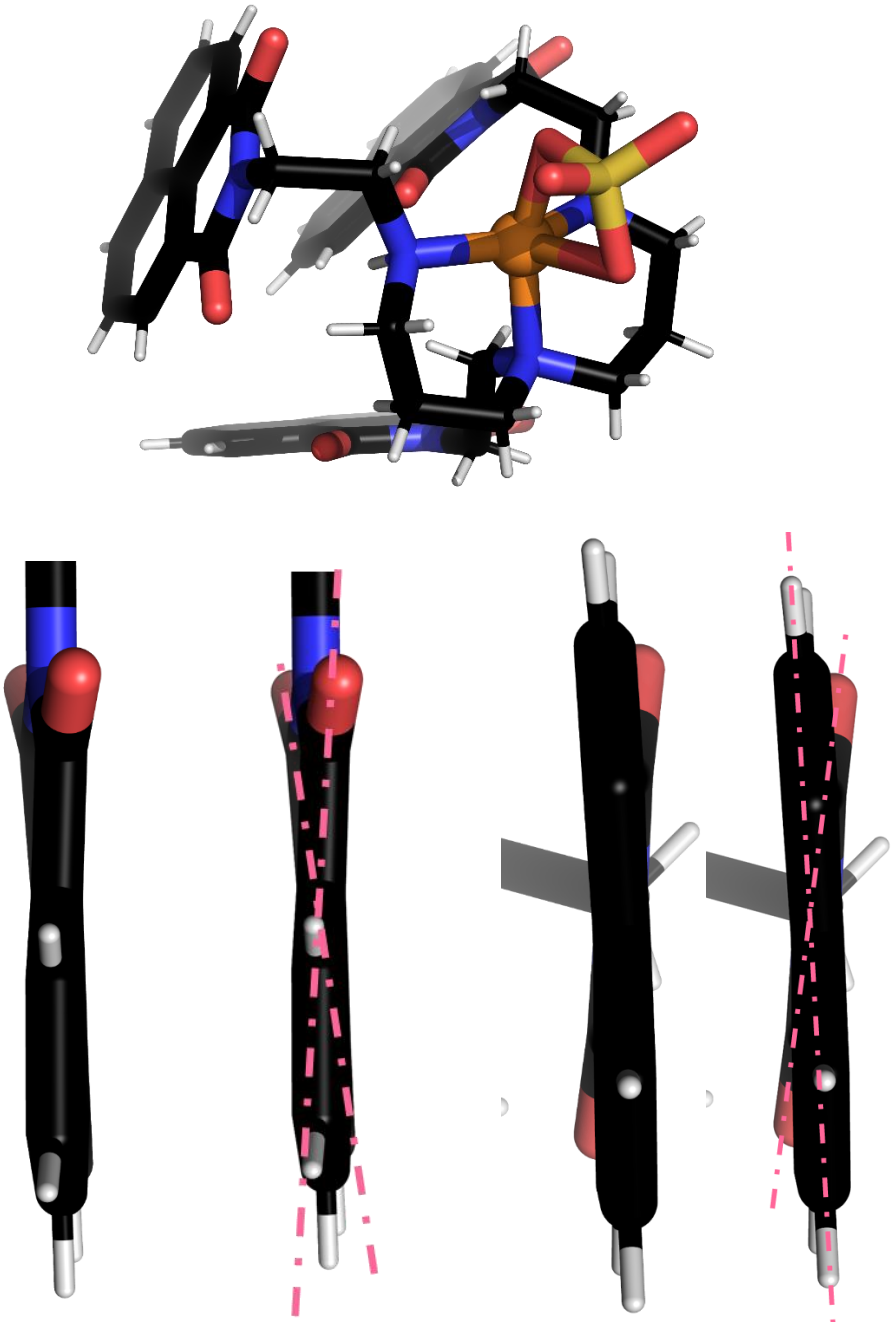

Figure 4.7: ***This figure illustrates the degree of twisting within the rings of the collected structure (top), 1,8-naphthalic anhydride[125] (middle) and naphthalimide[126] (lower). For the collected structure, dashed lines have been overlaid on a side by side image, where a single line designates a plane between a set of atoms, and the second line demonstrates how this plane is twisted compared to a second plane of atoms.***

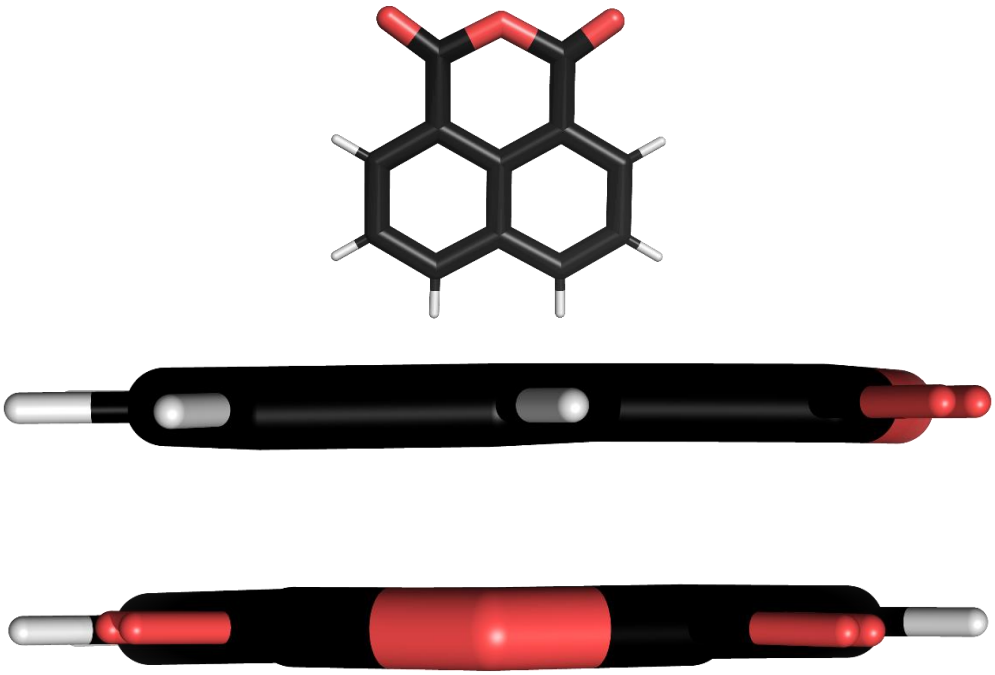

1,8-Naphthalic Anhydride

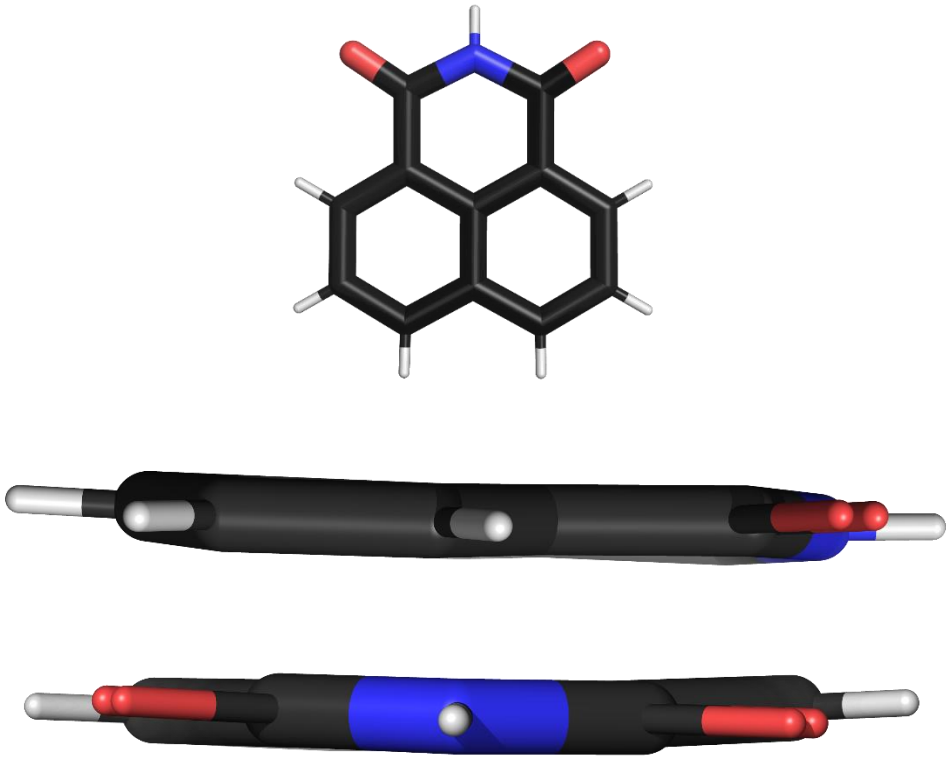

1,8-Naphthalimide

Figure 4.7 (continued).

251024[127]

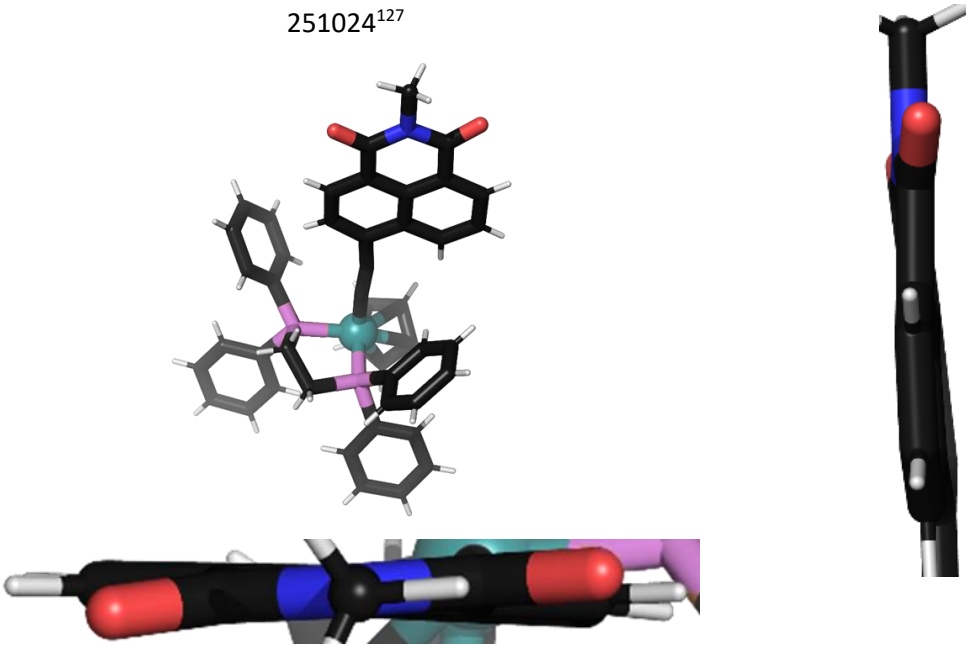

Figure 4.8: a) ***This structure includes a naphthalimidegroup coordinated to a metal centre via a carbon containing linker. The deformation of the napthalimide is demonstrated here as a twisting of the imide funtionality away from the naphthalene down the centre of the group from the nitrogen atom to the carbon atom at the bottom of the naphthalene ring fusing bond.***

253130[128]

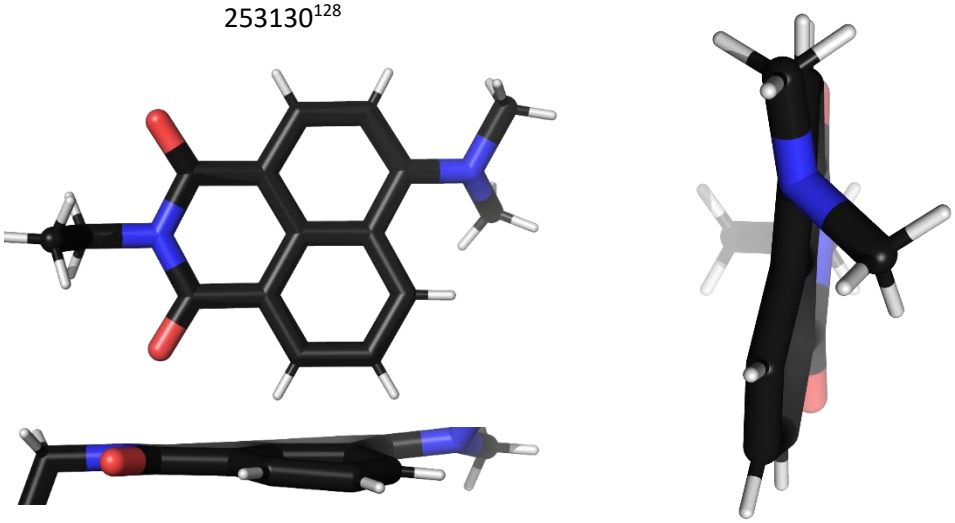

Figure 4.8: b) ***This structure showed very intense deformation to the naphthalimide system, with the ring adjacent to the amine substituent curving substantially. The ring with the amine substituent also appeared to bend sightly in the opposite direction.***

268888[129]

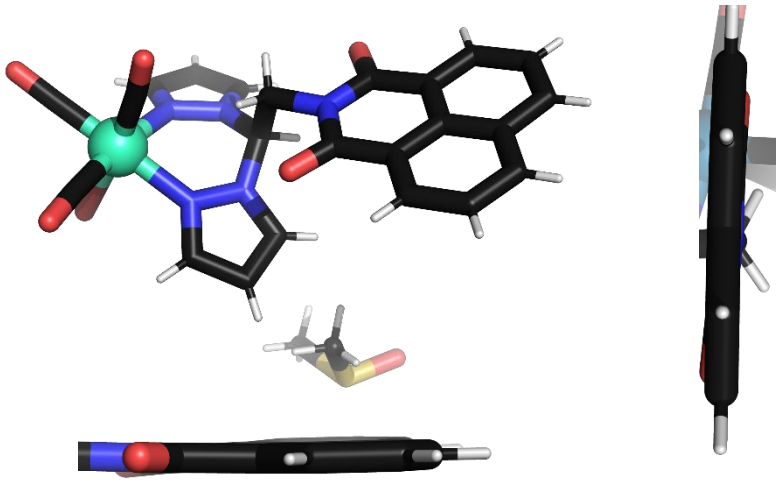

Figure 4.8: c) ***This structure demonstrates counterrotation of the naphthalimide, with the imide twisting in one direction and the naphthalene in the other. This deformation is like that observed in the structure reported in this work.***

274474[130]

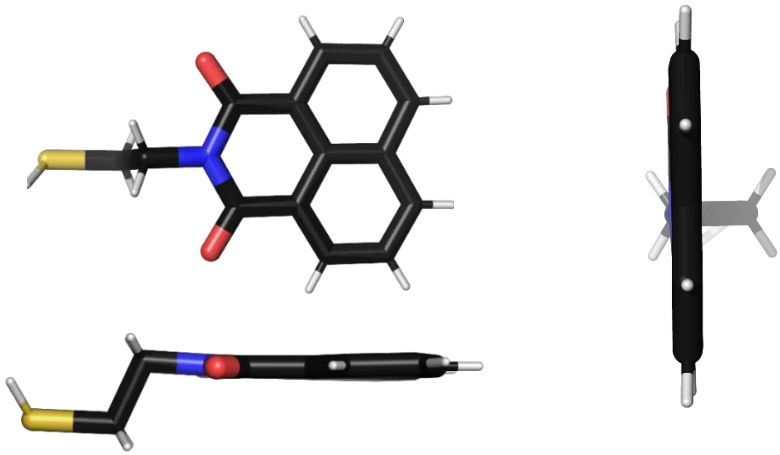

Figure 4.8: d) ***This structure again demonstrates counterrotation of the naphthalimide, with the imide twisting in one direction and the naphthalene in the other. This deformation was like that observed in the structure reported in this work to a lesser extent.***

274475[130]

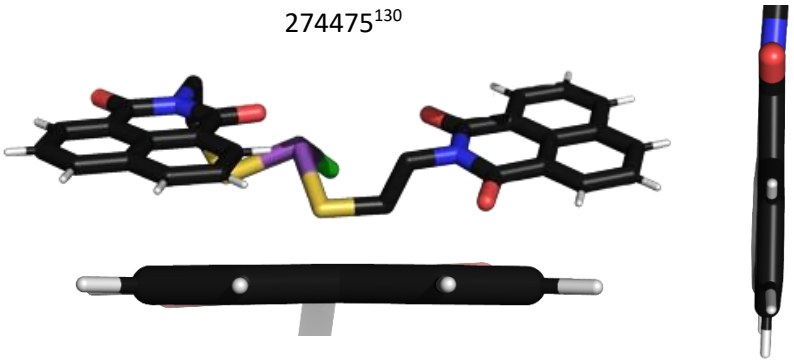

Figure 4.8: e) ***This structure also showed aa slight twisting deformation***

282516[131]

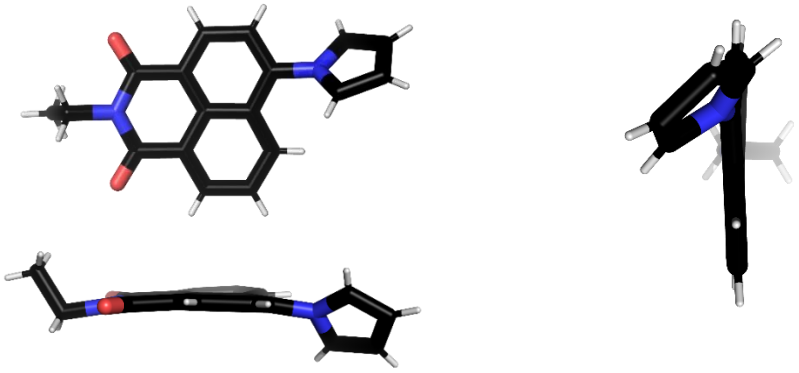

Figure 4.8: f) ***This structure also contains an amine substitution to the naphthalene moiety, and correspondingly experiences the same distortion to the adjacent ring resulting in an overall curved molecule in the direction of the non-substituted ring.***

604991[132]

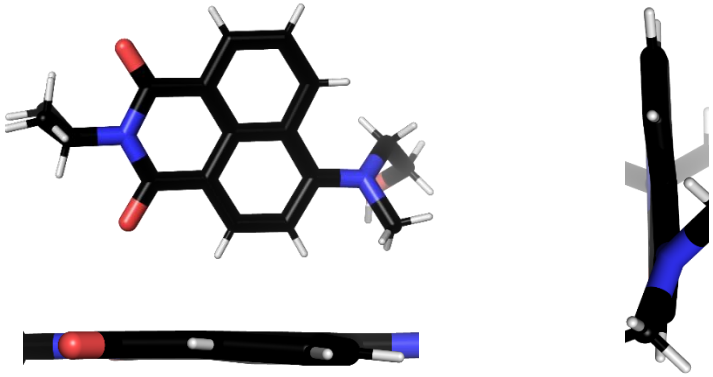

Figure 4.8: g) ***Another amine containing structure with adjacent ring curving.***

636004[91]

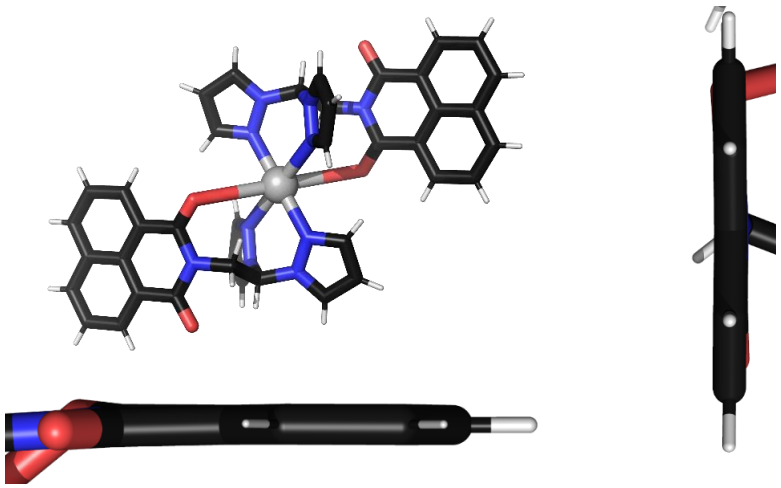

Figure 4.8: h) ***This structure contains a coordinated naphthalimide, including coordination of the oxygen to the metal centre. It is unclear as to whether this compound retains imide character, yet the same twisting deformation was observed.***

636006[91]

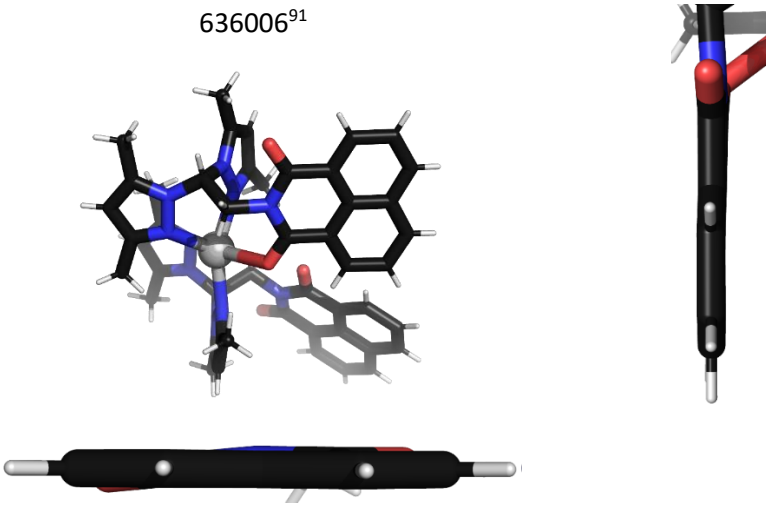

Figure 4.8: i) ***This molecule was also coordinated through the oxygen, and showed twisting. This indicated that the oxygen coordination did not alleviate the deformation.***

636007[91]

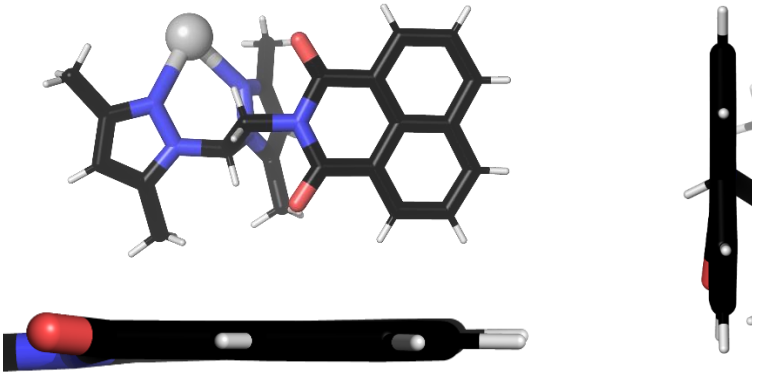

Figure 4.8: j) ***This coordinated naphthalimide was a similar distance from the metal centre as the naphthalimides in this work. This molecule demonstrates similar twisting to that in this work.***

677818[133]

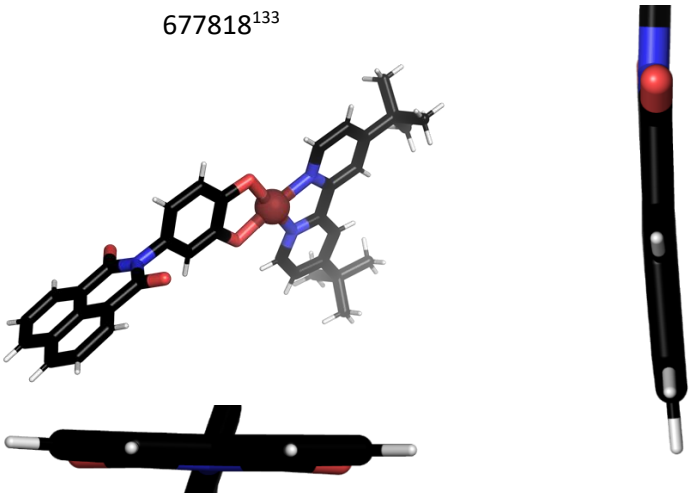

Figure 4.8: k) ***This naphthalimide was part of a ligand system, but was distant from the metal centre. In this structure, the naphthalimide was bent in the plane of the molecule, resulting in an overall curve to the naphthalimide.***

Figure 4.8: l) ***This naphthalimide showed very little deformation, despite the functionality. This may be due to the extended polycyclic aromatic substituent attached to the naphthalene moiety. Further analysis would be required to conclude this.***

The naphthalimides were not oriented symmetrically, with the central naphthalimide angling slightly towards one of the others. The cause of this interaction is unknown as the distance between the aromatic rings was likely too large for π interactions. It was possibly due to the packing of multiple molecules in the crystal structure.

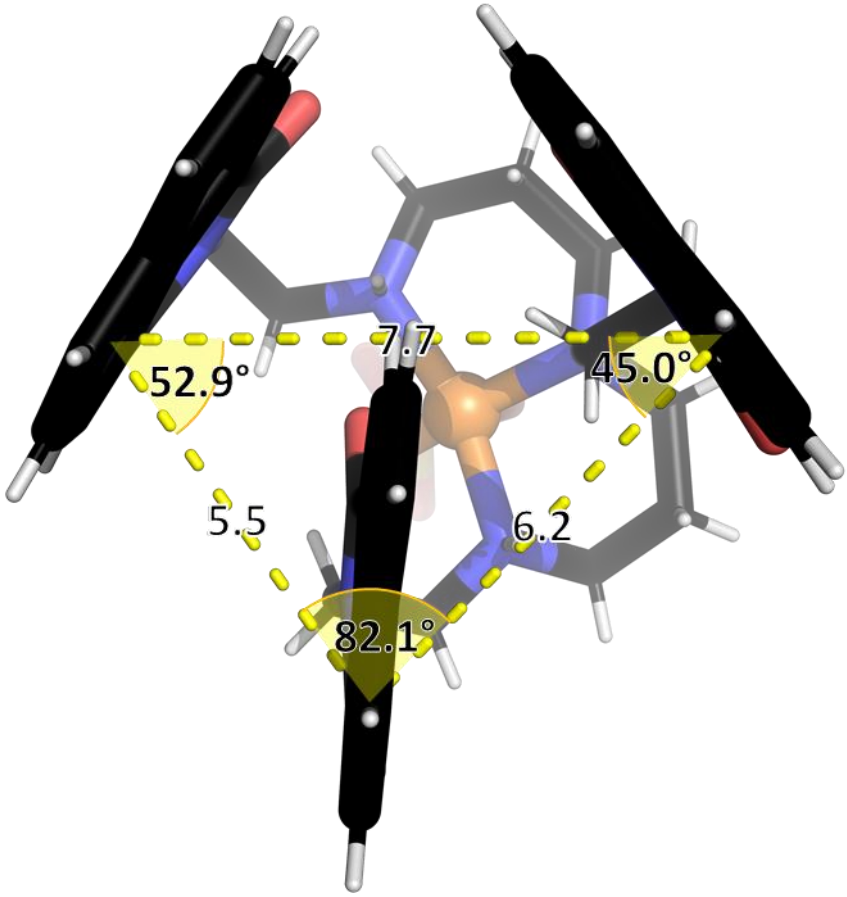

Figure 4.9*: Distances and angles shown for the naphthalimide pendants, measured from the centre of the same ring in each naphthalimide. The packing pace fill diagram is also shown***.**

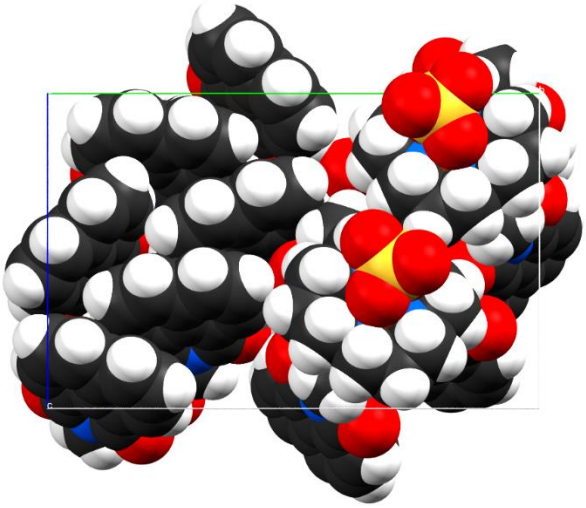

Figure 4.9 (continued)

4.4.2. Hexamine Starting Material and Ligand Synthesis

The naming and CAS number of the purchased amine indicated it was the linear polyamine 4.1, however, the crystal structure obtained as product of reaction with this amine showed that there was some of the branched isomer 4.2 present in the mixture.

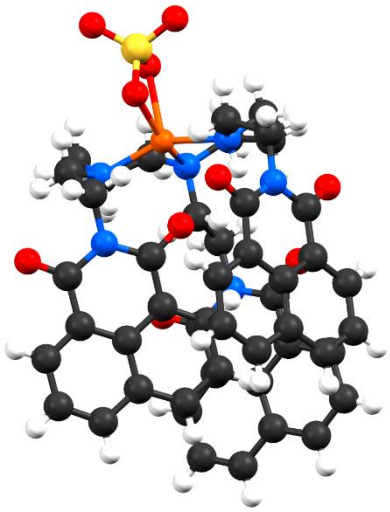

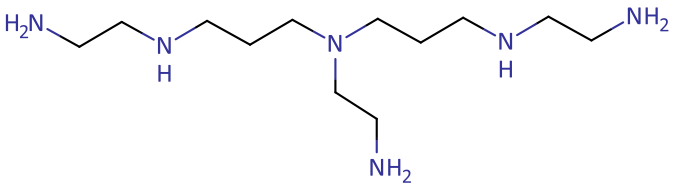

Figure 4.10: ***Crystal structure of the copper naphthalimide product, and structure of the amine starting material required to make this compound.***

It was possible for both species to be present, with the branched species preferentially forming crystals over the linear species due to the additional primary amine (and therefore additional naphthalimide pendant) that it possessed encouraging crystallisation. ESI-MS results indicate that there may be some of the linear species present as a dinaphthalimide was detected along with excess naphthalic anhydride, and increasing the amount of naphthalic anhydride did not

result in additional trinaphthalimide formation but rather increased detection of the free anhydride and the dinaphthalimide species with a naphthalamide attached. Further information on this can be observed in Appendix H.

4.5. Conclusions

This chapter explored the synthesis and characterisation of a novel copper polyamine complex possessing three pendant naphthalimide groups. The crystal structure was discussed and determined to have a distorted square pyramidal geometry around the copper centre with distortion of both bond lengths and bond angles occurring due to the sulfate ancillary ligand. The reproducibility of the experiment and the composition of the amine starting material were also explored. The amine was determined to be a mixture of both the compound named on the bottle; a linear polyamine, and a branched isomer that went on to form the ligand observed in the crystal structure. This was determined through X-ray crystallographic detection of the branched compound.

The initial intention for the synthesis of this ligand was to use as an alternative to the ligand in the previous chapter, facilitating physical blocking of the platinum centre of a heterodinuclear complex. The crystal structure showed that the formation of the naphthalimide ligands and their subsequent complexation was possible following the route examined in this thesis, from polyamine and anhydride starting materials. The structure indicated that the trinaphthalimide species 4.4 would be unsuitable for the purpose of heterodinuclear complex synthesis. Additionally, the fact that complex 4.7 was not detected in the mixture, despite ligand 4.3 being detected, suggests that further synthesis with this material was not likely to yield cobalt complexes suitable for use in heterodinuclear compounds.

Chapter 5:*Conclusions and Future Work*

This thesis explored the synthesis and analysis of complex polyamine ligand mixtures, their separation by copper complexation, and subsequent cobalt complexation. The ligand design of was based around the need for a motif that had the capacity to physically block associative ligand exchange to the platinum centre of a heterodinuclear drug candidate. This ligand should complex the redox-sensing cobalt centre while extending out over the platinum centre, and as such the tetradentate naphthalimide target 2.1 was selected.

Synthesis of the tetradentate naphthalimide ligand was based on imide formation from a hexamine starting material and 1,8-naphthalic anhydride. This reaction was performed using a mechanochemical procedure and afforded the desired ligand 2.1. Unfortunately, the amine starting material contained a range of impurities including branched compounds, piperazine derivatives and polyamines of different lengths. The purity of the dinaphthalimide ligand was judged by ESI-MS and NMR to be present as up to 35% of the reaction mixture. The side product compounds including 2.3, 2.4, 2.6, 2.8 and 2.13 contained different numbers of nitrogen atoms, some of which would be able to act as donor atoms for complexation. Many of the undesirable side products contained fewer donor atoms than the desired compound, and therefore the purification was attempted through complexation.

The crude ligand material was reacted with copper sulfate, producing an oily blue solid and a deep blue solution. The solid contained much of the copper dinaphthalimide complexation product, $[Cu(2.1)]^{2+}$, with many side products appearing in both phases when analysed by ESI-MS. Following complexation, both phases were treated with EDTA to remove the copper from the complexes formed, each producing a solid and a solution. As for the complexation liquor prior to treatment, the solid and solution produced by EDTA treatment both contained predominantly side products. The complexation solid also produced a solid and a solution. The solid produced showed an enrichment of the dinaphthalimide ligand 2.1 compared to the crude material, but still retained substantial presence of impurities. The solution ESI-MS showed a large enrichment of the desired free dinaphthalimide ligand product 2.1. Unfortunately, this perceived enrichment was tempered by the copper EDTA complex from the copper removal, which was present in large amounts in solution but was not detected by ESI-MS due to the neutral or negative charge.

To separate the dinaphthalimide 2.1 from the copper EDTA complex, the solution was extracted with chloroform. The chloroform extract only contained side products, which corresponded to

an increase of the enrichment of the remaining solution. This solution was then treated using anion exchange chromatography to varying results, producing a precipitate prior to loading one of the solutions to the column that contained predominantly the dinaphthalimide product 2.1. This was then used for further reactions. The purification by complexation process was performed following various modifications, with methanolic addition of 40% stoichiometric pentahydrate copper sulfate showing the greatest enrichment.

The procedure followed during the study of the complexation by purification process showed that, despite the substantial impurity of the amine starting material, the desired dinaphthalimide ligand product could be enriched following complexation by purification. During this work, this enrichment was achieved as both a slight increase observed in a large bulk of material, or a substantial increase in a small yield of material. This demonstrates that although the enrichment was possible, additional work would need to be done to improve upon the yield to make this material useful for further reactions. Additional work could also surround the further purification of the solid material produced following treatment of the copper complexation product with EDTA, as this solid showed some enrichment over the crude material and had a much greater mass than the more enriched material.

Following synthesis and purification of the ligand material, two cobalt complexes were successfully synthesised in impure form. The two complexes were the dinitrite and carbonate complexes, chosen for their ability to displace the coordinated anions in favour of water using acid. This displacement was critical for the further steps of complexation to platinum. Both compounds were detected using ESI-MS in syntheses using crude and enriched ligand material syntheses, with the crude material resulting in the expected contamination of side products. The enriched material did not appear to increase the relative intensity by ESI-MS of the desired complexes, and this appeared to be due to the detection of a side product. This side product features a cobalt coordinated to a deprotonated form of the tetradentate naphthalimide ligand which was often detected as the major peak of the ESI-MS spectra. It was unclear as to the true amount of this product, and whether it was a stable complex in solution or produced during the ESI process.

This complex could be detected during ESI-MS as a degradation product of the intended complexes, which would indicate the synthesis was largely successful, or it may be forming and precluding formation of the intended complexes, which would indicate that the desired complexation reaction was unfavourable. The fact that some reaction fractions did not contain the peak corresponding to this deprotonated complex, but did contain the peak corresponding

to the nitrite complex, indicates that this species is not solely a degradation product. As a result, further work on this species and the complexation procedures in general would need to be undertaken in order to determine the true complex yield, and therefore its fitness for use for heterodinuclear complex synthesis. Future work could also include synthesis of a broader range of complexes. Syntheses involving cobalt coordinated to chloride, sulfate, ammonia and ethane-1,2-diamine ligands have also been attempted during this work with only trace amounts of the complexes occasionally detected.

Alongside this process, a second tetradentate dinaphthalimide ligand 4.3 was proposed in an attempt to generate fewer side products. Synthesis of this ligand was performed in the same manner as the previous and the solid produced many peaks in the ESI-MS spectrum. To determine if any of the desired ligand was present and to purify it, the material was reacted with copper. This produced a blue solid and a blue solution, which was allowed to stand and yielded bright blue crystalline material. Analysis of these crystals by x-ray diffraction allowed for structural elucidation, showing that a complex 4.6 had formed of copper coordinated to a branched trinaphthalimide ligand 4.4 and a sulfate anion. The presence of this ligand indicated that the starting material amine contained the branched isomer that had led to this complex, and further ligand material synthesis showed that this was not the major component of the reaction but was present in substantial amounts; NMR analysis suggested 20%. The crystal structure analysis showed that the copper(II) centre was five coordinate, forming six-membered chelate rings with the nitrogen donor atoms of the trinaphthalimide ligand. The sulfate anion coordinated through a bidentate bonding mode, causing a small bond angle between the copper centre and the two donor oxygen atoms due to the four membered sulfate chelate ring. This resulted in a distortion of the square pyramidal coordination geometry.

To continue this work, more amine starting materials could be trialled to avoid the purity issues observed in this work. These amines could be manufactured or purified in a different manner to prevent side products from forming, or be composed of fewer repeating aminoethane units, resulting in fewer isomeric possibilities. Initial work has begun using two tetramine starting materials for this purpose and preliminary results indicated that some increase in enrichment can be achieved. Further work surrounding the use of different amines would give value to this project, especially if different hexaamines could be used for synthesis. The two tetramines used were chosen primarily due to their availability and lack of contamination, rather than their ability to form the tetradentate ligands required for dinuclear complex synthesis. Further work could trial various hexaamines in the attempt to find purer amines that can form tetradentate ligands.

A further issue surrounded the differing solubility of the ligands and the metal centres they were complexing. The solubility of both the free ligands and any complexation products was low and precludes convenient study. This was also an issue with regards to future drug efficacy – compounds that are insoluble in aqueous media tend to make poor candidates for therapeutics as they cannot be absorbed by the body or easily transported through the bloodstream. It is thus important to attempt to increase the solubility of the ligands, and subsequently, their complexes. Ideally, both the ligand and the metal centre would be soluble in the same solvent to allow for reaction as this allows both species to be dissolved in the minimum volume, encouraging product formation. The ligands studied in this work were most soluble in chloroform, and the metal salts were predominantly water soluble. Methanol was used as a middle ground for syntheses, however, the increased reaction volume due to the lower solubility could be identified as a possible cause for the limited complexation. Future work into increasing the solubility of the ligand material may be able to alleviate this issue. This could be approached through substitution on the naphthalimide moiety. Substitution for a charged or polar group with low ability to act as a donor atom for complexation to platinum would potentially make the ligand more soluble in aqueous solutions.

Preliminary exploration of this topic has focussed on substitution to the naphthalimide group using nitro and amino substituents, as well as through replacement of the naphthalimide group for the smaller phthalimide group. The nitro group was selected due to the increase in polarity this group may provide, while likely being a poor donor site to interact with the platinum centre it was designed to protect. Amino substitution was a further prospect for study due to the ready production from the nitro derivative and ability for further substitution to the amino group for other functional groups to produce a range of naphthalimide options. Preliminary syntheses in this area are ongoing. Work involving phthalimides was intended to increase the solubility by reducing the aromatic character of the diphthalimide product compared to the dinaphthalimide.

The synthesis and purification process used to source the amine starting material appeared to have had major bearing on the range and quantity of the contaminants present. Alternative methods of synthesising this material may allow for an improvement in the purity of the amine starting material by preventing formation of the side products. Many of the synthetic routes proposed for the production of the hexamine starting material would likely encounter some level of the side product formation seen in the industrially produced sample and would still require much purification.

Previous work indicated that the charge on the overall heterodinuclear complex prevented isolation of compounds[62]. It was highlighted that the complexes with a 3+ charge were too soluble to be isolated from side products, whereas the neutrally charged compounds were too insoluble to dissolve in solvents other than DMSO which then caused them to break down (Figure 1.5). The setting of my project surrounded the design of compounds that would physically block the platinum centre to prevent the interaction with solvent. Alternatively, future work could surround the synthesis of complexes with a different overall charge. This is beneficial for more than one reason; increasing the charge from neutral should prevent requiring DMSO for dissolution as it should be water soluble, which would prevent the unfavourable interaction, while additionally giving the compound more medicinal value as it would need to be water soluble to interact with the body. Ethylenediamine diacetic acid (EDDA) is a tetradentate ligand comprising two nitrogen donor atoms and two oxygen donor atoms. The acetic acid groups can be deprotonated to form coordinate bonds to the cobalt centre, giving the ligand a 2- charge. For a heterodinuclear complex with two bridging OH^- ligands, the overall complex charge would be 1+ if EDDA were used as the cobalt coordination sphere. Work using this ligand has begun and is ongoing.

To summarise, the results from this work indicate that synthesis of dinaphthalimide ligands was successfully able to produce the desired compound, 2.1, in an impure form due to the purity of the amine starting material used. Attempts to separate the desired ligand from the many impurities focussed on purification by complexation, relying on the different properties of the ligand 2.1, the complex Cu(2.1), and any side products to be sufficiently different to allow for their separation. This method showed moderate success, with enrichment of the desired compound observed. Cobalt complexes of 2.1 were also synthesised, although these were also faced with issues in purity. $[Co(2.1)CO_3]^+$ and $[Co(2.1)(NO_2)_2]^+$ were detected by ESI-MS analysis and further work is occurring surrounding optimisation of the conditions of the reaction to produce more of the desired complexes. A crystal structure was also reported in this work, showing a novel copper complex of tridentate naphthalimide ligand 4.4. This structure provided evidence of the naphthalimide moiety formation and the ability for these ligands to form stable complexes.

References

The programs Olex2[97] with ShelXL[99] and ShelXT[99] were used for structural elucidation within Chapter 4. PyMol Education version 2.0[135], Avogadro version 1.2.0[136] and Mercury[137] were used to generate the 3D rendered figures of both the crystal structures (PyMol, Mercury) and the theoretical models (Avogadro, PyMol) generated throughout this thesis. MestRe Nova[138] was used to render and label NMR spectra. External crystal structures were sourced from the CCDC[139] and are referenced by the paper associated with the structure.

1. IARC, Latest global cancer data: Cancer burden rises to 18.1 million new cases and 9.6 million cancer deaths in 2018. In *Press Release N° 263*, World Health Organisation: 2018.
2. Merletti, F.; Galassi, C.; Spadea, T., The socioeconomic determinants of cancer. *Environ. Health (London, U. K.)* **2011,** *10* (1), S7-S7.
3. WHO, Cancer: Key Facts. https://www.who.int/news-room/fact-sheets/detail/cancer, 2018.
4. Garrett, R. H.; Grisham, C. M., *Biochemistry*. Brooks/Cole, Cengage Learning: Belmont, CA, 2013.
5. Nelson, D. L.; Cox, M. M.; Lehninger, A. L., *Lehninger Principles of Biochemistry*. W.H. Freeman: New York, 2013.
6. Alberts, B.; Wilson, J.; Hunt, T., *Molecular Biology of the Cell*. Garland Science: New York, 2008.
7. Vermeulen, K.; Van Bockstaele, D. R.; Berneman, Z. N., The cell cycle: a review of regulation, deregulation and therapeutic targets in cancer. *Cell Proliferation* **2003,** *36* (3), 131-149.
8. Braña, M. F.; Cacho, M.; Gradillas, A.; Pascual-Teresa, B.; Ramos, A., Intercalators as Anticancer Drugs. *Curr. Pharm. Des.* **2001,** *7* (17), 1745-1780.
9. Boulikas, T.; Vougiouka, M., Cisplatin and platinum drugs at the molecular level (Review). *Oncol. Rep.* **2003,** *10* (6), 1663-82.
10. Dasari, S.; Tchounwou, P. B., Cisplatin in cancer therapy: molecular mechanisms of action. *Eur. J. Pharmacol.* **2014,** *0*, 364-378.
11. Greene, M. H., Is cisplatin a human carcinogen? *J. Natl. Cancer. Inst.* **1992,** *84* (5), 306-12.
12. Ryan, G. J.; Poynton, F. E.; Elmes, R. B. P.; Erby, M.; Williams, D. C.; Quinn, S. J.; Gunnlaugsson, T., Unexpected DNA binding properties with correlated downstream biological applications in mono vs. bis-1,8-naphthalimide Ru(II)-polypyridyl conjugates. *Dalton Trans.* **2015,** *44* (37), 16332-16344.
13. DeVita, V. T.; Chu, E., A History of Cancer Chemotherapy. *Cancer Res.* **2008,** *68* (21), 8643.
14. DeVita, V. T.; Rosenberg, S. A., Two Hundred Years of Cancer Research. *N. Engl. J. Med.* **2012,** *366* (23), 2207-2214.
15. Padma, V. V., An overview of targeted cancer therapy. *BioMedicine* **2015,** *5* (4), 19-19.
16. Dipple, A., DNA adducts of chemical carcinogens. *Carcinogenesis* **1995,** *16* (3), 437-441.
17. Tomasetti, C.; Li, L.; Vogelstein, B., Stem cell divisions, somatic mutations, cancer etiology, and cancer prevention. *Science* **2017,** *355* (6331), 1330.
18. Balendiran, G. K.; Dabur, R.; Fraser, D., The role of glutathione in cancer. *Cell Biochem. Funct.* **2004,** *22* (6), 343-352.
19. Chen, H. H. W.; Kuo, M. T., Role of Glutathione in the Regulation of Cisplatin Resistance in Cancer Chemotherapy. *Met.-Based Drugs* **2010,** *2010*.
20. Yadav, A.; Janaratne, T.; Krishnan, A.; Singhal, S. S.; Yadav, S.; Dayoub, A. S.; Hawkins, D. L.; Awasthi, S.; MacDonnell, F. M., Regression of lung cancer by hypoxia-sensitizing ruthenium polypyridyl complexes. *Mol. Cancer Ther.* **2013,** *12* (5), 643-53.

21. Zhu, Z.; Du, S.; Du, Y.; Ren, J.; Ying, G.; Yan, Z., Glutathione reductase mediates drug resistance in glioblastoma cells by regulating redox homeostasis. *J. Neurochem.* **2018,** *144* (1), 93-104.
22. Ravera, M.; Baracco, S.; Cassino, C.; Zanello, P.; Osella, D., Appraisal of the redox behaviour of the antimetastatic ruthenium(III) complex [ImH][$RuCl_4$(DMSO)(Im)] , NAMI-A. *Dalton Trans.* **2004,** (15), 2347-2351.
23. Fung, C.; Fossa, S. D.; Milano, M. T.; Oldenburg, J.; Travis, L. B., Solid Tumors After Chemotherapy or Surgery for Testicular Nonseminoma: A Population-Based Study. *J. Clin. Oncol.* **2013,** *31* (30), 3807-3814.
24. Zaki, M.; Arjmand, F.; Tabassum, S., Current and future potential of metallo drugs: Revisiting DNA-binding of metal containing molecules and their diverse mechanism of action. *Inorg. Chim. Acta* **2016,** *444*, 1-22.
25. Hasinoff, B. B.; Abram, M. E.; Barnabe, N.; Khelifa, T.; Allan, W. P.; Yalowich, J. C., The catalytic DNA topoisomerase II inhibitor dexrazoxane (ICRF-187) induces differentiation and apoptosis in human leukemia K562 cells. *Mol. Pharmacol.* **2001,** *59* (3), 453-61.
26. Visani, G.; Milligan, D.; Leoni, F.; Chang, J.; Kelsey, S.; Marcus, R.; Powles, R.; Schey, S.; Covelli, A.; Isidori, A.; Litchman, M.; Piccaluga, P. P.; Mayer, H.; Malagola, M.; Pfister, C., Combined action of PSC 833 (Valspodar), a novel MDR reversing agent, with mitoxantrone, etoposide and cytarabine in poor-prognosis acute myeloid leukemia. *Leukemia* **2001,** *15*, 764.
27. Nooter, K.; Sonneveld, P., Clinical relevance of P-glycoprotein expression in haematological malignancies. *Leuk. Res.* **1994,** *18* (4), 233-43.
28. Saez, R.; Craig, J. B.; Kuhn, J. G.; Weiss, G. R.; Koeller, J.; Phillips, J.; Havlin, K.; Harman, G.; Hardy, J.; Melink, T. J., Phase I clinical investigation of amonafide. *J. Clin. Oncol.* **1989,** *7* (9), 1351-1358.
29. Hu, P.; Wang, Y.; Zhang, Y.; Song, H.; Gao, F.; Lin, H.; Wang, Z.; Wei, L.; Yang, F., Novel mononuclear ruthenium(II) complexes as potent and low-toxicity antitumour agents: synthesis, characterization, biological evaluation and mechanism of action. *RSC Adv.* **2016,** *6* (36), 29963-29976.
30. Amr, A.; Michael, A. B., New Platinum and Ruthenium Complexes - the Latest Class of Potential Chemotherapeutic Drugs - a Review of Recent Developments in the Field. *Mini-Rev. Med. Chem.* **2009,** *9* (13), 1489-1503.
31. Sudhakar, A., History of Cancer, Ancient and Modern Treatment Methods. *J. Cancer Sci. Ther.* **2009,** *1* (2), 1-4.
32. Aderibigbe, B. A., Polymeric Prodrugs Containing Metal-Based Anticancer Drugs. *J. Inorg. Organomet. Polym. Mater.* **2015,** *25* (3), 339-353.
33. Banerjee, S.; Veale, E. B.; Phelan, C. M.; Murphy, S. A.; Tocci, G. M.; Gillespie, L. J.; Frimannsson, D. O.; Kelly, J. M.; Gunnlaugsson, T., Recent advances in the development of 1,8-naphthalimide based DNA targeting binders, anticancer and fluorescent cellular imaging agents. *Chem. Soc. Rev.* **2013,** *42* (4), 1601-1618.
34. Braña, M. F.; Ramos, A., Naphthalimides as anti-cancer agents: synthesis and biological activity. *Curr. Med. Chem. Anticancer Agents* **2001,** *1* (3), 237-55.
35. Houghton P, J.; Cheshire P, J.; Hallman J, C.; Gross J, L.; McRipley R, J.; Jung-Hui, S. U. N.; Behrens C, H.; Dexter D, L.; Houghton J, A., Evaluation of a novel bis-naphthalimide anticancer agent, DMP840, against human xenografts derived from adult, juvenile, and pediatric cancers. *Cancer Chemother. Pharmacol.* **1993,** *33* (4), 265-272.
36. Berman, H. M.; Young, P. R., The Interaction of Intercalating Drugs with Nucleic Acids. *Annu. Rev. Biophys. Bioeng.* **1981,** *10* (1), 87-114.
37. Bailly, C.; Braña, M.; Waring, M. J., Sequence-selective intercalation of antitumour bis-naphthalimides into DNA. *Eur. J. Biochem.* **1996,** *240* (1), 195-208.
38. Clayden, J.; Greeves, N.; Warren, S. G., *Organic Chemistry*. Oxford University Press: Oxford, 2012.

39. Hunter, C. A.; Sanders, J. K. M., The nature of π-π interactions. *J. Am. Chem. Soc.* **1990,** *112* (14), 5525-5534.
40. Haran, T. E.; Berkovich-Yellin, Z.; Shakked, Z., Base-Stacking Interactions in Double-Helical DNA Structures: Experiment Versus Theory. *J. Biomol. Struct. Dyn.* **1984,** *2* (2), 397-412.
41. Bousquet, P. F.; Braña, M. F.; Conlon, D.; Fitzgerald, K. M.; Perron, D.; Cocchiaro, C.; Miller, R.; Moran, M.; George, J.; Qian, X.-D.; Keilhauer, G.; Romerdahl, C. A., Preclinical Evaluation of LU 79553: A Novel Bis-naphthalimide with Potent Antitumor Activity. *Cancer Res.* **1995,** *55* (5), 1176-1180.
42. Braña, M. F., Castellano, J.M., Roldán, C.M., Synthesis and mode(s) of action of a new series of imide derivatives of 3-nitro-1,8 naphthalic acid. *Cancer Chemother. Pharmacol.* **1980,** *4* (1), 61-66.
43. Braña, M. F.; Cacho, M.; Ramos, A.; Dominguez, M. T.; Pozuelo, J. M.; Abradelo, C.; Rey-Stolle, M. F.; Yuste, M.; Carrasco, C.; Bailly, C., Synthesis, biological evaluation and DNA binding properties of novel mono and bisnaphthalimides. *Org. Biomol. Chem.* **2003,** *1* (4), 648-654.
44. Braña, M. F.; Castellano, J. M.; Moran, M.; deVega, M. J. P.; Perron, D.; Conlon, D.; Bousquet, P. F.; Romerdahl, C. A.; Robinson, S. P., Bis-naphthalimides 3: Synthesis and antitumor activity of N,N'-bis 2-(1,8-naphthalimido)-ethyl alkanediamines. *Anti-Cancer Drug Des.* **1996,** *11* (4), 297-309.
45. Keilhauer, G. R., Cynthia; Braña, M. F.; Qian, X.-D.; Bousquet, P. F.; Berlanga, J. M. C.; Moset, M. M.; de Vega, M. J. P. Bis-naphthalimides for the treatment of cancer. 1997.
46. Pérez, J. M.; López-Solera, I.; Montero, E. I.; Braña, M. F.; Alonso, C.; Robinson, S. P.; Navarro-Ranninger, C., Combined Effect of Platination and Intercalation upon DNA Binding of Novel Cytotoxic Pt−Bis(naphthalimide) Complexes. *J. Med. Chem.* **1999,** *42* (26), 5482-5486.
47. Roldan, C. M.; Braña, M. F.; Berlange, J. M. C. N-Aminoethyl-substituted-3-nitronaphthalimides. 1977.
48. Rosenberg, B.; Van Camp, L.; Krigas, T., Inhibition of Cell Division in *Escherichia coli* by Electrolysis Products from a Platinum Electrode. *Nature* **1965,** *205* (4972), 698-699.
49. Brabec, V.; Nováková, O., DNA binding mode of ruthenium complexes and relationship to tumor cell toxicity. *Drug Resist. Updates* **2006,** *9* (3), 111-122.
50. Brabec, V., *DNA Modification by Antitumor Platinum and Ruthenium Compounds: Their recognition and repair*. Elsevier Science (USA): 2002; Vol. 71.
51. Ohndorf, U.-M.; Rould, M. A.; He, Q.; Pabo, C. O.; Lippard, S. J., Basis for recognition of cisplatin-modified DNA by high-mobility-group proteins. *Nature* **1999,** *399* (6737), 708-712.
52. Kaushal, G. P.; Kaushal, V.; Hong, X.; Shah, S. V., Role and regulation of activation of caspases in cisplatin-induced injury to renal tubular epithelial cells. *Kidney Int.* **2001,** *60* (5), 1726-1736.
53. Oun, R.; Moussa, Y. E.; Wheate, N. J., The side effects of platinum-based chemotherapy drugs: a review for chemists. *Dalton Trans.* **2018,** *47* (19), 6645-6653.
54. Housecroft, C. E.; Sharpe, A. G., *Inorganic Chemistry*. Pearson: London, 2012.
55. Mclure, M., Synthesis and Symmetry of Two Cobalt(III) Complexes with Tetradentate Ligands. *J. Chem. Educ.* **2008,** *85* (3), 420-421.
56. Gable, R.; Hartshorn, R.; McFadyen, W.; Nunno, L., Preparation and Characterization of Some Cobalt(III) Complexes of 2-Aminomethylbenzimidazole. *Aust. J. Chem.* **1996,** *49* (5), 625-632.
57. Baruah, J.; Kashyap, K., A stable peroxo- and hydroxido-bridged dinuclear cobalt(III) ethylenediammine 2,4-dinitrophenolate complex. *Inorg. Chem. Comm.* **2017,** *84*.
58. Downward, A. M.; Jane, R. T.; Polson, M. I. J.; Moore, E. G.; Hartshorn, R. M., Heterodinuclear ruthenium(II)-cobalt(III) complexes as models for a new approach to selective cancer treatment. *Dalton Trans.* **2012,** *41* (47), 14425-14432.
59. Downward, A. M.; Moore, E. G.; Hartshorn, R. M., Photoinduced ligand release in a ruthenium(II)-cobalt(III) heterodinuclear system. *Chem. Commun. (Camb.)* **2011,** *47* (27), 7692-4.

60. Luo, H.; Sui, Y.; Luo, Z.-G.; Wen, J.-W.; Sui, H.-S., Dinuclear Co(III)/Pr(III) and Co(III)/Nd(III) complexes derived from a hexadentate Schiff base: synthesis, structure and magnetic properties. *J. Chem. Res.* **2014,** *38* (8), 486-489.
61. Piguet, C.; Bernardinelli, G.; Bocquet, B.; Schaad, O.; Williams, A. F., Cobalt(III)/Cobalt(II) Electrochemical Potential Controlled by Steric Constraints in Self-Assembled Dinuclear Triple-Helical Complexes. *Inorg. Chem.* **1994,** *33* (18), 4112-4121.
62. Tavakolinia, F. Synthesis and Study of Dinuclear Cobalt(III)-Platinum(II) Complexes as Potential Anti-cancer Pro-drugs. University of Canterbury, New Zealand, 2016.
63. Garnovskii, A. D.; Kharisov, B.; Blanco, L.; Sadimenko, A.; Uraev, A. I.; Vasilchenko, I.; Garnovskii, D., *Review: Metal Complexes as Ligands*. 2010; Vol. 55, p 1119-1134.
64. Chang, J. Y.-C.; Stevenson, R. J.; Lu, G.-L.; Brothers, P. J.; Clark, G. R.; Denny, W. A.; Ware, D. C., Syntheses of 8-quinolinolatocobalt(III) complexes containing cyclen based auxiliary ligands as models for hypoxia-activated prodrugs. *Dalton Trans.* **2010,** *39* (48), 11535-11550.
65. Crossland, B. E.; Staples, P. J., The acid-catalysed hydrolysis of nitro- and nitrito-pentammine complexes of cobalt(III), rhodium(III),and iridium(III). *J. Chem. Soc. A: Inorg. Phys. Theoret.* **1971**, 2853-2856.
66. Xu, W.; Louka, F. R.; Doulain, P. E.; Landry, C. A.; Mautner, F. A.; Massoud, S. S., Hydrolytic cleavage of DNA promoted by cobalt(III)–tetraamine complexes: Synthesis and characterization of carbonatobis[2-(2-pyridylethyl)]-(2-pyridylmethyl)aminecobalt(III) perchlorate. *Polyhedron* **2009,** *28* (7), 1221-1228.
67. Kimura, E.; Young, S.; Collman, J. P., Cleavage of amino acid esters and peptides with hydroxoaquo(2,2',2''-triaminotriethylamine)cobalt(III) ion. *Inorg. Chem.* **1970,** *9* (5), 1183-1191.
68. Fujimoto, T.; Sugimoto, H.; Kai, K.; Maeda, K.; Itoh, S., Oxido-Hydroxido- and Oxido-Aminato-Osmium(V) Complexes with a Cyclohexanediamine-Based Tetradentate Ligand as Active Oxidants for Dihydroxylation and Aminohydroxylation of Alkenes. *Eur. J. Inorg. Chem.* **2019,** (24), 2891-2898.
69. Antonini, I.; Volpini, R.; Dal Ben, D.; Lambertucci, C.; Cristalli, G., Design, synthesis, and biological evaluation of new mitonafide derivatives as potential antitumor drugs. *Bioorg. Med. Chem.* **2008,** *16* (18), 8440-8446.
70. Llombart, M.; Poveda, A.; Forner, E.; Fernández-Martos, C.; Gaspar, C.; Muñoz, M.; Olmos, T.; Ruiz, A.; Soriano, V.; Benavides, A.; Martin, M.; Schlick, E.; Guillem, V., Phase I study of mitonafide in solid tumors. *Invest. New Drugs* **1992,** *10* (3), 177-181.
71. Mahieu, T.; Mijatovic, T.; Van Quaquebeke, E.; Lefranc, F.; Van Vynckt, F.; Darro, F.; Kiss, R., UNBS5162 is a novel naphthalimide derivative that induces autophagy and senescence in human prostate cancer cells. *Mol. Cancer Ther.* **2007,** *6*, 3373S-3373S.
72. Lai, C.-M.; Garner, D. M.; Gray, J. E.; Brogdon, B. L.; Peterman, V. C.; Pieniaszek Jr, H. J., Determination of bisnafide, a novel bis-naphthalimide anticancer agent, in human plasma by high-performance liquid chromatography with UV detection. *J. Pharm. Biomed. Anal.* **1998,** *17* (3), 427-434.
73. Rong, R.-X.; Sun, Q.; Ma, C.-L.; Chen, B.; Wang, W.-Y.; Wang, Z.-A.; Wang, K.-R.; Cao, Z.-R.; Li, X.-L., Development of novel bis-naphthalimide derivatives and their anticancer properties. *MedChemComm* **2016,** *7* (4), 679-685.
74. Liu, H.-K.; Sadler, P. J., Metal Complexes as DNA Intercalators. *Acc. Chem. Res.* **2011,** *44* (5), 349-359.
75. Jennings, B. R.; Ridler, P. J., Interaction of chromosomal stains with DNA. *Biophys. Struct. Mech.* **1983,** *10* (1), 71-79.
76. Gottlieb, H. E.; Kotlyar, V.; Nudelman, A., NMR Chemical Shifts of Common Laboratory Solvents as Trace Impurities. *J. Org. Chem.* **1997,** *62* (21), 7512-7515.
77. National Toxicology Program *Pentaethylenehexamine*; National Toxicology Program: https://ntp.niehs.nih.gov/, 29th September 2005.

78. Weissermel, K.; Arpe, H.-J., *Industrial organic chemistry*. 2nd rev. ed.; VCH: New York, 1993.
79. Petraitis, D. M.; King, S. W.; Srnak, T. Z. Method of Manufacturing ethyleneamines. 2009.
80. Ma, L.; Yan, L.; Lu, A.-H.; Ding, Y., Effect of Re promoter on the structure and catalytic performance of Ni–Re/Al_2O_3 catalysts for the reductive amination of monoethanolamine. *RSC Adv.* **2018,** *8* (15), 8152-8163.
81. Akzo Nobel Ethylene Amines: EDC Process. http://web.archive.org/web/20080420232507/http://www.ethyleneamines.com:80/Startpage/Ethylene+Amines/Processes/EDC+process.htm (accessed June 2019).
82. Arya, S.; Kumar, S.; Rani, R.; Kumar, N.; Roy, P.; Sondhi, S. M., Synthesis, anti-inflammatory, and cytotoxicity evaluation of 9,10-dihydroanthracene-9,10-α,β-succinimide and bis-succinimide derivatives. *Med. Chem. Res.* **2013,** *22* (9), 4278-4285.
83. Bosnich, B.; Poon, C. K.; Tobe, M. L., Complexes of Cobalt(III) with a Cyclic Tetradentate Secondary Amine. *Inorg. Chem.* **1965,** *4* (8), 1102-1108.
84. Hay, R. W.; Lawrence, G. A., Transition-metal complexes of the macrocyclic ligand 5,12-dimethyl-1,4,8,11-tetra-azacyclotetradeca-4,11-diene. *J. Chem. Soc., Dalton Trans.* **1975,** (14), 1466-1471.
85. Chen, B.-H.; Lai, C.-Y.; Yuan, Y.; Chung, C.-S., Synthesis, characterization and aquation kinetics of a new trans diastereoisomer of dichloro(meso-5,12-dimethyl-1,4,8,11-tetraazacyclotetradecane)cobalt(III) perchlorate. *J. Chem. Soc., Dalton Trans.* **1994,** (20), 2959-2961.
86. McClintock, L. F.; Cavigliasso, G.; Stranger, R.; Blackman, A. G., The donor ability of the chelated carbonate ligand: protonation and metallation of $[(L)Co(O_2CO)]^+$ complexes in aqueous solution. *Dalton Trans.* **2008,** (37), 4984-4992.
87. McClintock, L. F.; Bagaria, P.; Kjaergaard, H. G.; Blackman, A. G., Co(III) complexes of the type $[(L)Co(O_2CO)]^+$ (L=tripodal tetraamine ligand): Synthesis, structure, DFT calculations and ^{59}Co NMR. *Polyhedron* **2009,** *28* (8), 1459-1468.
88. Utsuno, S.; Yoshikawa, Y.; Tahata, Y., Stereochemical studies of the diammine(triethylenetetramine)cobalt(III) complex. *Inorg. Chem.* **1985,** *24* (18), 2724-2726.
89. Mori, M.; Shibata, M.; Kyuno, E.; Hoshiyama, K., Studies on the Synthesis of Metal Complexes. III. Synthesis of Ethylenediamine-carbonato, Ammine-oxalato and Ethylenediamineoxalato Series of Cobalt (III) Complexes. *Bull. Chem. Soc. Jpn.* **1958,** *31* (3), 291-295.
90. Doerrer, L. H.; Bautista, M. T.; Lippard, S. J., Tuning of Electronic Properties and Reactivity in Four-Coordinate Cobalt(III) Complexes by the Tetraazamacrocyclic Tropocoronand Ligand. *Inorg. Chem.* **1997,** *36* (17), 3578-3579.
91. Reger, D. L.; Semeniuc, R. F.; Elgin, J. D.; Rassolov, V.; Smith, M. D., 1,8-Naphthalimide Synthon in Silver Coordination Chemistry: Control of Supramolecular Arrangement. *Cryst. Growth Des.* **2006,** *6* (12), 2758-2768.
92. Werner, A., Über die raumisomeren Kobaltverbindungen. *Justus Liebigs Ann. Chem.* **1912,** *386* (1-2), 1-272.
93. Vendilo, A. G.; Kovaleva, N. E.; Chistov, V. I.; Retivov, V. M., Potassium cobaltinitrite. *Russ. J. Inorg. Chem.* **2011,** *56* (4), 501.
94. Xia, J.; Jödecke, M.; Pérez-Salado Kamps, Á.; Maurer, G., Solubility of CO_2 in ($CH_3OH + H_2O$). *J. Chem. Eng. Data* **2004,** *49* (6), 1756-1759.
95. Springborg, J.; Schafferr, C. E., Dianionobis(ethylenediamine)cobalt(III) Complexes. In *Inorganic Syntheses*, pp 63-77.
96. Fumiyo, S.; Kiyoshi, I.; Shinichi, K., Reactions of the $[PtC_2L_2]$ Complexes (L=Sulfide or Tertiary Phosphine) with β-Diketonate Anions. *Bull. Chem. Soc. Jpn.* **1985,** *58* (2), 657-663.
97. Dolomanov, O. V.; Bourhis, L. J.; Gildea, R. J.; Howard, J. A. K.; Puschmann, H., OLEX2: A complete structure solution, refinement and analysis program. *J. Appl. Cryst.* **2009,** (42), 339-341.

98. Sheldrick, G. M., ShelXT. *Acta Cryst.* **2015,** (A71), 3-8.
99. Sheldrick, G. M., ShelXL. *Acta Cryst.* **2015,** (C71), 3-8.
100. Addison, A. W.; Rao, T. N.; Reedijk, J.; van Rijn, J.; Verschoor, G. C., Synthesis, structure, and spectroscopic properties of copper(II) compounds containing nitrogen–sulphur donor ligands; the crystal and molecular structure of aqua[1,7-bis(N-methylbenzimidazol-2'-yl)-2,6-dithiaheptane]copper(II) perchlorate. *J. Chem. Soc., Dalton Trans.* **1984,** (7), 1349-1356.
101. Beevers, C. A.; Lipson, H., Crystal Structure of Copper Sulphate. *Nature* **1934,** *133* (3354), 215-215.
102. Youngme, S.; Chaichit, N., Coordination geometries in bis(di-2-pyridylamine)copper(II) complexes. Crystal structures and spectroscopic properties of $[CuL_2(H_2O)_2](S_4O_6)$, $[CuL_2(CF_3SO_3)_2]$ and $[CuL_2(SO_4)]_2[CuL_2(H_2O)_2](PF_6)_2{\cdot}2H_2O$ (L=Di-2-pyridylamine). *Polyhedron* **2002,** *21* (2), 247-253.
103. Ghatak, I.; Mingos, D. M. P.; Hursthouse, M. B.; Malik, K. M. A., The crystal and molecular structure of bis{−(μ-sulphato-O'-O'-O")bis (triphenylphosphine) (sulphurdioxide)ruthenium(II)} · (toluene) $[Ru(SO_4)(SO_2)(PPh_3)_2]_2{\cdot}(C_7H_8)$. *Transition Met. Chem.* **1979,** *4* (4), 260-264.
104. Chunbai, Z.; Daisuke, I.; Takahiro, M.; Seiji, O., An Acid-stable Organoruthenium Complex Suitable as a Bidentate Building Block. *Chem. Lett.* **2010,** *39* (2), 130-131.
105. Thuéry, P.; Keller, N.; Lance, M.; Vigner, J.-D.; Nierlich, M., Bis(N,N-dimethylformamide)(μ-sulfato)dioxouranium(VI). *Acta Crystallogr., Sect. C* **1995,** *51* (8), 1526-1529.
106. Ng, C. H.; Lim, C. W.; Teoh, S. G.; Fun, H.-K.; Usman, A.; Ng, S. W., New Crown-Shaped Polyoxovanadium(V) Cluster Cation with a μ6-Sulfato Anion and Zwitterionic μ-(β-Alanine): Crystal Structure of $[V_6O_{12}(OH)_3(O_2CCH_2CH_2NH_3)_3(SO_4)][Na][SO_4]{\cdot}13H_2O$. *Inorg. Chem.* **2002,** *41* (1), 2-3.
107. Kozlevcar, B.; Leban, I.; Sieler, J.; Segedin, P., catena-Poly[diaquabis(nicotinamide-N1)copper(II)-[μ]-sulfato-O:O']. *Acta Crystallogr., Sect. C* **1998,** *54* (1), 39-41.
108. Sieron, L.; Bukowska-Strżyzewska, M., catena-Poly[[[diaqua(pyridine-2-carboxamide-N1,O)copper(II)]-μ-(sulfato-O:O')] monohydrate]. *Acta Crystallogr., Sect. C* **1999,** *55* (4), 491-494.
109. Melník, M.; Kabešová, M.; Dunaj-Jurčo, M.; Holloway, C. E., Copper (II) Coordination Compounds: Classification and Analysis of Crystallographic and Structural Data. *J. Coord. Chem.* **1997,** *41* (1-2), 35-182.
110. Aguilo, M.; Solans, X.; Castro, I.; Faus, J.; Julve, M., Two different (croconato)(2,2':6',2''-terpyridyl)copper(II) complexes in one single crystal: structure of $[Cu(C_{15}H_{11}N_3)(H_2O)(C_5O_5)][Cu(C_{15}H_{11}N_3)(C_5O_5)].4H_2O$. *Acta Crystallogr., Sect. C* **1992,** *48* (5), 802-806.
111. Kumar, R.; Guchhait, T.; Subramaniyan, V.; Mani, G., Mixed ligand Cu(II) complexes: Square pyramidal vs trigonal bipyramidal with the pyrrole-based dipodal ligand having hydrogen bond acceptors. *J. Mol. Struct.* **2019,** *1195*, 1-9.
112. Dittler-Klingemann, A. M.; Hahn, F. E., Trigonal-Bipyramidal Copper(II) Complexes with Symmetric and Unsymmetric Tripodal Tetramine Ligands. *Inorg. Chem.* **1996,** *35* (7), 1996-1999.
113. Wüstefeld, H.-U.; Kaska, W. C.; Schüth, F.; Stucky, G. D.; Bu, X.; Krebs, B., Transition Metal Complexes with the Proton Sponge 4,9-Dichloroquino[7,8-h]quinoline: Highly Twisted Aromatic Systems and an Extreme "Out-of-Plane" Position of the Coordinated Transition Metal Atom. *Angew. Chem., Int. Ed* **2001,** *40* (17), 3182-3184.
114. Shek, Iris P.-Y.; Yeung, W.-F.; Lau, T.-C.; Zhang, J.; Gao, S.; Szeto, L.; Wong, W.-T., Ni(II)Ru(II) and Cu(II)Ru(II) Coordination Polymers Constructed from $[Ru(CN)_6]^{4-}$. *Eur. J. Inorg. Chem.* **2005,** *2005* (2), 364-370.
115. Mautner, F. A.; Vicente, R.; Massoud, S. S., Structure determination of nitrito- and thiocyanato-copper(II) complexes: X-ray structures of $[Cu(Medpt)(ONO)(H_2O)]ClO_4$ (1), $[Cu(dien)(ONO)]ClO_4$ (2) and $[Cu_2(Medpt)_2(\mu N,S\text{-}NCS)_2](ClO_4)_2$ (3) (Medpt=3,3'-diamino-N-methyldipropylamine and dien=diethylenetriamine). *Polyhedron* **2006,** *25* (7), 1673-1680.
116. Maldonado, C. R.; Quirós, M.; Salas, J. M., Ternary Ni(II) and Cu(II) complexes with 4,6-dimethyl-1,2,3-triazolo-[4,5-d]pyrimidin-5,7-dionato and chelating aliphatic amines as auxiliary

ligands: Variability in the binding site and hydrogen-bond networks. *Polyhedron* **2010,** *29* (1), 372-378.
117. Al-Noaimi, M.; Choudhary, M. I.; Awwadi, F. F.; Talib, W. H.; Hadda, T. B.; Yousuf, S.; Sawafta, A.; Warad, I., Characterization and biological activities of two copper(II) complexes with dipropylenetriamine and diamine as ligands. *Spectrochim. Acta, Part A* **2014,** *127*, 225-230.
118. Halcrow, M. A., Jahn–Teller distortions in transition metal compounds, and their importance in functional molecular and inorganic materials. *Chem. Soc. Rev.* **2013,** *42* (4), 1784-1795.
119. Karan, N. K.; Sen, S.; Saha, M. K.; Mitra, S.; Tiekink, E. R. T., Crystal structure of [Cu(Hdabco)(dabco)Cl_3] (dabco = 1,4-diazabicyclo[2.2.2]octane), $C_{12}H_{25}Cl_3CuN_4$. *Z. Kristallogr. - New Cryst. Struct.* **1999,** *214* (2), 203-204.
120. Chandler, D. J.; Jones, R. A.; Whittlesey, B. R., The Jahn-Teller effect in a trigonal bipyramidal Ni(III) complex; synthesis and x-ray crystal structure of trans-NiI_3 $(PMe_3)_2$. *J. Coord. Chem.* **1987,** *16* (1), 19-24.
121. Bhattacharyya, B. D., Jahn-Teller Effect in the Ligand Field Theory of Trigonal Bipyramidal V^{4+} Complexes. *Phys. Status Solidi B* **1975,** *71* (2), 427-433.
122. Viossat, B.; Khodadad, P.; Rodier, N.; Dung, N.-H., Trichlorobis(diaza-1,4 bicyclo[2.2.2]octane)cuprate(II) d'hydrogene. *Acta Crystallogr., Sect. C* **1988,** *44* (2), 263-265.
123. Kabešová, M.; Boča, R.; Melník, M.; Valigura, D.; Dunaj-Jurčo, M., Bonding properties of thiocyanate groups in copper(II) and copper(I) complexes. *Coord. Chem. Rev.* **1995,** *140*, 115-135.
124. Pascal, R. A.; McMillan, W. D.; Van Engen, D.; Eason, R. G., Synthesis and structure of longitudinally twisted polycyclic aromatic hydrocarbons. *J. Am. Chem. Soc.* **1987,** *109* (15), 4660-4665.
125. Zhao, D.; Li, F.; Zhang, A., Naphthalene-1,8-dicarboxylic anhydride: a monoclinic polymorph. *Acta Crystallogr., Sect. E: Crystallogr. Commun.* **2010,** *66* (10), 2622.
126. Kovalevsky, A. Y.; Ponomarev, I. I.; Antipin, M. Y.; Ermolenko, I. G.; Shishkin, O. V., Influence of steric and electronic effects of substituents on the molecular structures and conformational flexibility of 1,8-naphthalenedicarboximides. *Russ. Chem. Bull.* **2000,** *49* (1), 70-76.
127. McAdam, C. J.; Manning, A. R.; Robinson, B. H.; Simpson, J., Group 8 and 10 metal acetylide naphthalimide dyads. *Inorg. Chim. Acta* **2005,** *358* (5), 1673-1682.
128. Sandip, B.; Anunay, S., Influence of Structure on the Unusual Spectral Behavior of 4-Dialkylamino-1,8-naphthalimide. *Chem. Lett.* **2005,** *34* (5), 722-723.
129. Reger, D. L.; Elgin, J. D.; Semeniuc, R. F.; Pellechia, P. J.; Smith, M. D., Directional control of π-stacked building blocks for crystal engineering: the 1,8-naphthalimide synthon. *Chem. Comm.* **2005,** (32), 4068-4070.
130. Carter, T. G.; Healey, E. R.; Pitt, M. A.; Johnson, D. W., Secondary Bonding Interactions Observed in Two Arsenic Thiolate Complexes. *Inorg. Chem.* **2005,** *44* (26), 9634-9636.
131. Shi, Y.-Q.; Xu, D.; Chen, B.; Cai, M.-J.; Zhu, Y., N-Eth-yl-5-(pyrrol-1-yl)-1,8-naphthalimide. *Acta Crystallogr., Sect. E: Crystallogr. Commun.* **2005,** *61* (8), o2436-o2437.
132. Bardajee, G. R.; Winnik, M. A.; Lough, A. J., 4-[N-(2-Hydroxy-ethyl)-N-methyl-amino]-N-isopropyl-1,8-naphthalimide. *Acta Crystallogr., Sect. E* **2006,** *62* (4), 1615-1617.
133. Shavaleev, N. M.; Davies, E. S.; Adams, H.; Best, J.; Weinstein, J. A., Platinum(II) Diimine Complexes with Catecholate Ligands Bearing Imide Electron-Acceptor Groups: Synthesis, Crystal Structures, (Spectro)Electrochemical and EPR studies, and Electronic Structure. *Inorg. Chem.* **2008,** *47* (5), 1532-1547.
134. Bezvikonnyi, O.; Gudeika, D.; Volyniuk, D.; Grazulevicius, J. V.; Bagdziunas, G., Pyrenyl substituted 1,8-naphthalimide as a new material for weak efficiency-roll-off red OLEDs: a theoretical and experimental study. *New J. Chem.* **2018,** *42* (15), 12492-12502.
135. DeLano, W. L., Pymol: An open-source molecular graphics tool. *CCP4 Newsletter on protein crystallography* **2002,** *40* (1), 82-92.

136. Hanwell, M. D.; Curtis, D. E.; Lonie, D. C.; Vandermeersch, T.; Zurek, E.; Hutchison, G. R., Avogadro: an advanced semantic chemical editor, visualization, and analysis platform. *Journal of Cheminformatics* **2012,** *4* (1), 17.
137. Macrae, C. F.; Sovago, I.; Cottrell, S. J.; Galek, P. T. A.; McCabe, P.; Pidcock, E.; Platings, M.; Shields, G. P.; Stevens, J. S.; Towler, M.; Wood, P. A., Mercury 4.0: from visualization to analysis, design and prediction. *Journal of Applied Crystallography* **2020,** *53* (1), 226-235.
138. Willcott, M. R., MestRe Nova. *J. Am. Chem. Soc.* **2009,** *131* (36), 13180-13180.
139. Groom, C. R.; Bruno, I. J.; Lightfoot, M. P.; Ward, S. C., The Cambridge Structural Database. *Acta Crystallographica Section B* **2016,** *72* (2), 171-179.
140. Grinberg, H.; Lamdan, S.; Gaozza, C. H., Heterocycles derived from the condensation of aliphatic diamines with succinic and glutaric acid derivatives. *J. Heterocycl. Chem.* **1975,** *12* (4), 763-766.
141. Zhou, X.; Day, A. I.; Edwards, A. J.; Willis, A. C.; Jackson, W. G., Facile C−H Bond Activation: Synthesis of the N4C Donor Set Pentadentate Ligand 1,4-Bis(2-pyridylmethyl)-1,4-diazacyclononane (dmpdacn) and a Structural Study of Its Alkyl−Cobalt(III) Complex [Co(dmpdacn-C)(OH_2)](ClO_4)$_2$·H_2O and Its Hydroxylated Derivative [Co(dmpdacnOH-O)Cl](ClO_4)$_2$·C_3H_6O. *Inorg. Chem.* **2005,** *44* (2), 452-460.
142. Piriz Mac-Coll, C. R., Carbonato complexes of cobalt(III). *Coord. Chem. Rev.* **1969,** *4* (2), 147-198.

Appendices

Appendix A. Additional Chapter 2 Methods

The methods detailed in this appendix were used to trial different reaction conditions in the purification by complexation process, intending to optimise the reaction conditions towards the most enriched material.

A.1 Ligand Synthesis and Purification by Complexation using 33% Stoichiometric Aqueous Copper Sulfate

This reaction utilised aqueous copper sulfate for the complexation reaction.

Ligand synthesis

This was performed following the procedure described in Section 2.2.6 with the following amendments:

- 10.00 g, 50 mmol of 1,8-naphthalic anhydride was placed in a smaller 10 cm mortar
- 20 mL of chloroform was added to the mortar
- 4 mL, 17 mmol of 3,6,9,12-tetraazatetradecane-1,14-diamine was used
- The reaction gave 17.19 g of a pale brown powder (m.p. 92-96°C decomposes) which was then analysed by ESI-MS (Table 2.1). Of note was the lower melting point which may be related to compositional differences between the attempts.

Attempted Purification by complexation

This reaction was performed following the procedure described in Section 2.2.6 with the following amendments:

- Crude ligand material (15.98 g) was placed in a 500 mL round bottom flask.
- 200 mL of methanol was then added with stirring.
- 2.21 g 8.88 mmol copper sulfate was dissolved in 6 mL warm water
- The oily blue solid produced was washed twice with less than 5 mL minimal methanol each wash

The solid and the reaction liquor were then characterised by ESI-MS (See Table B.1).

Treatment of the reaction liquor from the reaction of copper with crude ligand material

This reaction was performed following the procedure described in Section 2.2.6 with the following amendment:

- 3.30 g 8.88 mmol solid disodium EDTA was used

The solid and the reaction solution were then characterised by ESI-MS (See Table B.1).

Treatment of the solid material from the reaction of copper with crude ligand material

This reaction was performed following the procedure described in Section 2.2.6 with the following amendments:

- 200 mL of Water was added to the oily blue solid in the reaction vessel
- 3.30 g 8.88 mmol solid disodium EDTA was used

The oil and the reaction solution were then characterised by ESI-MS (See Table B.1).

A.2 Ligand Synthesis and Purification by Complexation using 33% Stoichiometric Methanolic Copper Sulfate

This reaction was the first described in this work to use methanolic copper sulfate for the addition of copper.

Ligand synthesis

This was performed following the procedure described in Section 2.2.6 with the following amendments:

- 10.00 g, 50 mmol of 1,8-naphthalic anhydride was placed in a smaller 10 cm mortar
- 20 mL of chloroform was added to the mortar
- 4 mL, 17 mmol of 3,6,9,12-tetraazatetradecane-1,14-diamine was used
- The reaction gave 17.00 g of a pale brown powder (m.p. 92-96°C decomposes).

Attempted Purification by complexation

This reaction was performed following the procedure described in Section 2.2.6 with the following amendments:

- Crude ligand material (15.99 g) was placed in a 500 mL two necked round bottom flask.
- 200 mL of methanol was then added with stirring
- 2.20 g 8.83 mmol copper sulfate was dissolved in 50 mL warm methanol
- The oily blue solid produced was washed twice with less than 5 mL methanol each wash

The solid and the reaction liquor were then characterised by ESI-MS (See Table B.2).

Treatment of the reaction liquor from the reaction of copper with crude ligand material

This reaction was performed following the procedure described in Section 2.2.6 with the following amendment:

- 3.30 g 8.88 mmol solid disodium EDTA was used

The solid and the reaction solution were then characterised by ESI-MS (See Table B.2).

Treatment of the solid material from the reaction of copper with crude ligand material

This reaction was performed following the procedure described in Section 2.2.6 with the following amendments:

- 200 mL of Water was added to the oily blue solid in the reaction vessel
- 3.30 g 8.88 mmol solid disodium EDTA was used

The solid and the reaction solution were then characterised by ESI-MS (See Table B.2).

A.3 Ligand Synthesis and Purification by Complexation using 40% Stoichiometric Methanolic Copper Sulfate

This reaction saw the quantity of copper sulfate increased from 33% stoichiometric to 40%. This reaction was also repeated once at the same scale, once at 3.5x scale and once at 7.5x scale (which is the method described in Section 2.2.6, Ligand Synthesis and purification by complexation).

Ligand synthesis

This was performed following the procedure described in Section 2.2.6 with the following amendments:

- 20.00 g, 100 mmol of 1,8-naphthalic anhydride was placed in the mortar
- 40 mL of chloroform was added to the mortar
- 8 mL, 34 mmol of 3,6,9,12-tetraazatetradecane-1,14-diamine was used
- The reaction gave 33.62 g of a pale brown powder (m.p. 75-78°C decomposes) which was then analysed by ESI-MS (Table 2.1). Of note was the lower melting point which may be related to compositional differences between the attempts.

Attempted Purification by complexation

This reaction was performed following the procedure described in Section 2.2.6 with the following amendments:

- Crude ligand material (8.00 g) was placed in a 250 mL round bottom flask.
- 125 mL of methanol was then added with stirring.
- 1.35 g 5.42 mmol copper sulfate was dissolved in 75 mL warm methanol
- The oily blue solid produced was washed twice with less than 5 mL minimal methanol each wash

The solid and the reaction liquor were then characterised by ESI-MS (See Tables B.3, B.4, B.6).

Treatment of the reaction liquor from the reaction of copper with crude ligand material

This reaction was performed following the procedure described in Section 2.2.6 with the following amendment:

- 2.00 g 5.37 mmol solid disodium EDTA was used

The solid and the reaction solution were then characterised by ESI-MS (See Tables B.3, B.4, B.6).

Treatment of the solid material from the reaction of copper with crude ligand material

This reaction was performed following the procedure described in Section 2.2.6 with the following amendments:

- 125 mL of Water was added to the oily blue solid in the reaction vessel
- 2.00 g 5.37 mmol solid disodium EDTA was used

The oil and the reaction solution were then characterised by ESI-MS (See Tables B.3, B.4, B.6).

Treatment of the Turquoise Solution Post EDTA

The solution from the previous step was taken and extracted five times with 50 mL of chloroform, which was then analysed by ESI-MS (See Tables B.3, B.4, B.6).

A.4 Ligand Synthesis and Purification by Complexation using 40% Stoichiometric Methanolic Anhydrous Copper Sulfate

This reaction used anhydrous copper sulfate (at 40% stoichiometry) as the copper source for complexation.

Ligand synthesis

This reaction was performed following the procedure described in Section 2.2.6 with the following amendment:

- 34.20 g of pale brown powder was produced and analysed by ESI-MS (See Table B.5)

Attempted Purification by complexation

This reaction was performed following the procedure described in Section 2.2.6 with the following amendments:

- Crude ligand material (4.00 g) was placed in a 500 mL round bottom flask.
- 70 mL of methanol was then added with stirring.
- 0.43 g 2.69 mmol anhydrous copper sulfate was dissolved in 175 mL warm methanol
- The oily blue solid produced was washed twice with less than 5 mL minimal methanol each wash

The solid and the reaction liquor were then characterised by ESI-MS (See Table B.5).

Treatment of the reaction liquor from the reaction of copper with crude ligand material

This reaction was performed following the procedure described in Section 2.2.6 with the following amendment:

- 0.65 g 1.75 mmol solid disodium EDTA was used

The solid and the reaction solution were then characterised by ESI-MS (See Table B.5).

Treatment of the solid material from the reaction of copper with crude ligand material

This reaction was performed following the procedure described in Section 2.2.6 with the following amendments:
- 275 mL of Water was added to the oily blue solid in the reaction vessel
- 0.65 g 1.75 mmol solid disodium EDTA was used

The oil and the reaction solution were then characterised by ESI-MS (See Table B.5).

Treatment of the Turquoise Solution Post EDTA

The solution from the previous step was taken and extracted six times with 30 mL of chloroform. Half of the aqueous phase was then run through DOWEX 1X8 resin in the chloride form to separate neutral and charged species by cation exchange. The sample was brought to pH 7-8 and loaded onto a 5 cm long 1 cm diameter column directly. The first fraction was eluted using 500 mL of distilled water, giving a pale turquoise solution. The bright blue band that remained on the column was then eluted using 0.25 M NaCl solution followed by 1 M NaCl solution to ensure complete elution. The fractions were then characterised by ESI-MS (See Table B.5).

Appendix B. Additional Chapter 2 Results Flowcharts and Summary Tables

The flowcharts in this appendix depict the distribution of compounds present at each stage of the reaction for the additional methods as presented in Appendix A1-4. These flowcharts were designed in the same way as Figure 2.4 on page 37. The flowcharts are followed by the summary tables compiled from the ESI-MS results for each iteration of the reaction.

B.1 Ligand Synthesis and Purification by Complexation using 33% Stoichiometric Aqueous Copper Sulfate

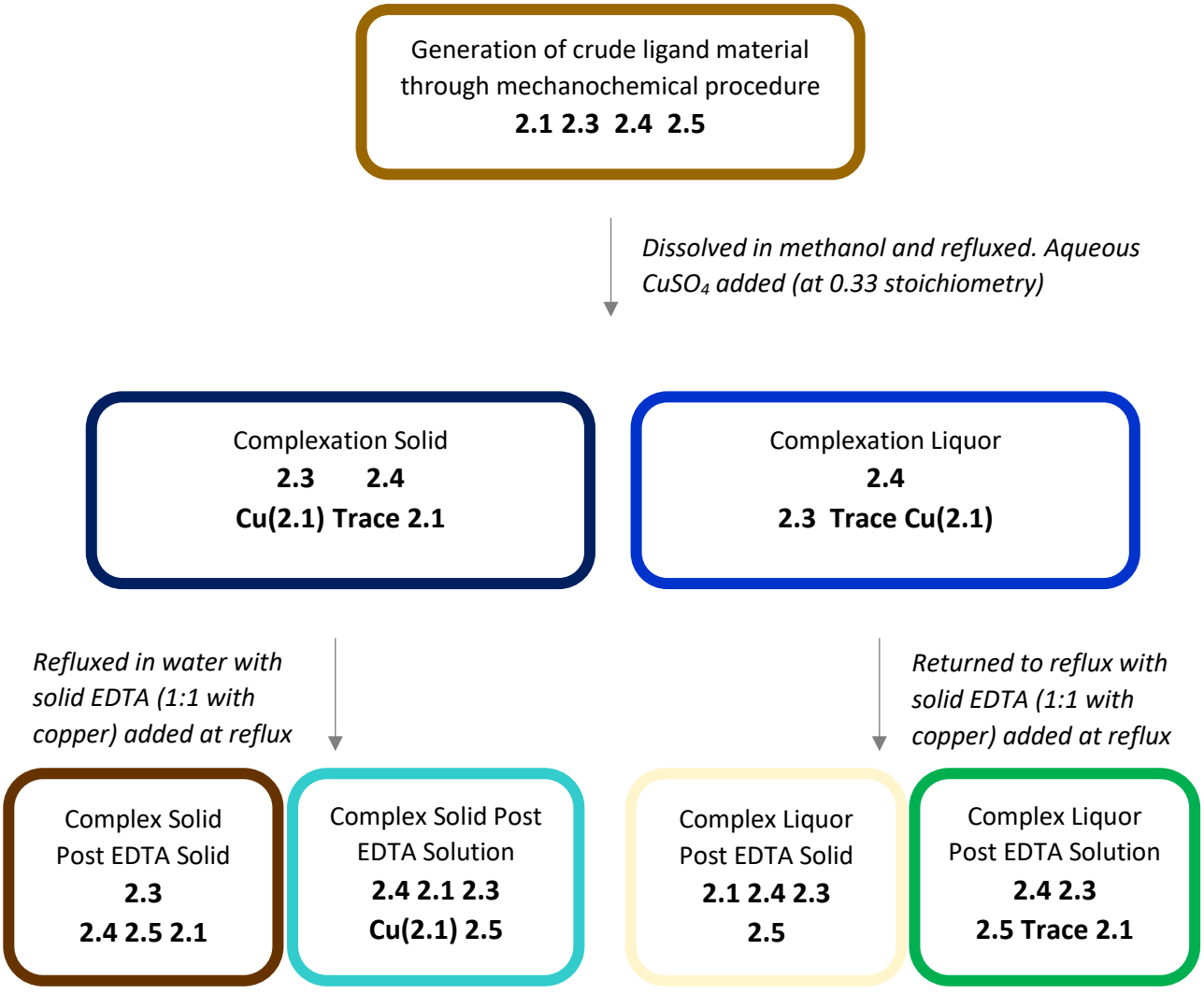

Figure B.1: ***Flowchart depicting the partitioning of the various major species in the reactions fractions of the variation on the method described in Section 2.2.6 using 33% aqueous copper sulfate. The exact method for this reaction can be found in Appendix A.1.***

Table B.1: *Summarised ESI-MS results from the 33% aqueous copper sulfate reaction fractions. The values are expressed as relative intensities for the species of interest compared to the largest peak in that spectrum. The final row percentages for the desired compound was calculated by the desired product divided by the sum of the most common side products. 2.1, 2.4, Cu(2.1), 2.3 and 2.5. The desired compound was 2.1 except in the second, third and fourth relative intensity columns where Cu(2.1) was the desired compound, as highlighted in green for 2.1 and blue for the complex.*

Identity	m/z	Predicted m/z	Relative Intensity									
			Crude Ligand	Complex Solid	Complex Liquor	Cooling Solid	Solid EDTA Solid	Solid EDTA Solution	Solid EDTA Solution oil	Liquor ETDA Solid	Liquor EDTA Solution	Liquor EDTA Solution oil
[**2.17**+2H$^+$] 2+	198.6231	198.6239 2+ for $C_{22}H_{31}N_5O_2$						0.02				
[M +1H$^+$] 1+	199.0388 1+	199.0395 1+ for $C_{12}H_7O_3$	0.17	0.10	0.12	0.07						0.13
[**2.2**+2H$^+$] 2+	207.1362 2+	207.1372 2+ for $C_{22}H_{40}N_6O_2$	0.09									
[**2.25**+2H$^+$] 2+	254.1047 2+	254.1055 2+ for $C_{30}H_{28}N_4O_4$		0.05		0.02			0.02	0.04	0.03	0.07
[**2.13**+2H$^+$] 2+	275.6268	275.6266 2+ for $C_{32}H_{33}N_5O_4$	0.12	0.15	0.06	0.15	0.05	0.28	0.08	0.12	0.11	0.07
[**2.18**+2H$^+$] 2+	288.6334	288.6345 2+ for $C_{34}H_{35}N_5O_4$		0.06	0.08	0.07					0.11	0.11
[**2.1**+2H$^+$] 2+	297.1459 2+	297.1477 2+ for $C_{34}H_{38}N_6O_4$	1.0	0.05	0.03	0.04	0.06	0.81	1.0	1.0	0.05	0.18
[**2.4**+2H$^+$] 2+	310.1548 2+	310.1556 2+ for $C_{36}H_{40}N_6O_4$	0.68	0.98	1.0	1.0	0.20	1.0	0.62	0.75	1.0	1.0
[**2.19**+2H$^+$] 2+	318.6673 2+	318.6688 2+ for $C_{36}H_{43}N_7O_4$	0.15									
[Cu(**2.1**)]$^{2+}$	327.6038 2+	327.6047 2+ for $[Cu(C_{34}H_{36}N_6O_4)]^{2+}$		0.29	0.13	0.36		0.58				
[**2.22**+2H$^+$] 2+	331.6756 2+	331.6767 2+ for $C_{38}H_{45}N_7O_4$	0.11		0.15				0.10			0.06
[Cu(**2.19**)]$^{2+}$	349.1249 2+	349.1257 2+ for $[Cu(C_{36}H_{41}N_7O_4)]^{2+}$		0.09	0.11	0.10					0.10	
2.26 or **2.29**	353.1963	353.1978 1+ for $C_{20}H_{25}N_4O_2$ or 2+ for $C_{40}H_{50}N_8O_4$										0.03
[**2.15**+2H$^+$] 2+	365.6361	365.6372 2+ for $C_{44}H_{35}N_5O_6$		0.03								0.03
[**2.12**+1H$^+$] 1+	370.2231 2+	370.2243 1+ for $C_{20}H_{28}N_5O_2$	0.06					0.06	0.07			
[**2.16**+2H$^+$] 2+	374.6400	374.6425 2+ for $C_{44}H_{39}N_5O_7$										0.05
[**2.3** +2H$^+$] 2+	387.1578 2+	387.1583 2+ for $C_{46}H_{42}N_6O_6$	0.49	1.0	0.36	0.86	1.0	0.77	0.62	0.69	0.86	0.85
[**2.5**+2H$^+$] 2+	396.1623 2+	396.1636 2+ for $C_{46}H_{44}N_6O_7$	0.26	0.19			0.15	0.37	0.24	0.13	0.23	0.18
[**2.20**+2H$^+$] 2+	408.6780 2+	408.6794 2+ for $C_{48}H_{47}N_7O_6$	0.23	0.22			0.11	0.31	0.30	0.17		
[**2.6**+2H$^+$] 2+	409.1703 2+	409.1714 2+ for $C_{48}H_{46}N_6O_7$			0.12						0.09	0.36
[**2.23**+2H$^+$] 2+	421.6852	421.6872 2+ for $C_{50}H_{49}N_7O_6$										0.10
[**2.24**+2H$^+$] 2+	430.6904	430.6925 2+ for $C_{50}H_{51}N_7O_7$										0.06
[Cu(**2.20**)]$^{2+}$	439.1355	439.1363 2+ for $[Cu(C_{48}H_{47}N_7O_6)]^{2+}$				0.08						
Percentage of desired compound (compared to major side products)			41%	12%	9%	16%	4%	23%	40%	39%	2%	8%

B.2 Ligand Synthesis and Purification by Complexation using 33% Stoichiometric Methanolic Copper Sulfate

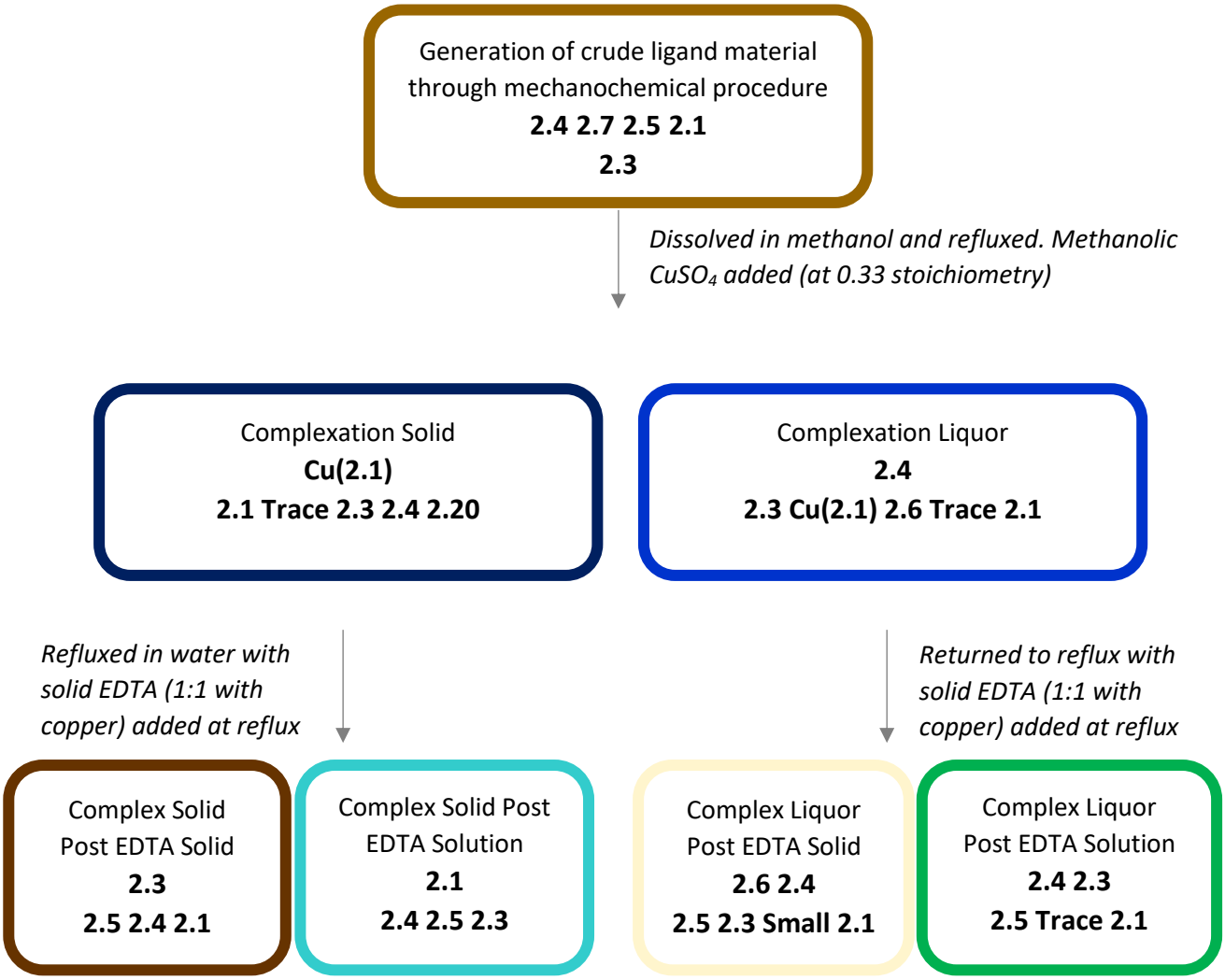

Figure B.2: *Flowchart depicting the partitioning of the various major species in the reactions fractions of the variation on the method described in Section 2.2.6 using 33% methanolic copper sulfate. The exact method for this reaction can be found in Appendix A.2.*

Table B.2: *Summarised ESI-MS results from the 33% methanolic copper sulfate reaction fractions. The values are expressed as relative intensities for the species of interest compared to the largest peak in that spectrum. The final row percentages for the desired compound was calculated by the desired product divided by the sum of the most common side products.* **2.1, 2.4, Cu(2.1), 2.3** *and* **2.5.** *The desired compound was* **2.1** *except in the second, third and fourth relative intensity columns where* **Cu(2.1)** *was the desired compound, as highlighted in green for 2.1 and blue for the complex.*

Identity	m/z	Predicted m/z	Relative Intensity									
			Crude Ligand	Complex Solid	Complex Liquor	Cooling Solid	Solid EDTA Solid	Solid EDTA Solution	Solid EDTA Solution oil	Liquor ETDA Solid	Liquor EDTA Solution	Liquor EDTA Solution oil
[**2.17**+2H$^+$] 2+	198.6231	198.6239 2+ for $C_{22}H_{31}N_5O_2$						0.03				
[**2.30** +1H$^+$] 1+	199.0388 1+	199.0395 1+ for $C_{12}H_7O_3$	0.49	0.03	0.26	0.10			0.02	0.29		
[**2.13**+2H$^+$] 2+	275.6268	275.6266 2+ for $C_{32}H_{33}N_5O_4$	0.11	0.03	0.09	0.10		0.16	0.10	0.08	0.13	0.10
[**2.18**+2H$^+$] 2+	288.6334	288.6345 2+ for $C_{34}H_{35}N_5O_4$			0.08	0.04					0.11	
[**2.1**+2H$^+$] 2+	297.1459 2+	297.1477 2+ for $C_{34}H_{38}N_6O_4$	0.89	0.42	0.04	0.05	0.10	1.0	1.0	0.12	0.09	0.14
[**2.7**+2H$^+$] 2+	306.1526 2+	306.1558 2+ for $C_{34}H_{40}N_6O_4$	0.94									
[**2.4**+2H$^+$] 2+	310.1557 2+	310.1556 2+ for $C_{36}H_{40}N_6O_4$	1.0	0.08	1.0	0.40	0.17	0.48	0.71	0.81	1.0	0.55
[Cu(**2.1**)]$^{2+}$	327.6046 2+	327.6047 2+ for $[Cu(C_{34}H_{36}N_6O_4)]^{2+}$		1.0	0.21	0.17						
[**2.22**+2H$^+$] 2+	331.6756 2+	331.6767 2+ for $C_{38}H_{45}N_7O_4$			0.18	0.07	0.03	0.11	0.10	0.04		
[Cu(**2.19**)]$^{2+}$	349.1258 2+	349.1257 2+ for $[Cu(C_{36}H_{41}N_7O_4)]^{2+}$			0.18			0.02			0.09	
2.26 or **2.29**	353.1963	353.1978 1+ for $C_{20}H_{25}N_4O_2$ or 2+ for $C_{40}H_{50}N_8O_4$								0.01		
[**2.12**+1H$^+$] 1+	370.2231 2+	370.2243 1+ for $C_{20}H_{28}N_5O_2$						0.06				
[**2.3** +2H$^+$] 2+	387.1582 2+	387.1583 2+ for $C_{46}H_{42}N_6O_6$	0.47	0.13	0.52	1.0	1.0	0.14	0.90	0.45	0.83	1.0
[**2.5**+2H$^+$] 2+	396.1623 2+	396.1636 2+ for $C_{46}H_{44}N_6O_7$	0.92		0.04	0.10	0.26	0.24	0.66	0.48	0.39	0.23
[**2.20**+2H$^+$] 2+	408.6775 2+	408.6794 2+ for $C_{48}H_{47}N_7O_6$		0.15								0.13
[**2.6**+2H$^+$] 2+	409.1727 2+	409.1714 2+ for $C_{48}H_{46}N_6O_7$	0.23		0.23	0.20			0.30?	1.0	0.14	
[**2.23**+2H$^+$] 2+	421.6852	421.6872 2+ for $C_{50}H_{49}N_7O_6$										
[**2.24**+2H$^+$] 2+	430.6904	430.6925 2+ for $C_{50}H_{51}N_7O_7$								0.10		
[Cu(**2.20**)]$^{2+}$	439.1343	439.1363 2+ for $[Cu(C_{48}H_{47}N_7O_6)]^{2+}$		0.01								
Percentage of desired compound (compared to major side products)			27%	61%	12%	10%	7%	54%	31%	6%	4%	7%

B.3 Ligand Synthesis and Purification by Complexation using 40% Stoichiometric Methanolic Copper Sulfate

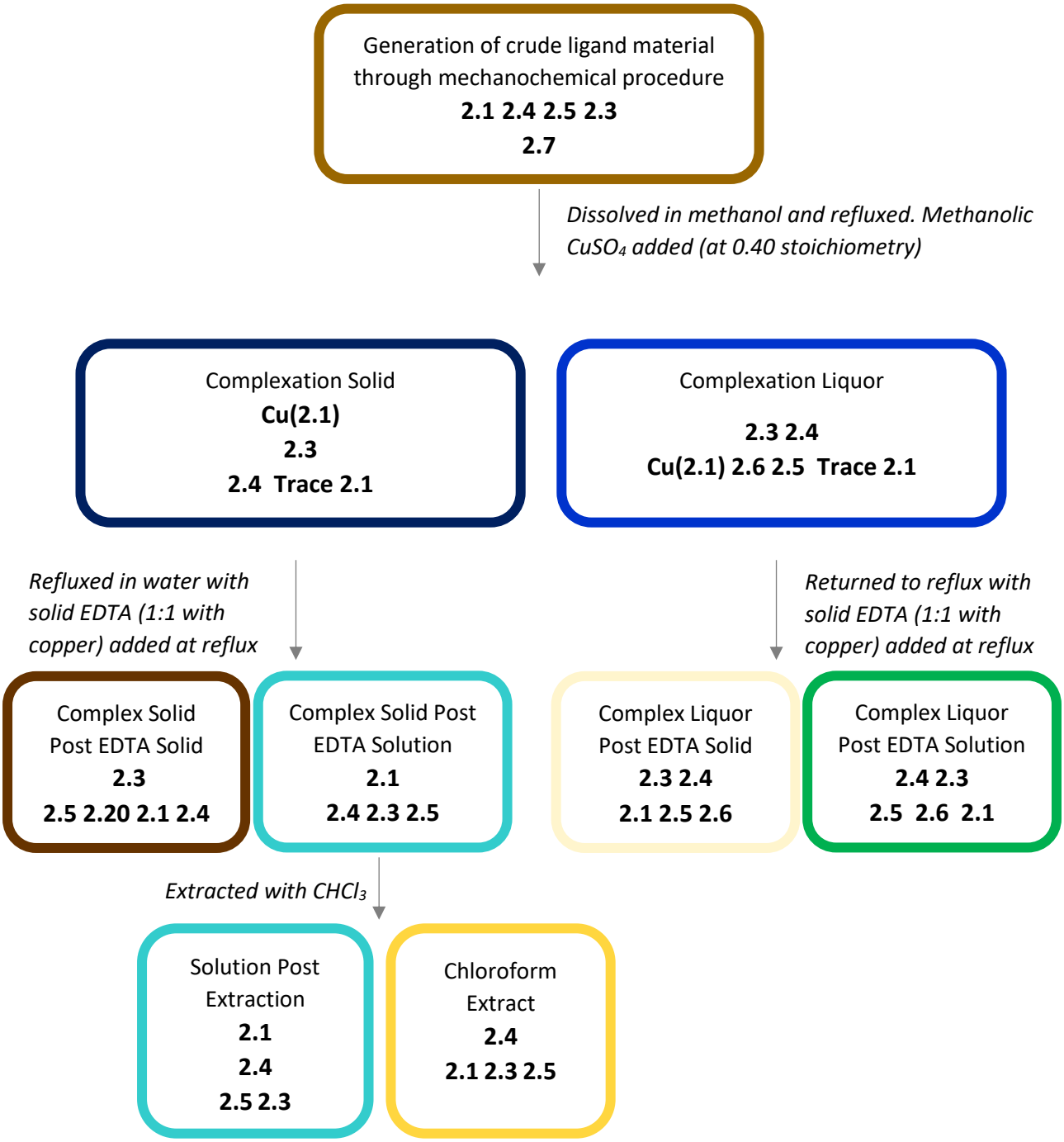

Figure B.3: ***Flowchart depicting the partitioning of the various major species in the reactions fractions of the variation on the method described in Section 2.2.6 using 40% methanolic copper sulfate. The exact method for this reaction can be found in Appendix A.3.***

Table B.3 *Summarised ESI-MS results from the repetition of the 40% methanolic copper sulfate reaction fractions. The values are expressed as relative intensities for the species of interest compared to the largest peak in that spectrum. The final row percentages for the desired compound was calculated by the desired product divided by the sum of the most common side products.* **2.1, 2.4, Cu(2.1), 2.3** *and* **2.5.** *The desired compound was* **2.1** *except where* **Cu(2.1)** *was the desired compound, as highlighted in green for 2.1 and blue for the complex.*

Identity	m/z	Predicted m/z	Relative Intensity Crude Ligand	Complex Solid	Complex Liquor	Cooling Solid	Solid EDTA Solid	Solid EDTA Solution	$CHCl_3$ Extract	Solution Post $CHCl_3$	Liquor ETDA Solid	Liquor EDTA Solution
[**2.30** +1H$^+$] 1+	199.0394 1+	199.0395 1+ for $C_{12}H_7O_3$	0.31	0.05					0.11			
[**2.2**+2H$^+$] 2+	207.1362 2+	207.1372 2+ for $C_{22}H_{40}N_6O_2$	0.15									
[**2.25**+2H$^+$] 2+	254.1047 2+	254.1055 2+ for $C_{30}H_{28}N_4O_4$							0.02			
[**2.13**+2H$^+$] 2+	275.6259 2+	275.6266 2+ for $C_{32}H_{33}N_5O_4$	0.10	0.07	0.09	0.02	0.02	0.10	0.25	0.08	0.15	0.11
[**2.18**+2H$^+$] 2+	288.6332	288.6345 2+ for $C_{34}H_{35}N_5O_4$			0.09							0.08
[**2.1**+2H$^+$] 2+	297.1470 2+	297.1477 2+ for $C_{34}H_{38}N_6O_4$	1.0	0.11	0.05	0.01	0.24	1.0	0.47	1.0	0.41	0.26
[**2.7**+2H$^+$] 2+	306.1520 2+	306.1558 2+ for $C_{34}H_{40}N_6O_4$	0.59									
[**2.4**+2H$^+$] 2+	310.1549 2+	310.1556 2+ for $C_{36}H_{40}N_6O_4$	0.93	0.44	0.90	0.34	0.22	0.70	1.0	0.65	0.95	1.0
[**2.19**+2H$^+$] 2+	318.6673 2+	318.6688 2+ for $C_{36}H_{43}N_7O_4$						0.09				0.11
[Cu(**2.1**)]$^{2+}$	327.6038 2+	327.6047 2+ for [Cu($C_{34}H_{36}N_6O_4$)]$^{2+}$		1.0	0.35	0.22						
[**2.22**+2H$^+$] 2+	331.6756 2+	331.6767 2+ for $C_{38}H_{45}N_7O_4$					0.03	0.13		0.11	0.09	0.14
[Cu(**2.19**)]$^{2+}$	349.1231 2+	349.1257 2+ for [Cu($C_{36}H_{41}N_7O_4$)]$^{2+}$		0.06	0.17	0.05						
2.26 or **2.29**	353.1963	353.1978 1+ for $C_{20}H_{25}N_4O_2$ or 2+ for $C_{40}H_{50}N_8O_4$							0.09			
[**2.12**+1H$^+$] 1+	370.2235 2+	370.2243 1+ for $C_{20}H_{28}N_5O_2$	0.07				0.02	0.16				
[**2.16**+2H$^+$] 2+	374.6421	374.6425 2+ for $C_{44}H_{39}N_5O_7$		0.03	0.04	0.02					0.03	0.05
[**2.3** +2H$^+$] 2+	387.1582 2+	387.1583 2+ for $C_{46}H_{42}N_6O_6$	0.71	0.87	1.0	1.0	1.0	0.54	0.46	0.18	1.0	0.89
[**2.5**+2H$^+$] 2+	396.1623 2+	396.1636 2+ for $C_{46}H_{44}N_6O_7$	0.77	0.18	0.20		0.29	0.42	0.32	0.18	0.40	0.61
[**2.20**+2H$^+$] 2+	408.6775 2+	408.6794 2+ for $C_{48}H_{47}N_7O_6$	0.37	0.16			0.28	0.25		0.10		
[**2.6**+2H$^+$] 2+	409.1727 2+	409.1714 2+ for $C_{48}H_{46}N_6O_7$			0.28	0.09			0.09		0.32	0.43
[**2.21**+2H$^+$] 2+	417.6829 2+	417.6847 2+ for $C_{48}H_{49}N_7O_7$	0.28					0.03			0.11	0.19
[**2.23**+2H$^+$] 2+	421.6866 2+	421.6872 2+ for $C_{50}H_{49}N_7O_6$		0.06	0.13	0.07	0.07					
[**2.24**+2H$^+$] 2+	430.6904	430.6925 2+ for $C_{50}H_{51}N_7O_7$									0.05	0.10
[Cu(**2.20**)]$^{2+}$	439.1341 2+	439.1363 2+ for [Cu($C_{48}H_{47}N_7O_6$)]$^{2+}$		0.16		0.09						
[Cu(**2.21**)]$^{2+}$	448.1413 1+	448.1416 2+ for [Cu($C_{48}H_{47}N_7O_7$)]$^{2+}$			0.09							
[**2.8**+2H$^+$] 2+	953.3300	953.3299 1+ for $C_{58}H_{45}N_6O_8$					0.03					
Percentage of desired compound (compared to major side products)			29%	38%	14%	14%	14%	38%	21%	50%	15%	9%

B.4 Ligand Synthesis and Purification by Complexation using 40% Stoichiometric Methanolic Copper Sulfate (Repetition)

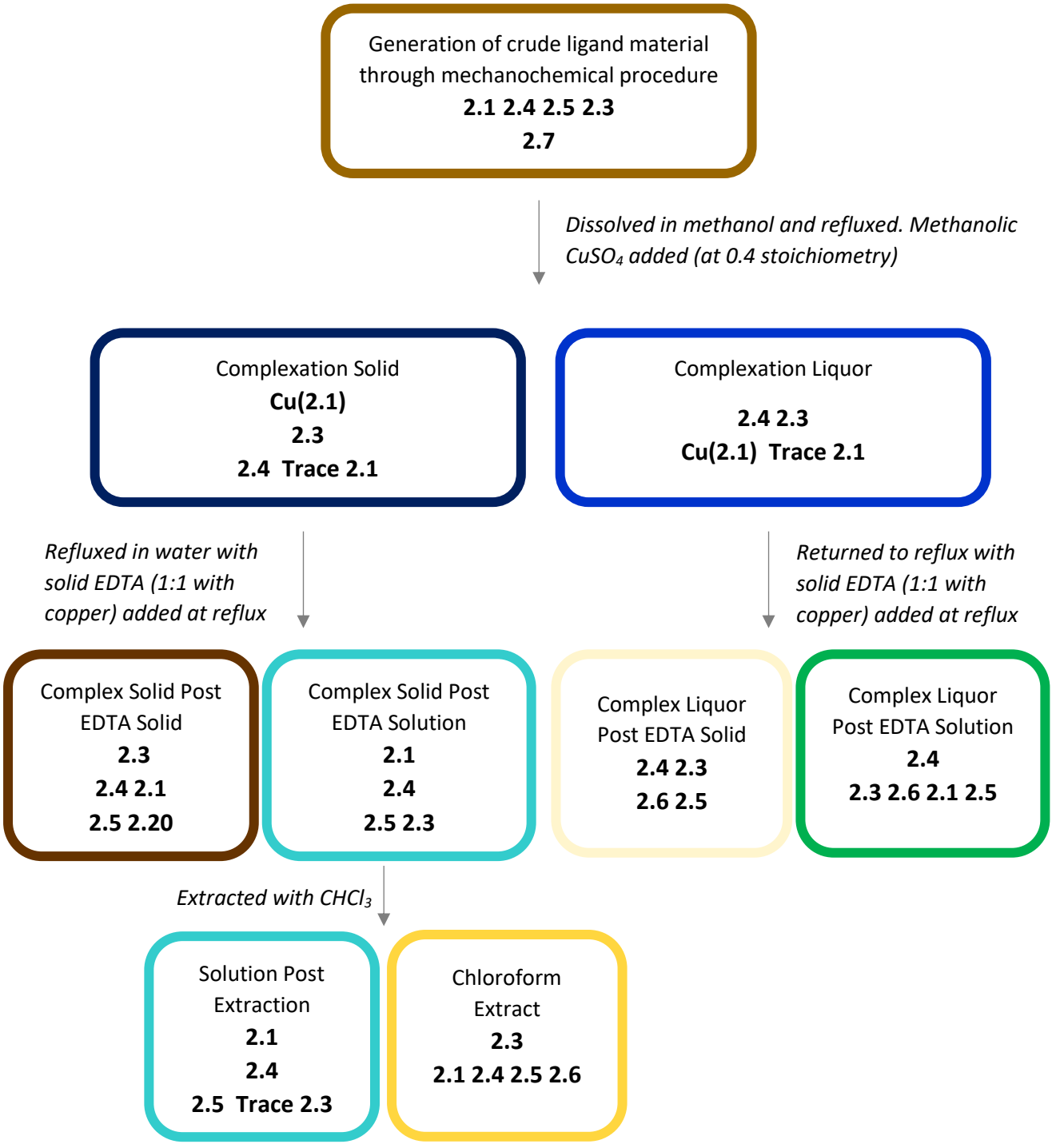

Figure B.4: ***Flowchart depicting the partitioning of the various major species in the reactions fractions of the variation on the method described in Section 2.2.6 using 40% methanolic copper sulfate. The general method for this reaction can be found in Appendix A.3.***

Table B.4: *Summarised ESI-MS results from the repetition of the 40% methanolic copper sulfate reaction fractions. The values are expressed as relative intensities for the species of interest compared to the largest peak in that spectrum. The final row percentages for the desired compound was calculated by the desired product divided by the sum of the most common side products.* **2.1, 2.4, Cu(2.1), 2.3** *and* **2.5.** *The desired compound was* **2.1** *except where* **Cu(2.1)** *was the desired compound, as highlighted in green for 2.1 and blue for the complex.*

Identity	m/z	Predicted m/z	Relative Intensity									
			Crude Ligand	Complex Solid	Complex Liquor	Cooling Solid	Solid EDTA Solid	Solid EDTA Liquor	Solid EDTA Liquor $CHCl_3$ Extract	Solid EDTA Liquor Post $CHCl_3$	Liquor ETDA Solid	Liquor EDTA Liquor
[**2.17**+2H$^+$] 2+	198.6243	198.6239 2+ for $C_{22}H_{31}N_5O_2$						0.04				
[**2.30** +1H$^+$] 1+	199.0391 1+	199.0395 1+ for $C_{12}H_7O_3$	0.31	0.06	0.23	0.04	0.03		0.08		0.10	0.25
[**2.2**+2H$^+$] 2+	207.1362 2+	207.1372 2+ for $C_{22}H_{40}N_6O_2$	0.15									
[**2.25**+2H$^+$] 2+	254.1056 2+	254.1055 2+ for $C_{30}H_{28}N_4O_4$					0.02		0.02			
[**2.13**+2H$^+$] 2+	275.6258 2+	275.6266 2+ for $C_{32}H_{33}N_5O_4$	0.10	0.08	0.09	0.04	0.08	0.06	0.06	0.13	0.08	0.12
[**2.18**+2H$^+$] 2+	288.6332	288.6345 2+ for $C_{34}H_{35}N_5O_4$			0.12							
[**2.1**+2H$^+$] 2+	297.1470 2+	297.1477 2+ for $C_{34}H_{38}N_6O_4$	1.0	0.09	0.06		0.65	1.0	0.14	1.0	0.10	0.28
[**2.7**+2H$^+$] 2+	306.1520 2+	306.1558 2+ for $C_{34}H_{40}N_6O_4$	0.59									
[**2.4**+2H$^+$] 2+	310.1544 2+	310.1556 2+ for $C_{36}H_{40}N_6O_4$	0.93	0.41	1.0	0.45	0.66	0.31	0.14	0.66	0.65	1.0
[Cu(**2.1**)]$^{2+}$	327.6035 2+	327.6047 2+ for [Cu($C_{34}H_{36}N_6O_4$)]$^{2+}$		1.0	0.29	0.39						
[**2.22**+2H$^+$] 2+	331.6757 2+	331.6767 2+ for $C_{38}H_{45}N_7O_4$					0.05			0.14		
[Cu(**2.19**)]$^{2+}$	349.1240 2+	349.1257 2+ for [Cu($C_{36}H_{41}N_7O_4$)]$^{2+}$		0.08	0.23	0.07						
[**2.15**+2H$^+$] 2+	365.6361	365.6372 2+ for $C_{44}H_{35}N_5O_6$			0.03							
[**2.12**+1H$^+$] 1+	370.2235 2+	370.2243 1+ for $C_{20}H_{28}N_5O_2$	0.07							0.09		
[**2.3** +2H$^+$] 2+	387.1583 2+	387.1583 2+ for $C_{46}H_{42}N_6O_6$	0.71	0.72	0.74	1.0	1.0	0.04	1.0	0.04	0.51	0.50
[**2.5**+2H$^+$] 2+	396.1623 2+	396.1636 2+ for $C_{46}H_{44}N_6O_7$	0.77	0.06		0.08	0.24	0.09	0.12	0.22	0.17	0.25
[**2.20**+2H$^+$] 2+	408.6776 2+	408.6794 2+ for $C_{48}H_{47}N_7O_6$	0.37	0.15		0.14	0.24					
[**2.6**+2H$^+$] 2+	409.1713 2+	409.1714 2+ for $C_{48}H_{46}N_6O_7$			0.18				0.10		0.22	0.32
[**2.21**+2H$^+$] 2+	417.6829 2+	417.6847 2+ for $C_{48}H_{49}N_7O_7$	0.28									
[**2.23**+2H$^+$] 2+	421.6849 2+	421.6872 2+ for $C_{50}H_{49}N_7O_6$					0.07					
[**2.24**+2H$^+$] 2+	430.6902	430.6925 2+ for $C_{50}H_{51}N_7O_7$										0.06
[Cu(**2.20**)]$^{2+}$	439.1346 2+	439.1363 2+ for [Cu($C_{48}H_{47}N_7O_6$)]$^{2+}$		0.11		0.10						
[Cu(**2.27**)]$^{2+}$	460.6548	460.6575 2+ for [Cu($C_{50}H_{50}N_8O_6$)]$^{2+}$				0.02						
Percentage of desired compound (compared to major side products)			29%	44%	14%	20%	25%	69%	10%	52%	7%	14%

B.5 Ligand Synthesis and Purification by Complexation using 40% Stoichiometric Methanolic Anhydrous Copper Sulfate

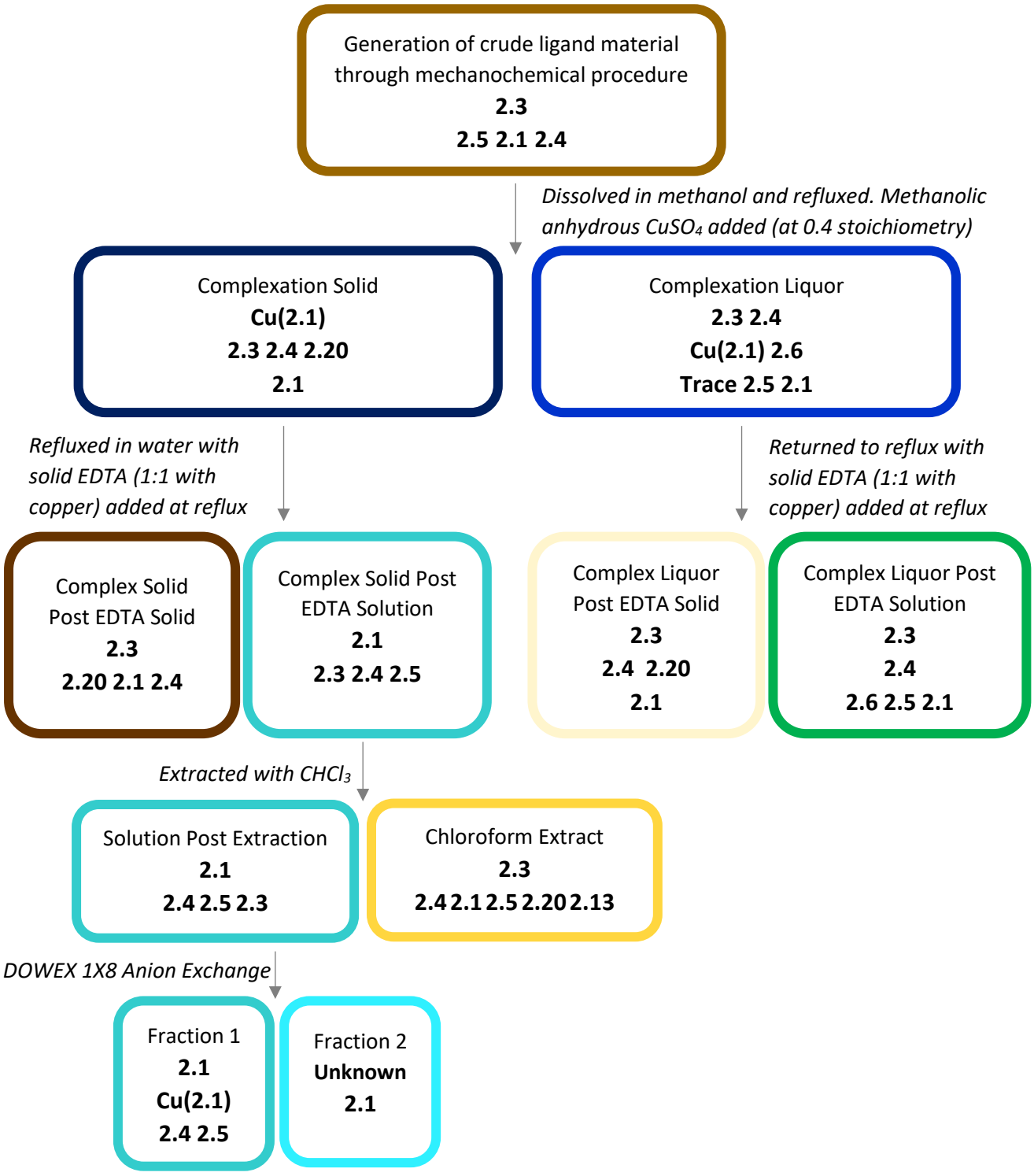

Figure B.5: ***Flowchart depicting the partitioning of the various major species in the reactions fractions of the variation on the method described in Section 2.2.6 using 40% methanolic anhydrous copper sulfate. The exact method for this reaction can be found in Appendix A.4.***

Table B.5*: Summarised ESI-MS results from the 40% methanolic anhydrous copper sulfate reaction fractions. The values are expressed as relative intensities for the species of interest compared to the largest peak in that spectrum. The final row percentages for the desired compound was calculated by the desired product divided by the sum of the most common side products.* **2.1, 2.4, Cu(2.1), 2.3** *and* **2.5***. The desired compound was* **2.1** *except where* **Cu(2.1)** *was the desired compound, as highlighted in green for 2.1 and blue for the complex.*

Identity	m/z	Predicted m/z	Relative Intensity													
			Crude Ligand	Solid	Liquor	Solid EDTA Solid	Solid EDTA Solution	$CHCl_3$ Extract	Solution Post $CHCl_3$	Column Band 1	Column Band 2 A	Column Band 2 B	Pre column oil	Oil on loading Column	Liquor ETDA Solid	Liquor EDTA Solution
[**2.30** +1H$^+$] 1+	199.0394 1+	199.0395 1+ for $C_{12}H_7O_3$	0.37	0.02	0.14	0.02	0.04	0.11							0.03	0.12
[**2.25**+2H$^+$] 2+	254.1043 2+	254.1055 2+ for $C_{30}H_{28}N_4O_4$	0.09			0.02		0.14							0.04	0.002
[**2.13**+2H$^+$] 2+	275.6260 2+	275.6266 2+ for $C_{32}H_{33}N_5O_4$		0.09	0.10	0.03		0.22	0.03	0.04	0.05		0.04		0.07	0.07
[**2.18**+2H$^+$] 2+	288.6332	288.6345 2+ for $C_{34}H_{35}N_5O_4$			0.09											0.07
[**2.1**+2H$^+$] 2+	297.1470 2+	297.1477 2+ for $C_{34}H_{38}N_6O_4$	0.20	0.05	0.09	0.25	1.0	0.50	1.0	1.0	1.0	1.0	1.0	1.0	0.04	0.07
[**2.4**+2H$^+$] 2+	310.1548 2+	310.1556 2+ for $C_{36}H_{40}N_6O_4$	0.19	0.17	0.79	0.15	0.20	0.53	0.07	0.07	0.10	0.23	0.35	0.03	0.21	0.57
[Cu(**2.1**)]$^{2+}$	327.6040 2+	327.6047 2+ for [Cu($C_{34}H_{36}N_6O_4$)]$^{2+}$		1.0	0.32	0.06				0.37	0.51	0.16	0.06	0.50		
[**2.22**+2H$^+$] 2+	331.6767 2+	331.6767 2+ for $C_{38}H_{45}N_7O_4$											0.06			
[Cu(**2.19**)]$^{2+}$	349.1231 2+	349.1257 2+ for [Cu($C_{36}H_{41}N_7O_4$)]$^{2+}$			0.24											
2.26 or **2.29**	353.1962	353.1978 1+ for $C_{20}H_{25}N_4O_2$ or 2+ for $C_{40}H_{50}N_8O_4$						0.03								
[**2.15**+2H$^+$] 2+	365.6353	365.6372 2+ for $C_{44}H_{37}N_5O_6$				0.04									0.03	0.04
[**2.3** +2H$^+$] 2+	387.1568 2+	387.1583 2+ for $C_{46}H_{42}N_6O_6$	0.41	0.24	1.0	1.0	0.27	1.0	0.05						1.0	1.0
Unknown	393.1487 2+	Unknown										0.56	0.54			
[**2.5**+2H$^+$] 2+	396.1623 2+	396.1636 2+ for $C_{46}H_{44}N_6O_7$	0.26		0.10		0.18	0.32	0.07	0.06	0.10	0.41	0.38	0.09		0.11
[**2.20**+2H$^+$] 2+	408.6769 2+	408.6794 2+ for $C_{48}H_{47}N_7O_6$		0.09		0.41	0.12	0.27					0.28		0.16	
[**2.6**+2H$^+$] 2+	409.1609 2+	409.1714 2+ for $C_{48}H_{46}N_6O_7$	0.13		0.23											0.29
[**2.23**+2H$^+$] 2+	421.6866 2+	421.6872 2+ for $C_{50}H_{49}N_7O_6$				0.08										
[Cu(**2.20**)]$^{2+}$	439.1338 2+	439.1363 2+ for [Cu($C_{48}H_{47}N_7O_6$)]$^{2+}$		0.05												
Percentage of desired compound (compared to major side products)			19%	68%	14%	17%	61%	21%	84%	67%	58%	56%	56%	62%	3%	4%

B.6 Ligand Synthesis and Purification by Complexation using 40% Stoichiometric Methanolic Copper Sulfate, 3.5x Scale (0.5 scale compared to Section 2.2.6)

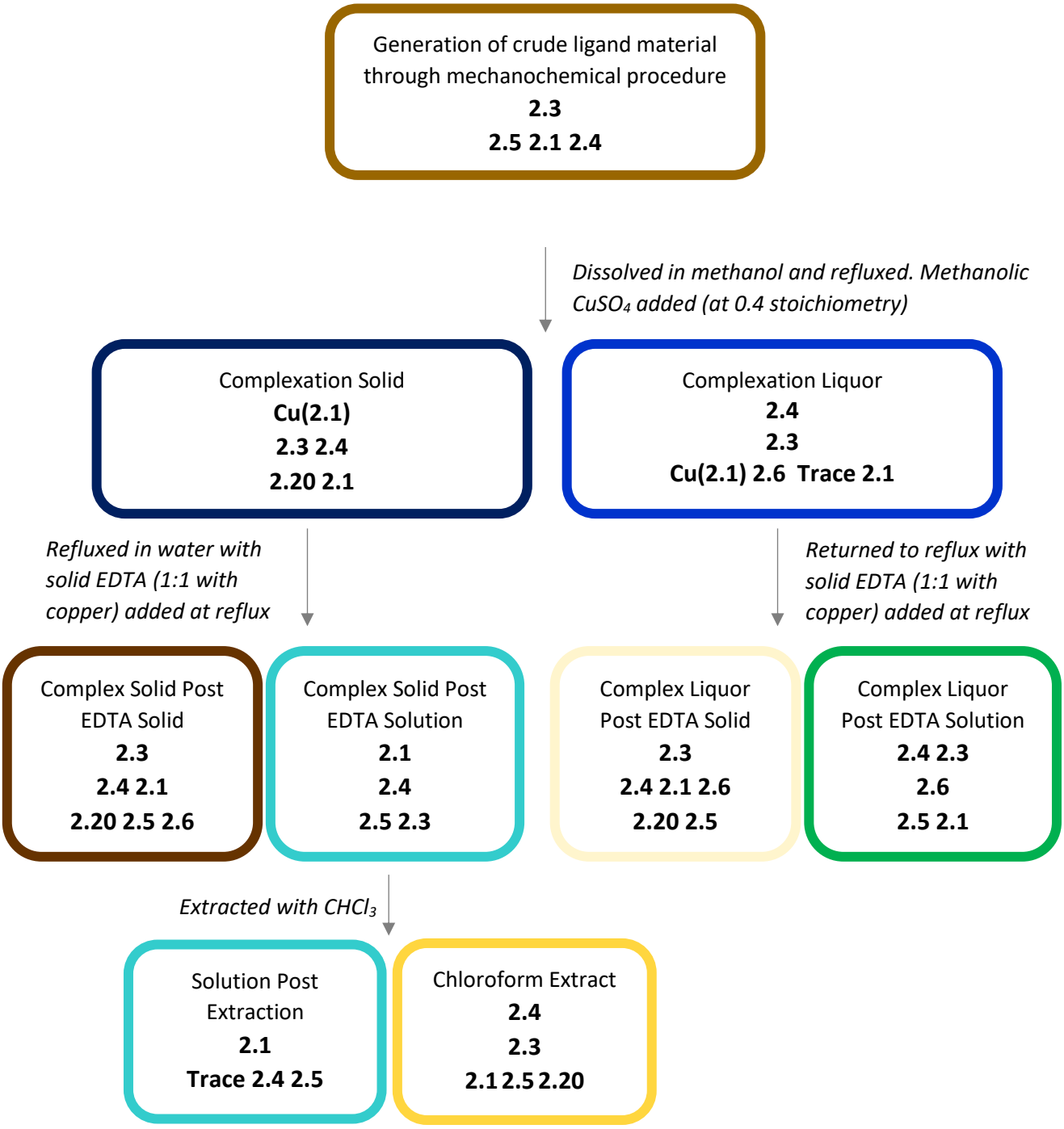

Figure B.6: ***Flowchart depicting the partitioning of the various major species in the reactions fractions of the variation on the method described in Section 2.2.6 using 40% methanolic copper sulfate. The general method for this reaction can be found in Appendix A.3.***

Table B.6: *Summarised ESI-MS results from the reaction fractions of the 40% methanolic copper sulfate reaction at 3.5x scale (0.5 compared to Section 2.2.6). The values are expressed as relative intensities for the species of interest compared to the largest peak in that spectrum. The final row percentages for the desired compound was calculated by the desired product divided by the sum of the most common side products.* **2.1, 2.4, Cu(2.1), 2.3** *and* **2.5**. *The desired compound was* **2.1** *except where* **Cu(2.1)** *was the desired compound, as highlighted in green for 2.1 and blue for the complex.*

Identity	m/z	Predicted m/z	Relative Intensity								
			Crude Ligand	Complex Solid	Complex Liquor	Solid EDTA Solid	Solid EDTA Solution	Solid EDTA Solution $CHCl_3$ Extract	Solid EDTA Solution Post $CHCl_3$	Liquor ETDA Solid	Liquor EDTA Solution
[**2.30** +1H$^+$] 1+	199.0395 1+	199.0395 1+ for $C_{12}H_7O_3$	0.37	0.06	0.13			0.04		0.05	0.15
[**2.25**+2H$^+$] 2+	254.1056 2+	254.1055 2+ for $C_{30}H_{28}N_4O_4$	0.09	0.02				0.04			
[**2.13**+2H$^+$] 2+	275.6255 2+	275.6266 2+ for $C_{32}H_{33}N_5O_4$		0.16	0.04	0.06	0.06	0.09	0.04	0.07	0.11
[**2.18**+2H$^+$] 2+	288.6332	288.6345 2+ for $C_{34}H_{35}N_5O_4$		0.05	0.10			0.09			
[**2.1**+2H$^+$] 2+	297.1472 2+	297.1477 2+ for $C_{34}H_{38}N_6O_4$	0.20	0.22	0.06	0.52	1.0	0.23	1.0	0.26	0.25
[**2.4**+2H$^+$] 2+	310.1544 2+	310.1556 2+ for $C_{36}H_{40}N_6O_4$	0.19	0.59	1.0	0.56	0.30	1.0	0.12	0.38	1.0
[Cu(**2.1**)]$^{2+}$	327.6032 2+	327.6047 2+ for [Cu($C_{34}H_{36}N_6O_4$)]$^{2+}$		1.0	0.28						
[**2.22**+2H$^+$] 2+	331.6757 2+	331.6767 2+ for $C_{38}H_{45}N_7O_4$				0.05	0.06		0.05		0.13
[Cu(**2.19**)]$^{2+}$	349.1240 2+	349.1257 2+ for [Cu($C_{36}H_{41}N_7O_4$)]$^{2+}$		0.14	0.18						
[**2.26** +1H$^+$] 1+	353.1965 1+	353.1978 1+ for $C_{20}H_{26}N_4O_2$						0.02			
[**2.12**+1H$^+$] 1+	370.2236 2+	370.2243 1+ for $C_{20}H_{28}N_5O_2$					0.08		0.06		
[**2.16**+2H$^+$] 2+	374.6400	374.6425 2+ for $C_{44}H_{39}N_5O_7$								0.05	
[**2.3** +2H$^+$] 2+	387.1566 2+	387.1583 2+ for $C_{46}H_{42}N_6O_6$	0.41	0.73	0.46	1.0	0.07	0.60		1.0	0.90
[**2.5**+2H$^+$] 2+	396.1623 2+	396.1636 2+ for $C_{46}H_{44}N_6O_7$	0.26			0.22	0.12	0.19	0.05	0.11	0.28
[**2.20**+2H$^+$] 2+	408.6776 2+	408.6794 2+ for $C_{48}H_{47}N_7O_6$		0.26		0.31		0.12		0.19	
[**2.6**+2H$^+$] 2+	409.1713 2+	409.1714 2+ for $C_{48}H_{46}N_6O_7$			0.12	0.20					0.61
[**2.23**+2H$^+$] 2+	421.6849 2+	421.6872 2+ for $C_{50}H_{49}N_7O_6$				0.07					
[Cu(**2.20**)]$^{2+}$	439.1346 2+	439.1363 2+ for [Cu($C_{48}H_{47}N_7O_6$)]$^{2+}$		0.10							
Percentage of desired compound (compared to major side products)			19%	39%	16%	23%	67%	11%	85%	15%	10%

Appendix C. Additional Chapter 2 Discussion on the Fractions of the Purification by Complexation Method

This appendix seeks to expand upon Section 2.4.3.1, Purification by Complexation Reaction Stages on page 63 by providing additional details around the speciation observed in each fraction of the complexation by purification method.

Complexation reaction of copper with the crude ligand material (Section 2.2.6.2)

The reaction of crude ligand with copper produced a deep blue solid and a deep blue liquor. Both the solid and the liquor contained a complex of the copper and desired compound, as identified by ESI-MS. The copper 2.1 complex was predominantly seen in the solid produced, with percentage compositions of 12% to 68% in the solid and 9% to 14% in the liquor (Tables B.1-B.6). The free dinaphthalimide piperazine and trinaphthalimide species (2.4 and 2.3, 310.1556 2+ and 387.1568 2+) were also found in both fractions, often as the major compounds. The deep blue colour of both fractions suggested the presence of copper bound to nitrogen donor atoms. This hints at the possibility of copper complex formation that was not detected by ESI-MS, such as neutral species or species that do not ionise well.

Aside from the partitioning of the desired compound and its complex between the two phases, the composition of the complexation solid and liquor was generally very similar in that each by-product component still appeared in each phase, albeit in slightly different ratios. In general, the relative intensity of the dinaphthalimide piperazine (2.4, 310.1556 2+) to the trinaphthalimide species showed greater presence of the trinaphthalimide (2.3, 387.1583 2+) species in the solid (around 0.73 versus 0.46 relative intensity), and greater presence of the dinaphthalimide piperazine in the reaction liquor (0.59 versus 1.0 relative intensity) . The exact ratio of the components varied between experiments.

The precipitate that formed during overnight refrigeration was also very similar between trials and was predominantly comprised of some of the remaining 2.3 compound precipitating from the liquor, along with more of the Cu(2.1) complex and some of 2.4. This fraction was collected and combined with the initial reaction solid to maximise the amount of the desired compound copper complex collected. This was done despite the greater presence of the trinaphthalimide side product 2.3 in the solid produced on cooling as this side product was already present in the complexation solid in large amounts, and thus collection of more complex was deemed more important than discarding the impurity at this step.

Treatment of the Reaction Solid with EDTA (Section 2.2.6.3)

Treatment of the reaction solid with EDTA resulted in the solid changing from a deep blue oily solid to a brown oil, and the solution went from the faint deep blue of the slightly dissolved solid to an intense bright blue, characteristic of the copper EDTA complex. The treatment of the solid with EDTA was of particular interest given that this fraction showed the highest ratio of desired compound to side products (average percentage composition 51% 2.1).

Despite the observation that the crude ligand material had a low solubility in water, the desired compound 2.1 appeared to have a high relative intensity in the aqueous phase following the removal of copper, appearing at an average of 51% composition and relative intensities up to 1.0 (Tables B.1-B.6, 2.18). The desired compound was the major component detected in this phase, however, substantial amounts of both copper EDTA and free EDTA (as the EDTA was used in slight excess) are also present in this phase. As the enrichment was determined by the relative intensities of the peaks observed in the ESI-MS spectra, the presence of the neutral and undetected Cu(EDTA) species was not included in the comparisons performed to determine enrichment. As a result, the perceived enrichment of the desired ligand in the aqueous phase was much higher than the true result. The desired compound was likely a minor component of the aqueous solution, which was further illustrated the poor yield of 1.5% for the precipitate from this solution (Section 2.3.2). The solid produced by this reaction contained large amounts of the side product along with a high relative intensity of the desired compound. This showed that despite the cleanness of the solution, the majority of the desired compound ended up in this solid phase and thus the purification was inefficient.

Treatment of the Reaction Liquor with EDTA (Section 2.2.6.4)

The treatment of the reaction liquor with EDTA was also performed to gain further information about the species present in the reaction mixture. The deep blue liquid produced a mixed brown solid and an emerald green solution upon addition of EDTA.

Both the solution and the solid following addition of EDTA contained the desired compound, the trinaphthalimide and naphthalamide species and the dinaphthalimide piperazine species in relative intensities of around 0.50, 1.00 and 1.00, respectively. This indicates that some of the desired compound 2.1 was lost to this fraction, but the recovery of it was unlikely to be worth the effort nor effective due to the excess of the by-products.

Chloroform Extraction of the Reaction Solid Post EDTA Aqueous Solution (Section 2.2.6.5)

To isolate the desired compound from the aqueous solution post EDTA treatment the solution was extracted using chloroform. The yield from this extraction was extremely low, around 0.6% of the mass of the initial crude ligand used, and the ESI-MS spectra for the chloroform extracts indicated that the extracted product was composed of primarily by-products. The nature and ratio of these side products varied greatly between the experiments. As a result, the extract was substantially less pure than the crude material.

This meant that although the extraction had not succeeded in isolating the desired compound from the copper and EDTA products, it had removed some of the other contaminants from the aqueous solution. The aqueous solution following extraction was less contaminated when analysed by ESI-MS, with a greater relative intensity of the desired compound to other side products than was seen pre-extraction (1.0 to 0.30 versus 1.0 to 0.12 as seen in Table B.6). This was seen as an increase in the percentage composition of the desired compound in the solution before and after extraction, going from an average of 51% and maximum of 69% to an average of 63% and maximum of 85% (Table 2.18).

Column of the Reaction Solid Post EDTA Aqueous Solution, Post Chloroform Extraction (Section 2.2.6.5)

The purpose of this column was to remove the free EDTA and the Copper EDTA complex from the free ligand. By adjusting the solution to pH 7.5, both the EDTA and the complex are likely to be negatively charged and can therefore be separated from the positively charged and neutral species. Running the pH 7.5 solution following extraction through the DOWEX 1X8 resin resulted in a pale blue fraction that ran through the column with the water as it was loaded and continued to elute with water. This fraction contained the desired compound when analysed by ESI-MS, along with some of the copper complex. This copper complex was not observed substantially in the solution prior to introduction in the column. This suggested the possibility of the complex forming in the column. A blue band was observed at the top of the column upon loading. This was likely to be the copper EDTA species as it did not move substantially under the water mobile phase, which would be expected as this complex would be negatively charged and therefore attracted to the positively charged resin.

The bright blue band that formed at the top of the resin was eluted with 0.25-1M NaCl and further concluded to be the copper EDTA species. A small amount of a yellow compound remained at the top of the column. Attempts to remove this from the column using acid and salt

were unsuccessful and required removal of the top layer of resin which was then washed with methanol to remove the compound. This compound was identified as ligand material that had crashed out due to poor solubility as determined by ESI-MS. This sample was also substantially contaminated by resin.

The amount of desired compound retrieved by the column was low despite the quantity of crude material used. The exact mass cannot be determined following *in vacuo* removal of water from the fraction due to the presence of salt and the blue species that remains in the product following washing of the material. This reinforces the conclusion drawn in the previous subsection for this aqueous solution, that while the reaction can produce relatively pure material (as seen by the column ESI-MS results in Table 2.15 and Table 2.18) the process was inefficient.

Precipitate following chloroform extraction of the complexation solid post EDTA solution

The purest sample of desired compound was collected during the work up of the post chloroform extraction solution to prepare it for ion exchange chromatography. This material was still a pale blue, suggesting presence of undetected complexes. The ESI-MS spectrum showed the material to be predominantly the desired compound (89%, Table 2.15). The precipitate upon drying weighed 0.5 g and was obtained from an initial reaction mass of 30 g, indicating that this process was also very low yielding. Unfortunately, attempts to collect an NMR spectrum of this compound to compare to the crude material were unsuccessful. An inability to gather NMR data even when using a large number of scans was also observed for the crude material so this was an unsurprising, although disappointing, finding.

Appendix D. Additional Chapter 2 Discussion comparing and contrasting the Variations to the Purification by Complexation method

Methanolic versus Aqueous Copper Sulfate (Appendix B.1 and B.2)

This variation surrounded the method by which copper was added to the methanolic solution of crude material. Using methanol resulted in a greater total reaction volume due to the lower solubility of the copper sulfate in methanol. The major difference between these two reactions surrounds the partitioning of the copper complex of the desired product versus the side products in the complexation solid, and subsequently, the solution produced following treatment of the this solid with EDTA (Tables B.1 and B.2). The initial reaction solid contains substantially greater amounts of the dinaphthalimide piperazine and trinaphthalimide compounds in the aqueous addition of copper versus the methanolic addition. This was likely due to the lower solubility of these species in the slightly more polar reaction solvent for the aqueous addition. The solid produced during the complexation reaction contained the majority of the copper complex of the desired compound and the methanolic addition showed the greater enrichment here, with 12% of the solid being complex for the aqueous reaction versus 61% for the methanolic addition.

33% Copper Versus 40% Copper (Appendix B.2 and B.3)

The amount of copper used in the complexation was also varied between experiments. The choice of 33% stoichiometric copper was somewhat arbitrary and based around a bottle label that may have corresponded to the purity, so it was likely that this ratio could be changed to improve the purification. Free ligand of the desired compound 2.1 was detected by ESI-MS following copper complexation at 33% stoichiometry indicating insufficient copper was used to complete complexation. The copper used was increased to 40% stoichiometric, with all other reaction conditions maintained.

The increase in copper increased the amount of the desired compound that was complexed, with the free desired ligand in the complexation solid going from 0.42 of the intensity of the complex peak to 0.09 of the intensity through increasing the amount of copper from 33% to 40% (Tables B.2 and B.3). The free ligand in the solvent remained low, at 0.04 and 0.06 of the dinaphthalimide piperazine compound in the 33% and 40% copper reactions, respectively.

The increased complex in the complexation solid corresponded to an increase in enrichment of the desired compound in the aqueous phase following EDTA treatment of this solid. The percentage of 2.1 in this fraction went from 54% to 69% upon increasing the copper stoichiometry. This increase was attributed to the additional complex present in the solid and could also be partially due to the extra solvent used to dissolve the additional copper allowing impurities to remain in solution and therefore not be observed in this step.

Based on the observation of greater complexation of the desired compound, as well as greater enrichment of this compound in the aqueous phase (following EDTA treatment), upon increasing the amount of copper it was decided that the further reactions would also be performed at this stoichiometry. Further increasing the stoichiometry was not attempted as it could only result in a slight improvement over this method, as very little free 2.1 remained, but would come with the risk of also complexing poorer ligands or complexing these compounds in greater quantities than already occurring.

Pentahydrate versus Anhydrous Copper Sulfate (Appendix B.3 and B.5)

Another modification made to this method surrounded the use of anhydrous copper sulfate as the source of copper. When compared to the pentahydrate synthesis a similar enrichment was observed by ESI-MS. Unfortunately, the anhydrous copper was also much more prone to precipitating out of the warm methanol as the solvent cooled slightly and required a much greater volume to dissolve. This resulted in difficulty keeping the solution warm during addition to the ligand solution. Both the volume and tendency to precipitate made performing the reaction impractical.

The complexation solid of the anhydrous reaction had a greater enrichment of the desired complex compared to the pentahydrate, appearing as 68% versus 44% (Table 2.18). This could be due to the increased reaction volume from the less soluble anhydrous copper favouring dissolution of the side products, as hypothesised in the previous subsection. This would reduce the amount of the side products present in the complexation solid, corresponding to the lower detection of the side products in the subsequent steps. As the methanol used was used without attempts to fully dry it, much of the water removed through the use of anhydrous copper may have been replaced in the increased methanol volume. This suggests that the increased volume may be the true reason for the increased enrichment, and further reactions using a greater reaction volume should be pursued as future work.

Following the EDTA treatment of this solid, the solution produced by the anhydrous reaction was slightly less enriched by comparison to the pentahydrate. The increased enrichment for the anhydrous reaction in the solid was somewhat offset by the slightly lower enrichment of the desired compound following treatment of the solid with EDTA. The obvious need for further optimisation at this step coupled with the more difficult reaction procedure led to the decision to continue using the pentahydrate copper sulfate salt for further reactions.

Reproducibility of the complexation process (Appendix B.3 and B.4)

Following the observation that slight changes to the reaction conditions led to the decision to repeat the reaction to determine the reproducibility of the method. The reaction of crude material with 40% stoichiometric copper was attempted following the same procedure as was applied in the first iteration.

The similarity between the two repetitions of this reaction (Tables B.3 and B.4) showed that this method was reproducible in terms of which compounds were detected in which fractions, however, the percentages of the desired compounds varied between the two trials. The aqueous solution following treatment with EDTA still showed the highest enrichment of the desired compound 38% and 69%). Across the different reaction fractions only minor differences in the compounds detected were observed.

Scale up of the process (Table 2.15, Appendix B.4 and B.5)

The reaction using 40% methanolic copper sulfate was also repeated at a 3.5x and 7.5x scale. As the scale increased, there was an observed decrease in the percentage of the desired compound in the fractions expected, even despite the slightly purer crude material used in the case of the 7.5x scale reaction (Table 2.15). The desired complex Cu(2.1) in the complexation solid decreased from 44% to 39% to 22%. Conversely, it increased in the liquor from 14% to 16% to 27%. The complex distribution has moved towards the reaction liquor. This could have been due to the fact that the volume required for dissolution did not increase by the same amount as the reactants, resulting in a more concentrated solution. This implies that decreasing the concentration of the solution may increase the enrichment of the desired complex Cu(2.1), which corresponds to the conclusion drawn in the previous subsection. Further work into this by varying the reaction volume would likely allow for further conclusions to be drawn.

The following step of the reaction was similarly affected; upon addition of EDTA to the complexation solid, the enrichment previously seen in the solution drops from 69% to 67 % to 44%, and the decrease seems to have been made up for by an increase of the desired ligand 2.1

in the solid produced (and lost to the complexation liquor in the previous step). The increase in the post EDTA solid is likely to be of benefit; as discussed in Section 2.4.3.1, the apparent enrichment in the solution was undermined by the lack of detection of the far more prevalent Cu(EDTA) complex. In the two scale up reactions, the solid produced in the also featured an enriched presence of the desired ligand 2.1 compared to the crude material, at 19% versus 23% for the 3.5x scale and 38% versus 44% for the 7.5x scale. Further investigation as to the payoff of this method still needs to be explored – while it produced a much greater yield of the enriched material in the solid material than observed in the solution in other iterations, the percentage composition was lower indicating less enrichment.

Appendix E. Analysis of the Components in the Chapter 2 Reaction Mixtures

E.1 Analysis of the Components in the Crude Ligand Reaction

Compounds Containing six nitrogen atoms

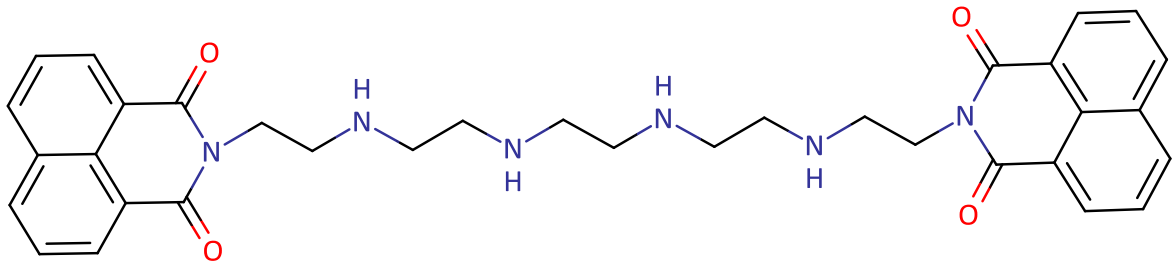

Figure E.1: ***Compound 2.1, ESI-MS peaks 593.2876 1+ and 297.1484 2+ (predicted 297.1477 2+ for $C_{34}H_{37}N_6O_4$ and 593.2876 1+ for $C_{34}H_{37}N_6O_4$)***

This desired compound was generally observed as a major component of the crude reaction mixture by ESI-MS relative intensities. The percentage of the crude ligand composition of this compound averaged 31% (judged by peak height versus total peak heights for identifiable compounds).

The linear form of this compound was the desired ligand for further synthesis, yet there are many other branched isomers that may be present.

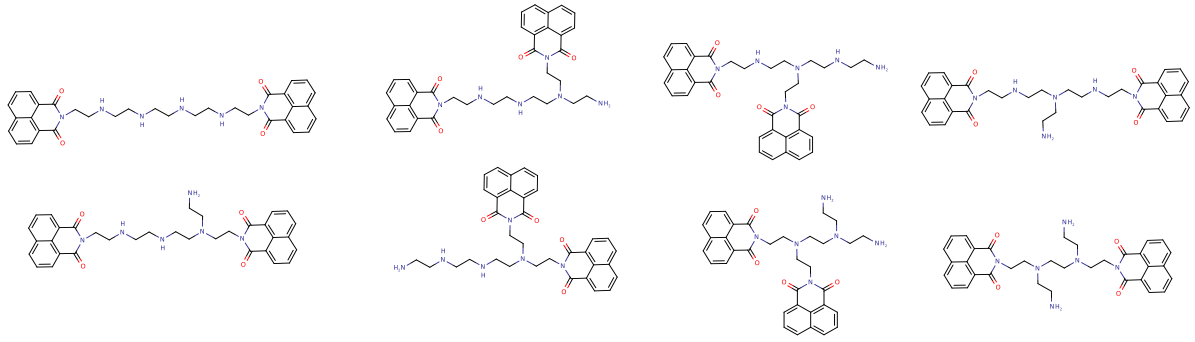

Figure E.2: ***Possible isomers of the desired product (top left) that may be contributing to the m/z signals at 593.2876 1+ and 297.1484 2+ (predicted 297.1477 2+ for $C_{34}H_{37}N_6O_4$ and 593.2876 1+ for $C_{34}H_{37}N_6O_4$).***

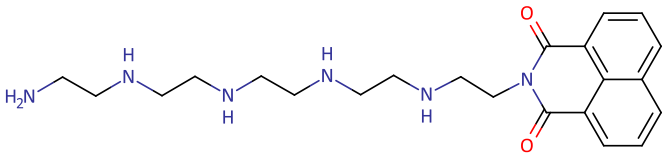

Figure E.3*: Compound 2.2, ESI-MS peak 207.1362 2+ (predicted 207.1372 2+ for $C_{22}H_{40}N_6O_2$)*

This compound was identified in the crude reaction mixtures in generally low amounts, less than 0.10 relative intensity. In order to have this mass, the amine starting material would have to contain at least two primary amines, with addition of a naphthalimide moiety to only one of them. This suggests that, despite the excess of naphthalic anhydride used, complete eradication of this species may not be possible. Unfortunately, this compound was likely to be a better ligand than the dinaphthalimide species, even if branched, due to the greater number of available donor atoms and the lower bulk from the singular naphthalimide.

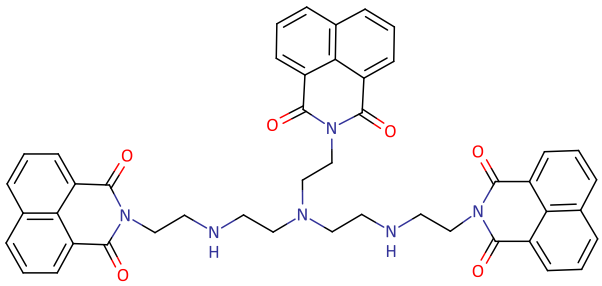

Figure E.4: ***Compound 2.3, ESI-MS peaks 387.1578 2+ and 773.3088 1+ (predicted 387.1583 2+ for $C_{46}H_{42}N_6O_6$ and 773.3088 1+ for $C_{46}H_{41}N_6O_6$)***

This compound mass could correspond to one of three main isomers, as well as the possibility of a less probable nine membered ring compound. These isomers correspond to the symmetric and asymmetric monobranched amine species, as well as the dibranched species with three pendants. Of these isomers, one compound was symmetrical which may encourage the formation of complexes with copper as seen in the crystal structure in Chapter 4. These compounds all have three available donor atoms, making them less likely to form complexes than the desired compound. As seen in the crystal structure in Chapter 4, a tripodal ligand may coordinate to the copper along with a sulfate, creating a neutral complex. Such a complex would be difficult to detect by ESI-MS, and as in the case of the crystal structure compound, only free ligand was detected. If these compounds are indeed present in the purification mixture, they were notndetected and instead may only be detected as free ligand upon complex degradation. Whether these species would form instead of copper complexes of the desired compound was unknown.

Heterocycles with nine members do exist in the literature, suggesting that the nine-membered ring diamide may be possible to form[140-141] (Figures E.5 and E.6).

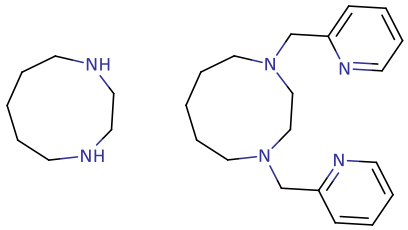

dacn and dmpdacn[141]

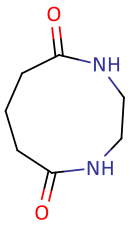

Core of a heterocycle with amides[140]

Figure E.5: ***Literature examples of nine-membered heterocycles.***

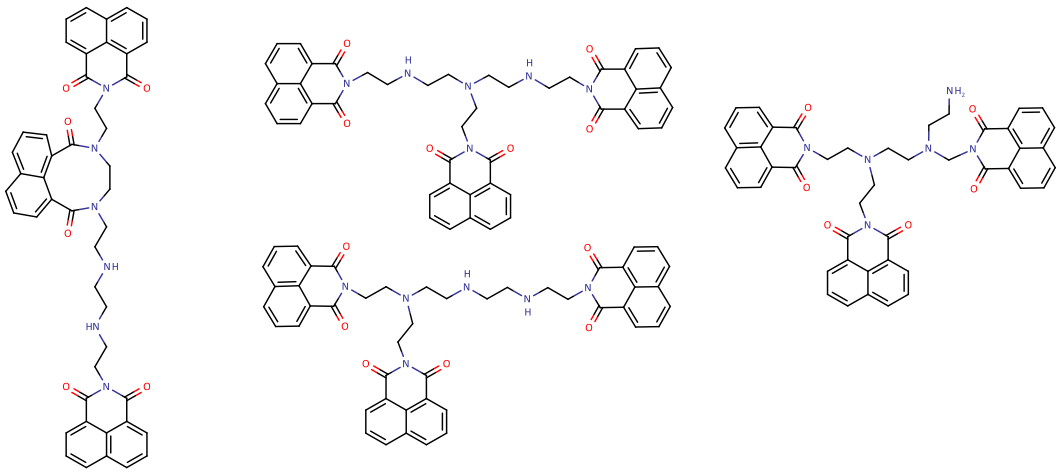

Figure E.6: ***Possible isomers that may be contributing to the m/z signals at 387.1578 2+ and 773.3088 1+ (predicted 387.1583 2+ for $C_{46}H_{42}N_6O_6$ and 773.3088 1+ for $C_{46}H_{41}N_6O_6$).***

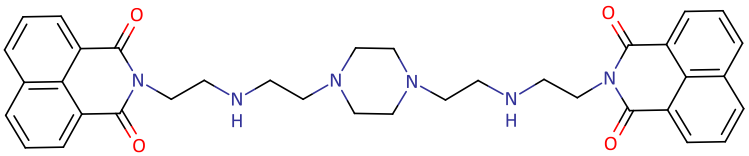

Figure E.7: ***Compound 2.4, ESI-MS peaks 310.1549 2+ and 619.3037 1+ (predicted 310.1556 2+ for $C_{36}H_{40}N_6O_4$ and 619.3033 1+ for $C_{36}H_{39}N_6O_4$)***

The dinaphthalimide piperazine compound was also detected by ESI-MS in the crude ligand mixture. In some iterations of the crude ligand synthesis, this piperazine compound (or its seven isomers) was the most detected product, which was interesting given that the piperazine peak in

the free amine ESI-MS spectrum was around one third of the relative intensity of the desired amine mass.

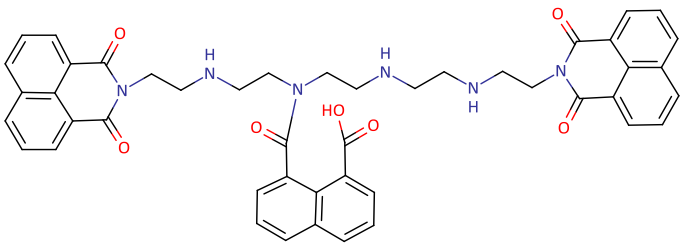

Figure E.8: ***Compound 2.5, ESI-MS peaks 396.1629 2+ and 791.3197 1+ (predicted 396.1636 2+ for $C_{46}H_{44}N_6O_7$ and 791.3194 1+ for $C_{46}H_{43}N_6O_7$)***

Formation of an amide in the ligand synthesis was an interesting observation. Despite the excess of anhydride used for a linear amine, the branched nature of some components of the amine mixture would suggest that any excess anhydride would form an imide with the additional terminal amines, rather than form amides with secondary amines of the chain. However, compounds with the correct mass for an additional pendant through an amide linkage frequently appear in the ESI-MS spectra. The relative intensity, when detected, varies from a trace component of the reaction mixture right through to the major component. This amide was likely to be a poorer ligand than the desired compound, both due to one of the donor atoms going from a secondary to tertiary amide (which would be a slightly poorer donor atom in the chelating system) as well as the added steric bulk of the additional naphthalimide. This compound could also exist as a number of isomers, some of which may have more steric strain than others due to the proximity of the naphthalimide and naphthalamide groups.

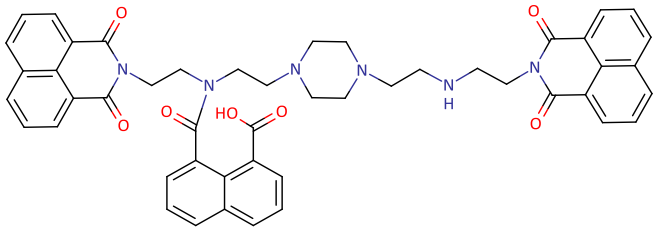

Figure E.9: ***Compound 2.6, ESI-MS peaks 409.1713 2+ and 817.3355 1+ (predicted 409.1714 2+ for $C_{48}H_{46}N_6O_7$ and 817.3350 1+ for $C_{48}H_{45}N_6O_7$)***

This compound appears frequently in the ESI-MS spectra and was the piperazine equivalent of compound 2.5. This compound will likely share many of the properties of both compound 2.4 and 2.5 with a reduction in available donor atoms due to the piperazine moiety as well as the

amide tertiary nitrogen. The relative intensity of this compound ranges greatly from not being detected right through to having the largest relative intensity.

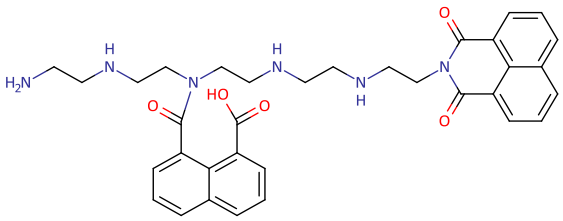

Figure E.10: ***Compound 2.7, ESI-MS peak 306.1526 2+ (predicted 306.1558 2+ for $C_{34}H_{40}N_6O_4$)***

As for the previous amide, this compound was not always detected but the fact that it was detected at all was an interesting finding. This compound was only substantially detected in the crude ligand, with a maximum relative intensity of 0.94, however, there was some evidence for trace amount peaks in ESI-MS spectra of other reaction steps. This suggests that this compound was disfavoured upon refluxing, wherein the amide has the opportunity to hydrolyse and equilibrate to a more favourable imide. There were 21 potential isomers of this compound.

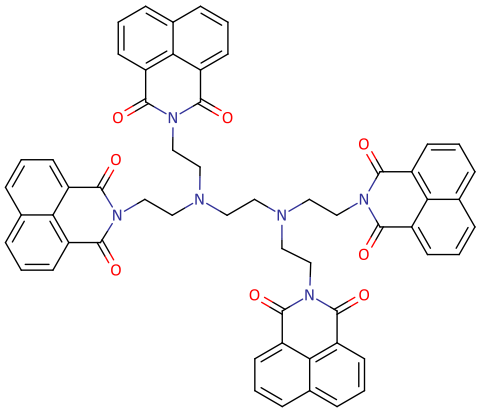

Figure E.11: ***Compound 2.8, ESI-MS peak 953.3300 1+ (predicted 953.3299 1+ for $C_{58}H_{45}N_6O_8$)***

The presence of this compound confirms that the dibranched isomer of the free amine exists. The number of pendants on this amine was greater than the number of equivalents of free anhydride added to the reaction mixture, making this compound less likely to form in favour of less substituted compounds. The steric bulk of the additional naphthalimides may also discourage the formation. Additionally, only one isomer of the desired amine could form this species, while the compounds with fewer naphthalimides could be formed from many of the isomers. These factors may explain the infrequent and low detection of this compound. Only one isomer exists.

The complexation ability of this compound was low as the only available donor atoms are tertiary nitrogen atoms and the steric bulk of the four pendants would likely preclude coordination to these nitrogen atoms. It was also possible that this compounds infrequent and low detection was due to the inability to become protonated from the steric hinderance and lower basicity of the tertiary nitrogen compared to the secondary nitrogen atoms available in other species.

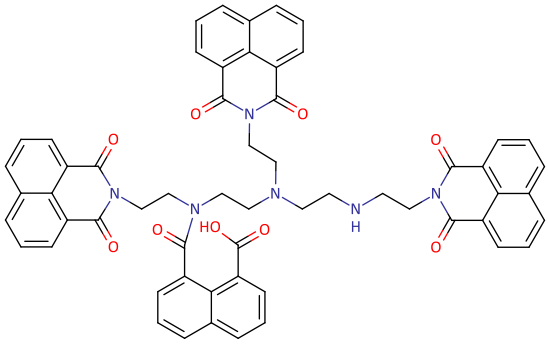

Figure E.12: ***Compound 2.9, ESI-MS peaks 486.1746 2+ and 971.3405 1+ (predicted 486.1741 2+ for $C_{58}H_{48}N_6O_9$ and 971.3404 1+ for $C_{58}H_{47}N_6O_9$)***

As for 2.8, the additional naphthalimides than the reaction stoichiometry as well as the steric bulk may disfavour this compounds formation. Despite this, this compound was frequently detected as at up to a relative intensity of 0.10. Interestingly, unlike compound 2.7, this compound was detected even after the crude material has been refluxed and therefore given an opportunity to equilibrate to the more stable imides, as was seen for compound 2.5. Detection of this compound may be better than for 2.8 due to the number of possible isomers (four) which arises from the greater number of free amine isomers that could lead to the formation of species matching this mass. The complexation ability of this compound was likely to be low.

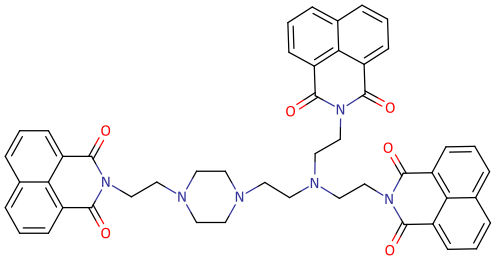

Figure E.13: ***Compound 2.10, ESI-MS peak 400.1664 2+ (predicted 400.1661 2+ for $C_{48}H_{44}N_6O_6$ and 799.3244 1+ for $C_{48}H_{43}N_6O_6$)***

This compound was detected in the ESI-MS spectra at relative intensities of 0.08. There was just one isomer of this compound, possibly explaining the lower detection. As for compound 2.6, this compound was likely to be a poor ligand.

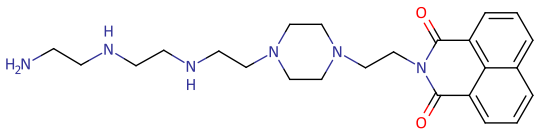

Figure E.14: ***Compound 2.11 ESI-MS peak 439.2807 1+ (predicted 439.2822 1+ for $C_{24}H_{35}N_6O_2$)***

This compound was detected as a trace component.

Compounds containing five nitrogen atoms

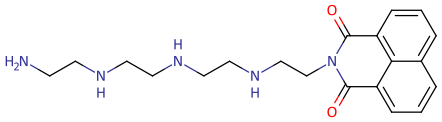

Figure E.15: ***Compound 2.12, ESI-MS peak 370.2243 1+ (predicted 370.2243 1+ for $C_{20}H_{28}N_5O_2$)***

The formation of this compound should be disfavoured by the reaction stoichiometry but was detected in the reaction mixture at relative intensities up to 0.16. This was similar to the detection of 2.2. This compound has four possible isomers.

Unfortunately, this compound was likely to be a better ligand than the desired compound as it possesses the same number of donor atoms but a lower steric bulk from the reduced number of pendants. Purification by complexation may not be able to remove this compound from the reaction mixture, and it was identified in the most enriched sample of the desired compound.

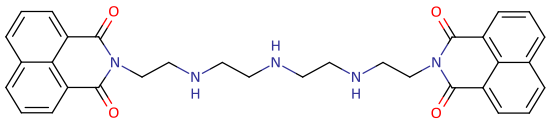

Figure E.16: ***Compound 2.13, ESI-MS peaks 275.6263 2+ and 550.2456 1+ (predicted 275.6266 2+ for $C_{32}H_{33}N_5O_4$ and 550.2455 1+ for $C_{32}H_{32}N_5O_4$)***

This compound was detected at relative intensities up to 0.28, which was expected considering the relative intensity of the free amine compared to the free hexamine in the crude amine was around 0.11, with the hexamine being composed of four different isomers.

This compound had fewer donor atoms than the desired compound and was likely to be outcompeted for coordination to copper.

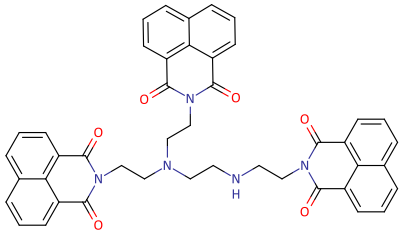

Figure E.17: ***Compound 2.14, ESI-MS peak 365.6361 2+ (predicted 365.6372 2+ for $C_{44}H_{37}N_5O_6$)***

This compound was detected in trace amounts at relative intensities of 0.04 in various reaction fractions. There was only one isomer. This compound had fewer donor atoms than the desired compound, and additional steric bulk from the third naphthalimide, and was likely to be outcompeted for coordination to copper.

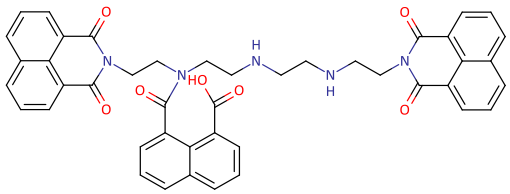

Figure E.18: ***Compound 2.16, ESI-MS peak 374.6423 2+ (predicted 374.6425 2+ for $C_{44}H_{39}N_5O_7$)***

ESI-MS peaks corresponding to this mass were identified in trace amounts, with relative intensities up to 0.05. There are 8 possible isomers of this compound. This compound had fewer donor atoms than the desired compound so was likely to be a poorer ligand.

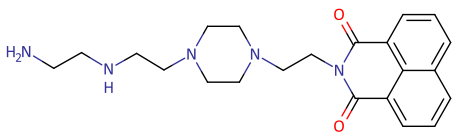

Figure E.19: ***Compound 2.17, ESI-MS peak 198.6234 2+ (predicted 198.6239 2+ for $C_{22}H_{31}N_5O_2$)***

This peak was identified in various reaction fractions in trace amounts up to 0.04 relative intensity. There are three possible isomers.

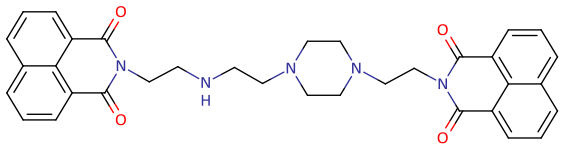

Figure E.20 ***Compound 2.18, ESI-MS peaks 288.6334 2+ and 576.2598 1+ (predicted 288.6345 2+ for $C_{34}H_{35}N_5O_4$ and 576.2611 1+ for $C_{34}H_{34}N_5O_4$)***

The highest relative intensity seen for this compound was 0.12 and there was only one isomer. This compound had two poorer donor atoms than the desired compound and was likely to be outcompeted for coordination to copper.

Compounds containing seven nitrogen atoms

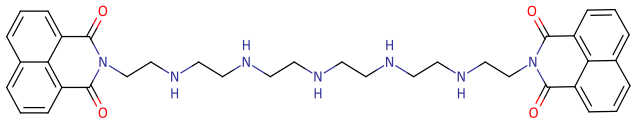

Figure E.21: ***Compound 2.19, ESI-MS peaks 318.6685 2+ (predicted 318.6688 2+ for $C_{36}H_{43}N_7O_4$)***

This compound had been detected by ESI-MS in amounts around 0.20 relative intensity. The heptamine was the largest peak aside from that of the desired hexamine in the free amine ESI-MS, so it would be expected that this compound would be detected in reasonable amounts.

Unfortunately, due to the greater number of donor atoms it was likely that this compound would outcompete the desired compound for complexation, and the free ligand was observed in the ESI-MS spectrum for the most enriched sample of the desired compound. This indicated that the purification by complexation was not able to sperate this compound from the desired ligand.

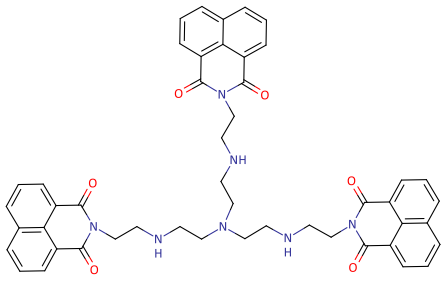

Figure E.22: ***Compound 2.20, ESI-MS peaks 408.6787 2+ 816.3502 1+ (predicted 408.6794 2+ for $C_{48}H_{47}N_7O_6$ and 816.3510 1+ for $C_{48}H_{46}N_7O_6$)***

This compound was detected extensively throughout the reactions with a maximum relative intensity of 0.41. There are four possible isomers of this compound. This compound had four

available donor atoms, the same number as the desired compound. The steric bulk of the third pendant may make this compound a poorer ligand than the desired compound.

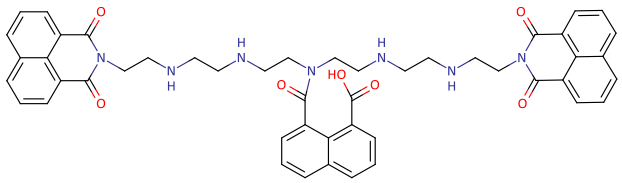

Figure E.23: ***Compound 2.21, ESI-MS peak 417.6847 2+ (predicted 417.6847 2+ for $C_{48}H_{49}N_7O_7$ and 834.3616 1+ for $C_{48}H_{48}N_7O_7$)***

This compound was also extensively detected in the ESI-MS in various reaction fractions at a relative intensity up to 0.28. As for 2.5 and 2.6, the amide was detected after the crude material had been at reflux. Similar to 2.20, this compound had five donor atoms, making it a potentially better ligand than the desired compound. The additional naphthalimide and tertiary nitrogen atom may mean the desired compound can outcompete this compound to coordinate copper.

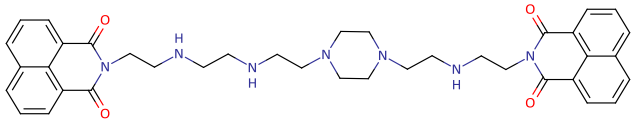

Figure E.24: ***Compound 2.22, ESI-MS peak 331.6756 2+ (predicted 331.6767 2+ for $C_{38}H_{45}N_7O_4$)***

The compound mass was detected in the ESI-MS spectra at relative intensities up to 0.28. This ligand had five donor atoms, more than the desired compound, two of which are constrained by the piperazine ring therefore potentially reducing the ability of this compound to complex.

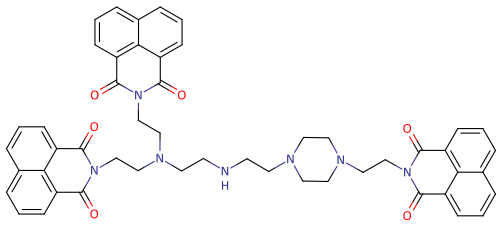

Figure E.25: ***Compound 2.23, ESI-MS peak 421.6866 2+ (predicted 421.6872 2+ for $C_{50}H_{49}N_7O_6$)***

The peak corresponding to this mass was detected with relative intensities up to 0.13. This compound contains both a ring constrained piperazine moiety as well as a third naphthalimide reducing the number of donor atoms. This indicates that this was likely to be a poorer ligand than the desired compound.

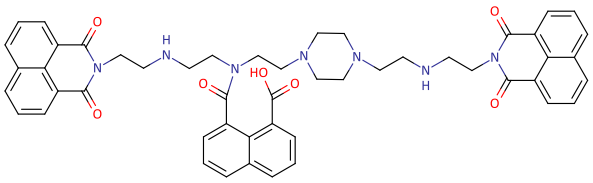

Figure E.26*: Compound 2.24, ESI-MS peak 430.6930 2+ (predicted 430.6925 2+ for $C_{50}H_{51}N_7O_7$)*

The compound mass was detected in the ESI-MS spectra at relative intensities around 0.10. As for 2.23, this ligand had both ring strain, a tertiary nitrogen and steric strain and therefore was likely to be a poorer ligand than the desired compound.

Compounds containing four nitrogen atoms

These compounds contain fewer donor atoms than the desired compound which would therefore be likely to outcompete these compounds. The tetramine and piperazine-derived tetramine compounds were detected in low amounts in the free amine, 0.05 and 0.13 respectively, and these compounds were detected in trace amounts.

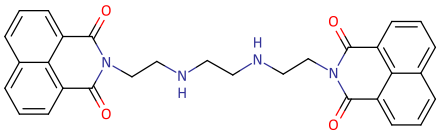

Figure E.27: ***Compound 2.25, ESI-MS peaks 254.1055 2+ and 507.2022 1+ (predicted 254.1055 2+ for $C_{30}H_{28}N_4O_4$ and 507.2033 1+ $C_{30}H_{27}N_4O_4$)***

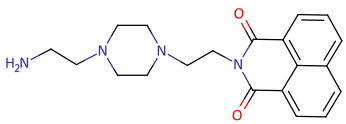

Figure E.28: ***Compound 2.26, ESI-MS peaks 177.1018 2+ and 353.1965 1+ (predicted 177.1028 2+ for $C_{20}H_{26}N_4O_2$ and 353.1978 1+ for $C_{20}H_{26}N_4O_2$)***

E.2 Complexes Detected

Although the intention of this process was to isolate the desired compound through complexation and subsequent separation of the complexation product, the presence of other potentially better ligands indicated that the desired tetradentate ligand compound would not be isolated. The possibility for neutral complexes had been discussed previously in the relevant sections, yet as they were by nature undetectable by ESI-MS unless they became charged, it was unsurprising that no complex was detected.

Future work to identify other complexes, including to determine the presence of neutral species, could involve the comparison of relative intensities of compounds in the crude material versus the complexation products to detect any reduction in the height of peaks that correspond to compounds forming neutral complexes. A better understanding of any complexes forming may allow for better refinement of the purification conditions.

During the analysis of the various ESI-MS spectra across the reactions, the following copper complexes were detected (Figures E29-35):

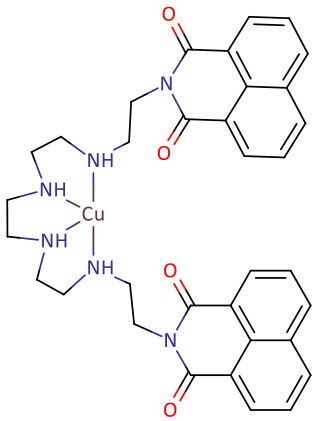

Figure E.29: ***Complex [Cu(2.1)]$^{2+}$, ESI-MS peak 327.6047 2+ (predicted 327.6046 2+ for [Cu($C_{34}H_{36}N_6O_4$)]$^{2+}$). Largest relative intensity: 1.00.***

This was the complex of the desired compound for purification and was detected extensively throughout the study.

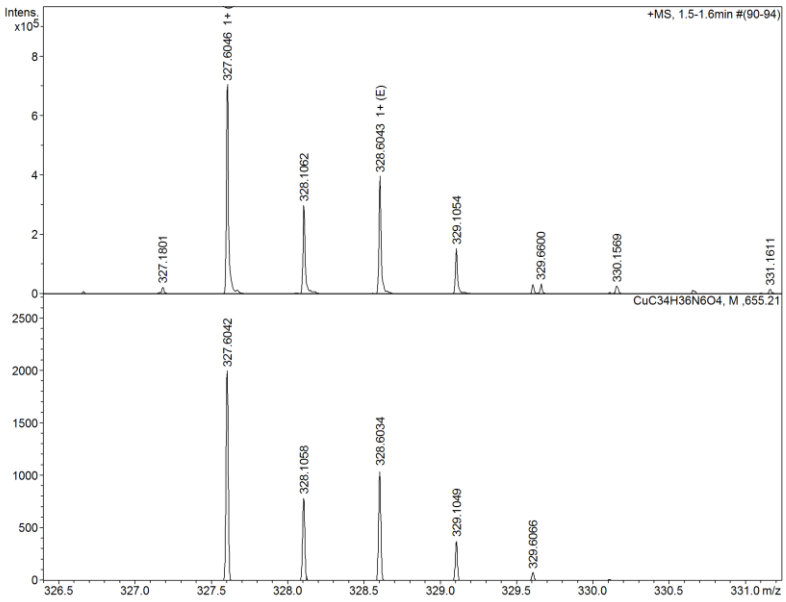

Figure E.30: ***ESI-MS of [Cu(2.1)]$^{2+}$, showing the isotope pattern for the native (above) and simulated (below) spectra.***

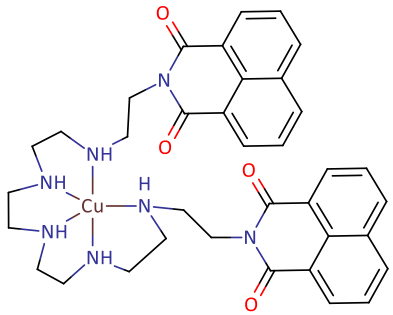

Figure E.31: ***Compound [Cu(2.19)]$^{2+}$ ESI-MS peak 349.1258 2+ (predicted 349.1258 2+ for [Cu($C_{36}H_{41}N_7O_4$)]$^{2+}$). Largest relative intensity: 0.24.***

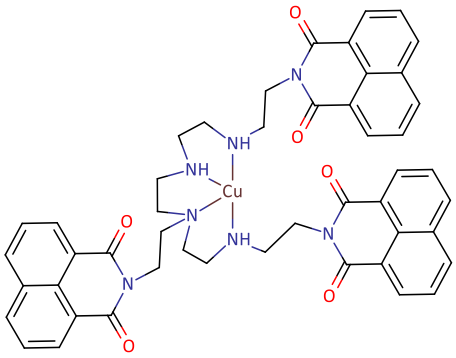

Figure E.32: ***Compound [Cu(2.20)]$^{2+}$, ESI-MS peak 439.1370 2+ (predicted 439.1364 2+ for [Cu($C_{48}H_{45}N_7O_6$)]$^{2+}$). Largest relative intensity: 0.16***

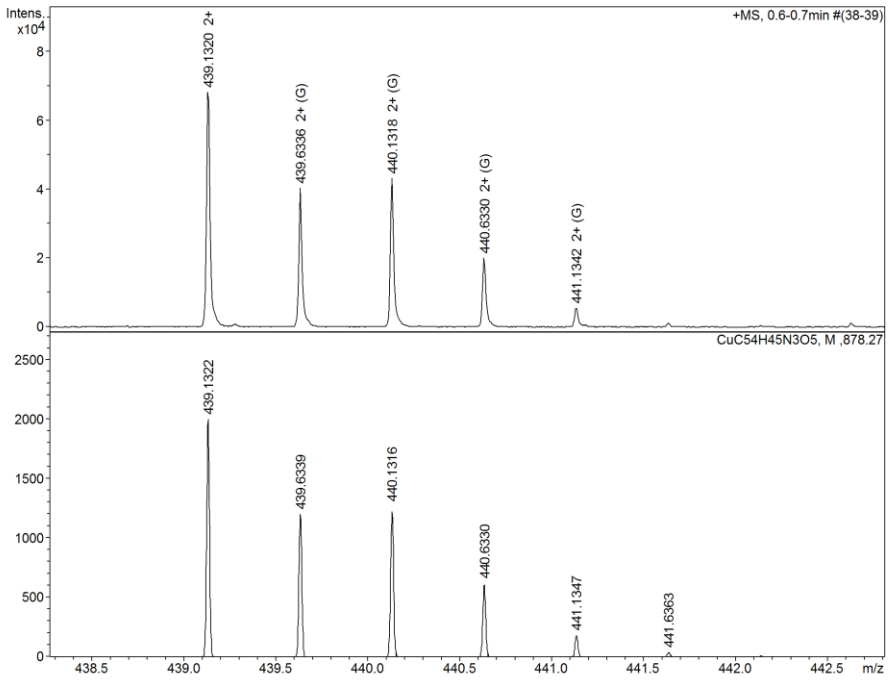

Figure E.33: ***ESI-MS of [Cu(2.20)]$^{2+}$, showing the isotope pattern for the native (above) and simulated (below) spectra.***

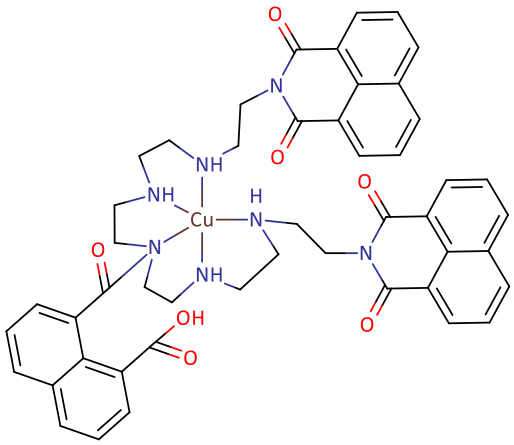

Figure E.34: ***Compound [Cu(2.21)]$^{2+}$, ESI-MS peak 448.1413 2+ (predicted 448.1416 2+ for [Cu($C_{48}H_{47}N_7O_7$)]$^{2+}$). Largest relative intensity: 0.09***

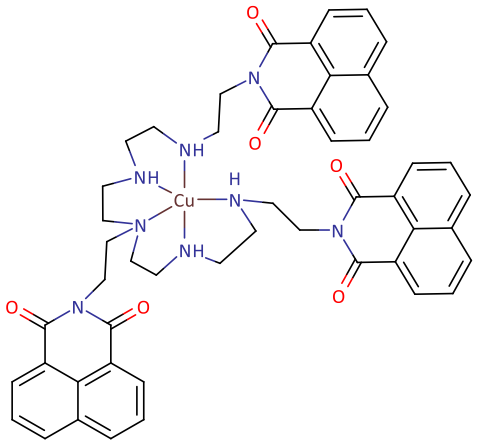

Figure E.35: ***Compound [Cu(2.27)]$^{2+}$, ESI-MS peak 460.6548 2+ (predicted 460.6575 2+ for [Cu($C_{50}H_{50}N_8O_6$)]$^{2+}$). Largest Relative Intensity: 0.02***

Appendix F. Additional Chapter 3 Discussion

F.1 Cobalt Carbonate Complex Synthesis

The reaction to produce the carbonate complex can be divided into two stages – formation of the cobalt starting material and reaction of this material with the ligand. The formation of the cobalt starting material had to be done immediately prior to using it as the $K_3[Co(CO_3)_3]$ complex degrades over time, shifting from the bright deep green to a brownish green[142]. This complex was synthesised and added to the reaction in two different ways. The literature method[89] describes taking the slurry of the complex produced and using it directly. This reaction produced KCl as a by-product, and using the slurry directly resulted in adding this KCl into the reaction with the ligand material. In order to avoid having to desalt the mixture, the green slurry produced from the reaction of cobalt chloride with potassium bicarbonate was filtered and rinsed with water to remove any residual salt. Some of the finer particles of the solid were lost during filtering, and further loss was experienced during the rinsing as the complex had a slight solubility in water. Unfortunately, the process of filtering appears to have degraded some of the material, as observed by the darkening of the filter cake. It also meant the amount of the product present was unknown due to the losses experienced during the filtering process. Filtering of the slurry was abandoned, and the slurry used directly. The reaction of this slurry with the ligand material resulted in the solution changing colour from the amber of dissolved ligand to sap green upon addition of the slurry and slowly to burgundy as the reaction proceeds. The reaction produced a solid and a liquor, which then formed an oil upon cooling.

The solid from this reaction was a deep green colour, suggesting it contained excess starting material that did not react or starting material that degraded prior to interacting with the ligand material. This starting material itself would not be detected by ESI-MS in positive ion mode as it was a negatively charged species. Additionally, it may not be detected at all due to decomposition of the carbonates from the formic acid generally added to encourage ionisation during the ESI process.

Aside from the discussed detection of the deprotonated ligand complex in both syntheses, there was also potential evidence of other complexes in this material – a complex of cobalt to the desired ligand with an ancillary hydroxide ligand (334.1068 2+, predicted 334.1079 2+ for $[Co(C_{34}H_{36}N_6O_4)(OH)]^{2+}$) detected with a relative intensity of 0.37, as well as a peak possibly corresponding to the desired complex and an associated water molecule (which may also be a hydroxide and a hydrogen carbonate, 729.2101 1+, a higher error match for the predicted 729.2083 1+ for $[Co(C_{34}H_{36}N_6O_4)(CO_3)(OH_2)]^+$ or $[Co(C_{34}H_{36}N_6O_4)(HCO_3)(OH)]^+$). It was unclear how

viable these complexes are to exist as both seem unlikely; the former due to the possibly five coordinate cobalt and the latter due to the error in the predicted monoisotopic mass.

The reaction with enriched material showed evidence of unreacted starting material that was not observed in the crude ligand reaction. This was likely because the reactions were each performed using the amount of cobalt required to react with the ligand in a 1:1 ratio, assuming the entirety of the ligand material was the desired compound. In both cases this was untrue, but the true proportion was unable to be determined. The crude material was likely to be around 30% desired compound, while the enriched ligand was likely to be around 80% of the mass of the solid. This would mean that the crude ligand procedure was likely performed at a substantially higher cobalt excess compared to the enriched ligand procedure.

The enriched ligand procedure did not produce an oil upon cooling. This may be in part due to the greater reaction volume required by comparison to the scale.

F.2 Cobalt Nitrite Complex Synthesis

The reaction performed with excess cobalt and crude ligand material resulted in the production of the purest sample of the desired complex. The excess cobalt was used following the observation that the material had low solubility in methanol. Increased solid presence would give a greater surface area of the suspended powder in solution which was done to attempt to increase the chances of reaction with the dissolved ligand material.

The reaction liquor still contained substantial amounts of the desired complex even following the formation of the oil. This indicates that more of the desired complex could be recovered from this liquor, either by concentrating further and allowing to stand, or by completely removing the solvent. The colour difference between the solution and the solid does, however, suggest that they may not be composed of the same compounds as the oil was an orangey brown, while the solution was a brighter orange. This may be due presence of starting material or due to the formation of neutral complexes. In this reaction, the predominant side products from the crude ligand material (2.3, 2.4) would again be poorer ligands than the desired compound. Due to both the ring strain and presence of additional tertiary nitrogen atoms compared to the desired compound, the side products may have fewer donor atoms. The desired complex had two nitrite ligands remaining from complexation of the ligand, forming a 1+ charge overall. If the side products complexed using fewer donor atoms, the complexes would potentially retain more of the nitrite ligands, forming neutral (or negative) species that would not be detected by ESI-MS.

The stoichiometric cobalt reaction produced an oil upon cooling; however, it was a much brighter orange than the oil seen in the excess cobalt reaction and the composition of this oil appears to be very similar to the liquor itself. Unlike the previous reaction with excess cobalt, this oil contains a decent proportion of the tripendanted side product. There was also an oil that formed immediately in the bottom of the Buchner flask upon hot filtration of the reaction mixture. This oil also resembles the liquor and cooling oil in that it was predominantly composed of the side products from the crude ligand mixture.

The reaction preformed using the enriched ligand material was performed on a much smaller scale than the previous reactions and produced slightly different results. The most notable difference was the lack of oil produced by cooling the reaction liquor. This may have occurred due to the slightly larger volume of methanol used than was proportional for the scale of the reaction encouraging the contents that would form the oil to instead remain in solution upon cooling. Another difference was the presence of blue solid in this reaction. This was presumed to be from the enriched ligand material, which retained some of the blue colour from the copper procedure. The reaction liquor was in this case similar to the orange solid collected on the filter paper. In the previous reactions the reaction liquor and the oil produced upon cooling were very similar, so it was possible that the oil did not form after filtering in this reaction but just prior to filtering instead. This reaction was performed on a much smaller scale than the previous reactions, which would allow it to cool a lot more rapidly. In each reaction the refluxing reaction mixture was cooled on the hot plate until the mixture had ceased boiling. The smaller scale of this reaction may have allowed it to cool down to the point of oil formation prior to filtering as opposed to afterwards as in the previous reactions. In the reaction liquor, remaining free ligand was detected suggesting that the reaction may not have been complete either due to insufficient cobalt starting material or insufficient reaction duration.

The purest sample of the desired 2.1 dinitrito complex was detected in the excess cobalt synthesis at a possible 5-10% yield. While this was a low yield, the reaction was performed using the crude material. This means the yield may be greater than observed as the desired mass was only around 30% of the species detected in the crude reaction. The fact that the crude material was used for this reaction also reduces the impact that a low yield had as the cobaltinitrite material was purchased and could potentially be recovered due to its high aqueous solubility. The ligand material appeared to be enriched during this reaction which would reduce the amount of work required to get to this step, which also reduces the impact low yield had on the reaction.

Appendix G. Additional Chapter 4 Methods and Results

G.1 Methods

Repetition of reaction using excess 1,8-naphthalic anhydride

The synthesis that led to crystal formation was repeated using excess 1,8-naphthalic anhydride ($C_{12}H_6O_3$ 15.00 g, 75 mmol), chloroform (35 mL) and 3,7,10,14-tetraazahexadecane-1,16-diamine ($C_{12}H_{32}N_6$, 5 mL approx. 20 mmol) giving 19.92 g crude material.

15 g of this crude material was then dissolved in methanol (150 mL) in a 500 mL round bottom flask and placed on a hot plate with a magnetic stirrer. The flask was fitted with a condenser and the reaction mixture brought to reflux. Copper sulfate ($CuSO_4{\cdot}5H_2O$, 4.66 g, 18.7 mmol) was dissolved in warm methanol (125 mL) and added dropwise down the condenser. The reaction was refluxed for four hours. Once cool, the liquor (275 mL) was decanted and the solid in the round bottom flask was treated with EDTA by adding 300 mL of distilled water and returning the flask to reflux. Solid disodium EDTA ($Na_2C_{10}H_{14}N_2O_8{\cdot}2H_2O$, 6.96 g 18.7 mmol) was added in five roughly equal portions to the refluxing mixture and the flask neck rinsed with 5 mL of distilled water. The reaction mixture was refluxed for three hours producing a bright blue solution and a brown oily solid.

Separately, the methanolic liquor was allowed to stand for one week to encourage crystal formation. The liquor was then decanted off the solid that formed, leaving the solid in a small amount of liquor to be analysed by powder diffraction. The liquor that was decanted was placed in a 500 mL round bottom flask and returned to reflux. Solid disodium EDTA ($Na_2C_{10}H_{14}N_2O_8{\cdot}2H_2O$, 6.96 g 18.7 mmol) was added in five roughly equal portions to the refluxing mixture and the flask neck rinsed with 5 mL of methanol. The reaction was refluxed overnight, producing a turquoise solution and a beige solid.

G.2 Results

Repetition of Crystallisation Conditions

Synthesised Naphthalimide Ligand Material

Largest peak unable to be assigned, many unassignable peaks

Mass: [M +2H$^+$] 2+: *m/z* 401.1712 2+ (predicted 401.1739 2+ for $C_{48}H_{46}N_6O_6$)
Relative Intensity: 1.0

[M +2H$^+$] 2+: *m/z* 410 (predicted 410.1792 2+ for $C_{48}H_{48}N_6O_7$)
Relative Intensity: 0.99

[M +2H$^+$] 2+: *m/z* 311 (predicted 311.1633 2+ for $C_{36}H_{42}N_6O_4$)
Relative Intensity: 0.61

[M +2H$^+$] 2+: *m/z* 199.0398 1+ (predicted 199.0395 1+ for $C_{12}H_7O_3$)
Relative Intensity: 0.23

Copper Complexation Solid

Mass: [M +2H$^+$] 2+: *m/z* 401.1720 2+ (predicted 401.1739 2+ for $C_{48}H_{46}N_6O_6$)
Relative Intensity: 1.0

[M +2H$^+$] 2+: *m/z* 311.1624 2+ (predicted 311.1633 2+ for $C_{36}H_{42}N_6O_4$)
Relative Intensity: 0.69

[M +2H$^+$] 2+: *m/z* 199.0399 1+ (predicted 199.0395 1+ for $C_{12}H_7O_3$)
Relative Intensity: 0.06

[M +2H$^+$] 2+: *m/z* 410 (predicted 410.1792 2+ for $C_{48}H_{48}N_6O_7$)
Relative Intensity: 0.06

$C_{36}H_{40}N_6O_4Cu$ 341.6204 2+, not detected.

$C_{48}H_{44}N_6O_6Cu$ 431.6309 2+, not detected.

$C_{36}H_{42}N_6O_4CuSO_4$ 390.6040 2+, $C_{36}H_{41}N_6O_4CuSO_4$ 780.2003 1+, not detected.

$C_{48}H_{46}N_6O_6CuSO_4$ 480.6146 2+, $C_{48}H_{45}N_6O_6CuSO_4$ 960.2214 1+, not detected.

Copper Complexation Solution

Mass: [M +2H$^+$] 2+: *m/z* 311.1622 2+ (predicted 311.1633 2+ for $C_{36}H_{42}N_6O_4$)
[M +1H$^+$] 1+: *m/z* 621.3166 1+ (predicted 621.3189 1+ for $C_{36}H_{41}N_6O_4$)
Relative Intensity: 1.0

[M +2H$^+$] 2+: *m/z* 199.0393 1+ (predicted 199.0395 1+ for $C_{12}H_7O_3$)
Relative Intensity: 0.36

[M +2H$^+$] 2+: *m/z* 410.1759 2+ (predicted 410.1792 2+ for $C_{48}H_{48}N_6O_7$)
Relative Intensity: 0.12

[M +2H$^+$] 2+: *m/z* 401 (predicted 401.1739 2+ for $C_{48}H_{46}N_6O_6$)
Relative Intensity: 0.06

Excess Anhydride

Synthesised Naphthalimide Ligand Material

Many unassignable peaks

Mass: [M +2H$^+$] 2+: *m/z* 401.1713 2+ (predicted 401.1739 2+ for $C_{48}H_{46}N_6O_6$)
Relative Intensity: 0.17

[M +2H$^+$] 2+: *m/z* 410.1770 (predicted 410.1792 2+ for $C_{48}H_{48}N_6O_7$)
Relative Intensity: 0.97

[M +2H$^+$] 2+: *m/z* 311.1622 (predicted 311.1633 2+ for $C_{36}H_{42}N_6O_4$)
Relative Intensity: 0.49

[M +2H$^+$] 2+: *m/z* 199.0398 1+ (predicted 199.0395 1+ for $C_{12}H_7O_3$) Relative Intensity: 1.0

Copper Complexation Solid

Mass: [M +2H$^+$] 2+: *m/z* 311.1613 2+ (predicted 311.1633 2+ for $C_{36}H_{42}N_6O_4$)
[M +1H$^+$] 1+: *m/z* 621.3166 1+ (predicted 621.3189 1+ for $C_{36}H_{41}N_6O_4$)
Relative Intensity: 1.0

[M +2H$^+$] 2+: *m/z* 401.1707 2+ (predicted 401.1739 2+ for $C_{48}H_{46}N_6O_6$)
Relative Intensity: 0.73

[M +2H$^+$] 2+: *m/z* 410.1758 2+ (predicted 410.1792 2+ for $C_{48}H_{48}N_6O_7$)
Relative Intensity: 0.36

[M +2H$^+$] 2+: *m/z* 199.0392 (predicted 199.0395 1+ for $C_{12}H_7O_3$)
Relative Intensity: 0.06

Copper Complexation Liquor

Mass: [M +2H$^+$] 2+: *m/z* 311.1625 2+ (predicted 311.1633 2+ for $C_{36}H_{42}N_6O_4$)
Relative Intensity: 1.0

[M +2H$^+$] 2+: *m/z* 410.1770 2+ (predicted 410.1792 2+ for $C_{48}H_{48}N_6O_7$)
Relative Intensity: 0.21

[M +2H$^+$] 2+: *m/z* 199.0401 (predicted 199.0395 1+ for $C_{12}H_7O_3$)
Relative Intensity: 0.20

[M +2H$^+$] 2+: *m/z* 401 2+ (predicted 401.1739 2+ for $C_{48}H_{46}N_6O_6$)
Relative Intensity: 0.01

Complexation Liquor Post EDTA Solid

Mass: [M +2H$^+$] 2+: *m/z* 311.1626 2+ (predicted 311.1633 2+ for $C_{36}H_{42}N_6O_4$)
[M +1H$^+$] 1+: *m/z* 621.3177 1+ (predicted 621.3189 1+ for $C_{36}H_{41}N_6O_4$)
Relative Intensity: 1.0

[M +2H$^+$] 2+: *m/z* 410.1769 2+ (predicted 410.1792 2+ for $C_{48}H_{48}N_6O_7$)
Relative Intensity: 0.22

[M +2H$^+$] 2+: *m/z* 401 2+ (predicted 401.1739 2+ for $C_{48}H_{46}N_6O_6$)
Relative Intensity: 0.01

[M +2H$^+$] 2+: *m/z* 199.0398 (predicted 199.0395 1+ for $C_{12}H_7O_3$)
Relative Intensity: 0.06

Complexation Liquor Post EDTA Solution

Mass: [M +2H$^+$] 2+: *m/z* 311.1610 2+ (predicted 311.1633 2+ for $C_{36}H_{42}N_6O_4$)
Relative Intensity: 1.0

[M +2H$^+$] 2+: *m/z* 410.1754 2+ (predicted 410.1792 2+ for $C_{48}H_{48}N_6O_7$)
Relative Intensity: 0.92

[M +2H$^+$] 2+: *m/z* 401 (predicted 401.1739 2+ for $C_{48}H_{46}N_6O_6$)
Relative Intensity: 0.01

[M +2H$^+$] 2+: *m/z* 199.0386 (predicted 199.0395 1+ for $C_{12}H_7O_3$)
Relative Intensity: 0.06

$C_{36}H_{40}N_6O_4Cu$ 341.6204 2+, possible trace.

Complexation Solid Post EDTA Solid

Mss: [M +2H$^+$] 2+: *m/z* 401.1720 2+ (predicted 401.1739 2+ for $C_{48}H_{46}N_6O_6$)
Relative Intensity: 1.0

[M +2H$^+$] 2+: *m/z* 199.0394 1+ (predicted 199.0395 1+ for $C_{12}H_7O_3$)
Relative Intensity: 0.20

[M +2H$^+$] 2+: *m/z* 311.1618 2+ (predicted 311.1633 2+ for $C_{36}H_{42}N_6O_4$)
Relative Intensity: 0.16

[M +2H$^+$] 2+: *m/z* 410 (predicted 410.1792 2+ for $C_{48}H_{48}N_6O_7$)
Relative Intensity: 0.01

Complexation Solid Post EDTA Solution

Mass: [M +2H$^+$] 2+: *m/z* 311.1621 2+ (predicted 311.1633 2+ for $C_{36}H_{42}N_6O_4$)

[M +2H$^+$] 2+: *m/z* 621.3182 1+ (predicted 621.3189 1+ for $C_{36}H_{41}N_6O_4$)
Relative Intensity: 1.0

[M +2H$^+$] 2+: *m/z* 401.1714 2+ (predicted 401.1739 2+ for $C_{48}H_{46}N_6O_6$)
Relative Intensity: 0.15

Appendix H. Additional Chapter 4 Discussion

H.1 Amine Starting Material

The number of peaks in the ^{13}C NMR spectrum of the amine stating material shows six inequivalent carbon environments, which was expected for the linear compound 4.1. The branched compound 4.2, however, would likely have seven inequivalent carbon environments. The number of peaks in the ^{13}C spectrum indicates that there was presence of at least one other compound (approximately one third as much as the main species, representing 25% of the mixture present based on integrals) yet the number of peaks of this height was greater than the expected seven so they cannot be assigned.

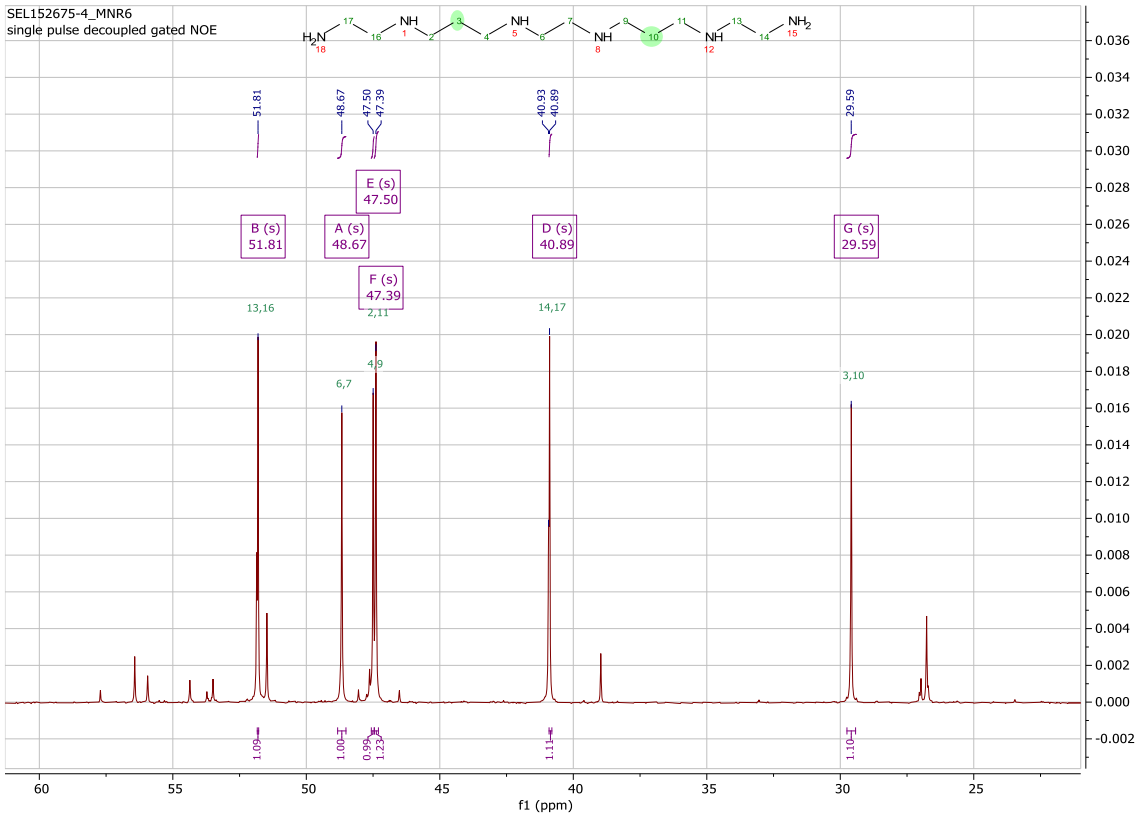

H.2 Crude Ligand Material

A substantial amount of branched amine 4.2 was present in the starting material which lead to formation of a trinaphthalimide species. Both the dinaphthalimide 4.3 and trinaphthalimide 4.4 species were detected by ESI-MS, with either present as the major peak across the syntheses. A compound mass matching that of a compound with two naphthalimide groups and a naphthalamide, 4.5, was also detected. This was more likely to be the product of additional substitution to the linear dinaphthalimide 4.3, as it appears that the primary amines react with naphthalic anhydride before the secondary amines (as observed by the crystal structure and in the previous chapters), yet in the previous chapter a compound (2.7) was identified by ESI-MS

that could only have formed if a secondary amine reacted without both primary amines reacting first. Therefore this peak cannot be attributed solely to the additional reaction to 4.3, but the majority was assumed to have arisen from this source as the presence of 2.7 in the previous chapter was inconsistent and often low.

Complexation of Ligand Material

The copper complex 4.5 was not detected by ESI-MS. This ligand may also form a copper complex with a sulfate ancillary ligand, resulting in a neutral complex that was not detected. This seems unlikely given that the analogous tetradentate dinaphthalimide ligand **2.1** formed a charged complex with copper as detected by ESI-MS. The reason for the lack of detection of this compound was unknown.

Reproduction of Crystallisation Conditions

Following the structural elucidation of the crystallised compound, efforts were focussed on reproducing the result. This is useful for multiple reasons – if the compound could be reliably crystallised it would allow the ligand to be collected in a very pure form. So far the evidence suggests that the 4.4 compound was formed from a minor component of the starting material, and as such its use for further syntheses was limited even if it was relevant for use in heterodinuclear complex synthesis unless it can be readily purified. Additionally, reproducibility indicates whether the complex formed was a consistent observation or if it was a random event caused by an irreproducible environment.

During the repetition, the reaction scale and duration were maintained but the method of heating was switched from a steambath to a hotplate as the hot plate had fewer issues with effective use. The repeat reaction was visually indistinguishable from the original throughout. When the copper reaction liquor was allowed to stand once the reaction was complete, the liquid did not produce crystals as was observed in the first reaction but instead resulted in formation of a pale blue powder that resembled the colour of the crystals collected previously. This solid was collected and work to compare the powder diffraction pattern to the crystal structure is ongoing.

In both reactions, the peak corresponding to 4.4 was the major peak, with small amounts of the other reaction components. The 4.3 species was detected predominantly in the solution. As mentioned previously, the copper complex of 4.4 was not detected directly in either reaction, only the free ligand.

Excess Anhydride

The synthesis of the crystallised complex showed that the amine starting material was not composed solely of the named compound. The material observed by crystallography indicated that a branched species was also present in the reaction mixture, and NMR was insufficient to determine the proportions of the compounds. To determine what proportion of the amine starting material was present, the mechanochemical reaction to produce the ligand was repeated using excess naphthalic anhydride. If the relative intensities of the dinaphthalimide and trinaphthalimide species shifted further towards the trinaphthalimide species, then this would indicate greater presence of the branched isomer.

The relative intensity of ligand 4.3 to ligand 4.4 product mass in the original stoichiometry was 0.61:1.0 as observed by ESI-MS. This indicated that there were still substantial amounts of a dinaphthalimide species present. Following the reaction with excess anhydride, the relative intensity of the 4.3 to 4.4 peaks went from 0.61:1.0 to 0.49:0.17. This suggested that the amount of 4.4 had actually decreased. The formation of a dinaphthalimide with an additional naphthalamide, 4.5, was also observed in the reaction mixture and went from 0.99 relative intensity in the initial reaction (approximately the same amount as 4.4) to 0.97 in the excess anhydride reaction (five times that of 4.4) when observed by ESI-MS. As free anhydride was detected in both ESI-MS spectra, the evidence indicates that the branched isomer was likely a minor component of the reaction which corresponds to the NMR interpretation.

The excess anhydride reaction was also followed through with treatment of the complexation liquor and solid with EDTA. This was done to determine if either of the major species (the trinaphthalimide and the dinaphthalimide) could be isolated using the purification by complexation technique covered in Chapter 2. Upon complexation, the trinaphthalimide 4.4 species is detected as the major species in the complexation solid, while the dinaphthalimide 4.3 and the dinaphthalimide with the additional naphthalamide 4.5 were the predominant species in the complexation liquor. Following removal of copper with EDTA, the same trend continued, with the dinaphthalimide detected as the major species in both the solid and the solution produced following treatment of EDTA, and the trinaphthalimide appearing as the major species in the solid produced following treatment of the complexation solid following treatment with EDTA. This suggests that the complexation by purification technique could be employed to separate these compounds for further studies, including the use of the enriched dinaphthalimide for cobalt complexation.